12-2012

# Experimental Determination of Colburn and Friction Factors in Small Plate Heat Exchangers with High Surface Enlargement Factors

Pike

# EXPERIMENTAL DETERMINATION OF COLBURN AND FRICTION FACTORS IN SMALL PLATE HEAT EXCHANGERS WITH HIGH SURFACE ENLARGMENT FACTORS

by

Andrew H. Pike

A Thesis
Submitted to the
Faculty of The Graduate College
in partial fulfillment of the
requirements for the
Degree of Master of Science in Engineering (Mechanical)
Department of Mechanical and Aeronautical Engineering
Advisor: HoSung Lee, Ph.D.

Western Michigan University
Kalamazoo, Michigan
December 2012

# EXPERIMENTAL DETERMINATION OF COLBURN AND FRICTION FACTORS IN SMALL PLATE HEAT EXCHANGERS WITH HIGH SURFACE ENLARGMENT FACTORS

Andrew H. Pike, M.S.E

Western Michigan University, 2012

Experiments were conducted to measure the performance of several small brazed plate heat exchangers. A test apparatus was designed and constructed that allowed for the easy switching of the plate heat exchangers, as well as having the ability to electronically monitor and record the inlet and outlet temperatures, pressures, and flow rates. The flow rates and applied electrical power were controlled electronically by the same program which recorded the data. De-ionized water was used as the heat transfer medium to reduce the uncertainty related to fluid properties.

An existing mathematical model was used to create Colburn and friction factors based on empirical correlations and the given geometric parameters of the heat exchangers. The experimental data was then expressed in terms of these factors, and were then compared to predictions. It was found that there was reasonable agreement for the Colburn and friction factors, despite the fact that the existing correlations were formulated using data from plate heat exchangers with significantly lower surface enlargement factors.

ACKNOWLEDGMENTS

I would like to thank my thesis advisor Dr. HoSung Lee, for teaching me the myriad of things that were necessary for me to complete this work, and for helping me to be a better engineer. I have no doubt that I wouldn't have been nearly as successful as a graduate student without his help and guidance.

Also, I would like to thank Abdulmohsen Alothman, who helped me to construct of the test apparatus in this study. Additionally the technicians here at WMU, Glenn Hall and Peter Thannhauser, deserve a good deal of thanks in aiding me turning an assortment of parts in to a complex working system.

Lastly, I would like to thank my parents, Gregory and Susan Pike who have been nothing but supportive of all my endeavors, as well as my other family and friends. I also want to thank my dearest Anell, who has stuck by me through all these difficult years of study.

Andrew H. Pike

TABLE OF CONTENTS

ACKNOWLEDGMENTS ..... ii

LIST OF TABLES ..... vi

LIST OF FIGURES ..... viii

CHAPTER

1. INTRODUCTION ..... 1

1.1 Overview of heat exchangers ..... 1

1.1.1 Performance of heat exchangers ..... 3

1.2 Objective of experiment ..... 7

2. LITERATURE REVIEW ..... 9

2.1 Chevron type plate heat exchangers ..... 9

2.1.1 Experimental results ..... 12

2.1.2 Correlations ..... 18

2.2 Heat exchanger test apparatuses ..... 20

3. DESIGN AND CONSTRUCTION OF EXPERIMENT ..... 25

3.1 Previous apparatus ..... 25

3.2 System design ..... 25

3.2.1 Flow loops ..... 29

3.2.2 Bulk heaters and power supply ..... 30

3.2.3 Instrumentation ..... 30

CHAPTER

3.2.4 Data acquisition and control ..... 31

Table of Contents—Continued

CHAPTER


3.2.5 Test section ..... 34

3.3 Analytical method ..... 35

4. EXPERIMENTAL PROCEDURE AND UNCERTAINTY ..... 36

4.1 Heat exchanger specifications ..... 36

4.2 Procedure ..... 39

4.2.1 Heat exchanger installation ..... 40

4.2.2 Flow loop preparation ..... 41

4.2.3 Experimental parameters ..... 41

4.3 Uncertainty discussion in the literature ..... 41

4.4 Uncertainty and calibration ..... 43

4.4.1 Primary measurements ..... 46

4.4.2 Calculated values ..... 51

4.5 Effect of temperature dependent properties on results ..... 52

4.6 Correction of pressure drop due to hoses ..... 54

5. EXPERIMENTAL RESULTS ..... 56

5.1 Fp3x8-10 ..... 56

5.1.1 Isothermal pressure drop ..... 57

5.1.2 High heat transfer ..... 58

5.1.3 Low heat transfer ..... 60

5.2 Fg3x8-14 ..... 61

Table of Contents—Continued

CHAPTER

5.2.1 Isothermal pressure drop ..... 62

5.2.2 High heat transfer ..... 63

5.2.3 Low heat transfer ..... 65

5.3 GB220H-20 ..... 67

5.3.1 Isothermal pressure drop ..... 67

5.3.2 High heat transfer ..... 68

5.3.3 Low heat transfer ..... 70

5.4 GB240H-20 ..... 72

5.4.1 Isothermal pressure drop ..... 72

5.4.2 High heat transfer ..... 73

5.4.3 Low heat transfer ..... 75

6. CONCLUSION ..... 77

APPENDICES

A. MATHCAD for Fp3x8-10 ..... 78

B. MATHCAD for Fg3x8-14 ..... 102

C. MATHCAD for GB220H-20 ..... 126

D. MATHCAD for GB240H-20 ..... 150

E. Averaged Experimental Results in Table Format ..... 175

F. Table of Experimental Hose Pressure Drops ..... 183

G. Power Measurement ..... 186

H. Instrumentation and Experimental Equipment Information ..... 191

Table of Contents—Continued

BIBLIOGRAPHY ..... 203

LIST OF TABLES

2.1 Review of Experiments in Literature ..... 17

4.1 Heat Exchanger Parameters ..... 39

4.2 Statistical Characteristics of Experimental Data ..... 44

4.3 Hot Side Pressure Drop Offset and Uncertainty ..... 48

4.4 Range of Measured Temperature Offsets ..... 49

4.5 Temperature Offsets ..... 50

4.6 Experimental Uncertainties ..... 51

5.1 Experimental Results of Fp3x8-10 at 22kW ..... 58

5.2 Experimental Results of Fp3x8-10 at 11kW ..... 60

5.3 Experimental Results of Fg3x8-14 at 25kW ..... 63

5.4 Experimental Results of Fg3x8-14 at 14kW ..... 65

5.5 Experimental Results of GB220H-20 at 28kW ..... 68

5.6 Experimental Results of GB220H-20 at 14kW ..... 70

5.7 Experimental Results of GB240H-20 at 27kW ..... 73

5.8 Experimental Results of GB240H-20 at 13.7kW ..... 75

LIST OF FIGURES


1.1 Drawing of a Brazed Plate Heat Exchanger .....2

2.1 Diagram of a Chevron Type Plate .....10

2.2 Internal Section of Stacked Chevron Plates.....10

2.3 Legend for Experimental Systems .....21

2.4 Muley and Manglik Experimental System .....21

2.5 Warnakulasuriya and Worek Experimental System .....22

2.6 Durmuş et al. Experimental System.....23

2.7 Khan et al. Experimental System.....23

2.8 Faizal and Ahmed Experimental System.....24

3.1 Logical Diagram of Experimental System.....26

3.2 Path of Energy Flow at Steady State Conditions .....27

3.3 Picture of Experimental System.....28

3.4 Picture of Labview Program Interface.....33

3.5 Picture of Labview Block Diagram .....33

3.6 Picture of Test Section .....34

4.1 Picture of Heat Exchangers Tested .....36

4.2 View of Fp3x8-10 Flow Passages.....37

4.3 View of Sectioned Fp3x8-10 .....37

4.4 GEA Plate Dimensions .....38

4.5 Graph of Steady State Temperatures .....45

4.6 Graph of Steady State Flow Rates .....45

List of Figures—Continued

4.7 Graph of Uncorrected Steady State Pressure Drop ..... 46
4.8 February 26th Overnight Temperature Measurements ..... 49
4.9 Graph of Colburn Factor and Effect of Property Variation ..... 53
4.10 Effect of Hose Pressure Drop Correction ..... 55
5.1 Isothermal Friction Factor Fp3x8-10 ..... 57
5.2 Colburn and Friction Factor Fp3x8-10 22kW ..... 59
5.3 Colburn and Friction Factor Fp3x8-10 11kW ..... 61
5.4 Isothermal Friction Factor Fg3x8-14 ..... 62
5.5 Colburn and Friction Factor Fg3x8-14 25kW ..... 64
5.6 Colburn and Friction Factor Fg3x8-14 14kW ..... 66
5.7 Isothermal Friction Factor GB220H-20 ..... 67
5.8 Colburn and Friction Factor GB220H-20 28kW ..... 69
5.9 Colburn and Friction Factor GB220H-20 14kW ..... 71
5.10 Isothermal Friction Factor GB240H-20 ..... 72
5.11 Colburn and Friction Factor GB240H-20 27kW ..... 74
5.12 Colburn and Friction Factor GB240H-20 13.7kW ..... 76

# CHAPTER 1

# INTRODUCTION

## 1.1 Overview of heat exchangers

Heat transfer can take place through three mechanisms, Conduction, Convection, and Radiation. It is often necessary to transfer heat between different fluids without mixing them, when this is the case a heat exchanger is often employed. A heat exchanger is a device that transfers thermal energy between two or more fluids. This occurs by directing the two flows past each other in separately wetted channels. The heat from one of the fluids will move into the material separating the two flows via convection, is then conducted across the material, and will finally pass into the second fluid by convection again.

It is not necessary that both of the fluids be liquids, the flows can be gas, liquid, or a combination of the two. There are many types of heat exchangers, an example of a common gas/liquid heat exchanger would be an automotive radiator. The type of heat exchanger will usually be dictated by state of the fluids that are being handled, although for a given set of fluid states there can be a variety of types.

The common types of heat exchangers for liquid/liquid heat transfer are double pipe heat exchangers, shell and tube heat exchangers, and plate heat exchangers (PHEs). Shell and tube heat exchangers have been employed in industry for well over a century, but they are often bulky and have lower compactness relative to some of their counterparts (Dović et al., 2009). Heat exchanger manufacturers have been continually striving to increase compactness and surface area density. PHEs have existed for over a century, with one of the first patents being issued in 1890 in Germany (Ayub, 2003). These heat exchangers use a stack of thin plates

with flows of different temperature passing between them in alternating layers of hot and cold, allowing heat to be transferred between the fluids.

Plate heat exchangers have the benefit of being suited to be deployed in configurations which are very compact. Traditionally, heat exchangers have been rather large devices, with PHEs consisting of a stack of plates with gaskets in between but a type of PHE called the brazed plate heat exchanger has been in service since the 1970s (Hesselgreaves, 2001). These PHEs have stacks of plates pressed together, and then brazed in to form a single part capable of withstanding high pressures. These devices are generally smaller, sometimes almost fitting in a hand and weighing several pounds. It is this type of heat exchanger which will be the focus of this thesis. Figure 1.1 is a drawing of a typical brazed plate heat exchanger.

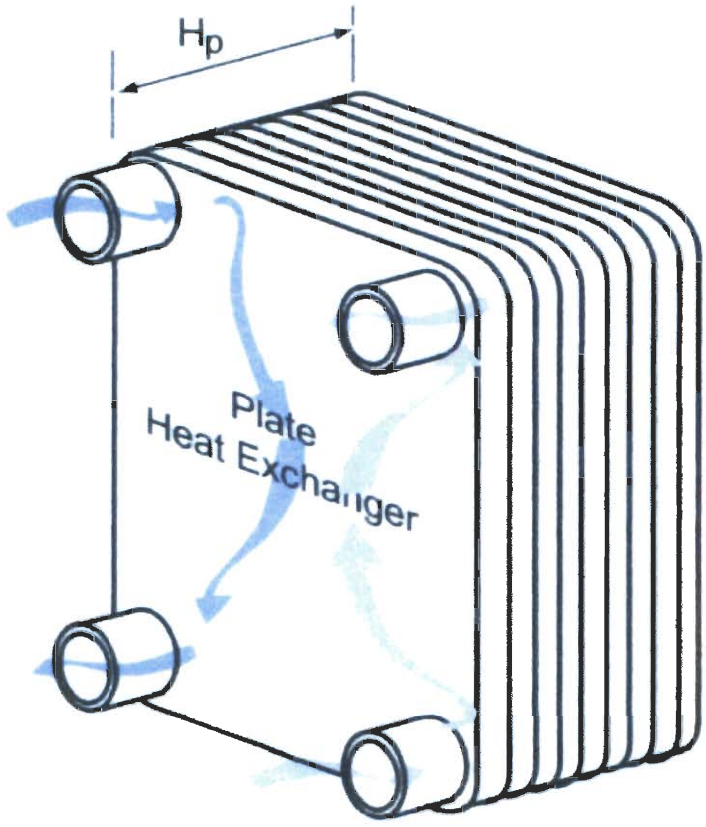


Figure 1.1 Drawing of a Brazed Plate Heat Exchanger, Lee (2010)

### 1.1.1 Performance of heat exchangers

In order to better understand the remainder of this thesis, a discussion is necessary regarding the meaning of the word performance in relation to heat exchangers. There are two primary methods for defining the thermal performance, these are the Log Mean Temperature Difference (LMTD) method, and the Effectiveness and Number of Transfer Units (e-NTU) method. For this study, the e-NTU method will be used. Effectiveness is the actual heat transfered divided by the maximum possible heat transfer, and is dimensionless. For a plate heat exchanger, the overall heat transfer coefficient can be defined by Equation 1.2. For the remainder of the discussion in this study, the descriptor 1 will refer to hot side values, 2 shall refer to the cold side, 3 refers to the cooling loop, i will represent the inlet and o will represent the outlet conditions. $\delta$ is the thickness of the wall, $k_{wall}$ is the thermal conductivity of the wall separating the fluids, A represents the respective areas, and h is the convection coefficient.

The convection coefficient is an important factor in determining the rate of heat transfer between a moving fluid and an adjacent surface, it depends on several things including Reynolds number and physical properties of the fluid as well the geometry of the channel in which the fluid is flowing through. The convection coefficient h is very important as a design consideration, and many experiments have done to determine the value under different conditions. An arbitrary heat transfer rate can be found through the use of Equation 1.1. $T_\infty$ is the bulk temperature of the fluid while $T_{wall}$ is the temperature of the wall or surface the fluid is flowing past. The heat transfer rate can also be defined in terms of the mass flow, specific heat, and the temperature difference across the inlet and outlet. It should be noted that h cannot be directly solved through Equation 1.1, as that would require measuring the temperature difference between the fluid and wall.

$$q = h * A * (T_{\infty} - T_{wall}) \tag{1.1}$$

$$q = \dot{m} * c_p * (T1_i - T1_o) \tag{1.2}$$

Another important concept in heat transfer is effectiveness, which has direct physical meaning, it being the actual rate of heat transfer divided by maximum theoretically possible heat transfer. The maximum theoretical heat transfer can be determined through thermodynamic relationships, and is based upon the inlet temperatures, flow rates, and fluid properties for the hot and cold sides respectively.

$$\varepsilon = \frac{q}{q_{max}} \tag{1.3}$$

In order to define effectiveness, it is necessary to introduce a value known as mass capacitance. It is the product of mass flow rate and the specific heat of the fluid.

$$C = \dot{m} * c_p \tag{1.4}$$

The heat capacity ratio, $C_r$, is defined as the ratio of minimum and maximum mass capacitances, $C_{min}$ and $C_{max}$ respectively.

$$C_r = \frac{(\dot{m} * c_p)_{min}}{(\dot{m} * c_p)_{max}} \tag{1.5}$$

It is now possible to define effectiveness in terms of C and temperature. The derivations for this relationship are widely available in the literature so the details will not be shown. As all of the testing was done with the test fluids in counter flow operation, as it is generally more effective, and therefore only the effectiveness for this case is shown.

$$\varepsilon = \frac{C_1*(T1_i - T1_o)}{C_{min}*(T1_i - T2_i)} \tag{1.6}$$

The number of transfer units (NTU), is a dimensionless value, and represents the ratio of UA and Cmin, where Cmin is the minimum value of mass capacitance in the system, it being the limiting of the two mass flows. It is also possible to define NTU in terms of Cr and temperature.

$$NTU = \frac{1}{1-C_r} * \ln\left(\frac{1-\varepsilon*C_r}{1-\varepsilon}\right) \tag{1.7}$$

NTU can also be defined in terms of UA, the overall heat transfer coefficient.

$$NTU = \frac{UA}{C_{min}} \tag{1.8}$$

Where UA can also be expressed as

$$UA = \frac{1}{\frac{1}{h_1 A_1} + \frac{\delta}{k_{wall}} + \frac{1}{h_2 A_2}} \tag{1.9}$$

For the type of heat exchanger used in this study, the areas of A1, A2, Aw are equivalent. Setting the experimental flow rates equal to one another allows for the assumption that $h_1 = h_2$. Equation 1.7 can now be rearranged so that h can be solved for as U is measured experimentally and the various geometry values are known.

$$h_{exp} = \frac{2}{\frac{1}{U} + \frac{\delta}{k_{wall}}} \tag{1.10}$$

Now that h has been found empirically, it is possible to calculate the Colburn factor j. It is a non-dimension quantity, and is a relation between the convection coefficient,

fluid properties, flow conditions and geometry. It is also necessary to introduce a new term, $A_c$, which is the free-flow area.

$$j_{exp} = \frac{h_{exp} * A_c}{c_p * \dot{m}} * P_r^{\frac{2}{3}} \tag{1.11}$$

Another important design parameter for heat exchangers is the pressure drop, or alternatively the friction factor. The friction factor gives the ability to calculate a pressure drop given the flow rate and geometry. It is important as a design factor, as a reduction in pressure drop directly correlates to lower frictional losses in the heat exchanger, which also equates to a lower level of pumping power required. The pressure drop is very simply the difference in pressure between the inlet and outlet ports of a heat exchanger, as shown in Equation 1.12.

$$\Delta P_{total} = P_i - P_o \tag{1.12}$$

The total pressure drop across the heat exchanger is comprised of two intrinsic pressure drops which are separable mathematically. These are the frictional pressure drop of the channels, and the pressure drop from the ports, $\Delta P_f$ and $\Delta P_p$ respectively. In order to calculate these, a new term is introduced in Equation 1.13, which is the mass velocity. The descriptors f and p refer to the frictional and port associated terms. $G_p$ is the mass velocity across the port area.

$$G = \frac{\dot{m}}{A_c} \tag{1.13}$$

$$G_p = \frac{4 * \dot{m}}{\pi * {D_p}^2} \tag{1.14}$$

An empirical correlation for the port pressure drop has been determined by several authors, including Kays and London (1984). It is shown in Equation 1.15.

$$\Delta P_p = \frac{1.5 * {G_p}^2}{2 * \rho} \tag{1.15}$$

It is now possible to determine $\Delta P_f$ by subtracting the port pressure drop from the total pressure drop, as seen in Equation 1.16.

$$\Delta P_f = \Delta P_t - \Delta P_p \tag{1.16}$$

The friction factor for the flow channels in the heat exchanger, sometimes referred to as the core friction factor, can now be calculated using Equation 1.17. It should be noted that this is the Fanning friction factor, not the Darcy friction factor.

$$f = \frac{D_h * {A_c}^2 * \Delta P_f}{2 * \rho * Q^2} \tag{1.17}$$

Where $D_h$ is the hydraulic diameter, $L_p$ is the length of the plate in the PHE, ρ is the density, and Q is the flow rate.

## 1.2 Objective of experiment

The purpose of this work was to experimentally determine the steady state convection heat transfer coefficient and pressure drops for four compact brazed plate heat exchangers. These values were used to compute Colburn factor and friction factor curves based on their internal geometry. GEA PHE systems contributed four heat exchangers of the type required for this study. De-ionized water was used as the heat transfer media so that there would be little doubt about the make up of the working fluid.

In order to calculate the convection coefficient and friction factor, it is necessary to monitor the inlet and outlet ports of both the hot and cold sides of the heat exchangers. The primary measurements that made were the temperature difference and pressure drop across both sides of the PHE, as well as the flow rate of water passing through each side respectively. In addition, to verify the overall heat transfer

of the system, the flow rate and temperature difference of the stream of cooling water was also measured.

It was therefore necessary to construct two flow loops, one for the hot side of the heat exchanger, and another for the cold side. An existing flow loop was modified, and another constructed alongside it. Attached to the second loop was a third loop, interacting with a stream of water taken from the building mains allowing the system to be cooled and finally sending the heat generated by the electric heaters to be sent down the drain.

With the ultimate goal of these experiments being the determination of convection coefficients and friction factors, care was taken to choose the proper conditions. Computing the fanning friction factor is a relatively straightforward task, as it is purely a function of pressure drop, flow rate, and geometry. Determining the convection coefficient required more scrutiny when choosing test conditions. Muley and Manglik calculated the convection coefficient using a calibration strategy employing modified Wilson plots (1999). This technique has the downside of basing the calibration on a linear regression taken from previous experimental work. An alternative method for calculation was employed by setting the hot and cold side convection coefficients equal to one another as done by Khan et al. (2010).
In order for this technique to be valid experimentally, it is therefore necessary that the hot loop and cold loop flow rates to be equal to one another. For each of the heat exchangers in the study, two levels of heat transfer were applied for each set of flow rates. Over the course of the study, the maximum heat transfer applied was 28 kW, and the sets of flow rates ranged from 3 to 11 gallons per minute in counter flow operation.

# CHAPTER 2

# LITERATURE REVIEW

There have been many investigators of the subject of heat exchanger performance. Compact heat exchangers have been a subject of study since for several decades (London and Kays, 1984). The literature survey was undertaken for two primary purposes. First, it served to provide a background on what type of experimental data would be useful to generate. Secondly, it provided a set of examples of the experimental apparatuses used in conducting heat exchanger testing. While there are many types of heat exchangers, the survey primarily focused on chevron type PHEs.

## 2.1 Chevron type plate heat exchangers

In order to provide a larger heat transfer area and encourage turbulent flow (reference), PHE manufacturers will often corrugate the plates. A common geometry used is a repeating pattern of sinusoidal corrugations, commonly referred to as a chevron pattern. Plate heat exchangers consist of multiple plates stacked upon one another, so that there are alternating flow passages of hot and cold fluid channels, with the plates providing the primary heat transfer area. In order to increase the surface area of the plates, it is often common to corrugate or in some other way change the surface profile of the plate. Durmuş et al (2009) investigated the effect of plates with asterisk and washboard type corrugations, however chevron plate configurations are one of the most common. Below in Figure 2.1 an example of a chevron type plate can be seen.

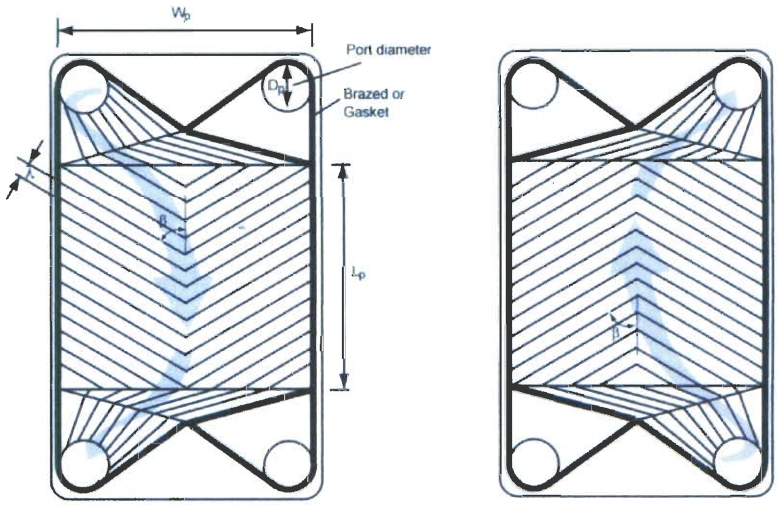


Figure 2.1 Diagram of a Chevron Type Plate, Lee (2010)

It is a rather straightforward assumption that changes in the geometry of the plate will affect the performance of the heat exchanger, this was verified by the literature review of plate heat exchangers by Ayub (2003). In order for the reader to better understand the workings of this type of heat exchanger, Figure 2.2 is shown below and provides some information on the various geometric parameters which impact performance.

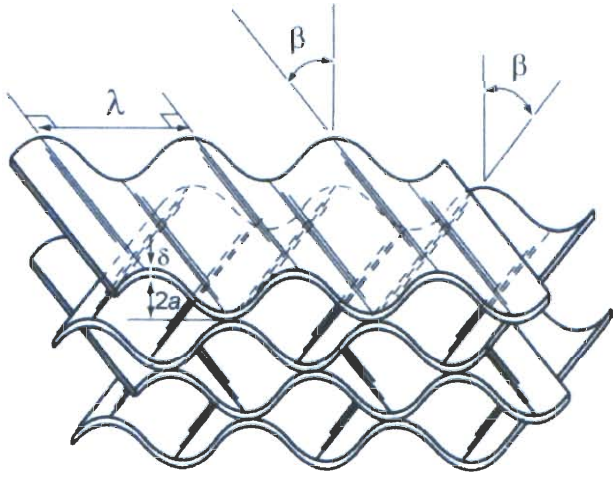


Figure 2.2 Internal Section of Stacked Chevron Plates, Lee (2010)

The figure shows many of the important geometric parameters that concern chevron type plates. The chevron angle, β, is the angle that the corrugation makes with respect to the longitudinal axis of the plate and can vary from 0 to 90 degrees. The plate thickness is often given as δ. The corrugation pitch, λ, represents the wavelength of the repeating sinusoidal pattern. The 2a term refers to the height, or twice the amplitude, of the corrugation. Different companies will specify different geometries with regards to the chevron angle β, the corrugation wavelength λ, and the amplitude of the corrugation in addition to many other factors. Despite a long history of use, there is lack of reliable data and generalized correlations for PHEs (Dovic, 2009).

While all of these parameters have impacts on performance, there are two factors which can largely summarize the characteristics of a chevron type plate. These are the chevron angle β, and another value named the surface enlargement factor Φ. The latter of these two is simply the total surface area of the plate divided by the projected area of the plate (Lee, 2010). A reduced form of this equation is shown below.

$$\Phi = \frac{corrugated\ area}{projected\ area} = \frac{L_\lambda N_\lambda}{W_p} \tag{2.1}$$

Where $L_\lambda$ is the enlarged length per wavelength, $N_\lambda$ is the number of wavelengths per plate, and $W_p$ is the width of the plate. To put this in perspective, a perfectly flat plate would have a Φ value of 1. There are several methods of calculating this factor in the literature, and while they differ slightly in form they have roughly equivalent meanings. Martin (1996) defines Φ similar to Lee, however he arrives at the value through an approximation of a three point integration using a dimensionless corrugation parameter based on the amplitude and wavelength of the pitch, opposed to the method employed by Lee which allows direct calculation based on geometric parameters. In his literature survey in 2003, Ayub defined Φ as the ratio of the developed length of the sinusoidal wave over the protracted length. He stated there is

a lack of design information in the public literature due to the proprietary state of the heat exchanger industry.

Another relevant factor is the surface area density β, not to be confused with the chevron angle. It has units of m^2/m^3, and is defined as the ratio of heat transfer area to the volume it occupies (Lee, 2010). In general, a heat exchanger will be considered compact when it's β is greater than 600.

### 2.1.1 Experimental results

As stated previously, there have been many investigators which have studied the performance of PHEs. Such that the experimental results can be better understood, context will be given by summarizing several papers in the open literature, while highlighting important variables and listing the ranges of factors relevant to the work done in this study. This is by no means an exhaustive review of available literature, but does give a broad view of the state of experimental heat exchanger testing done in recent times.

One set of investigators, Muley and Manglik (1999), undertook a wide ranging experimental study of PHEs with chevron plates, experimenting with many different plate configurations. Their study focused on single phase, counter flow with a single pass U type flow configuration. The plates which they used had β values of 30, 45, and 60 degrees and another so-called mixed configuration approximating a β of 45 degrees by using a mixed arrangement of 30 and 60 degree chevron angle plates in combination. Additionally, the observation is reached that there seems to be no significant advantage from using a mixed 30 and 60 degree plate arrangement relative to a stack of plates with β=45 degrees. They go on to state based upon their own literature review for chevron plate configurations, the transition to turbulent from laminar flow will occur at a Reynolds number between 400 and 800. For the plates used in their experiments, the Φ values were 1.29 and 1.46. Their data and conclusion show that by increasing Φ the heat transfer performance will increase relative to that of a flat plate configuration. However, this comes with a penalty of a higher pressure drop at a given pumping power, or equivalently a rise in the friction

factor. There is also a corresponding gain and penalty for increasing values of β, for the Nusselt number and friction factor respectively. In addition, they conducted similar experiments with vegetable oil as a working fluid.

Hsieh et al. (2002) investigated subcooled flow boiling of R-134a in a PHE. The PHE used in this study employed chevron type plates, with a β of 60 degrees. During their experiments they used hot water to induce boiling in the subcooled working fluid. For their study the boiling heat flux varied from 0 to 35 kW per square meter, and the refrigerant mass flux varied from 50 to 200 kg per square meter. Additionally, their work only made use of two PHEs, one for measuring heat transfer data, and another for visualization of the refrigerant flow.

Jokar et al. studied condensation heat transfer and pressure drop in brazed plate heat exchangers using R-134a (2004). They characterize brazed plate heat exchangers as a type of compact PHE, and performed experiments with single pass counter flow operation. For the non-refrigerant loop, working fluids of water as well as a glycol/water mixture were used. They then employed the Wilson technique, similar to Muley and Manglik, to obtain the single phase heat transfer coefficient. They state that due to the different corrugation patterns and geometries, it is difficult to predict performance with generalized correlations. Two brazed PHEs were employed in this study, one with 40 plates and another with 54. The plates used in these heat exchangers had chevron type corrugations, with a β of 60 degrees. The range of glycol/water flow rates employed in this study ranged from 0.15 to .45 kg per second, and used several expansion valves for the refrigerant loop with capacities ranging from 7 to 35 kW. The paper goes on to describe testing single phase fluid performance, with one loop containing water and the other containing a glycol/water mixture. However, there is some ambiguity with regards to this part of the testing and the method and amount of heating applied. Again, they employed the Wilson technique for calibrating and determining the heat transfer coefficients for single phase flow. For the single phase flow investigations, the Reynolds number was varied between 70 and 900.

Galeazzo et al. (2006) undertook an experimental and numerical study of heat transfer in a PHE. The experimental study used an Armfield FT-43 laboratory plate pasteurizer, operating in both parallel and counter flow configuration. The plates were comprised of stainless steel, and were flat, having no corrugations and the working fluid used was distilled water. Their paper states that the cold loop of the heat exchanger was provided water from a chiller and experienced flow rates of 0.6, 0.8, and 1.0 Liters per minute, while the hot loop had water provided from a thermostatic bath at temperatures of 50, 70 and 80 degrees Celcius. The hot loop was run in closed loop configuration with flow rates of 0.6, 0.8 and 1.0 Liters per minute. They compared the experimental results of the different test conditions with those generated by a 3D computational fluid dynamics (CFD) model, and also with predictions made using a 1D plug flow model. In general, they found that the CFD model provided better agreement to the experimental results relative to that of the plug flow model. For their study, the stated range of Re was from 136 to 1528, and the heat load varied from 70 to 749 W.

Dwivedi and Das (2007) conducted dynamic tests of PHEs subject to flow variations. They tested a PHE from Alfa Laval comprised of a stack of 40 chevron plates with a $\beta$ of 60 degrees, and operating in a U type configuration. Their experimental procedure consisted of introducing step changes in flow rates of the hot and cold water flow rates, with the tested flow rates in the range 0.93 Liters per second to 1.86 Liters per second. These flow rates correspond to Re ranging from 877 to 1756. The applied heat load came from a hot water tank with immersion heaters having 42 kW of capacity. The results presented provide a non-dimension time at which steady state was reached after various steps in flow rates, and they conclude that flow maldistribution has considerable effect on the transient response.

Research has also been done on the heat transfer and pressure drop of viscous salt solutions in PHEs. Warnakulasuriya and Worek (2008) investigated the performance characteristics of an absorbent salt solution in an ALFA-LAVAL PHE, with a rated heat capacity of 14,650 W. They describe it as having cross-corrugated

plates, with the angle between corrugations being 120 degrees. They stated that the inlet temperature differences ranged from 14 to 20 degrees Celsius, with hot side inlet temperatures ranging from 55 to 77 Celsius. However, they did not calculate the convection coefficients, and only provided the overall heat transfer coefficients measured. Based on the correlations referenced in the paper, they stated that the calculated overall heat transfer and fanning friction factors show very good agreement with the experimental results at Reynolds numbers above 400, but below that there was considerable deviation. For the course of their study, the flow rates ranged from 0.30 – 0.58 kg/s, and Re ranged from approximately 250 to 1075.

As noted earlier, Durmuş et al. (2009) investigated PHEs with different surface geometries in both parallel and counter flow. They chose water as a working fluid, and list the hot loop flow rates ranging from 0.03 kg/s to 0.16 kg/s, with hot inlet temperature ranging from 45 to 80 degrees Celsius. For the experiments undertaken, Re was between 50 and 1000. They used the method of solving for Nu by taking the experimental heat transfer for both the hot and cold sides respectively, and setting it equal to the product of convection coefficient, heat transfer area, and temperature difference across each side. It was also shown that corrugated plates provided a greater level of heat transfer when compared to both the flat and asterisk type plates.

Khan et al. conducted an investigation of single phase flow in PHEs with multiple plate configurations (2010). Chevron type plates were used, with $\beta$ values of 30 and 60 degrees, along with another mixed configuration using plates having an alternating $\beta$ of 30 and 60 degrees. During the experiments they solved for the convection heat transfer coefficient by keeping the Reynolds number same on both sides of the plate, allowing the assumption that the hot and cold side coefficients were equal. The surface enlargement factor $\Phi$ for all of the plates in this study was 1.117. A stack of three plates was used, providing one channel each for the hot and cold flows. Based on the results of the experiments undertaken, they suggest that the Nusselt number increased linearly with Re, and also increased with $\beta$.

Another study comparing CFD simulation and chevron PHEs was undertaken by Han et al. (2010). They did not provide specifications on plates used in the PHE, although it was specified that five plates were used, providing two channels of flow for the hot and cold sides respectively. A CFD model was set up also having four fluid channels, and it was found that there was not significant difference in thermal performance between them. Five flow rates were employed in the study, ranging from 50 to 90 liters/hour. The results presented showed a large discrepancy between the simulation and experimental values, on the order of 35%, however they did not discuss the uncertainty of their measurements. For the simulation settings used, the model under predicted the pressure drop as well as the outlet temperature of the hot side water flow.

Faizal and Ahmed (2012) conducted experimental studies on a corrugated PHE at low temperature differences. The plates were corrugated in a washboard fashion, the equivalent of a β of 90 degrees. As they were interested in ocean thermal energy conversion, low temperature differences were used in testing, and greater scrutiny was applied to the pressure drop. During the tests the hot side flow rate was varied, as well as the vertical spacing between the plates. A stack of 20 plates was used, and it was found that the smallest plate spacing of 6mm provided the highest heat transfer, but also produced the highest pressure drop. Over the course of the study, the temperature difference between the hot and cold inlets was held constant at 23 degrees Celsius, and the hot side flow was varied from 0.18 to 0.63 L/s while the cold side flow was held constant at 0.16 L/s.

The data in Table 2.1 represents various parameters regarding the experimental ranges of variables in the literature.

Table 2.1 Review of Experiments in Literature

| Authors | Year | Type | Fluid | Chevron Angle β (degrees) | Number of plates | Φ | Flow Rates Stated and (gpm) | Re |
|---|---|---|---|---|---|---|---|---|
| Muley, Manglik | 1999 | Gasketed PHE | Water, Veg. Oil | 30/30, 30/60, 60/60 | 12, 24 | 1.29, 1.46 | Not given | 600 – 10,000 |
| Hsieh, et al. | 2002 | PHE | R-134a | 60 | 3 | Not given, calculable | Not given | N/A |
| Jokar et al. | 2004 | BPHE | Water, Water/Glycol, R-134a | 60 | 40, 54 | Not given, calculable | 0.15 – 0.45 kg/s (2.38 – 7.14) | 70 – 900 |
| Galeazzo et al. | 2006 | Gasketed PHE | Water | N/A | 4 | 1 | 0.3 – 0.8 L/s (4.76 – 12.70) | Not given |
| Dwivedi, Das | 2007 | Gasketed PHE | Water | 60 | 40 | Not given, calculable | 0.93 – 1.86 L/s (14.76 – 29.52) | 877 - 1756 |
| Warnakulasuriya, Worek | 2008 | PHE | Absorbent salt solution LZB | N/A | Not given | Not given | 0.30 – 0.58 kg/s | 250 - 1100 |
| Durmuş et al. | 2009 | Gasketed PHE | Water | N/A | 15 | Not given | 0.03 – 0.16 kg/s (0.48 - 2.54) | 50 - 1000 |

Table 2.1 Continued

| Authors | Year | Type | Fluid | Chevron Angle β (degrees) | Number of plates | Surface Enlargement factor Φ | Flow Rates Stated and (gpm) | Re |
|---|---|---|---|---|---|---|---|---|
| Khan et al. | 2010 | Gasketed PHE | Water | 30/30, 30/60, 60/60 | 3 | 1.117 | Not given | 500 - 2500 |
| Han et al. | 2010 | BPHE | Water | Not given | 5 | Not given | 50 – 90 L/hr (.22 – 0.40) | Not given |
| Faizal, Ahmed | 2012 | Gasketed PHE | Water | N/A | 20 | Not given, calculable | 0.18 – 0.63 L/s (2.86 - 10) | Not given |

### 2.1.2 Correlations

One of the primary objectives in testing the performance of heat exchangers is to gather data that can be analyzed, allowing for empirical correlations to be developed. These empirical correlations are very important, as they can help to aide and guide the design process, allowing for better and more predictable performance of heat exchangers.

Martin (1996) collected a list of correlations from the literature and worked on developing a generalized correlation that could be used for design. By applying analytical techniques to the unit cell of flow area between two chevron type plates, and incorporating data from the literature along with reported geometric properties of the respective plates, he developed a generalized set of correlations for the heat transfer and pressure drop.

In 2003, Ayub conducted a literature survey for PHEs and their related heat transfer and pressure drop correlations. In that study, he compiled a list containing correlations for the Nusselt number and friction factor, the associated geometric parameters when given, and the range of values for which the correlations are valid. It should be noted that in his definitions, he defines the chevron angle β as the angle between the corrugations and the axis perpendicular to the main direction of flow, where as Lee and several other authors define β with respect to the longitudinal axis.

Dović and his co-authors worked to expand upon the work done by Martin in striving to develop generalized correlations for PHEs of an arbitrary geometry (2009). In their study they chose to define the chevron angle with respect to the longitudinal axis of the heat exchanger, contrary to the manner used by Ayub, which appears to be the general convention regarding this factor. The work done had the benefit of having additional experimental studies conducted, and it was found that there was reasonable agreement between their heat transfer correlations and those developed by Martin. However, it was concluded that there was larger disagreement between the new correlations developed and experimental data when regarding the friction factor. They state that this due to the fact that the correlation for friction factor was developed from a largely theoretical stand point, as no empirical correction factors are employed, but then stated that it is a worthwhile technique due to the large discrepancies within the experimental data.

Selbaş et al. (2009) investigated an alternative method for analyzing heat exchanger performance. They made use a neural network, trained with preliminary experimental results. Predictions were then made using this technique and compared against further experimental results. They found that once properly trained, predictions of heat transfer and effectiveness were within 1% of experimental results.

In 2011, Alothman undertook a comparison between these correlations. It was necessary for him to construct a theoretical heat exchanger with an arbitrary geometry, with parameters chosen such that it was possible to compare Martin's predictions to those developed by Dović et al.. He found that in general that was

reasonable agreement between the two with regards to the Colburn and friction factors, although the level of agreement depended on the geometric parameters selected, particularly with differing values of the chevron angle β.

## 2.2 Heat exchanger test apparatuses

For all heat exchangers which are of the liquid/liquid type, there are some basic elements which are required to conduct testing. For the purposes of this discussion these requirements will refer to tests of a steady state nature. Perhaps the most important, is the need to provide the inlet ports of the heat exchanger with hot and cold streams of fluid at steady flow rates and temperatures. As the nature of these tests is to discover useful information about performance, it is necessary to measure the inlet and outlet conditions for each port of the heat exchanger, as well as the respective flow rates.

For the experimental studies in the literature, some of the test apparatuses will now be described and schematics shown, so the workings of the system used in this study can be better understood. The key features of the experimental setups will all make use of the same iconography, indicated below. Experiment specific components which are not common to the rest of the diagrams will be noted where appropriate. The diagrams which are presented may represent a simplified schematic of the systems, and are intended to provide an idea of their nature, not to be definitive. Minor features such as static mixers, line pressure gauges, etc. will be omitted, as will valves unless they are critical to system operation. Pressure taps and thermocouple locations will be marked on the schematic as in the legend, although not every location may be labeled directly. For more detailed descriptions of the experimental systems refer to the original works. Figure 2.3 represents a legend of the iconography used in the various system diagrams.

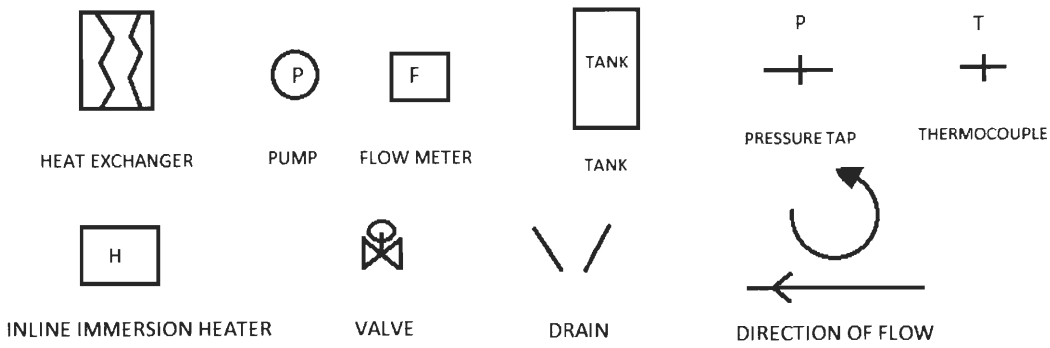


Figure 2.3 Legend for Experimental Systems

The work done by Muley and Manglik (1999) conducted tests over a wide range of operating conditions. While they reached a relatively high value of Re, this was only in the hot side of the heat exchangers. Their system is shown below in Figure 2.4.

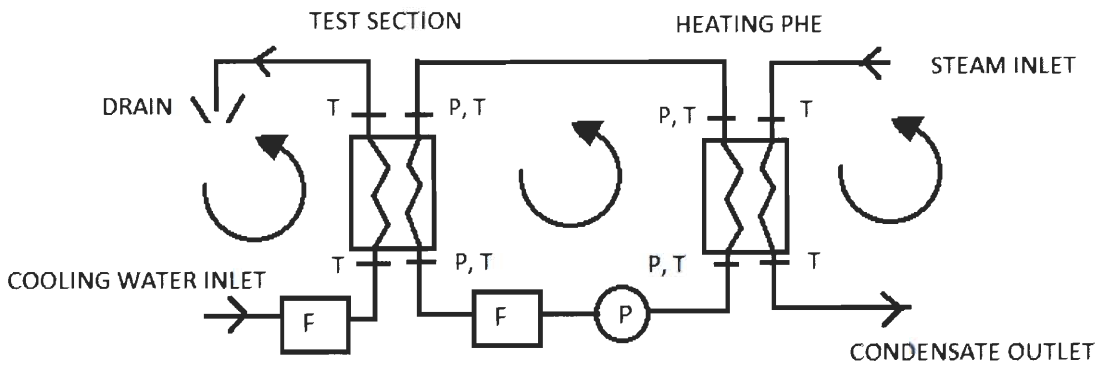


Figure 2.4 Muley and Manglik Experimental System

The process stream, being the loop in the middle of the diagram, is continuously heated by steam in the heating PHE, and cooled in the test section. A variable speed pump is used to control the flow rate in the process loop. They describe a time frame of approximately 25-30 minutes to reach state, presumably from the last change to

pump speed or steam flow rate. They also define the steady state in terms of maintaining an energy balance, q, across the hot and cold sides of the heat exchanger to within ±5%.

Warnakulasuriya and Worek (2008) constructed an experiment for testing the performance of a viscous absorption salt solution within a PHE. The paper does not specify the means of controlling the flow rates within various parts of the system, although the diagram does show recirculating loops with adjustable valves so it is presumably by means of adjusting said valves. It is redrawn in Figure 2.5.

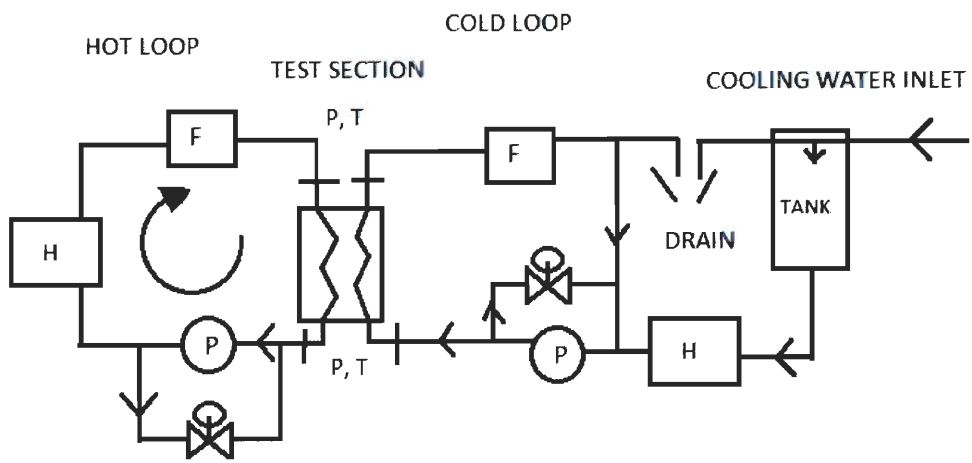


Figure 2.5 Warnakulasuriya and Worek Experimental System

Heat is generated in the system in both hot loop as well as the cold loop, as they were seeking to vary the Prandtl numbers of the fluids at the inlets of the test section.

In 2009 Durmuş et al. investigated the effect of various plate types in a PHE. A series of bypass valves, not shown in the schematic, allowed the system to be operated in both counter and parallel flow by means of adjusting the valves. No specific mention was made of how the flow rates were controlled, but it is a reasonable assumption that a variable speed pump was used as there was no recirculating loop was located near the pump in the experimental diagram in Figure 2.6.

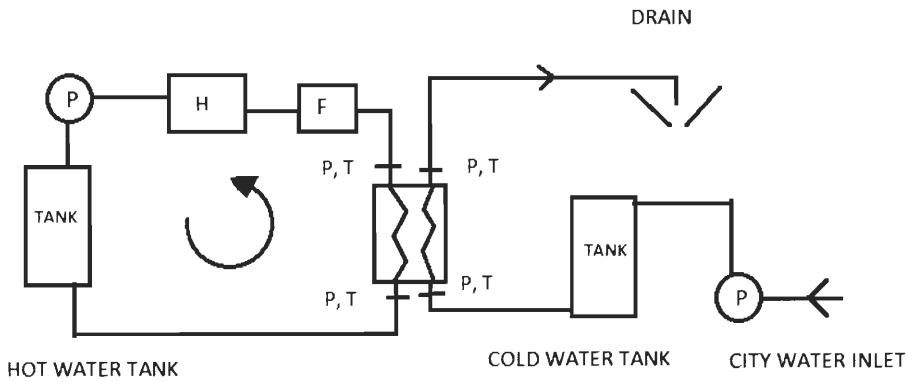


Figure 2.6 Durmuş et al. Experimental System

It is unclear as to how the flow rate of the cold/city water loop is measured, other than a reference on the diagram near the drain that reads "measurement container". The pump in the cold loop serves to augment the pressure of the incoming city water supply.

Khan et al. conducted a performance study of PHEs with multiple plate configurations by varying the Prandtl and Reynolds numbers (2010). The hot water tank contained several immersion heaters controlled by an RTD to maintain the desired temperature. The experimental system is shown in Fig 2.7.

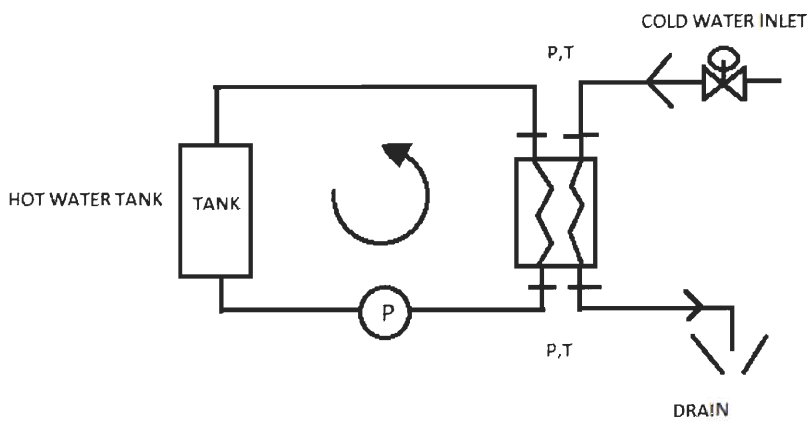


Figure 2.7 Khan et al. Experimental System

A 2.2 kW pump with an inverter was used to control the flow rate on the hot side of the system. It is presumed that the cold side flow rate was controlled by adjusting the valve on the cold water inlet line. No flow meter was included in the system, and they describe using a 5L graduated cylinder and stopwatch to measure the flow rate.

Faizal and Ahmed used a simplified system in their study of a PHE (2012). A hot water heater with steam heating was used to maintain a constant temperature of 49 degrees Celsius at the hot side inlet across all testing conditions, and the cold side inlet temperature was held constant at 26 degrees Celsius, although it was not stated how this was achieved. No flow meters were shown in the experimental diagram, and no mention was made as to how the flow rates were measured. Only the inlet gauge pressures were measured, and both the hot and cold flows were discharged into the atmosphere.

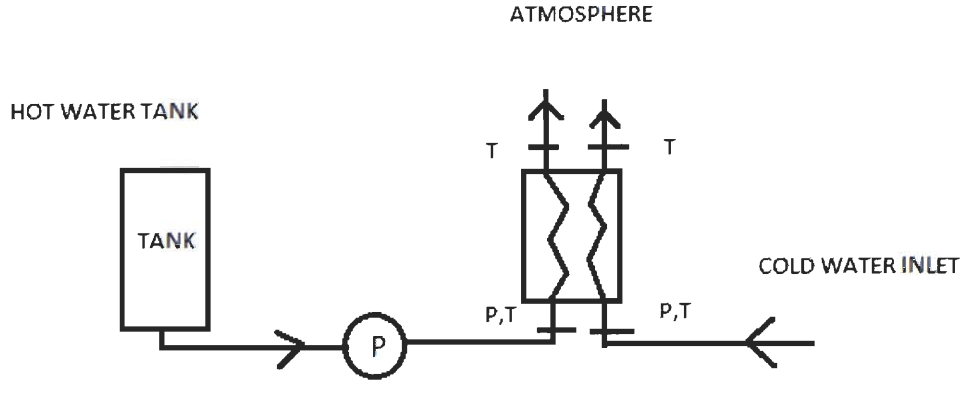


Figure 2.8 Faizal and Ahmed Experimental System

# CHAPTER 3

# DESIGN AND CONSTRUCTION OF EXPERIMENT

## 3.1 Previous apparatus

The initial portion of the test apparatus created for this study was from an existing experiment. It consisted of a single flow loop, constructed of stainless steel and being approximately 1.5 meters tall by 3 meters long. Immersion heaters were installed in the flow loop, to heat working fluid, and pumping power was provided by a 0.5 hp electrical motor coupled to a centrifugal pump. An expandable bellows allowed the system to operate at elevated temperature without system failure due to thermal expansion of the fluid inside. Pressure taps and thermocouples were installed to measure pressures and temperatures at various points in the loop.

## 3.2 System design

Three flow loops were used in the experimental set up. The hot loop, which was pre-existing and modified for this study, and the cold loop which was designed and constructed as part of the study. The last flow loop, referred to as the cooling loop, was also constructed and functioned largely as an extension of the cold loop.

Each of the flow loops in the system are isolated from one another in terms of flow and pressure, but are interconnected with regard to temperature and heat transfer. The hot and cold loops operate as closed loops, while the cooling loop is an open system as it is connected to the building water supply and eventually sends this flow down the drain. Isolating the primary experimental loops from the cooling source allows for a high degree of stability under steady state conditions. The other experimental systems in the literature have the fluid cooling flow as part of the

respective cold loops, and as such perturbations in the temperature and flow rate of the cooling water will be directly applied to the test section. Making the cooling loop a separate entity allows these fluxuations at steady to be dampened by the mass of the fluids in the hot and cold loops. At steady state the heat generation from the immersion heaters will be passed through the test section heat exchanger from the hot loop to the cold loop, and will be again passed from the cold loop to the cooling loop by means of the cooling heat exchanger as evident in Figure 3.2.

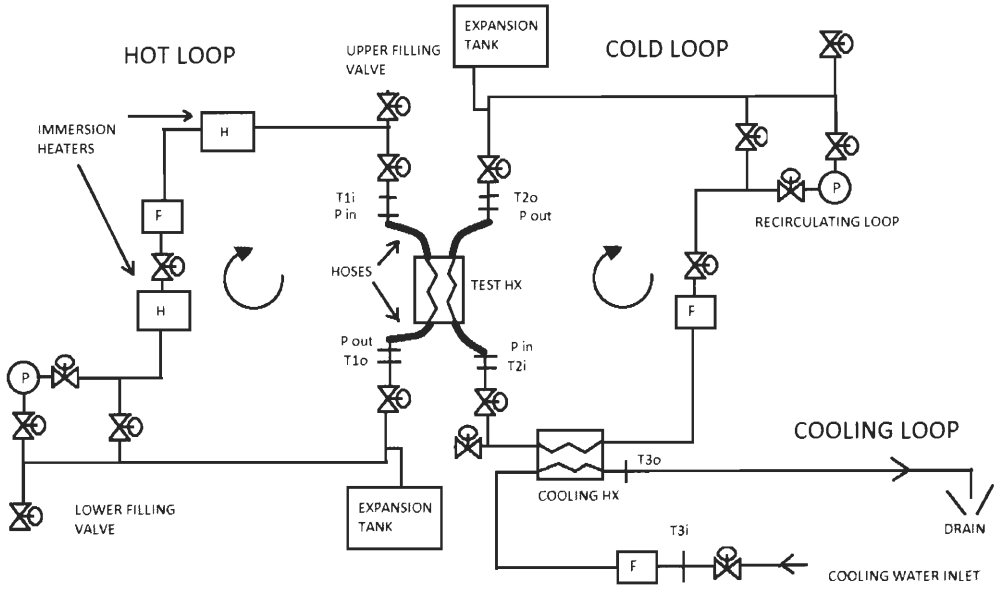


Figure 3.1 Logical Diagram of Experimental System

The flow loops are vertically oriented and mounted on a movable test frame having a central support structure with the hot and cold loops on opposite sides. A picture of the system can be seen below in Figure 3.3.

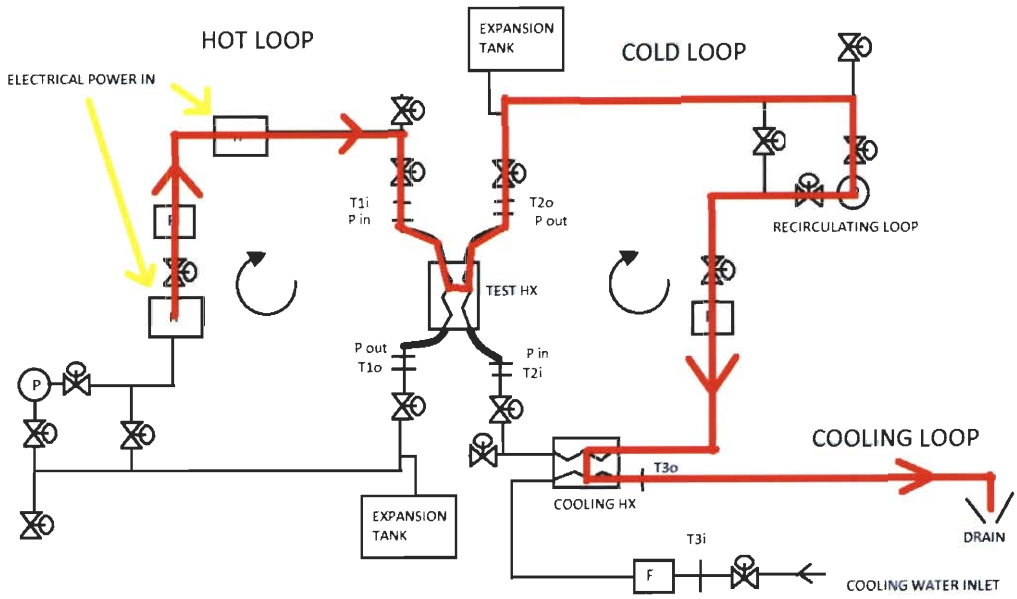


Figure 3.2 Path of Energy Flow at Steady State Conditions

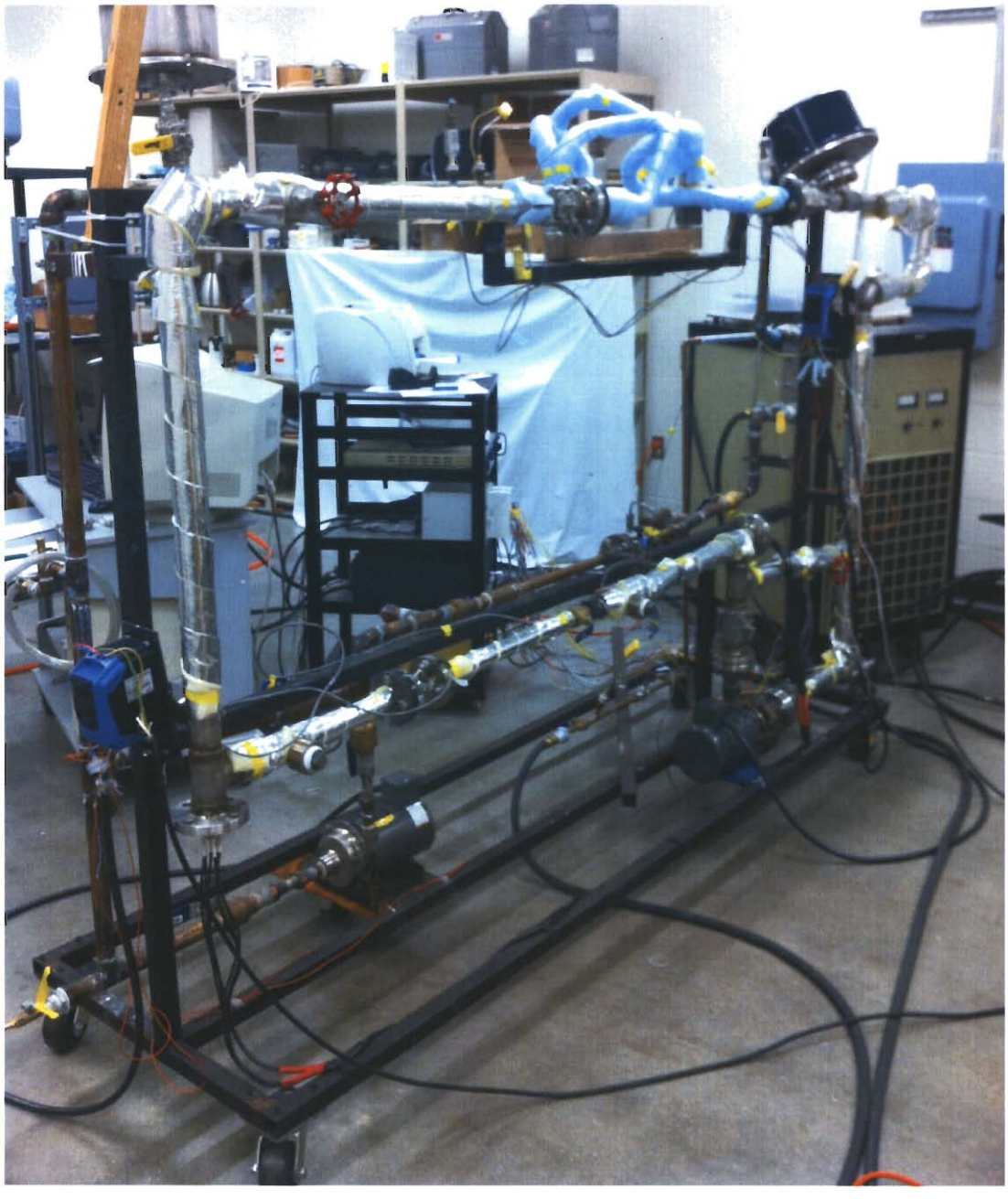

Figure 3.3 Picture of Experimental System

### 3.2.1 Flow loops

The hot loop was largely constructed of schedule 10 1 ½ inch 316 stainless steel piping, with the exception of the entry and exit regions of the flow meter section, which had 1 inch piping to match the diameter of the flow meter. A reducing tee was installed at the start and end of the flow meter section, so that additional branches to handle flow meters requiring different sizes of pipe could be installed at a later date without significant modification to the system. This design feature was replicated in the cold loop.

The cold loop was constructed with 1 ¼ inch copper pipe, with the exception of the flow meter section. The position of valves, instrumentation, and pumps were placed in relatively similar locations to their counterparts in the hot loop although the loop as a whole was "mirrored" on the opposite side of the test stand frame since the primary flow configuration of the system was chosen to be for counter flow. A flat plate FP5x12-50 PHE was installed in the cold loop, allowing heat to be extracted from the system by the flow of cooling water passing through the alternate channels. Expansion tanks with expandable bellows of sufficient size were installed on both loops, to ensure no damage would occur from thermal expansion of the water in the closed systems. The total volume of the hot loop was approximately 4.5 gallons, and the cold loop was approximately 3 gallons.

The hot loop had a centrifugal pump, a Goulds 3642, with a fixed speed ½ hp motor. The motor was replaced with a ½ hp Baldor 3-phase motor, so that motor speed could be controlled electronically through the use of a motor drive. For the cold loop, a centrifugal pump was also chosen, a Dayton 4JMY2, which provided similar performance to the other pump. A motor of the same type was attached to it. Each motor had a ½ hp drive powering it, an Invertek ODE-2-11005-1H012. These drives converted common 120V 60hz electricity from the building mains into the 3-phase power used by the motors, and controlled their speed by means of changing the output frequency.

### 3.2.2 Bulk heaters and power supply

Heat was generated within the hot loop through means of two immersion heaters. They were purchased from Vulcan Electric, and have the part number SF-1524B. Their locations can be seen in the figure below. Each of the heaters operate using DC current, having a maximum rated voltage of 240V, and capable of generating 15kW of heat, providing a maximum heat generation within the system of 30kW. A programmable power supply, model EMHP 300-200 was used to supply power to the heaters, converting 480V three phase power taken from the building mains and converting it to DC current. It has a maximum output of 300V and 200A.

### 3.2.3 Instrumentation

In order to acquire the data necessary to determine the heat transfer and friction factor coefficients, four types of primary measurements were necessary. These were temperature, pressure, flow rate, and electrical. The descriptions of the instruments and data acquisition system will be discussed in this chapter, while the calibration procedures and results will be presented in chapter 4.

The three existing thermocouples installed were kept in place, and an additional four stainless steel sheathed grounded Omega K-type thermocouples with diameters of 1/16 of an inch were installed, meeting or exceeding special limits of error, in order to match those already in place (part# KQSS-116U-12). The appropriate grade of Omega brand thermocouple extension wire was used to make the connections to the data acquisition system.

Static pressure measurements were taken at the inlet and outlets for both the hot and cold sides of the heat exchanger test section. These were taken using four Omega brand PX32B1-100AV pressure transducers, which were selected for their ability to operate at elevated temperatures and durable construction. They measure absolute pressure from 0 to 100 psi. These pressure transducers are a type with a mV/V output, and a Measurements Group 3800 wide range strain indicator was used to provide a 10 V excitation to the transducers, with the excitation voltage being measured separately so that the recorded pressure values could be normalized. For

each loop respectively, the heights of the wetted pressure transducer diaphragms from the pipe centerline were within a ¼ inch, so changes in pressure differences due to height were neglected.

The flow rate measurements were made with using turbine style flow meters. The rotating turbine within the meter produces an oscillating voltage which is monitored with a magnetic pick up. This oscillating voltage is analyzed in term of frequency, which can then be converted to a corresponding flow rate. In both the hot and cold loops, Omega model FTB-1424 flow meters were used, having a calibrated flow range of 3 to 30 gallons per minute (gpm). The accuracy of the flow meters is discussed in the following chapter, and copies of the calibration reports appear in the appendix. Straight pipes of a length of 18 pipe diameters upstream and 10 pipe diameters downstream, exceeding the minimum entry and exit lengths specified by the manufacturer. For the cooling loop, an Omega FTB-1412 flow meter was used having a calibrated flow range of 0.75 to 7.5 gpm, also with upstream and downstream straight pipes exceeding the minimum specified length.

The SCXI-1102 module was used to measure all of the signal data with the exception of the flow rates, and the voltage of the power supply. Appropriate gains were selected for the expected input levels automatically within the NI software DAQmx.

### 3.2.4 Data acquisition and control

The data acquisition system for this experiment consisted of a Dell PC running Windows XP, and fitted with National Instruments (NI) hardware and Labview software. Two data acquisition cards (DAQs) were installed in the computer, a NI PCI-6221 and a NI PCI-6040E. The NI PCI-6221 has 16 bit analog to digital conversion, having a least count of 1 out of 65536, and the NI PCI-6040E has 12 bit analog to digital conversion, having a least count of 1 out of 4096. A SCXI-1000 chassis housed the three SCXI modules used in the study, and was connected to the NI PCI-6221 DAQ. The three flow meters installed in the system were directly inputted to the other DAQ through the use of a CB-68LPR breakout board.

A SCXI-1102 module was used in conjunction with a SCXI-1303 isothermal terminal block. The terminal block provided a built in thermistor measuring the cold junction temperature with a certainty of ±0.5 degrees Celsius. It has internal programmable amplifiers, with gains ranging from 1 to 100 which are able to be applied independently to the different measurement channels. Each gain was chosen based on the expected range of signal input for each channel.

In order to directly measure the voltage across the bulk heater power supply, a SCXI-1122 module was used, along with a high voltage SCXI-1322 terminal block. This allowed for the dangerous DC voltage to be safely measured, as well as ensuring that the maximum rated voltage of the immersion heaters was not exceeded.

A SCXI-1124 module with a SCXI-1325 terminal block was used to send control signals to the two motor drives and as well as the programmable power supply. The use of a dedicated high accuracy voltage output module allowed the motor drives and power supply to be independently controlled with a high degree of precision. During testing it was found that the reported rpm of the motors could be controlled to ±2 rpm.

All control signals were generated from within the Labview program that was written for use in this study. The program was capable of controlling three commanded values independently, these being the power output of the bulk heater and the percent speed signal sent to the motor drives.

The same program was also responsible for recording the data being generated by the experimental system. In total, there were 19 independent measurements being taken, seven temperatures, three flow rates, four pressure transducer excitations, the pressure transducer excitation voltage, the bulk heater voltage, and three shunt voltages. The SCXI-1102 module read 1000 samples for each of the measured channels each second at a rate of 1000 samples per second, then reported this value. The SCXI-1122 high voltage module read the voltage of main power supply twice a second, took the average of these two samples, and reported the value every second.

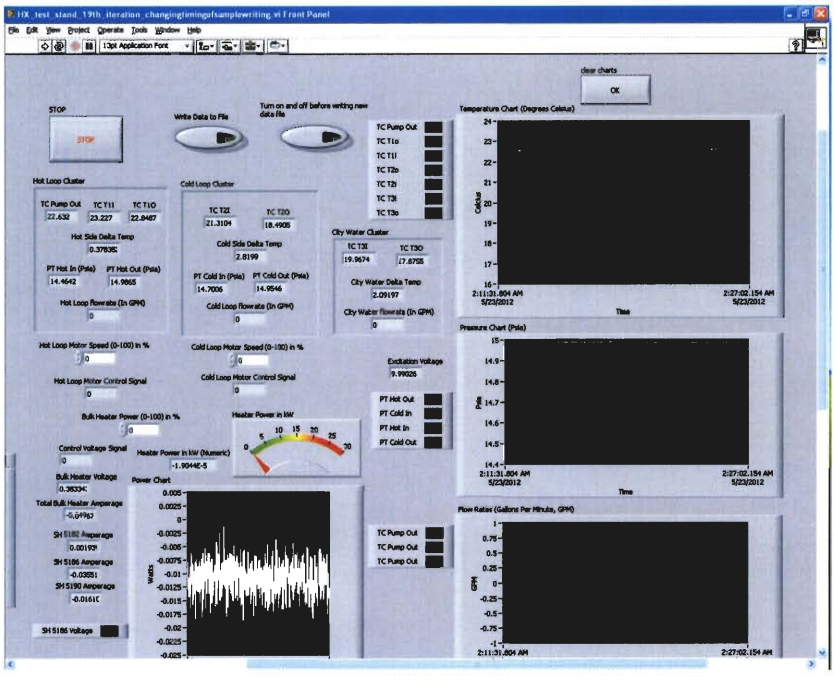


Figure 3.4 Picture of Labview Program Interface

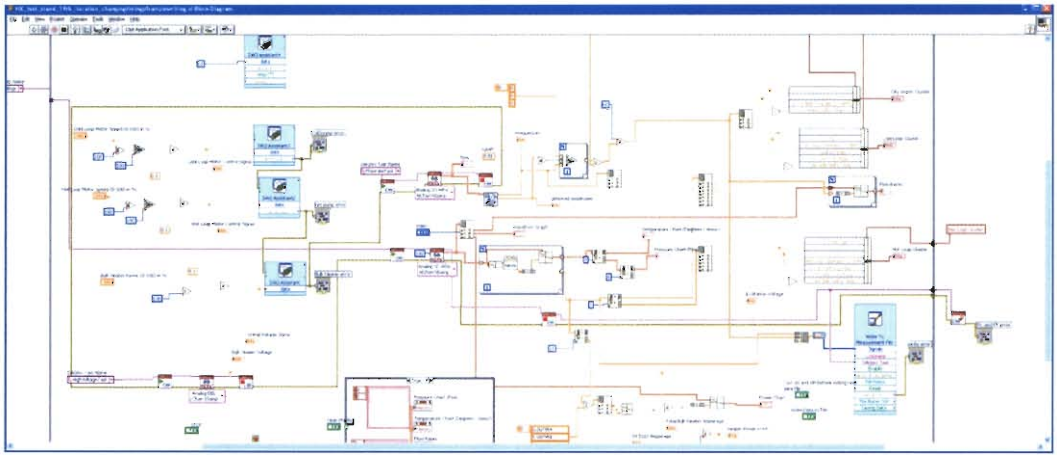

Figure 3.5 Picture of Labview Block Diagram

All three flow meters were connected to the NI PCI-6040E, and each channel was sampled at 20kHz. 20,000 samples were taken for each and the average frequency was reported by the program. Measuring and recording the flow rates with

a separate DAQ card allowed for less possibility of signal interference from the other instruments to affect the reported flow rates and vice versa, while allowing a higher than otherwise obtainable sampling rate for all of the measurements within the system.

### 3.2.5 Test section

The primary goal of the study was to measure the temperature difference and pressure drop across the heat exchanger under various testing conditions. The temperature difference across the test section was measured using two thermocouples and taking the difference between them, likewise with the pressure transducers. The thermocouples were located midstream, with their tips along the centerline of the piping. Pressure taps were installed with the pressure transducers oriented vertically which took measurements of the static pressure.

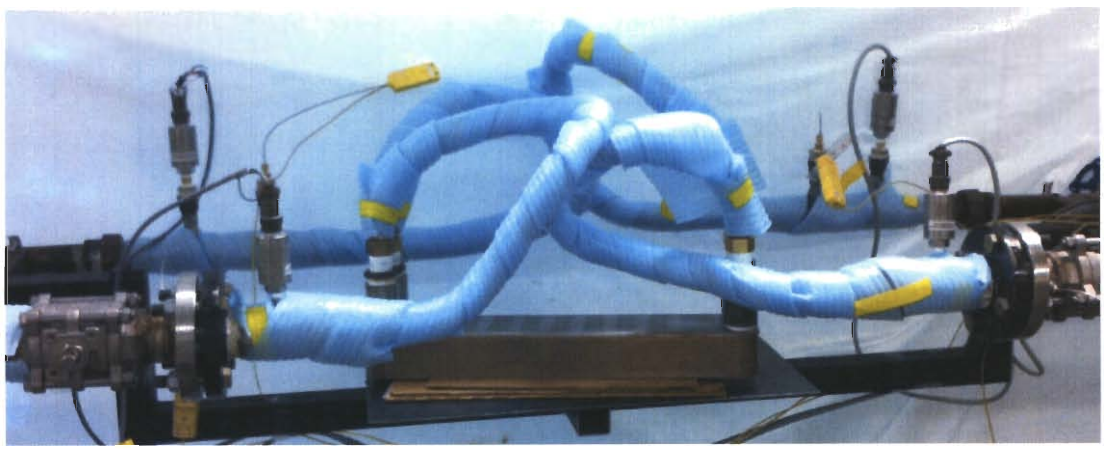

Figure 3.6 Picture of Test Section

After the instrumentation portion of the test section, 1 ¼ to ¾ inch reducer and expansion fittings were installed, on the fixed portion of the piping for the inlet and outlet respectively. This allowed for stainless steel braided coolant hoses to be installed, having internal diameters of ¾ an inch with a smooth interior, and a length of 30 inches. The flexible hoses allowed for easy installation of heat exchangers of varying sizes and port configurations.

## 3.3 Analytical method

MathCAD was used to perform the data analysis in this study. The analytical methods used in this study are largely based on those employed by Alothman (2011) in his thesis. The models generated by him were modified to allow comparison between the experimental values generated and those predicted by Martin's correlation (1996). Detailed MathCAD programs are omitted from this section but do appear in the appendix.

When comparing the results of experiments to the prediction made by Martin's correlation, a principle factor affecting the predictions is the surface area of the plate. The method employed by Muley and Manglik (1999) of directly measuring the plates was not possible for all of the heat exchangers as they were brazed together. While the major geometric parameters were provided by the manufacturer, there are some assumptions made with regards to the plate area due to the nature of the entry region near the heat exchanger ports. This is discussed further in chapter 4.

# CHAPTER 4

# EXPERIMENTAL PROCEDURE AND UNCERTAINTY

## 4.1 Heat exchanger specifications

This study comprised performance testing of four compact brazed plate heat exchangers. All of them were provided by the manufacturer, GEA PHE Systems. All of these are compact brazed plate heat exchangers. The four heat exchangers used were: Fp3x8-10, Fg3x8-14, GB220H-20, and a GB240H-20. They can be seen in that order from right to left in Figure 4.1.

Figure 4.1 Picture of Heat Exchangers Tested

All of the heat exchangers have plates comprised of AISI 316 stainless steel, and feature four ports, one inlet and outlet port for each side. Additionally, all of the PHEs feature an even number of plates. This has the effect of creating an uneven number of flow channels, and can be seen in figure 4.2. The same heat exchanger was then sectioned, to allow pictures and measurements of the internal features, this can be seen in figure 4.3.

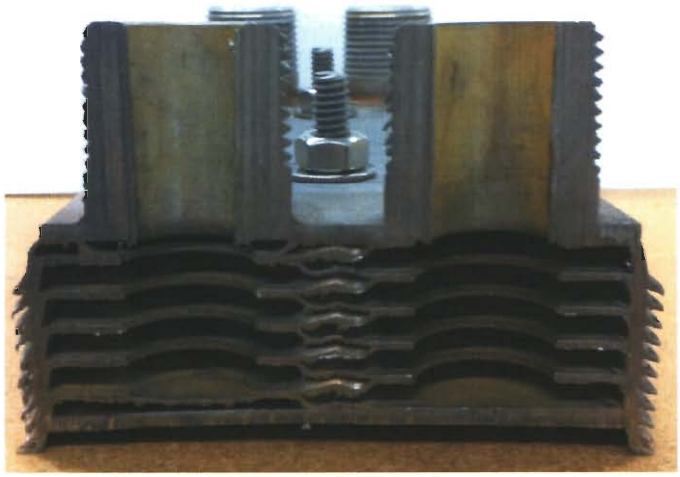

Figure 4.2 View of Fp3x8-10 Flow Passages

Figure 4.3 View of Sectioned Fp3x8-10

The plates in the PHEs were all of the chevron type, having a chevron angle of 60 degrees, provided by the manufacturer GEA PHE Systems. Measurements were made to verify the values provided by the manufacturer, and the two were found to be in good agreement. As only one heat exchanger was sectioned, assumptions were made for the other heat exchangers in the study based on the measurements taken from the Fp3x8-10. GEA uses the method shown in Figure 4.4 for defining the geometry of the plates in their heat exchangers.

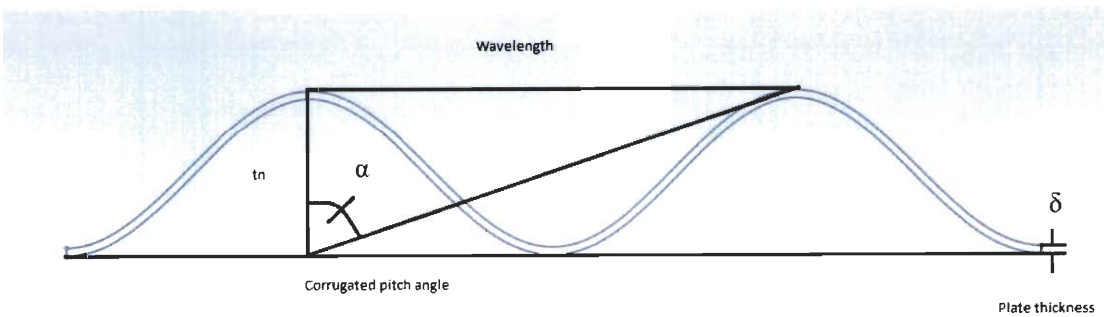


Figure 4.4 GEA Plate Dimensions

Rather than specify the wavelength of the corrugation directly, GEA defines the plates in terms of a corrugated pitch angle, α, the total height of the plate, tn, and the plate thickness δ. Additionally, all of the heat exchangers tested had plates with an α of 40 degrees, and a δ of .6mm, as stated by the manufacturer. Alothman (2011), defined the wavelength, λ, and amplitude of the sinusoidal wave, a, in terms of these factors.

$$\lambda = tn * \tan(\alpha) \tag{4.1}$$

$$a = \frac{tn-\delta}{2} \tag{4.2}$$

As part of his work in creating models for the heat exchangers, Alothman compiled a list of the geometric properties of the heat exchangers experimentally

tested in this study. This is recreated below in Table 4.1, with certain values changed to reflect the measurements made.

Table 4.1 Heat Exchanger Parameters

| Model | $W_p$ (in) | $L_p$ (in) | $L_{p2p}$ (in) | Nt | tn (in) | $H_p$ (in) | λ (in) | a (in) | Φ | $D_p$ (in) |
|---|---|---|---|---|---|---|---|---|---|---|
| Fp3x8-10 | 3 | 5 | 6 | 10 | 0.093 | 0.93 | 0.078 | 0.035 | 2.1072 | .75 |
| Fg3x8-14 | 3 | 6.2 | 7.2 | 14 | 0.087 | 1.12 | 0.073 | 0.032 | 2.0705 | .75 |
| GB220H-20 | 3 | 10 | 11 | 20 | 0.087 | 1.74 | 0.073 | 0.032 | 2.0705 | .75 |
| GB240H-20 | 3 | 15.3 | 16.3 | 20 | 0.087 | 1.78 | 0.073 | 0.032 | 2.0705 | 1 |

$W_p$ represents the width of the plate, $L_{p2p}$ is the port to port length, Nt is the number of plates, $H_p$ is the overall depth, λ is the wavelength, and $D_p$ is the port diameter. These dimensions can be seen in Figures 2.1, 2.2, and 4.4. Based on the sectioned Fp3x8-10 PHE, a distance of 0.5 inches was measured between the center of the port and the start of $L_p$. Therefore for the modeling, one inch was subtracted from $L_{p2p}$ to determine$L_p$. This was a direct measurement for the Fp3x8-10, and an assumption applied to the other heat exchangers in this study. For the GB240H-20, a distance of 0.75 inches from the center of the port to start of Lp was used to compensate for the larger port size.

## 4.2 Procedure

With the goal of producing Colburn factor and friction factor curves, the experimental procedure was established with this in mind. First and foremost, all of the data generated were collected at steady state system operation. In the manner of setting the flow rates in the hot and cold loops equal to one another, one level of heat generation was applied to a range of flow rate sets. This allowed for the j factor to be compared against a range of Re. For each heat exchanger two levels of heat

generation were applied. The first was determined by setting both loops to their lowest flow rate at which the flow meters had valid calibration, 3gpm, and increasing the heat generation until the highest steady state temperature of the system was close to but below the boiling point of water, or the capacity of the immersion heaters, 30kW, was reached. After reaching steady state and recording the run, the heat generation was held constant and the next set of flow rates would be applied. This was repeated until the entire range of flow rate sets had been tested. Heat generation of approximately half the maximum value for the same heat exchanger was commanded and held constant, and the same sets of flow rates were tested for the second data set. Highly conservative estimates were made in terms of the amount of time given for the loops to reach steady state conditions after changes to flow rate, on the order of 15 minutes, although the actual time to reach steady state decreased with increasing flow rates.

After letting the system reach steady state conditions for a given testing point, data recording started. For all of the data presented in this study, 300 sequential data points representing 5 minutes of system behavior were taken and then averaged to ensure a high level of confidence in the steady state nature of the data. The working fluid for all of the experiments was De-Ionized water taken from the building DI water supply from the College of Engineering and Applied Sciences at Western Michigan University.

### 4.2.1 Heat exchanger installation

All of the heat exchangers were installed in the test section of the system by means of the flexible coolants hoses previously mentioned. The ends of the hoses featured a ¾ inch brass fittings with NPSM female threads, allowing direct coupling to the ports of the heat exchangers, except for the GB240H-20 which had port diameters of 1 inch. In order to install this heat exchanger, 1 inch couplings with reducer bushings were used to form the appropriate connections. Installation was only done after purging both loops of the working fluid. All of the heat exchangers were installed with the hot side connected to the side of the heat exchanger with

higher number of flow channels, as was found to be the common practice in the manufacturers literature.

### 4.2.2 Flow loop preparation

Prior to installation of the heat exchangers, both loops were drained of water, the loops were purged with compressed air to ensure that they were sufficiently evacuated. With the heat exchanger installed, both the hot and cold sides are closed loops and not exposed to the atmosphere. A vacuum pump was attached to the top fill valve, and ran until the system was deemed to be of sufficiently low pressure. It was necessary to evacuate the loops of air before filling, as it was found during early testing that pockets of air trapped within the system would generate flow instability, leading to random fluxuations in flow rates and invalidating the steady state nature of the experiments to be conducted. While it was impossible to achieve a perfect vacuum within the loops, it was determined through trial and error than an absolute pressure below 0.5 psi before filling was sufficient to provide stable flow rates.

### 4.2.3 Experimental parameters

There are three independent variables controllable by the experimental system. These are the level of heat generation (or heat transfer at steady state operation), and the flow rate of each of the loops. Each of these was adjusted in the manner described previously such that the necessary data could be collected. The raw averaged data sets generated are presented in table form and graphs in chapter 5.

## 4.3 Uncertainty discussion in the literature

There is much discussion in the literature regarding experimental uncertainty, and it is considered good practice to include the uncertainty for the values presented, however not all authors will include these values. All instruments report a measured value, which may or may not differ from the actual value being measured, with the error being the difference between the two. Many authors describe different methods and techniques for calculating uncertainty. Moffat (1988) describes a widely used method for determining uncertainty, by taking the square root of the sum of a series

of partial derivatives taken with respect to the variables in question. However, he goes on to state that for more complex experiments, of which the type in this study is unquestionably, using a data interpretation program and creating perturbations to the input values and comparing the nominal values to the program output is also an acceptable method.

As part of the literature review, it was discovered that there is a wide range of what uncertainties, if any at all, are reported regarding experimental results. Some authors include uncertainties about the areas of the plates, other do not. For this study, uncertainties regarding the plate geometries will not be considered and values given by the manufacturer shall be treated as true. Also, other than the discussion regarding the method of calculating fluid properties based on temperature, it shall be assumed there is no uncertainty attributed due to property variations.

The majority of the experimental results found in the literature are for steady state conditions, although different authors have different definitions of what constitutes steady state. While there is a great deal of discussion about the steadiness of heat transfer, there is little said about the steadiness of flow rates, particularly for that of the cooling water. For temperature related uncertainty, there are several methods which are common. One definition is based on the principle of energy balance using the measured heat transfer, q. Muley and Manglik (1999), described a method for determining steady state by comparing the hot and cold side q values with the average measured q, as shown in equation 4.4.

$$q_{avg} = \frac{q_{hot}+q_{cold}}{2} \tag{4.3}$$

$$\%\ error\ q = \frac{q_{hot,cold}-q_{avg}}{q_{avg}} * 100 \tag{4.4}$$

In their work, they state that the majority of their heat transfer data had an energy balance of ±5%. In 2010 Khan et al. reported that they calculated the average heat transfer in the same manner as Muley and Manglik, and had measured energy

balances of under ±3% for the majority of their data, with the a maximum difference of 7%. Warnakulasuriya and Worek stated that both experimental and calculated overall heat transfer coefficient, UA, had uncertainties of 2.0 and 2.25% respectively. An alternative method is to define steady state conditions based on the fluxuation of temperatures for the inlets of the heat exchanger ports. In the study done by Jokar et al. (2004), the experimental system was considered steady when the temperatures at the inlets varied by ±1 degrees Celsius for single phase flows. Galeazzo et al. (2004) stated that experimental runs were only accepted if the difference in q between the hot and cold sides were less than 15% and the standard deviation of the stream temperatures were under 1 degree Celsius.

## 4.4 Uncertainty and calibration

Great care was taken to ensure the steady state nature of the experimental runs in this study. The design of the experimental system, particularly the isolation of the two primary flow loops created extremely steady conditions when compared to those in the literature. For temperature related stability, experimental runs were discarded if the fluxuation of temperature at any inlet was greater than ±0.25 degrees Celsius, with a majority of data being in a range of ±0.12 degrees Celsius. Experimental runs were also discarded if there were significant fluxuations in either the temperature or flow rate of the cooling water taken from the building water supply, as these changes would also be evident in changing inlet temperatures.

As the analytical method of setting the hot and cold side convection coefficients was used in this study, great care was taken in ensuring that the flow rates of the hot and cold loops were as close as possible. The maximum difference between the measured hot and cold loop flow rates for all the data in this study was under 1.0%, and the majority were under 0.5%.

The steadiness of the cooling water flow was also an important factor in determining the steady state nature of the conditions within the two measurement loops. It was found during testing that it took approximately one hour for the incoming cooling water taken from the building supply to reach steady state

temperatures, which is comparable to the experimental procedure of Han et al. (2010) who allowed an hour of system operation so that that gas would be discharged from the flow of cooling water although no discussion was made regarding change in temperature.

A sample of various statistical characteristics of the data is given in Table 4.2. It represents a single data point from one data set for one heat exchanger, but is representative of the general nature of deviations and variations found across all the data presented in this study.

Table 4.2 Statistical Characteristics of Experimental Data

| | T1i (C) | T1o (C) | T2i (C) | T2o (C) | HL flow rate (gpm) | CL flow rate (gpm) | HL ΔP (psi) | CL ΔP (psi) |
|---|---|---|---|---|---|---|---|---|
| Average | 77.50 | 57.87 | 40.78 | 59.70 | 4.997 | 4.992 | 2.0021 | 3.2503 |
| Std. Dev. | 0.0457 | 0.0315 | 0.0536 | 0.0390 | 0.0117 | 0.0216 | 0.0071 | 0.0225 |
| Min | 77.40 | 57.78 | 40.65 | 59.56 | 4.950 | 4.925 | 1.9835 | 3.1674 |
| Max | 77.65 | 57.94 | 40.91 | 59.79 | 5.022 | 5.045 | 2.0265 | 3.3451 |

The graph of temperatures, pressure drops, and flow rates for the data in Table 4.2 are shown below in the following figures. They data presented in them are raw data taken from the file generated by the Labview program, and do not contain offsets. The values were calculated from the data point of the 28kW, nominal 5gpm test conditions for the Fg3x8-14 heat exchanger.

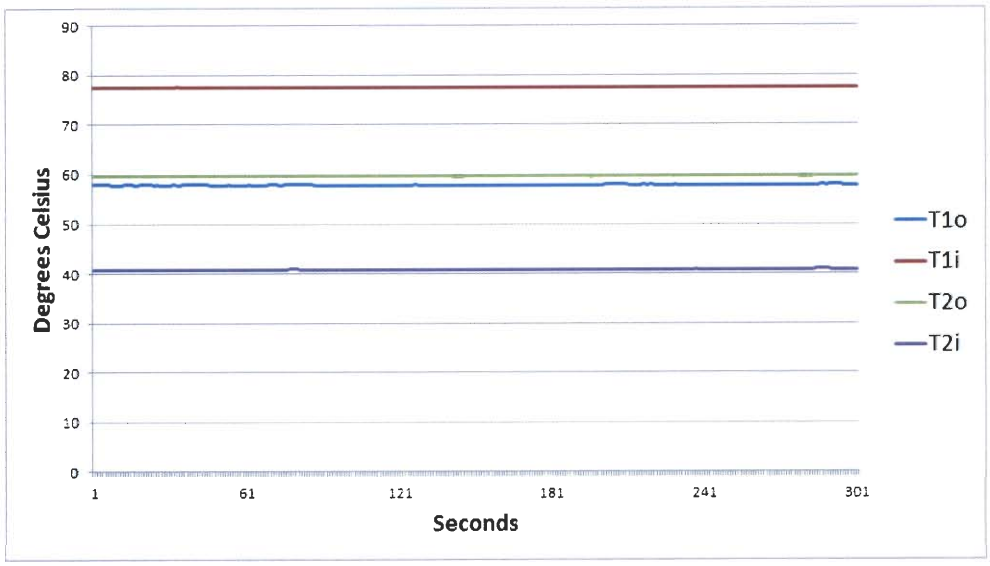


Figure 4.5 Graph of Steady State Temperatures

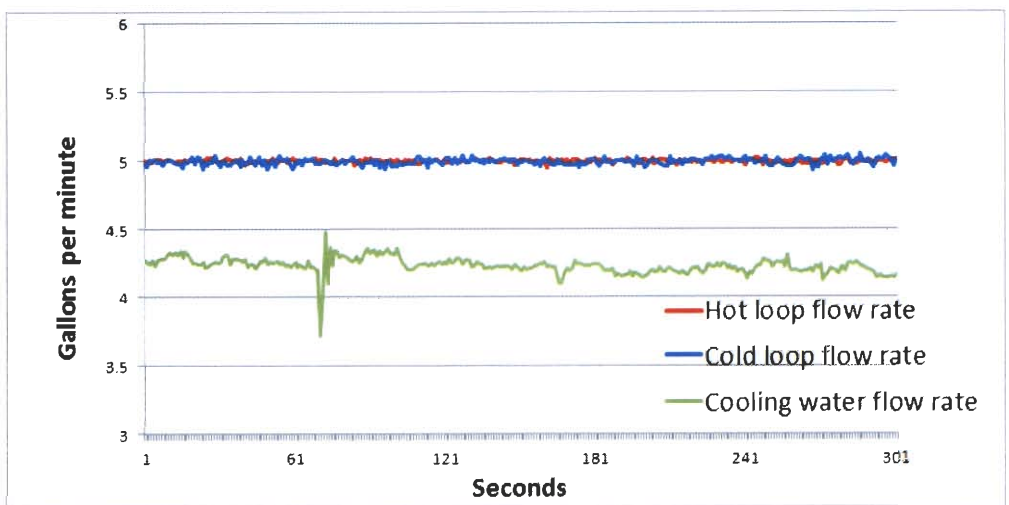


Figure 4.6 Graph of Steady State Flow Rates

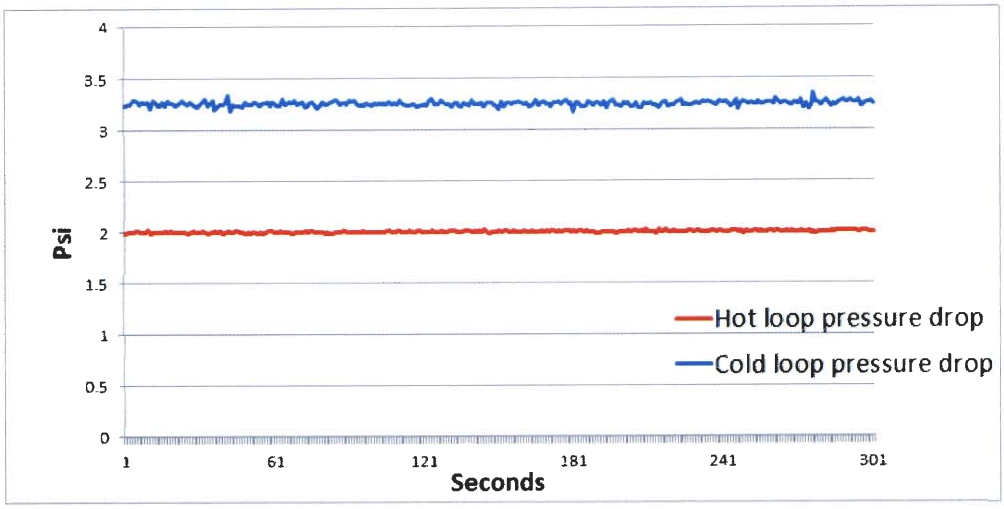


Figure 4.7 Graph of Uncorrected Steady State Pressure Drop

### 4.4.1 Primary measurements

Flow Rate

As noted earlier, the flow rates were measured using OMEGA FTB-1424 flow meters. These were calibrated under NIST traceable conditions, and had reported uncertainties of ±0.51% and ±0.33% for the hot and cold loops respectively. The calibration is given as a K value, which is equivalent to the number of pulses or turbine rotations per unit flow. By measuring the frequency output of the flow meters and converting the values using the appropriate nominal K values flow rates can be calculated. For the range of flow rates tested, the maximum output expected was approximately 500Hz, while the DAQ card took samples at a rate of 20kHz. The uncertainty for the onboard timer of the DAQ card was .01%, and due to the extremely high sampling rate other factors were neglected giving total uncertainties of ±0.52% and ±0.34% for the hot and cold loops respectively.

Additional steps were taken to validate the flow meters. Each flow meter was tested independently by passing a stream of water from the building water supply through the flow meter in question, and then verifying the flow rates using a 5 gallon bucket and a stop watch, with the determination that both flow meters were accurate. Another test consisted of rearranging the test section to create a single closed loop.

The hot side inlet hose was connected to the cold side outlet hose with a 4 inch steel nipple, and the same was done for the remaining connections. The a pump was then run at a constant speed, and the reported flow rates of the hot and cold loop flow meters were compared. It was found that there was a discrepancy between the two measured flow rates, but the difference was within the combined calibrated uncertainties so the flow meters were deemed to report trustworthy values.

Pressure Drop

The pressure drop is the difference in pressure between the inlet and outlet of the heat exchanger. All of the pressure transducers used were OMEGA brand PX32B1-100AVs. The factory calibrations were applied for each of the respective transducers, with the values being reported in absolute psi. It was determined experimentally that the pair of pressure transducers in the cold loop exhibited a wider range of variation in offset at steady state non-flow conditions than the pair mounted in the hot loop test section. As such, a calibration was only created for the hot side pressure drop, and although a rough estimation is made for the cold loop pressure drop the graphs and tables presented in chapter 5 will only contain values pertaining to the hot loop. The pressure offset was developed by recording the steady state pressure difference under still conditions, as well as the measured pressure difference when the valve to the flow meter section was closed with the pump running in the recirculating loop. During the course of these trials, the maximum deviation in the hot loop pressure offset varied from -0.5046 psi to -0.6033 psi. This lead to an uncertainty due to offset fluxuation of ±0.049 psi. The estimated offset for the cold loop pressure difference was 0.112 psi. During recording the overnight single point calibration on the 26$^{th}$ of February, the hot side pressure difference had a deviation of 0.000767 psi, far below the reported accuracy of ±0.25% for each pressure transducer, and as such was neglected. For the gain setting used by the SCXI-1102 module, each transducer reading has an uncertainty of 0.035%. These uncertainties combine to give a pressure difference uncertainty of ±.049 psi ±0.57%, and an offset of 0.54 psi to be added to the measured hot side pressure drop. The excitation voltage

was separately measured, and was used to normalize the transducer output to their respective factory calibrations, but the uncertainty associated with this process was neglected as the uncertainty applied to the difference between the applied voltage and factory calibrated voltage was trivial.

Table 4.3 Hot Side Pressure Drop Offset and Uncertainty

| Pressure offset | Uncertainty in pressure drop |
|---|---|
| 0.540 psi | $P_1 * (\pm 0.285\%) - P_2 * (\pm 0.285\%) \pm 0.049\ psi$ |

Temperature

Due to the fact that some of the thermocouples used in this study were permanently affixed to the previous test apparatus, it was not practical to employ a calibration of the thermocouples using a controlled temperature bath. A method of taking multiple steady state single point measurements was used to create a set of calibrated offsets for the thermocouples in the test section. At each instant in time, all of the measured temperatures in the system fell well within the range of uncertainty specified for K-type thermocouples, ± 1.1 C. The average of all the temperatures within the system was then taken, and was chosen to represent the baseline from which offsets would be determined. At each point in time, a comparison was made between the individual temperatures in the test section and baseline temperature by subtracting the baseline from the thermocouple reading, respectively for each of the thermocouples in question. An example of one of the measurements can be seen in Figure 4.8.

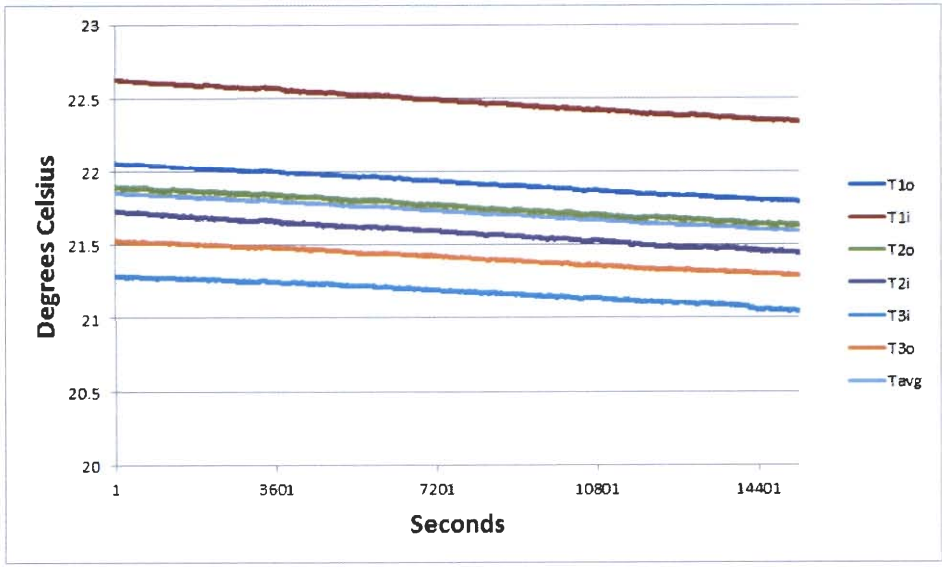


Figure 4.8 February 26th Overnight Temperature Measurements

These offsets were then averaged over the steady state measurement. Calculating the offsets for each time interval allowed the small changes in temperature to be neglected. Table 4.4 shows the averaged offsets for three sets of steady state measurements, representing the extremes and median of the median offsets. Other measurements of the same nature were made, but fell within the range described in the associated table.

Table 4.4 Range of Measured Temperature Offsets

| | T1o | T1i | T2o | T2i |
|---|---|---|---|---|
| February 16th | 0.2052 C | 0.8130 C | -0.0235 C | -0.1366 C |
| February 20th | 0.2107 C | 0.6389 C | 0.2165 C | 0.1773 C |
| February 26th | 0.2003 C | 0.7555 C | 0.0407 C | -0.1408 C |

The standard deviations of the offsets were very small, for the T1o February 16th data the standard deviation was 0.0046 C, well below the range of observed deviation within the offsets and as such they are neglected. The sensitivity of the SCXI-1102 module at the amplifier gain selected was 0.05% for the thermocouple readings, much

smaller than the observed deviations of the offsets and as such was neglected. The individual temperature offsets are calculated by taking the average of the maximum and minimum of the observed offsets. These are presented in Table 4.5. The uncertainty was then defined as the maximum observed variation for each of the temperature offsets in question. The largest deviation was seen in the offset for T2i, ranging from -0.1366 C to 0.1773 C. This corresponds to an uncertainty of the corrected temperature of ±0.16 C. This uncertainty was then used for all of the temperatures, as it was the largest. As the offsets were created by subtracting the baseline temperature from the respective temperatures, the offsets are subtracted from the related temperatures.

Table 4.5 Temperature Offsets

| T1i offset | T1o offset | T2i offset | T2o offset |
|---|---|---|---|
| 0.73 C | 0.21 C | 0.02 C | .10 C |

Electrical Power

The primary purpose of this study was focused on the temperature, pressure, and flow measurements, and as such less focus was placed on calibrating the instrumentation involved with calculating the applied power. Three voltage shunts with known resistances were used in parallel to handle the high level of current being generated by the large power supply. Shunt voltages were then converted to amperages and were added together. The total current was multiplied by the measured voltage of said power supply. There was good general agreement between the measured power and with the average heat transfer in the test section heat exchanger, on the order of 3-7%. All the values were also positive, this is likely due to the fact that heat loss from system has been neglected, with the larger differences corresponding to the higher sets of temperatures in the system. Further details appear in Appendix G.

The resulting uncertainties of the primary measurements are shown in Table 4.6.

Table 4.6 Experimental Uncertainties

| | Hot loop uncertainties | Cold loop uncertainties |
|---|---|---|
| Flow rate matching | 1% | 1% |
| Flow meters | ±0.52% | ±0.34% |
| Temperature | +-0.16 C | +-0.16 C |
| Pressure drop | $P_1 * (\pm 0.285\%) - P_2 * (\pm 0.285\%)$ $\pm\ 0.049\ psi$ | |

### 4.4.2 Calculated values

Uncertainty calculations were undertaken for the various heat exchangers using the maximum heat transfer data sets. The method of inducing perturbations of the data as suggested by Moffat (1988) was used, with the determined uncertainties used as the values. As the performance of the system is highly interconnected, various values were adjusted with either positive or negative changes to the nominally measured values. The combination of various disturbances were tried until the appropriate combination resulted in the biggest percent difference relative to the nominal values. This method was not applied exhaustively to the various data sets, but various parameters were examined so that a reasonable assumption of experimental uncertainty could be made. The values were calculated using the maximum heat transfer for each heat exchanger, so uncertainties which depend on temperature differences, such as h and j, will be higher for the data set which had the lower power levels and temperature differences.

Mass flow

As the effects of temperature were neglect per the discussion to follow in chapter 4.5, the variation in mass flow was solely due to the contribution of the flow meters, 0.52% and 0.34% for the hot and cold loops respectively.

Reynolds number

Again as with mass flow, temperature effects were neglected, and the contributions to uncertainty in Re was to be considered purely from the flow rates.

Heat transfer

Based on the method used by Muley and Manglik (1999), measured heat transfer across the hot and cold sections were compared to the average of the hot and cold side heat transfers. For all of the heat exchangers tested, the maximum measured difference was 2.8%. The largest uncertainty of heat transfer, due to instrument accuracy, was 3.89% for the GB220H-20.

Convection coefficient

By using the defined uncertainties to create perturbations in the data, the maximum error in the convection coefficient across all of the heat exchangers in the study was found to be 13.38% for the GB240H-20.

Colburn factor

From the same method used in calculated uncertainty for the convection coefficient, the largest difference in the Colburn factor was found to be 12.93%.

Friction factor

Of all the calculated values, the friction factor had the highest level of uncertainty. For the GB220H-20, that which had most uncertainty for all of the heat exchangers in the study, the calculated uncertainty ranged from 32.29% at 3gpm to 3.96% at 11gpm. The relatively small pressure drop at the lowest flow rate was the reason for such a large value. Of the total maximum uncertainty, approximately 10% was due to the deviation in the pressure drop offset, while the uncertainty of the flow rates accounted for roughly and addition 5%.

## 4.5 Effect of temperature dependent properties on results

There is some uncertainty in the literature with regards to the presentation of experimental values, and the effect of temperature dependent properties on series of data. It is however accepted practice for fluids passing through a heat exchanger to compute the fluid properties at the average of the inlet and outlet temperatures as shown in Equation 4.4.

$$T_{avg} = \frac{T_i + T_o}{2} \tag{4.4}$$

It is unclear what is accepted practice when comparing a range of data when each point has a different temperature ($T_{avg}$) associated with it. For a given set of data of the type in this study, each data point can have the fluid properties calculated using the respective $T_{avg}$, or the fluid properties can be calculated by the average $T_{avg}$ of the entire data set. Regardless of which temperature was used to calculate properties, the method of calculating properties was done by linearly interpolating between the values found in table A-12 of Thermal Design (Lee, 2010). The data in Figure 4.9 uses that of the GB220H-20 PHE.

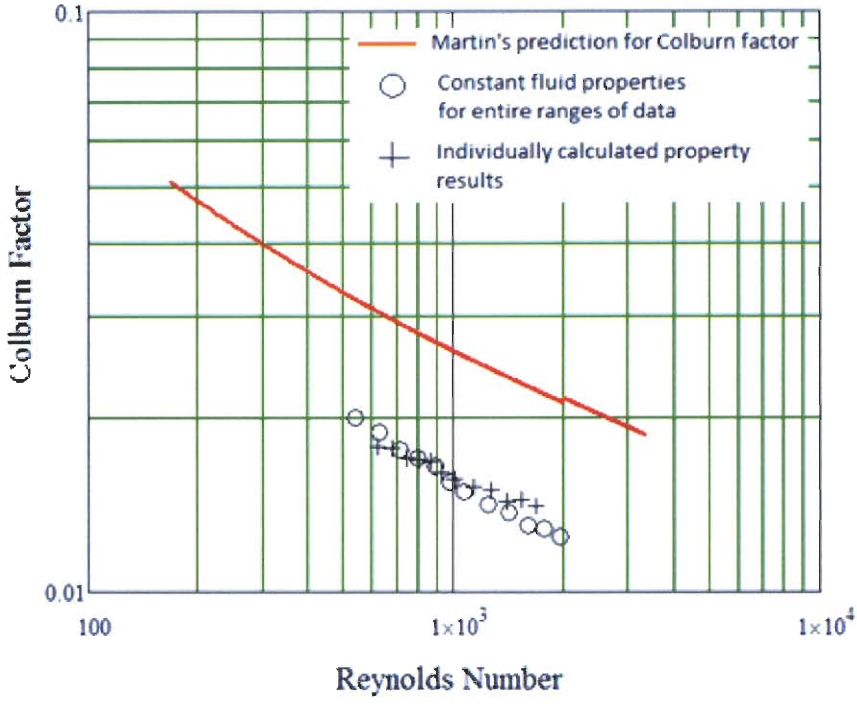


Figure 4.9 Graph of Colburn Factor and Effect of Property Variation

The data points with crosses are for individually calculated properties, while the points with circles use the averaged $T_{avg}$ of the entire data range. The largest effect of choosing one temperature for property values vs. calculating the property values independently for each data point can be seen in the Reynolds number, where the different methods for calculation can produce changes in Re as large as 15%. This corresponded to a difference in the Colburn factor of over 12%. Choosing to calculate fluid properties for each experimental run in the series independently also has the effect of diminishing the overall range of Re. For the graphs and tables presented, the use of individually calculated property values will be used, so the effects of property variation on uncertainty can be reasonably neglected.

## 4.6 Correction of pressure drop due to hoses

When an initial run of experimental data was inputted into the MathCAD model, it was found that the calculated friction factor had significantly higher pressure drop then that predicted by Martin's correlation. It was then surmised that this could be attributed to the additional pressure drop of the hoses which are used to connect the heat exchanger in the test section. The heat exchanger was removed, and a four inch steel nipple was used to connect the respective inlet and outlet hoses of both sides. The associated pressure drops for the hoses and fittings were then measured by measuring the isothermal pressure drops over the replicated flow rates used over the course of this study. After applying the appropriate offsets, the experimentally determined pressure drops from the hoses at the closest matching flow rate were then able to subtracted from the measured pressure drops of the experimental runs with heat exchangers installed. This can be seen in Figure 4.10, which is the friction factor vs. Re for the series of isothermal pressure drops for the Fg3x8-14 PHE. The crosses represent the uncorrected friction factor, and the circles represent the calculated friction factor with the hose corrections applied while the line represents Martin's prediction. The graphs and tables in chapter 5 represent values with the hose corrections applied, the uncorrected values are omitted.

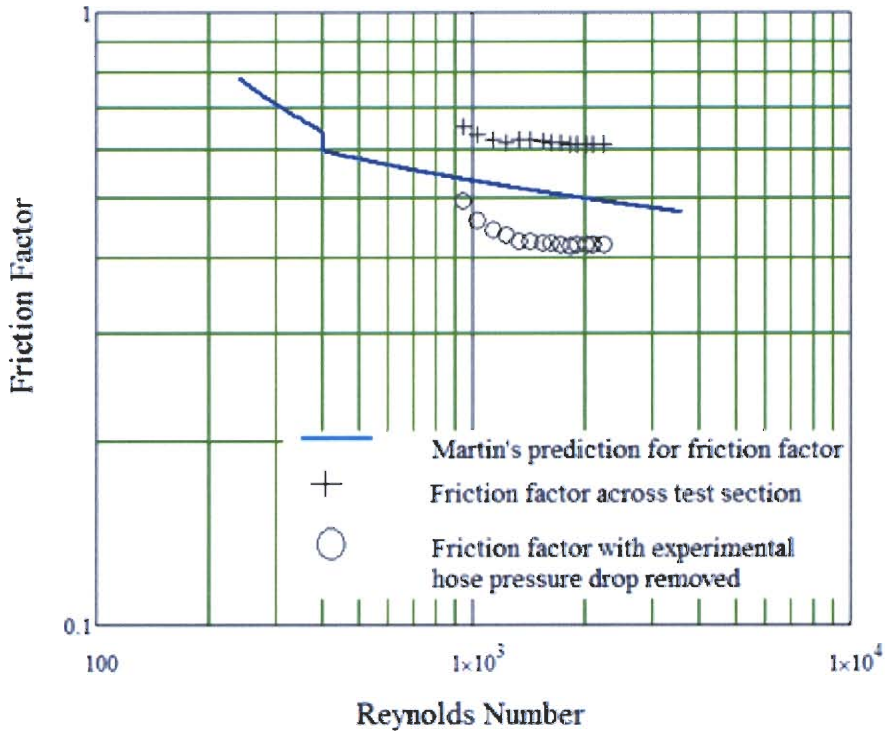


Figure 4.10 Effect of Hose Pressure Drop Correction

The table in Appendix F represents the hot and cold side hose pressure drops, with the pressure drop offsets applied. They were calculated by subtracting the averaged outlet pressure from the averaged inlet pressure. With the pressure drop offsets applied, they amount to a significant difference, having a pressure drop of over four psi at 12 gpm.

# CHAPTER 5

# EXPERIMENTAL RESULTS

The averaged compensated data will be presented in table format in the section relevant to that heat exchanger and test condition. While data was collected for both the hot and cold loops, and Colburn and friction factors calculated for both sides, only graphs for the hot side values will be shown, as the trends were similar for both. Only the primary results of the experimental data are presented in this chapter, more detailed lists of experimental values appear in appendix E. The friction factor listed in the tables are those that account for the measured pressure drops in the hoses. The axis for all the graphs are non-dimensional, the vertical representing the Colburn and friction factors, while the horizontal axis is the corresponding Reynolds number. The data points in the graphs are experimental data, while the lines represent Martin's prediction.

## 5.1 Fp3x8-10

This was the smallest of the heat exchangers tested. It also had the highest pressure drop of all the heat exchangers at a given flow rate, thereby limiting the maximum flow rate to the lowest value of all the heat exchangers tested. It did exhibit pressure drops much higher than those predicted by the literature, however the measured values did correspond to data for this model provided by the manufacturer.

### 5.1.1 Isothermal pressure drop

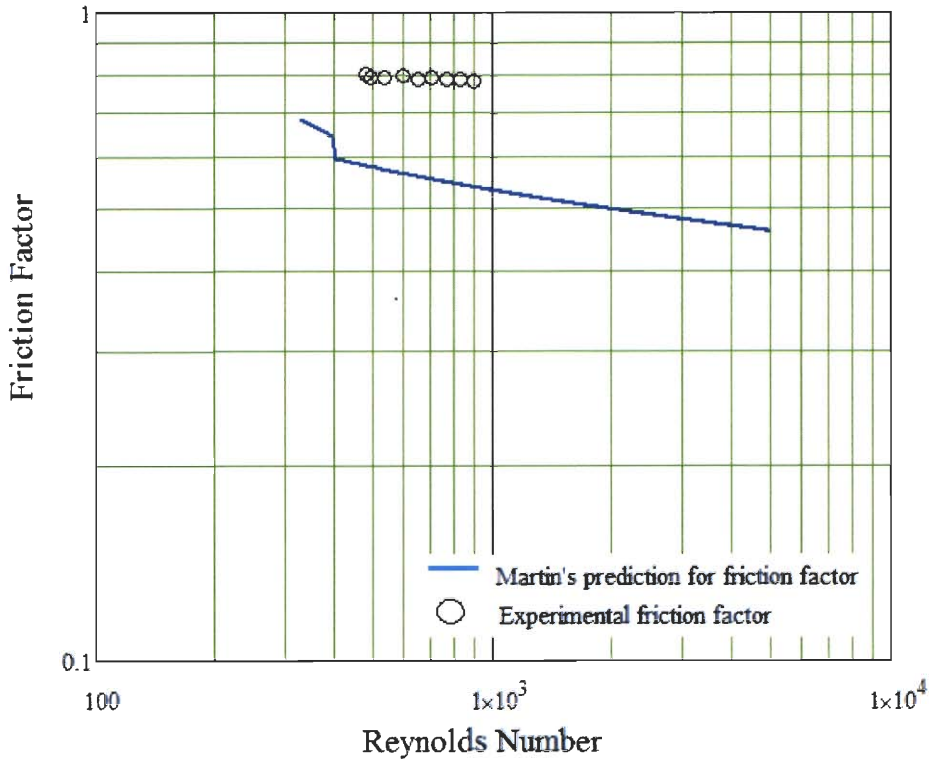


Figure 5.1 Isothermal Friction Factor Fp3x8-10

As can be seen clearly in Figure 5.1, the measured friction factor was significantly higher than that in the prediction. Although the measurements vary greatly from those predicted, they do correspond to values provided by the manufacturer.

### 5.1.2 High heat transfer

Table 5.1 Experimental Results of Fp3x8-10 at 22kW

| HL flow (gpm) | CL flow (gpm) | T1i (C) | T1o (C) | T2i (C) | T2o (C) | hexp (W/m^2K) | J1exp | f1exp | Re1 |
|---|---|---|---|---|---|---|---|---|---|
| 3.015 | 3.015 | 93.59 | 66.48 | 36.98 | 63.22 | 10819 | 0.0159 | 0.8083 | 1301 |
| 3.484 | 3.504 | 87.58 | 64.14 | 36.63 | 59.34 | 11799 | 0.0156 | 0.8015 | 1430 |
| 3.994 | 4.002 | 83.11 | 62.44 | 36.45 | 56.59 | 12922 | 0.0153 | 0.7808 | 1575 |
| 4.505 | 4.506 | 79.47 | 61.11 | 36.57 | 54.47 | 13999 | 0.015 | 0.7748 | 1719 |
| 4.993 | 4.995 | 76.71 | 60.14 | 36.79 | 52.99 | 14979 | 0.0148 | 0.7627 | 1856 |
| 5.512 | 5.511 | 74.25 | 59.34 | 37.05 | 51.77 | 15828 | 0.0144 | 0.7736 | 2003 |
| 6.004 | 6.01 | 72.26 | 58.51 | 37.1 | 50.65 | 16836 | 0.0143 | 0.7667 | 2138 |
| 6.506 | 6.513 | 70.55 | 57.86 | 37.24 | 49.78 | 17756 | 0.0141 | 0.765 | 2277 |
| 6.992 | 6.996 | 69.14 | 57.33 | 37.4 | 49.08 | 18651 | 0.0139 | 0.7625 | 2412 |
| 7.497 | 7.485 | 67.94 | 56.9 | 37.58 | 48.52 | 19593 | 0.0137 | 0.7599 | 2555 |

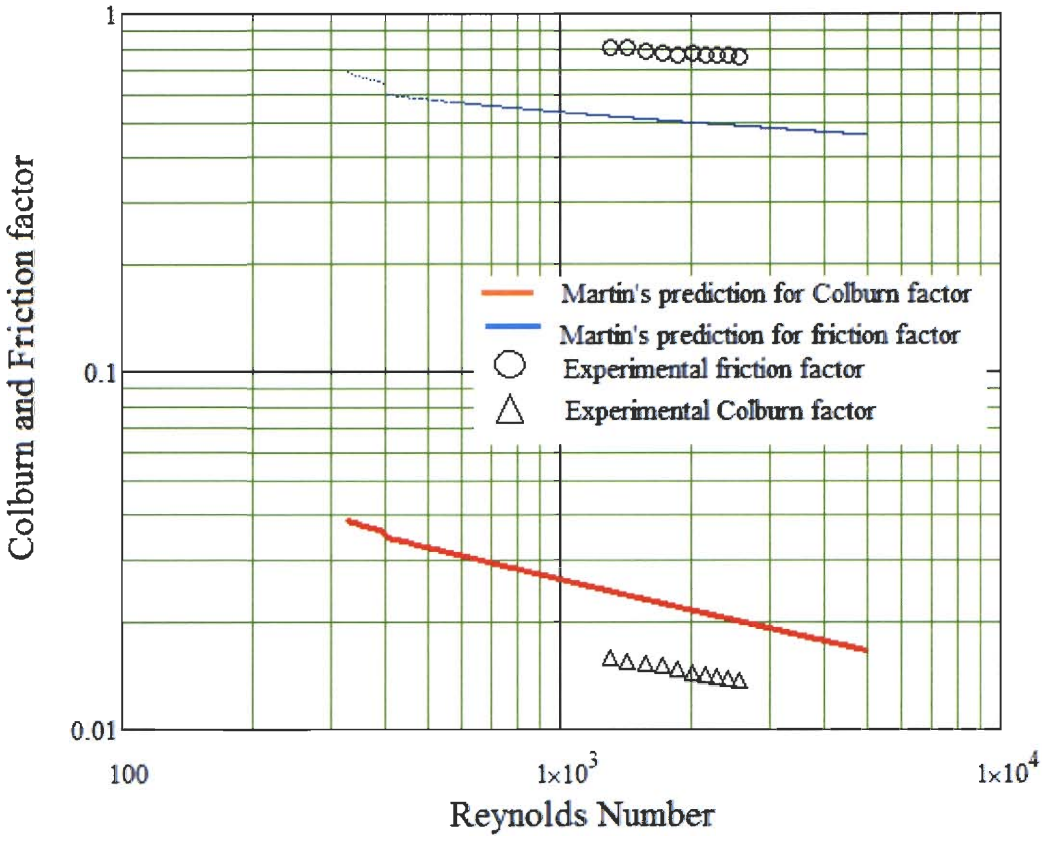


Figure 5.2 Colburn and Friction Factor Fp3x8-10 22kW

Figure 5.2 shows the highest level of heat transfer achieved in the smallest heat exchanger in the study. The discrepancy between pressure drops has been discussed earlier. Martin's prediction is larger than the experimental values, however the trend is the same as those predicted.

### 5.1.3 Low heat transfer

Table 5.2 Experimental Results of Fp3x8-10 at 11kW

| HL flow (gpm) | HL flow (gpm) | T1i (C) | T1o (C) | T2i (C) | T2o (C) | hexp (W/m^2K) | jexp | fexp | Re1 |
|---|---|---|---|---|---|---|---|---|---|
| 3.008 | 3.007 | 54.74 | 41.11 | 24.43 | 37.62 | 9532 | 0.0197 | 0.8261 | 818 |
| 3.5 | 3.504 | 51.42 | 39.64 | 24.1 | 35.54 | 10476 | 0.0191 | 0.8047 | 915 |
| 4.005 | 4.009 | 49.45 | 39.14 | 24.66 | 34.72 | 11472 | 0.0186 | 0.7961 | 1026 |
| 4.496 | 4.508 | 47.79 | 38.6 | 24.96 | 33.95 | 12385 | 0.0181 | 0.7915 | 1132 |
| 5.007 | 5.01 | 46.32 | 38.06 | 25.12 | 33.25 | 13291 | 0.0176 | 0.7798 | 1240 |
| 5.512 | 5.519 | 45.07 | 37.56 | 25.22 | 32.63 | 14163 | 0.0173 | 0.7805 | 1345 |
| 6.013 | 6.019 | 43.75 | 36.85 | 25.02 | 31.82 | 15035 | 0.017 | 0.7799 | 1443 |
| 6.51 | 6.504 | 42.97 | 36.56 | 25.16 | 31.49 | 15944 | 0.0167 | 0.7745 | 1549 |
| 7.008 | 6.993 | 41.57 | 35.61 | 24.56 | 30.47 | 16676 | 0.0165 | 0.7742 | 1636 |

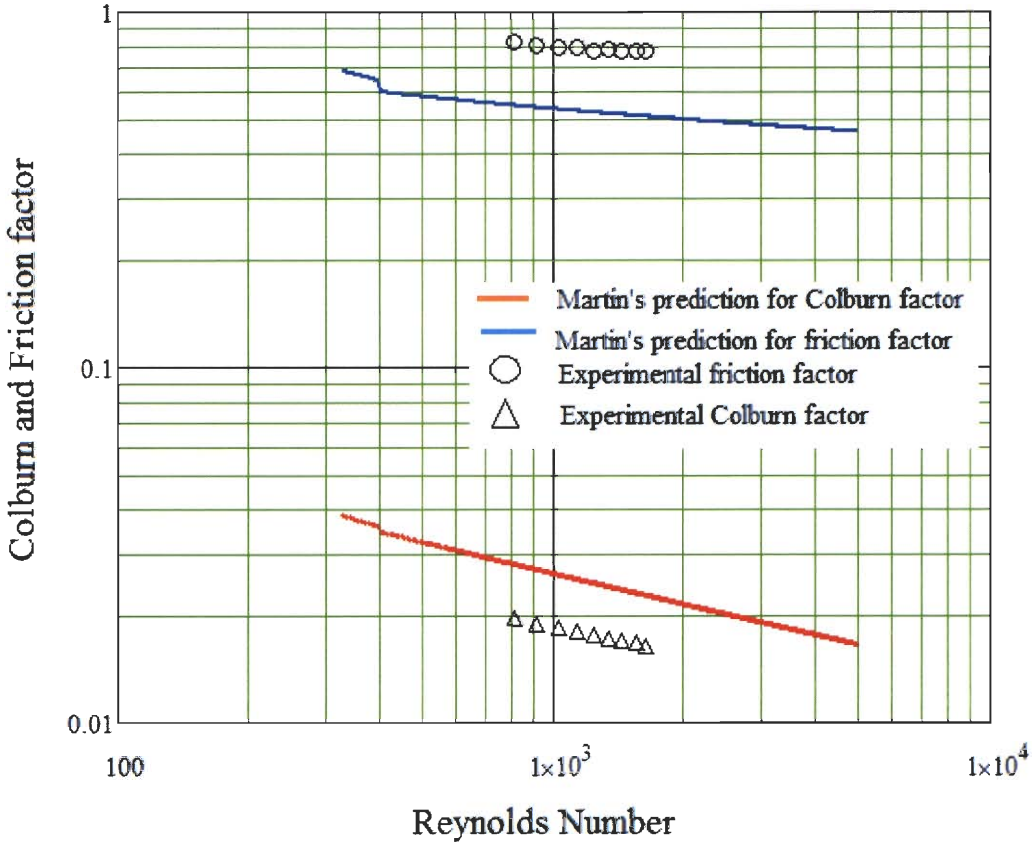


Figure 5.3 Colburn and Friction Factor Fp3x8-10 11kW

Again, as with the maximum heat transfer graph for this heat exchanger, both of the trends can be clearly seen. The largest difference between the graphs for high and lower power is the difference in Reynolds numbers. The hotter fluids have higher values, shifting the respective graph to the right.

## 5.2 Fg3x8-14

This was the second smallest PHE in the study. The additional four plates create a lower pressure drop at a given flow rate when compared to the Fp3x8-10, allowing it to reach a higher maximum flow rate.

### 5.2.1 Isothermal pressure drop

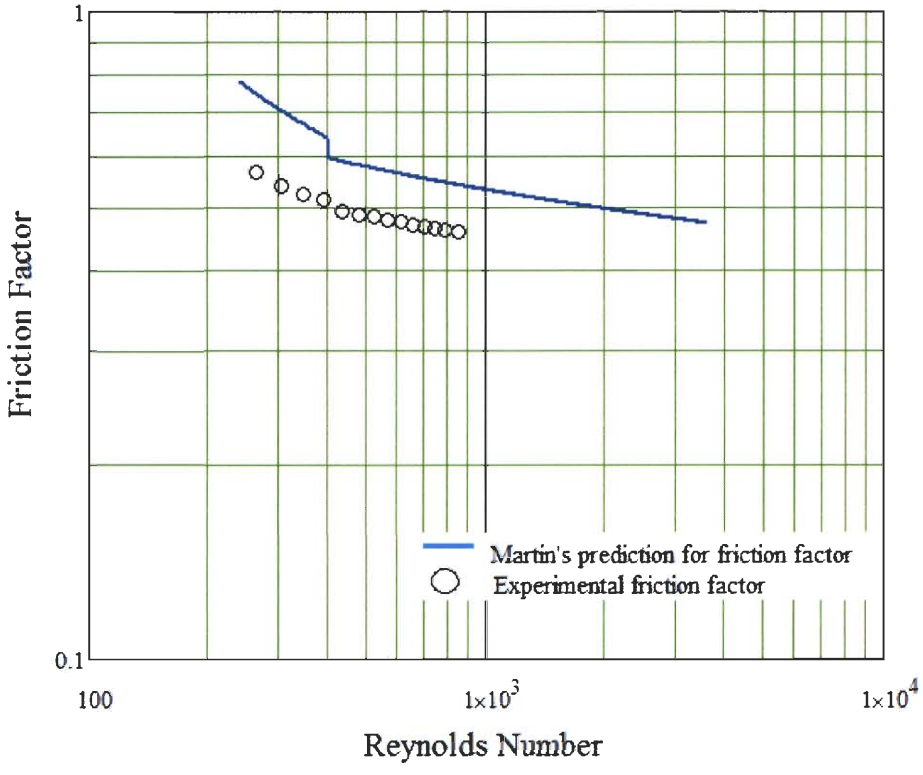


Figure 5.4 Isothermal Friction Factor Fg3x8-14

It can be seen in Figure 5.6 that there is a transition from linear to turbulent regimes, occurring at a Reynolds number of approximately 400. The measured friction factor is lower than that of the predicted one, but the trends are in good agreement.

### 5.2.2 High heat transfer

Table 5.3 Experimental Results of Fg3x8-14 at 25kW

| HL flow (gpm) | HL flow (gpm) | T1i (C) | T1o (C) | T2i (C) | T2o (C) | hexp (W/m^2K) | jexp | fexp | Re1 |
|---|---|---|---|---|---|---|---|---|---|
| 3.01 | 3.003 | 95.24 | 64.05 | 42.57 | 73.02 | 9048 | 0.0171 | 0.4907 | 940 |
| 3.513 | 3.509 | 87.97 | 61.07 | 41.08 | 67.31 | 9979 | 0.0169 | 0.4589 | 1030 |
| 4.011 | 4.02 | 83.46 | 59.64 | 40.84 | 64.07 | 10908 | 0.0166 | 0.4424 | 1131 |
| 4.503 | 4.521 | 79.98 | 58.75 | 41 | 61.79 | 11739 | 0.0163 | 0.4334 | 1233 |
| 4.997 | 4.992 | 76.77 | 57.66 | 40.76 | 59.6 | 12545 | 0.016 | 0.4239 | 1328 |
| 5.504 | 5.504 | 73.86 | 56.5 | 40.39 | 57.52 | 13365 | 0.0158 | 0.4226 | 1420 |
| 6.014 | 6.027 | 72.34 | 56.49 | 41.21 | 56.81 | 14270 | 0.0156 | 0.4216 | 1535 |
| 6.514 | 6.507 | 70.06 | 55.41 | 40.68 | 55.15 | 15055 | 0.0155 | 0.4196 | 1622 |
| 7.001 | 7.014 | 68.38 | 54.73 | 40.53 | 54 | 15831 | 0.0153 | 0.4186 | 1712 |
| 7.515 | 7.524 | 67.11 | 54.38 | 40.68 | 53.28 | 16668 | 0.0152 | 0.4157 | 1816 |
| 8.007 | 8.067 | 65.48 | 53.54 | 40.33 | 52.07 | 17461 | 0.0151 | 0.4173 | 1899 |
| 8.509 | 8.508 | 64.41 | 53.18 | 40.29 | 51.44 | 18155 | 0.0149 | 0.4169 | 1996 |
| 9.009 | 9.035 | 63.12 | 52.51 | 40.02 | 50.54 | 18972 | 0.0149 | 0.4174 | 2082 |
| 9.745 | 9.758 | 61.89 | 52.08 | 40.06 | 49.82 | 20084 | 0.0147 | 0.418 | 2223 |

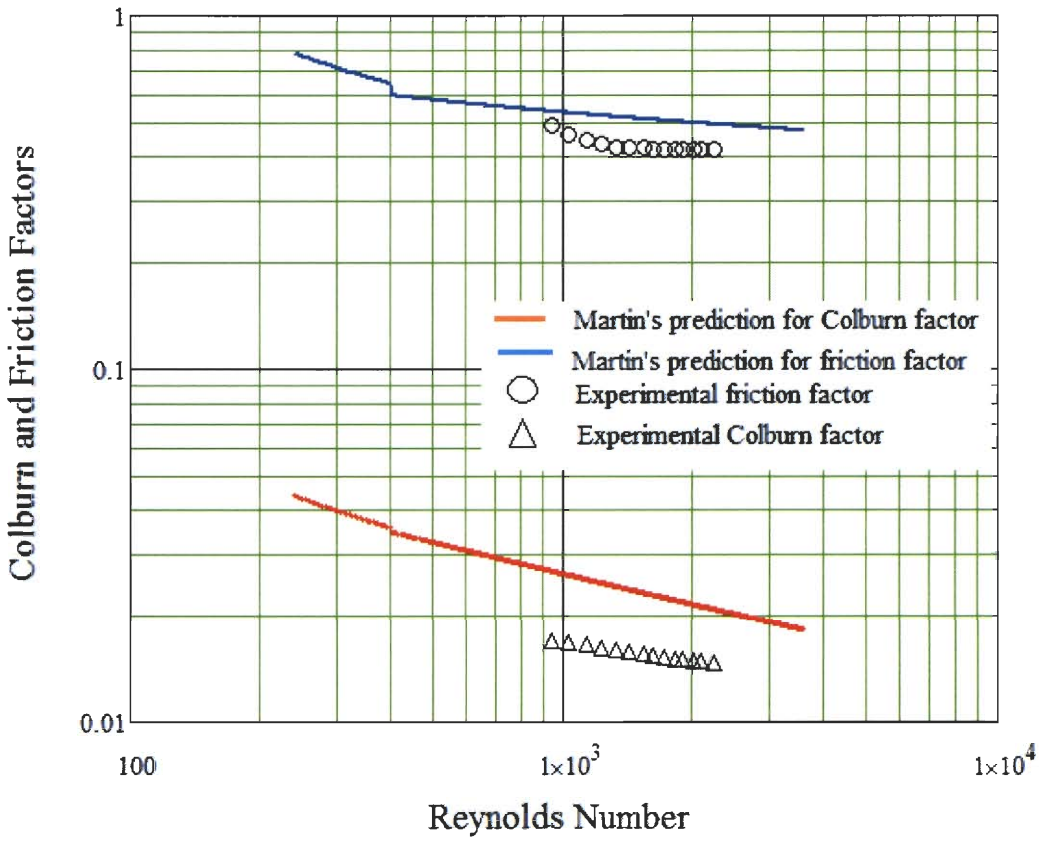


Figure 5.5 Colburn and Friction Factor Fg3x8-14 25kW

As with the earlier results described, there is an over estimation of the steady state heat transfer. Also it can be clearly seen that there is again a transition from laminar to turbulent for the friction factor data in Figure 5.5, however the transition now occurs at a Re of roughly 1200.

### 5.2.3 Low heat transfer

Table 5.4 Experimental Results of Fg3x8-14 at 14kW

| HL flow (gpm) | HL flow (gpm) | T1i (C) | T1o (C) | T2i (C) | T2o (C) | hexp (W/m^2K) | jexp | fexp | Re1 |
|---|---|---|---|---|---|---|---|---|---|
| 3.011 | 3.001 | 59.15 | 41.74 | 28.46 | 45.46 | 8167 | 0.0209 | 0.5273 | 620 |
| 4 | 4.002 | 52.04 | 38.85 | 27.24 | 40.25 | 9674 | 0.0198 | 0.5251 | 759 |
| 4.498 | 4.5 | 50.18 | 38.45 | 27.6 | 39.15 | 10521 | 0.0194 | 0.5091 | 838 |
| 4.999 | 5.011 | 48.25 | 37.67 | 27.39 | 37.81 | 11282 | 0.019 | 0.4996 | 911 |
| 5.527 | 5.531 | 47.08 | 37.5 | 27.8 | 37.22 | 12176 | 0.0187 | 0.476 | 997 |
| 5.997 | 5.992 | 46.26 | 37.39 | 28.09 | 36.81 | 12945 | 0.0184 | 0.4652 | 1073 |
| 6.505 | 6.504 | 45.5 | 37.31 | 28.42 | 36.47 | 13752 | 0.0181 | 0.4617 | 1156 |
| 7.017 | 7.034 | 44.48 | 36.88 | 28.35 | 35.81 | 14525 | 0.0179 | 0.4567 | 1232 |
| 7.503 | 7.5 | 43.58 | 36.47 | 28.22 | 35.23 | 15224 | 0.0177 | 0.453 | 1303 |
| 7.994 | 8.009 | 42.9 | 36.23 | 28.25 | 34.83 | 15896 | 0.0174 | 0.4501 | 1378 |
| 8.528 | 8.525 | 42.27 | 35.98 | 28.26 | 34.46 | 16794 | 0.0173 | 0.4462 | 1460 |
| 9.021 | 9.038 | 41.88 | 35.94 | 28.46 | 34.31 | 17501 | 0.0171 | 0.4441 | 1539 |
| 9.782 | 9.741 | 41.35 | 35.87 | 28.68 | 34.12 | 18575 | 0.0168 | 0.4491 | 1660 |

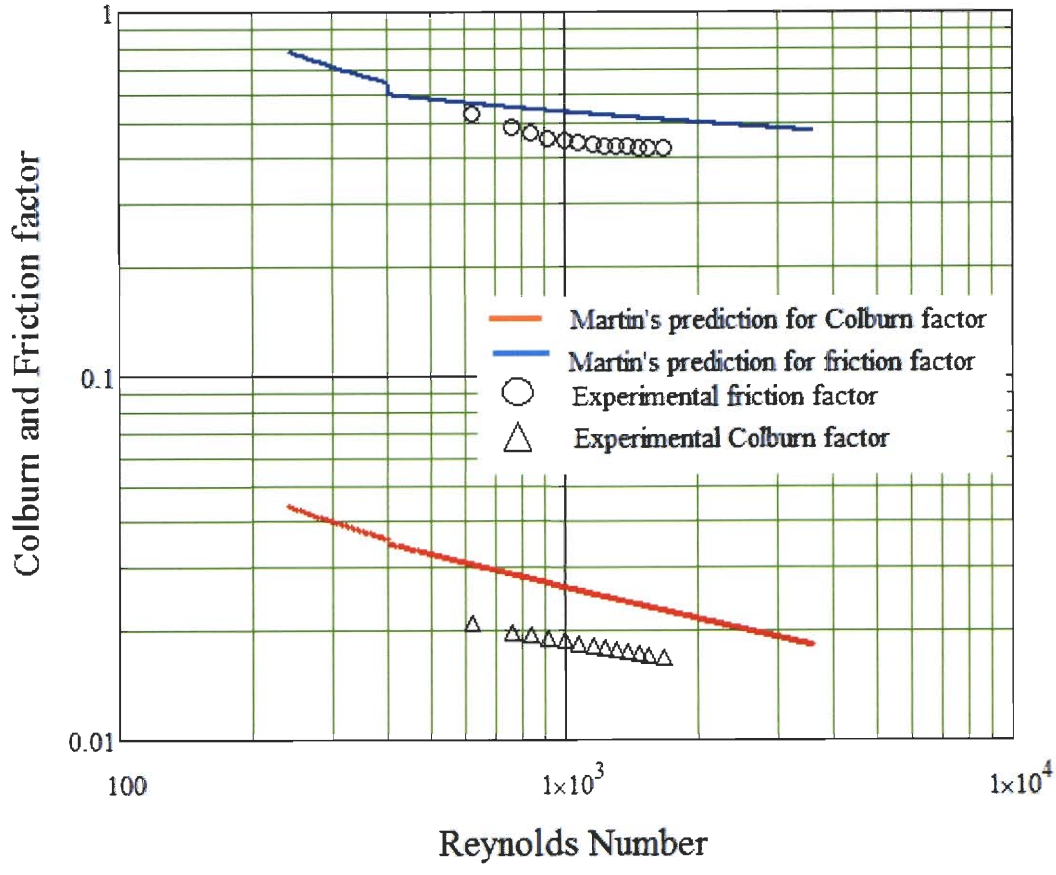


Figure 5.6 Colburn and Friction Factor Fg3x8-14 14kW

There is also a transition point in Figure 5.6, at Re 1000, but it has been shifted to the left relative to that found in Figure 5.5, likely due to the lower range of temperatures in this course of the data. It is important to note that the amount of heat transfer does not greatly effect the discrepancy between the measured and predicted heat transfer.

## 5.3 GB220H-20

This heat exchanger had the largest range of flow rates in the study, due to having 20 plates. Its large size also allowed for the largest amount of power in the study, 28kW, to be applied to the immersion heaters in the system.

### 5.3.1 Isothermal pressure drop

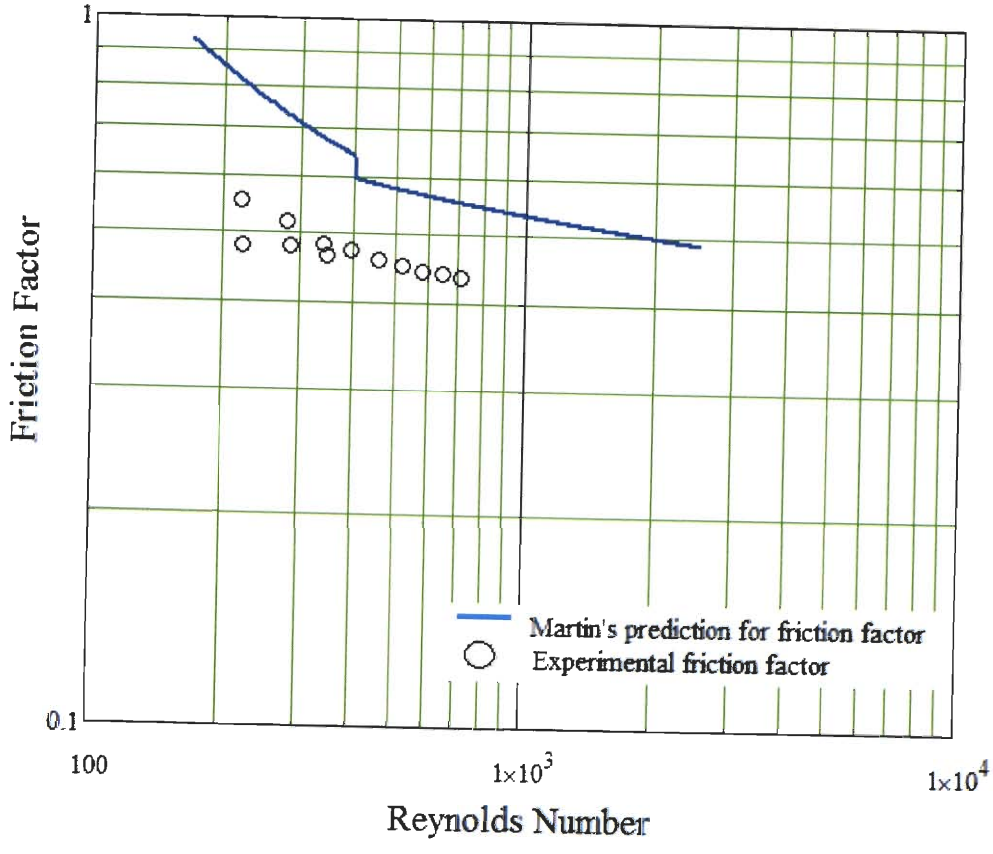


Figure 5.7 Isothermal Friction Factor GB220H-20

There is an erratic early portion of the trend of the friction factor data in Figure 5.7. This is due to slightly changing temperatures of the course of this data series, which has notable impact on the calculated results. For the higher portion of the range, the values are below those predicted, but do follow the same trend.

### 5.3.2 High heat transfer

Table 5.5 Experimental Results of GB220H-20 at 28kW

| HL flow (gpm) | HL flow (gpm) | T1i (C) | T1o (C) | T2i (C) | T2o (C) | hexp (W/m^2K) | jexp | fexp | Re1 |
|---|---|---|---|---|---|---|---|---|---|
| 3.016 | 3.015 | 91.42 | 56.85 | 44.03 | 77.7 | 6652 | 0.0188 | 0.5084 | 616 |
| 3.511 | 3.506 | 84.33 | 54.39 | 42.48 | 71.57 | 7349 | 0.0187 | 0.4606 | 673 |
| 4.022 | 4.011 | 79.66 | 53.45 | 42.2 | 67.85 | 7913 | 0.0181 | 0.4418 | 741 |
| 4.504 | 4.536 | 75.66 | 52.23 | 41.71 | 64.46 | 8484 | 0.0178 | 0.4336 | 799 |
| 5.003 | 5.011 | 72.47 | 51.33 | 41.26 | 61.92 | 9043 | 0.0174 | 0.4042 | 861 |
| 5.497 | 5.507 | 69.96 | 50.78 | 41.09 | 60.01 | 9448 | 0.0169 | 0.4031 | 925 |
| 6.016 | 6.03 | 67.94 | 50.45 | 41.2 | 58.46 | 9979 | 0.0165 | 0.4036 | 994 |
| 7.021 | 7.019 | 64.75 | 49.76 | 41.17 | 56.04 | 10987 | 0.0159 | 0.394 | 1126 |
| 7.999 | 8.005 | 62.36 | 49.21 | 41.19 | 54.23 | 11971 | 0.0155 | 0.389 | 1254 |
| 8.999 | 9.018 | 60.83 | 49.14 | 41.61 | 53.2 | 12972 | 0.015 | 0.3858 | 1393 |
| 9.996 | 10.066 | 59.43 | 48.91 | 41.8 | 52.2 | 13918 | 0.0147 | 0.3841 | 1528 |
| 11.005 | 11.016 | 58.24 | 48.69 | 41.88 | 51.41 | 14818 | 0.0143 | 0.3849 | 1663 |

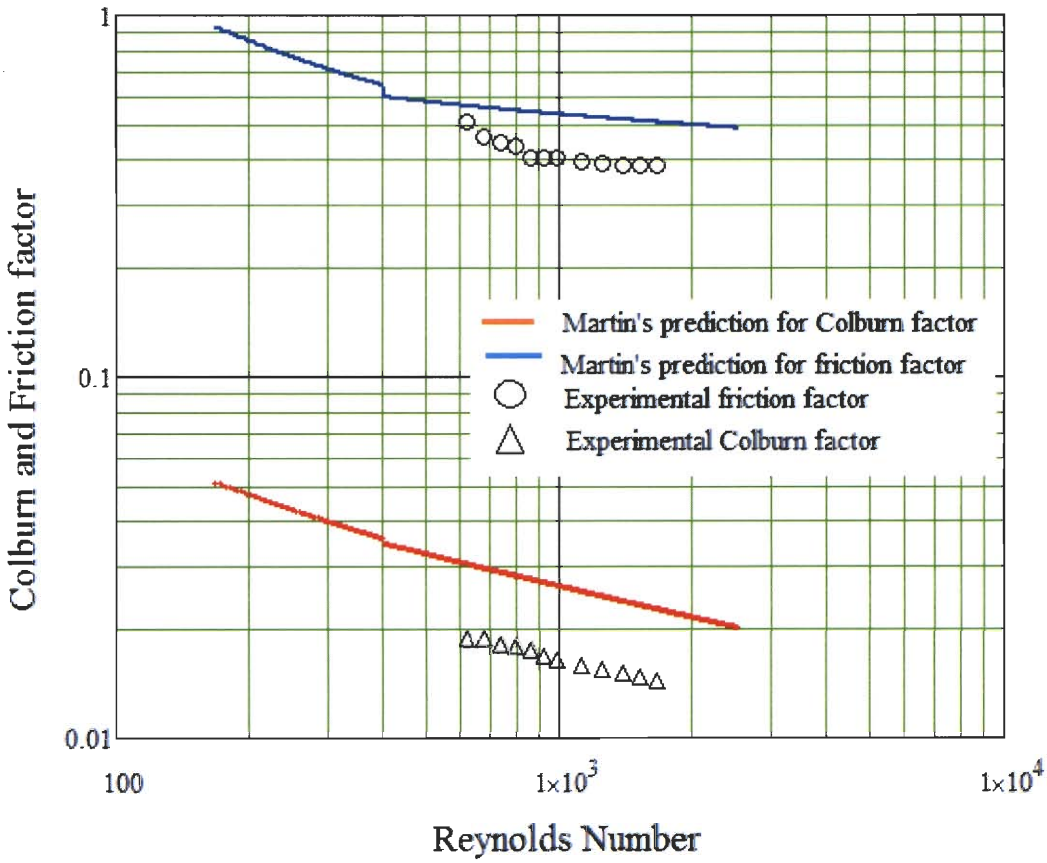


Figure 5.8 Colburn and Friction Factor GB220H-20 28kW

Figure 5.8 shows the experimental results for the highest level of heat transfer in the study across all of the different PHEs. As with the previous model, there is an under prediction for both the friction and Colburn factor, although the difference is largest for the Colburn factor. There is a clearly defined laminar to turbulent transition occurring for the friction factor around Re 800.

### 5.3.3 Low heat transfer

Table 5.6 Experimental Results of GB220H-20 at 14kW

| HL flow (gpm) | HL flow (gpm) | T1i (C) | T1o (C) | T2i (C) | T2o (C) | hexp (W/m^2K) | jexp | fexp | Re1 |
|---|---|---|---|---|---|---|---|---|---|
| 3.021 | 3.02 | 51.07 | 33.6 | 26.42 | 43.31 | 6042 | 0.0242 | 0.5411 | 382 |
| 3.516 | 3.523 | 50.14 | 34.7 | 27.92 | 42.93 | 6644 | 0.0229 | 0.4703 | 445 |
| 4.036 | 4.037 | 46.15 | 32.91 | 26.67 | 39.58 | 7209 | 0.0224 | 0.4787 | 487 |
| 4.508 | 4.511 | 46.1 | 33.98 | 27.99 | 39.84 | 7756 | 0.0214 | 0.4468 | 548 |
| 4.991 | 5.033 | 42.93 | 32.25 | 26.67 | 37.11 | 8131 | 0.0209 | 0.44 | 583 |
| 5.498 | 5.528 | 43.47 | 33.56 | 28.16 | 37.88 | 8706 | 0.0201 | 0.4277 | 652 |
| 6 | 6.018 | 40.6 | 31.67 | 26.59 | 35.35 | 9218 | 0.02 | 0.4275 | 684 |
| 6.996 | 7.038 | 38.92 | 31.27 | 26.6 | 34.12 | 10176 | 0.0192 | 0.4202 | 783 |
| 8.038 | 8.041 | 37.71 | 31.02 | 26.65 | 33.26 | 11182 | 0.0186 | 0.4129 | 888 |
| 9.012 | 9.027 | 36.69 | 30.72 | 26.61 | 32.51 | 12080 | 0.018 | 0.4056 | 983 |
| 10.013 | 10.016 | 35.94 | 30.55 | 26.66 | 31.99 | 13034 | 0.0176 | 0.4009 | 1083 |
| 11.016 | 11.019 | 35.31 | 30.4 | 26.7 | 31.55 | 13956 | 0.0172 | 0.3992 | 1183 |

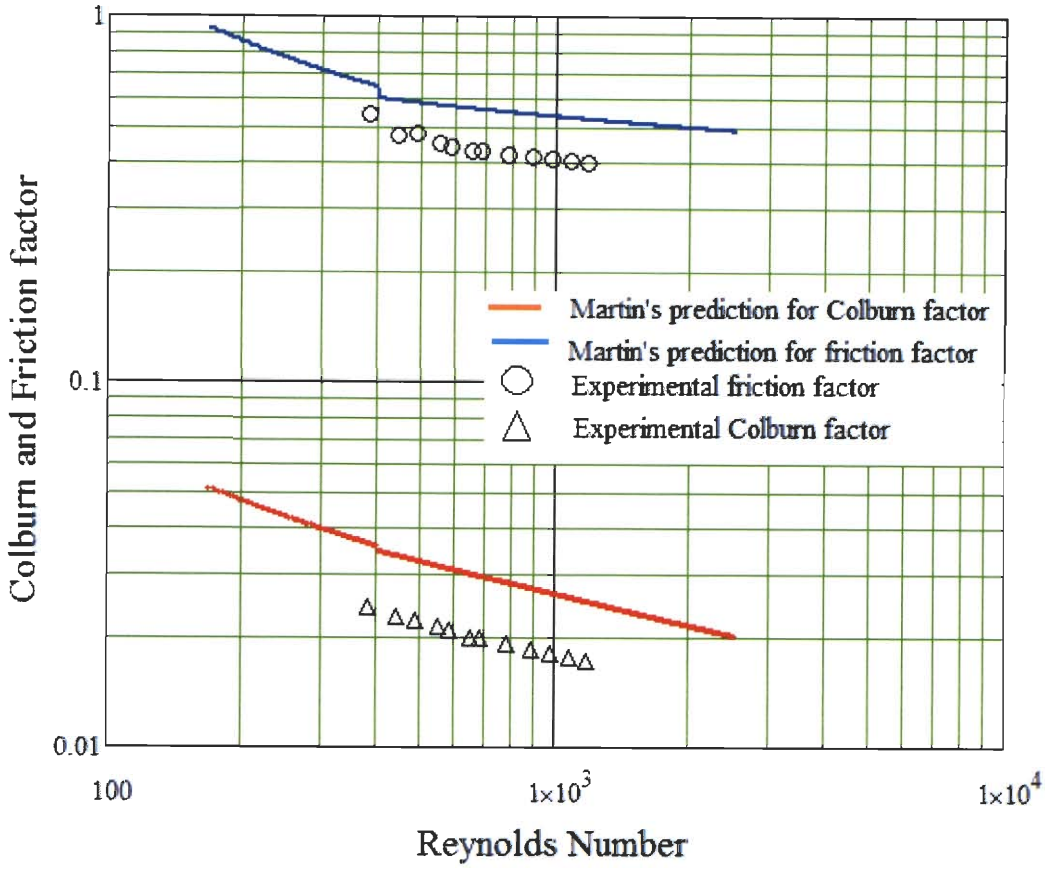


Figure 5.9 Colburn and Friction Factor GB220H-20 14kW

Figure 5.9 shows similar results, again showing that the level of heat transfer does not effect the trend of measured Colburn factors. There is also a transition region, occurring at around Re 650, which is again shifted relative to the data for 28kW of heat transfer for this heat exchanger.

## 5.4 GB240H-20

This heat exchanger was the largest tested in the study, having the same width and number of plates as the GB220H-20 but with longer plates. This additional length increased the pressure drop and lowered the maximum flow rate.

### 5.4.1 Isothermal pressure drop

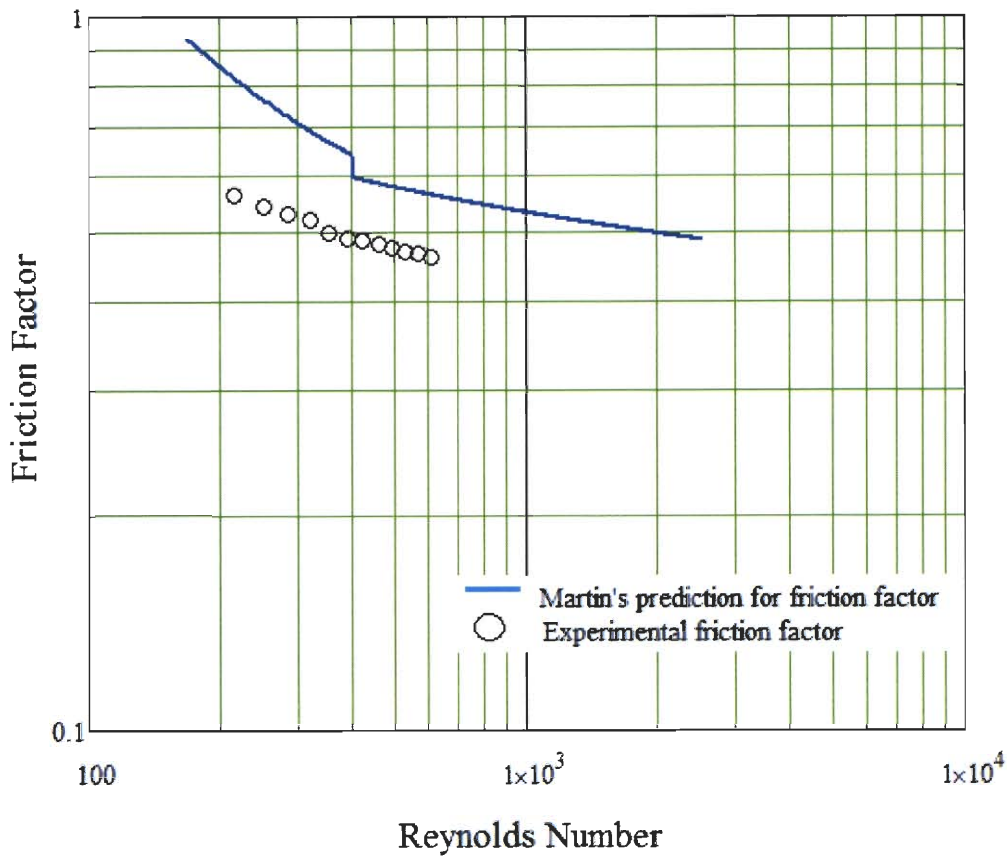


Figure 5.10 Isothermal Friction Factor GB240H-20

This was the largest PHE in the study, and consequently has the lowest Re values in the study. As with both the Fg3x8-14 and GB220H-20, there is an over prediction of the friction factor.

### 5.4.2 High heat transfer

Table 5.7 Experimental Results of GB240H-20 at 27kW

| HL flow (gpm) | HL flow (gpm) | T1i (C) | T1o (C) | T2i (C) | T2o (C) | hexp (W/m^2K) | jexp | fexp | Re1 |
|---|---|---|---|---|---|---|---|---|---|
| 2.997 | 3.016 | 89.58 | 56.76 | 48.32 | 80.72 | 6326 | 0.0182 | 0.518 | 605 |
| 3.514 | 3.515 | 83.92 | 55.43 | 47.68 | 75.61 | 7236 | 0.0183 | 0.4769 | 676 |
| 3.999 | 3.992 | 78.76 | 53.62 | 46.32 | 70.98 | 7850 | 0.0181 | 0.4616 | 733 |
| 4.517 | 4.515 | 74.98 | 52.72 | 45.86 | 67.7 | 8443 | 0.0177 | 0.4532 | 800 |
| 5.006 | 5.013 | 72.26 | 52.14 | 45.61 | 65.36 | 8955 | 0.0172 | 0.4319 | 865 |
| 5.511 | 5.523 | 71.11 | 52.87 | 46.67 | 64.6 | 9504 | 0.0166 | 0.4258 | 950 |
| 6.002 | 6.024 | 69 | 52.25 | 46.26 | 62.8 | 9901 | 0.0161 | 0.4252 | 1013 |
| 6.523 | 6.516 | 66.74 | 51.3 | 45.52 | 60.82 | 10462 | 0.016 | 0.42 | 1075 |
| 7.013 | 7.01 | 64.78 | 50.36 | 44.79 | 59.07 | 11008 | 0.0159 | 0.4164 | 1130 |
| 7.509 | 7.523 | 64.95 | 51.51 | 46.14 | 59.44 | 11452 | 0.0153 | 0.4119 | 1222 |
| 8.013 | 8.016 | 62.36 | 49.72 | 44.49 | 57.02 | 11938 | 0.0154 | 0.4112 | 1261 |
| 8.519 | 8.513 | 62.99 | 51.13 | 46.07 | 57.85 | 12428 | 0.0149 | 0.4086 | 1362 |
| 9.012 | 9.024 | 60.67 | 49.45 | 44.52 | 55.67 | 12840 | 0.0149 | 0.4078 | 1397 |
| 9.522 | 9.524 | 61.42 | 50.81 | 46.02 | 56.59 | 13329 | 0.0144 | 0.4061 | 1500 |
| 10.013 | 10.006 | 59.35 | 49.21 | 44.52 | 54.62 | 13823 | 0.0145 | 0.4066 | 1533 |

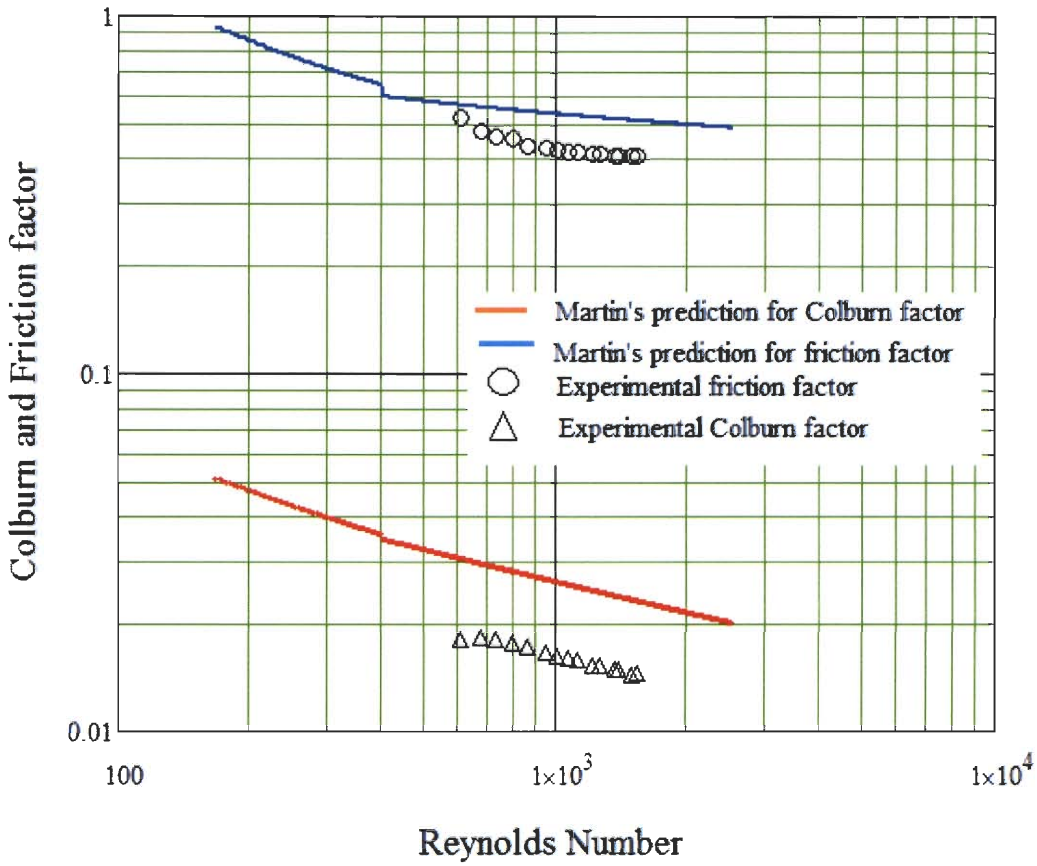


Figure 5.11 Colburn and Friction Factor GB240H-20 27kW

As was expected based on the analysis of the smaller PHEs, there is an over prediction of both friction and Colburn factor by Martin for this plate geometry. Compared to the isothermal data, there is now a well defined transition region around Re 900. Despite the difference in predictions, the trends are very well followed by the experimental data.

### 5.4.3 Low heat transfer

Table 5.7 Experimental Results of GB240H-20 at 13.7kW

| HL flow (gpm) | HL flow (gpm) | T1i (C) | T1o (C) | T2i (C) | T2o (C) | hexp (W/m^2K) | jexp | fexp | Re1 |
|---|---|---|---|---|---|---|---|---|---|
| 3.018 | 3.011 | 51.24 | 34.22 | 29.53 | 46.06 | 6113 | 0.0244 | 0.5262 | 384 |
| 3.509 | 3.508 | 48.8 | 34.11 | 29.73 | 44.07 | 6616 | 0.0231 | 0.4986 | 437 |
| 4.017 | 4.01 | 46.55 | 33.7 | 29.6 | 42.21 | 7177 | 0.0222 | 0.4884 | 489 |
| 4.507 | 4.501 | 44.98 | 33.51 | 29.64 | 40.92 | 7688 | 0.0214 | 0.474 | 541 |
| 4.999 | 5.009 | 44.05 | 33.72 | 30.09 | 40.19 | 8236 | 0.0208 | 0.4534 | 597 |
| 5.51 | 5.514 | 42.43 | 33.02 | 29.55 | 38.8 | 8757 | 0.0203 | 0.4482 | 645 |
| 6.009 | 6.005 | 42.26 | 33.65 | 30.34 | 38.82 | 9265 | 0.0197 | 0.4432 | 706 |
| 6.501 | 6.518 | 40.98 | 33 | 29.86 | 37.69 | 9865 | 0.0196 | 0.4389 | 752 |
| 7.001 | 7.015 | 40.91 | 33.53 | 30.5 | 37.77 | 10266 | 0.0189 | 0.4345 | 813 |
| 7.499 | 7.514 | 39.96 | 33.04 | 30.11 | 36.94 | 10763 | 0.0186 | 0.4304 | 860 |
| 8.007 | 8.006 | 40.07 | 33.6 | 30.76 | 37.16 | 11201 | 0.0181 | 0.4284 | 923 |
| 8.5 | 8.502 | 39.48 | 33.37 | 30.62 | 36.67 | 11697 | 0.0179 | 0.4247 | 973 |
| 9.004 | 9 | 39.18 | 33.41 | 30.73 | 36.46 | 12103 | 0.0175 | 0.4224 | 1029 |
| 9.505 | 9.506 | 38.85 | 33.38 | 30.78 | 36.22 | 12585 | 0.0173 | 0.4204 | 1083 |
| 10.006 | 10.012 | 38.72 | 33.52 | 31 | 36.16 | 13106 | 0.0171 | 0.4197 | 1140 |

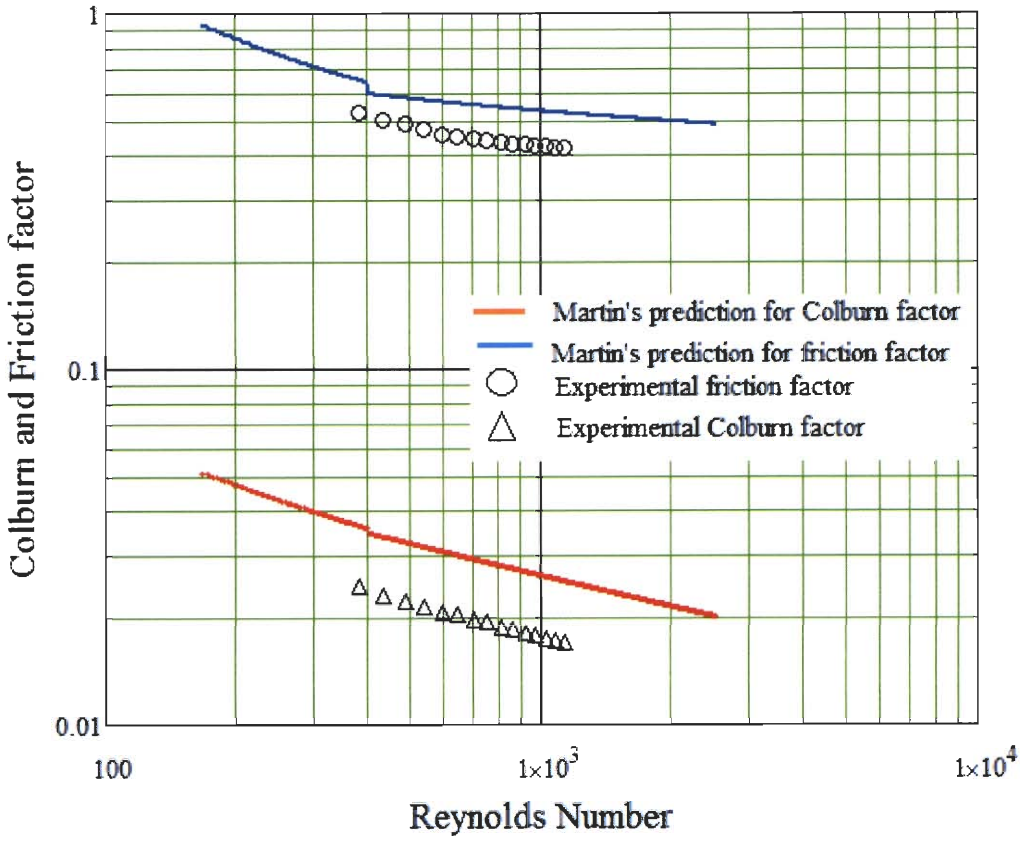


Figure 5.12 Colburn and Friction Factor GB240H-20 13.7kW

As a result of lower temperatures in the system, the range of Reynolds numbers has been shifted lower, while the trends of the data remain the same. A transition is also seen in Figure 5.12, at approximately Re 700. It is worthwhile to note that although the transitions are occurring at different Re between the full and half power data, the flow rates at which the transitions occur appear to be similar, despite the differences in temperatures between the two ranges.

# CHAPTER 6

# CONCLUSION

The experimental procedure and system performed well in comparison to other experiments undertaken in the literature. The design choice of isolating the primary flow loops from the cooling flow resulted in an extremely stable system

The comparison of the experimental data with that of the predicted performance by Martin's models yielded very interesting results. For the most part, the prediction of friction factors was very close to those observed in the system, even at a significantly higher surface enlargement factor than what was found in the literature at the time.

What is most notable is the wide discrepancy between the predicted Colburn factor and those experimentally determined in this study. All of the data generated in regards to this was significantly below that predicted by Martin, on the order of 2/3 the expected value. This is an important result, that high surface enlargement factors have a serious impact on the thermal performance of small heat exchangers. Notably, the smallest heat exchanger in the study had very large differences with regards to both the Colburn and friction factors. The data generated in this study should provide a good basis for further investigations.

# Appendix A

## MATHCAD for Fp3x8-10

GEA Fp3x8-10

**MathCAD format solution:**

## Test Heat Exchanger Fp3x8-10

Hot and cold water properties at Tf

$T_{hot\_water} := 50\,°C$ $T_{cold\_water} := 40\,°C$

Hot water (subscript 1) Cold water (subscript 2)

$\rho_1 := 985\frac{kg}{m^3}$ $\rho_2 := 994\frac{kg}{m^3}$

$c_{p1} := 4184\frac{J}{kg \cdot K}$ $c_{p2} := 4178\frac{J}{kg \cdot K}$

$k_1 := 0.639\frac{W}{m \cdot K}$ $k_2 := 0.628\frac{W}{m \cdot K}$

$\mu_1 := 471 \cdot 10^{-6}\frac{N \cdot s}{m^2}$ $\mu_2 := 654 \cdot 10^{-6}\frac{N \cdot s}{m^2}$

$Pr_1 := 3.02$ $Pr_2 := 4.34$

Thermal conductivity of the plate (Stainless Steel AISI 316)

$k_w := 13.4\frac{W}{m \cdot K}$

**Given information**

Volume flow rates for hot and cold water

$Q_1 := 10gpm$ $Q_2 := 10gpm$

Mass flow rates

$mdot_1(Q_1) := \rho_1 \cdot Q_1$ $mdot_1(Q_1) = 0.6214\frac{kg}{s}$

$mdot_2(Q_2) := \rho_2 \cdot Q_2$ $mdot_2(Q_2) = 0.6271\frac{kg}{s}$

**Geometric parameters:**

$N_p := 1$ Number of passes

$\beta := 60deg$ Corrugation inclination angle (chevron angle)

$N_t := 10$ Total number of plates

$D_p := \frac{3}{4}in$ Port diameter

$t_n := 0.093in$ spacing between plates

$\alpha := 40deg$ Corrugation Pitch angle

$\lambda := t_n \cdot \tan(\alpha)$ Corrugation Pitch (=wavelengtht) $\lambda = 0.078 \cdot in$

$\delta := 0.6mm$ Thickness of the plates

Use the dimensions of the test heat exchanger

$W_p := 3in$ $L_{p2p} := 6in$ $L_p := L_{p2p} - 1in$ $L_p = 5 \cdot in$

$H_p := t_n \cdot N_t$ $H_p = 0.93 \cdot in$

Number of wavelength per single plate

$$N_\lambda := \frac{W_p}{\lambda}$$

Number of channels for hot and cold fluid

$$N_{c1} := \frac{N_t}{2N_p} \qquad N_{c1} = 5$$

$$N_{c2} := \frac{N_t}{2N_p} - 1 \qquad N_{c2} = 4$$

Amplitude of corrugation and channel spacing

$$a := \frac{1}{2}\cdot\left(\frac{H_p}{N_t} - \delta\right) \qquad a = 0.0347 \cdot in \qquad 2 \cdot a = 0.0694 \cdot in \qquad 2 \cdot a + \delta = 0.093 \cdot in$$

Corrugation ratio γ

$\gamma := 4\cdot\frac{a}{\lambda}$ $\gamma = 1.7781$

Corrugated length

$$L_\lambda := \int_0^\lambda \sqrt{1 + \left(\frac{2\cdot\pi\cdot a}{\lambda}\right)^2 \cdot \cos\left(\frac{2\cdot\pi}{\lambda}\cdot x\right)^2}\, dx$$

Heat transfer area for hot fluid (fluid1)

$A_1 := 2\cdot L_\lambda \cdot N_\lambda \cdot L_p \cdot N_{c1}$ $A_1 = 0.2039\,m^2$

$A_2 := 2\cdot L_\lambda \cdot N_\lambda \cdot L_p \cdot N_{c2}$ $A_2 = 0.1631\,m^2$

Now setting the heat transfer area equal to the minimum area, which is A2

$A_w := A_2$

Projected area for the plates

$A_{p1} := 2\cdot W_p \cdot L_p \cdot N_{c1}$ $A_{p2} := 2\cdot W_p \cdot L_p \cdot N_{c2}$

**Enlargement factor φ**

$\Phi := \frac{L_\lambda \cdot N_\lambda}{W_-}$ $\Phi = 2.1072$

Exact hydraulic diameter

$D_h := \frac{4\cdot a}{\Phi}$ $D_h = 1.6725\,mm$

Minimum free-flow area

$A_{c1} := 2\cdot a\cdot W_p \cdot N_{c1}$ $A_{c1} = 1.0407\,in^2$

$A_{c2} := 2\cdot a\cdot W_p \cdot N_{c2}$ $A_{c2} = 0.8325\,in^2$

Surface area density

$\beta_1 := \frac{A_1}{W_p\cdot 2\cdot a\cdot L_p\cdot N_{c1}}$ $\beta_1 = 1.9132\times 10^3\,\frac{1}{m}$

Mass velocity

$G_1(Q_1) := \frac{mdot_1(Q_1)}{A_{c1}}$ $v_1 := \frac{G_1(Q_1)}{\rho_1} = 0.9397\,\frac{m}{s}$

$Re_1(Q_1) := \frac{G_1(Q_1)\cdot D_h}{\mu_1}$ $Re_1(Q_1) = 3.2868\times 10^3$

$$G_2(Q_2) := \frac{mdot_2(Q_2)}{A_{c2}} \qquad v_2 := \frac{G_2(Q_2)}{\rho_2} = 1.1746\frac{m}{s}$$

$$Re_2(Q_2) := \frac{G_2(Q_2)\cdot D_h}{\mu_2} \qquad Re_2(Q_2) = 2.9859 \times 10^3$$

**Friction factors**

Martin's correlation (1996) for the Darcy friction factor is modified by the Fanning friction factor.

Martin, H., 1996, A theoretical approach to predict the performance of chevron-type plate heat exchanger, Chem. Eng. Processing, Vol.35, pp. 301-310.

$$f_{o1}(Q_1) := \begin{cases} \left(1.56\cdot\ln(Re_1(Q_1)) - 3.0\right)^{-2} & \text{if } Re_1(Q_1) \geq 400 \\ \dfrac{16}{Re_1(Q_1)} & \text{otherwise} \end{cases}$$

$$f_{o2}(Q_2) := \begin{cases} \left(1.56\cdot\ln(Re_2(Q_2)) - 3.0\right)^{-2} & \text{if } Re_2(Q_2) \geq 400 \\ \dfrac{16}{Re_2(Q_2)} & \text{otherwise} \end{cases}$$

$$f_{m1}(Q_1) := \begin{cases} \dfrac{9.75}{Re_1(Q_1)^{0.289}} & \text{if } Re_1(Q_1) \geq 400 \\ \dfrac{149.25}{Re_1(Q_1)} + 0.9625 & \text{otherwise} \end{cases}$$

$$f_{m2}(Q_2) := \begin{cases} \dfrac{9.75}{Re_2(Q_2)^{0.289}} & \text{if } Re_2(Q_2) \geq 400 \\ \dfrac{149.25}{Re_2(Q_2)} + 0.9625 & \text{otherwise} \end{cases}$$

$$f_1(Q_1) := \left[\frac{\cos(\beta)}{\left(0.045\cdot\tan(\beta) + 0.09\cdot\sin(\beta) + \dfrac{f_{o1}(Q_1)}{\cos(\beta)}\right)^{0.5}} + \left(\frac{1-\cos(\beta)}{\sqrt{3.8\cdot f_{m1}(Q_1)}}\right)\right]^{-2}$$

$$f_1(Q_1) = 0.4745$$

$$f_2(Q_2) := \left[ \frac{\cos(\beta)}{\left(0.045\cdot\tan(\beta) + 0.09\cdot\sin(\beta) + \frac{f_{b2}(Q_2)}{\cos(\beta)}\right)^{0.5}} + \left( \frac{1-\cos(\beta)}{\sqrt{3.8\cdot f_{m2}(Q_2)}} \right) \right]^{-2}$$

$$f_2(Q_2) = 0.4784$$

Heat transfer coefficients

$$h_1(Q_1) := \frac{k_1}{D_h}\cdot\left[0.205\cdot Pr_1^{\frac{1}{3}}\cdot 1^{\frac{1}{6}}\cdot\left(f_1(Q_1)\cdot Re_1(Q_1)^2\cdot\sin(2\cdot\beta)\right)^{0.374}\right]$$

$$h_1(Q_1) = 3.4672\times 10^4\cdot\frac{W}{m^2\cdot K}$$

$$h_2(Q_2) := \frac{k_2}{D_h}\cdot\left[0.205\cdot Pr_2^{\frac{1}{3}}\cdot 1^{\frac{1}{6}}\cdot\left(f_2(Q_2)\cdot Re_2(Q_2)^2\cdot\sin(2\cdot\beta)\right)^{0.374}\right]$$

$$h_2(Q_2) = 3.5899\times 10^4\cdot\frac{W}{m^2\cdot K}$$

Overall heat teansfer coefficient

$$U_2(Q_1,Q_2) := \frac{1}{\frac{A_2}{h_1(Q_1)\cdot A_1} + \frac{\delta}{k_w} + \frac{1}{h_2(Q_2)}}$$

$$U_2(Q_1,Q_2) = 9.8548\times 10^3\cdot\frac{W}{m^2 K}$$

$$U_2(Q_1,Q_2)\cdot A_2 = 1.6077\times 10^3\cdot\frac{W}{K}$$

**Effectiveness-NTU Method**

$$C_1(Q_1) := mdot_1(Q_1)\cdot c_{p1} \qquad C_1(Q_1) = 2.6001\times 10^3\,\frac{m^2\cdot kg}{K\cdot s^3}$$

$$C_2(Q_2) := mdot_2(Q_2) \cdot c_{p2} \qquad C_2(Q_2) = 2.6201 \times 10^3 \frac{m^2 \cdot kg}{K \cdot s^3}$$

$$C_{min}(Q_1, Q_2) := \min(C_1(Q_1), C_2(Q_2)) \qquad C_{min}(Q_1, Q_2) = 2.6001 \times 10^3 \frac{m^2 \cdot kg}{K \cdot s^3}$$

$$C_{max}(Q_1, Q_2) := \max(C_1(Q_1), C_2(Q_2)) \qquad C_{max}(Q_1, Q_2) = 2.6201 \times 10^3 \frac{m^2 \cdot kg}{K \cdot s^3}$$

$$C_r(Q_1, Q_2) := \frac{C_{min}(Q_1, Q_2)}{C_{max}(Q_1, Q_2)} \qquad C_r(Q_1, Q_2) = 0.9924$$

$$NTU(Q_1, Q_2) := \frac{U_2(Q_1, Q_2) \cdot A_2}{C_{min}(Q_1, Q_2)} \qquad NTU(Q_1, Q_2) = 0.6183$$

Counterflow effectiveness

$$\varepsilon_{PHE}(Q_1, Q_2) := \frac{1 - \exp\left[-NTU(Q_1, Q_2) \cdot (1 - C_r(Q_1, Q_2))\right]}{1 - C_r(Q_1, Q_2) \cdot \exp\left[-NTU(Q_1, Q_2) \cdot (1 - C_r(Q_1, Q_2))\right]}$$

$$\varepsilon_{PHE}(Q_1, Q_2) = 0.3826$$

$Q_m := 1gpm, 2gpm .. 15gpm$

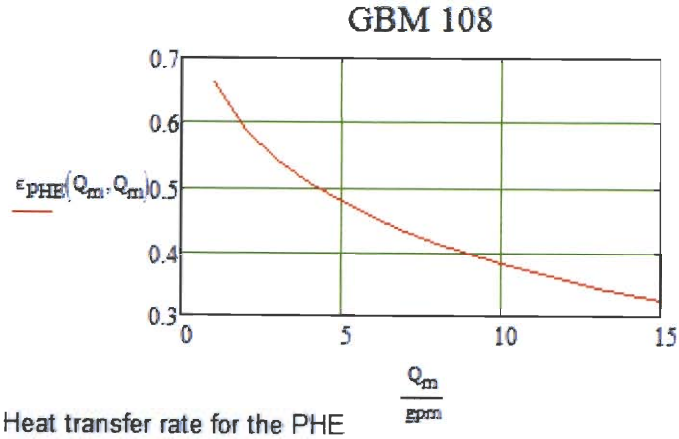


Heat transfer rate for the PHE

$$q(T_{1i}, T_{2i}, Q_1, Q_2) := \varepsilon_{PHE}(Q_1, Q_2) \cdot C_{min}(Q_1, Q_2) \cdot (T_{1i} - T_{2i})$$

Since $\varepsilon_{PHE} = \frac{C_1 \cdot (T_{1i} - T_{1o})}{C_{min} \cdot (T_{1i} - T_{2i})} = \frac{C_2 \cdot (T_{2o} - T_{2i})}{C_{min} \cdot (T_{1i} - T_{2i})}$

$$T_{1o}(T_{1i}, T_{2i}, Q_1, Q_2) := T_{1i} - \varepsilon_{PHE}(Q_1, Q_2) \cdot \frac{C_{min}(Q_1, Q_2)}{C_1(Q_1)} \cdot (T_{1i} - T_{2i})$$

$$T_{2o}(T_{1i}, T_{2i}, Q_1, Q_2) := T_{2i} - \varepsilon_{PHE}(Q_1, Q_2) \cdot \frac{C_{min}(Q_1, Q_2)}{C_2(Q_2)} \cdot (T_{1i} - T_{2i})$$

$$j_1(Q_1) := \frac{h_1(Q_1) \cdot Pr_1^{\frac{2}{3}}}{G_1(Q_1) \cdot c_{p1}}$$

$T_{1i} := 70\,°C$ $T_{2i} := 30\,°C$

$Q_m := 0.1gpm, 0.11gpm .. 12gpm$

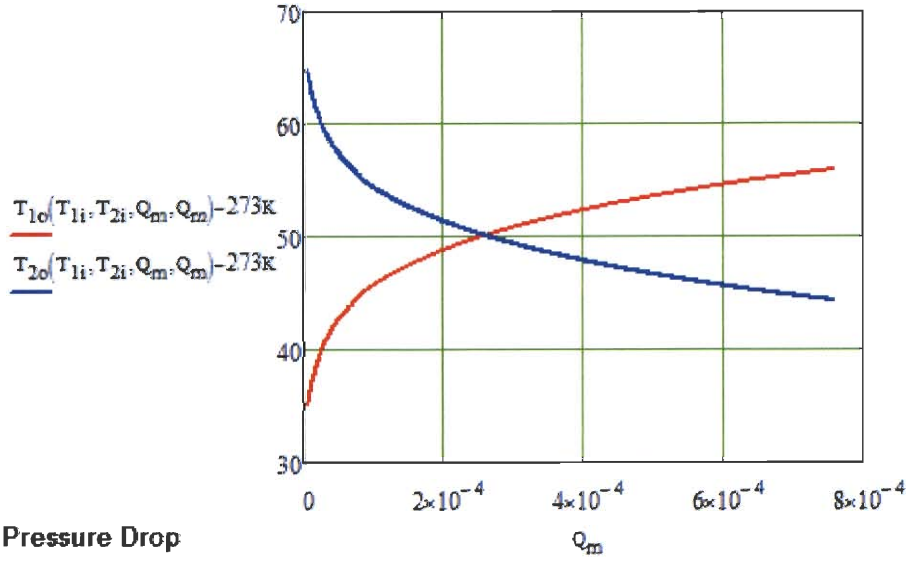


**Pressure Drop**

The frictional channel pressure drop

$$\Delta P_{fl}(Q_1) := \frac{2 \cdot f_1(Q_1) \cdot L_p}{D_h} \cdot \frac{G_1(Q_1)^2}{\rho_1} \cdot N_p \qquad \Delta P_{fl}(Q_1) = 9.0907 \cdot psi$$

$$\Delta P_{f2}(Q_2) := \frac{2 \cdot f_2(Q_2) \cdot L_p}{D_h} \cdot \frac{G_2(Q_2)^2}{\rho_2} \cdot N_p \qquad \Delta P_{f2}(Q_2) = 14.4519 \cdot psi$$

The connection and port pressure drop

$$G_{p1}(Q_1) := \frac{4 \cdot mdot_1(Q_1)}{\pi \cdot D_p^{\,2}} \qquad G_{p1}(Q_1) = 2.1803 \times 10^3 \ \frac{kg}{m^2 \cdot s}$$

$$G_{p2}(Q_2) := \frac{4 \cdot mdot_2(Q_2)}{\pi \cdot D_p^{\,2}}$$

$$\Delta P_{p1}(Q_1) := 1.5 \cdot N_p \cdot \frac{G_{p1}(Q_1)^2}{2 \cdot \rho_1} \qquad \Delta P_{p1}(Q_1) = 0.525 \cdot psi$$

$$\Delta P_{p2}(Q_2) := 1.5 \cdot N_p \cdot \frac{G_{p2}(Q_2)^2}{2 \cdot \rho_2} \qquad \Delta P_{p2}(Q_2) = 0.5298 \cdot psi$$

$$\Delta P_1(Q_1) := \Delta P_{fl}(Q_1) + \Delta P_{p1}(Q_1) \qquad \Delta P_1(Q_1) = 9.6156 \cdot psi$$

$$\Delta P_2(Q_2) := \Delta P_{f2}(Q_2) + \Delta P_{p2}(Q_2) \qquad \Delta P_2(Q_2) = 14.9816 \cdot psi$$

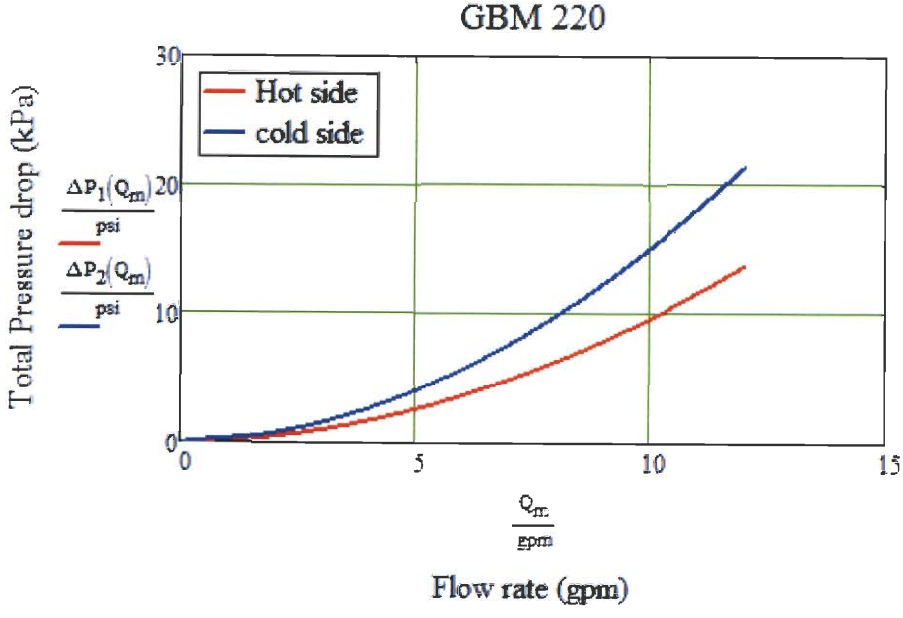

$$f_1(Q_1) := \left(\Delta P_1(Q_1) - \frac{1.5 \cdot G_{p1}(Q_1)^2}{2 \cdot \rho_1}\right) \cdot \frac{D_h \cdot \rho_1}{2 \cdot L_p \cdot G_1(Q_1)^2 \cdot N_p}$$

Experimental Data

ORIGIN := 1

$i := 1, 2 .. 10$

$M_{i,1} := i$

$M_{i,2} := \frac{T_{1i} - 273K}{K}$

$M_{i,3} := \frac{T_{1o}(T_{1i}, T_{2i}, i \cdot gpm, i \cdot gpm) - 273.15K}{K}$

$M_{i,4} := \frac{T_{2i} - 273K}{K}$

$M_{i,5} := \frac{T_{2o}(T_{1i}, T_{2i}, i \cdot gpm, i \cdot gpm) - 273.15K}{K}$

$M_{i,6} := \frac{\Delta P_1(i \cdot gpm)}{psi}$ $\quad$ $M_{i,7} := \frac{\Delta P_2(i \cdot gpm)}{psi}$

Predictions

$M =$

| | 1 | 2 | 3 | 4 | 5 | 6 | 7 |
|---|---|---|---|---|---|---|---|
| 1 | 1 | 70.15 | 43.4467 | 30.15 | 56.3507 | 0.1363 | 0.2197 |
| 2 | 2 | 70.15 | 46.557 | 30.15 | 53.2641 | 0.447 | 0.7009 |
| 3 | 3 | 70.15 | 48.3742 | 30.15 | 51.4607 | 0.9631 | 1.5067 |
| 4 | 4 | 70.15 | 49.7651 | 30.15 | 50.0804 | 1.6649 | 2.6015 |
| 5 | 5 | 70.15 | 50.9012 | 30.15 | 48.9531 | 2.5487 | 3.9793 |
| 6 | 6 | 70.15 | 51.864 | 30.15 | 47.9976 | 3.6118 | 5.6356 |
| 7 | 7 | 70.15 | 52.7 | 30.15 | 47.168 | 4.8518 | 7.5668 |
| 8 | 8 | 70.15 | 53.4381 | 30.15 | 46.4355 | 6.2668 | 9.7698 |
| 9 | 9 | 70.15 | 54.0983 | 30.15 | 45.7803 | 7.8552 | 12.2422 |
| 10 | 10 | 70.15 | 54.6947 | 30.15 | 45.1885 | 9.6156 | 14.9816 |

Adding temperature dependent properties

Temperature dependent properties of water taken from table A.12 Thermal Design

temperature range of properties, in deg celsius

$$tx := \begin{pmatrix} 0 \\ 20 \\ 40 \\ 60 \\ 80 \\ 100 \end{pmatrix}$$

liquid density information, in kg/m3

$$dly := \begin{pmatrix} 1002 \\ 1000 \\ 994 \\ 985 \\ 974 \\ 960 \end{pmatrix}$$

$dly1 := dly$

$dls1 := lspline(tx, dly1)$

$\rho 1(t_{avg1}) := interp(dls1, tx, dly1, t_{avg1}) \cdot \frac{kg}{m^3}$

$dly2 := dly$

$dls2 := lspline(tx, dly2)$

$\rho 2(t_{avg2}) := interp(dls2, tx, dly2, t_{avg2}) \cdot \frac{kg}{m^3}$

$dly3 := dly$

$dls3 := lspline(tx, dly3)$

$\rho 3(t_{avg3}) := interp(dls3, tx, dly3, t_{avg3}) \cdot \frac{kg}{m^3}$

specific heat information, in J/(kg*K)

$$dcpy := \begin{pmatrix} 4217 \\ 4181 \\ 4178 \\ 4184 \\ 4196 \\ 4216 \end{pmatrix}$$

$dcp1 := dcpy$ $dcp2 := dcpy$

$dcps1 := lspline(tx, dcp1)$ $dcps2 := lspline(tx, dcp2)$

$c_{p1}(t_{avg1}) := interp(dcps1, tx, dcp1, t_{avg1}) \frac{J}{kg \cdot K}$

$c_{p2}(t_{avg2}) := interp(dcps2, tx, dcp2, t_{avg2}) \frac{J}{kg \cdot K}$

$dcp3 := dcpy$

$dcps3 := lspline(tx, dcp1)$

$c_{p3}(t_{avg3}) := interp(dcps3, tx, dcp3, t_{avg3}) \frac{J}{kg \cdot K}$

thermal conductivity information, in W/(m*K)

$$dky := \begin{pmatrix} .552 \\ .597 \\ .628 \\ .651 \\ .668 \\ .68 \end{pmatrix}$$

$dk1 := dky$ $dk2 := dky$

$dks1 := lspline(tx, dk1)$ $dks2 := lspline(tx, dk2)$

$k_1(t_{avg1}) := interp(dks1, tx, dk1, t_{avg1}) \frac{W}{m \cdot K}$ $k_2(t_{avg2}) := interp(dks2, tx, dk2, t_{avg2}) \frac{W}{m \cdot K}$

$dk3 := dky$

$dks3 := lspline(tx, dk3)$

absolute viscosity information, in N*s/m^2

$k_3(t_{avg3}) := interp(dks3, tx, dk3, t_{avg3}) \frac{W}{m \cdot K}$

$$dvsy := \begin{pmatrix} 1792 \\ 1006 \\ 654 \\ 471 \\ 355 \\ 288 \end{pmatrix}$$

$dv1 := dvsy$ $dv2 := dvsy$ $dv3 := dvsy$

$dvs1 := lspline(tx, dv1)$ $dvs2 := lspline(tx, dv2)$ $dvs3 := lspline(tx, dv3)$

$$\mu_1(t_{avg1}) := interp(dvs1, tx, dv1, t_{avg1}) \cdot 10^{-6} \cdot \frac{N \cdot s}{m^2}$$

$$\mu_2(t_{avg2}) := interp(dvs2, tx, dv2, t_{avg2}) \cdot 10^{-6} \cdot \frac{N \cdot s}{m^2}$$

$$\mu_3(t_{avg3}) := interp(dvs3, tx, dv3, t_{avg3}) \cdot 10^{-6} \cdot \frac{N \cdot s}{m^2}$$

Prantle number information

$$pry := \begin{pmatrix} 13.6 \\ 7.02 \\ 4.34 \\ 3.02 \\ 2.22 \\ 1.74 \end{pmatrix}$$

$pry1 := pry$ $pry2 := pry$ $pry3 := pry$

$prs1 := lspline(tx, pry1)$ $prs2 := lspline(tx, pry2)$ $prs3 := lspline(tx, pry3)$

$$Pr_1(t_{avg1}) := interp(prs1, tx, pry1, t_{avg1})$$

$$Pr_2(t_{avg2}) := interp(prs2, tx, pry2, t_{avg2})$$

$$Pr_3(t_{avg3}) := interp(prs3, tx, pry3, t_{avg3})$$

Experiments. For the model and data that follows, when regarding side A and side B of the heat exchangers, the hot side (A) will have a subscript 1, the cold side (B) will have a subscript 2

Description of matrix columns: 1) hot loop flow rate, 2) cold loop flow rate, 3) T1i, 4) T1o, 5) T2i, 6) T2o, 7) normalized hot loop inlet pressure, 8) normalized hot loop pressure outlet, 9) normalized cold loop inlet pressure, 10) normalized cold loop outlet pressure, 11) T3i, 12) T3o, 13) city water flow rate, 14) power applied to bulk heaters (accounts for voltage drop across shunts in power calc)

f represents full power, h represents half power, i represents isothermal

$$Mf22 := \begin{pmatrix} 3.015 & 3.015 & 94.32 & 66.69 & 37 & 63.32 & 26.725 & 25.604 & 20.852 & 18.27 & 12.91 & 30.82 & 4.526 & 22346 \\ 3.484 & 3.504 & 88.31 & 64.35 & 36.65 & 59.44 & 23.819 & 22.12 & 20.713 & 17.252 & 12.72 & 30.65 & 4.562 & 22342 \\ 3.994 & 4.002 & 83.84 & 62.65 & 36.47 & 56.69 & 22.466 & 20.114 & 20.876 & 16.469 & 12.7 & 30.7 & 4.562 & 22330 \\ 4.505 & 4.506 & 80.2 & 61.32 & 36.59 & 54.57 & 21.63 & 18.499 & 21.733 & 16.17 & 12.78 & 30.86 & 4.567 & 22329 \\ 4.993 & 4.995 & 77.44 & 60.35 & 36.81 & 53.09 & 21.181 & 17.199 & 22.822 & 16.038 & 12.56 & 31.29 & 4.403 & 22317 \\ 5.512 & 5.511 & 74.98 & 59.55 & 37.07 & 51.87 & 21.661 & 16.625 & 23.836 & 15.648 & 12.59 & 31.5 & 4.375 & 22302 \\ 6.004 & 6.01 & 72.99 & 58.72 & 37.12 & 50.75 & 22.232 & 16.21 & 24.701 & 15.046 & 12.56 & 31.58 & 4.352 & 22277 \\ 6.506 & 6.513 & 71.28 & 58.07 & 37.26 & 49.88 & 22.939 & 15.781 & 26.043 & 14.792 & 12.55 & 31.58 & 4.329 & 22269 \\ 6.992 & 6.996 & 69.87 & 57.54 & 37.42 & 49.18 & 23.825 & 15.491 & 27.545 & 14.634 & 12.58 & 31.83 & 4.307 & 22253 \\ 7.497 & 7.485 & 68.67 & 57.11 & 37.6 & 48.62 & 24.857 & 15.22 & 29.244 & 14.553 & 12.63 & 32 & 4.293 & 22254 \end{pmatrix}$$

$i := 1..10$

$$Mh22 := \begin{pmatrix} 3.008 & 3.007 & 55.47 & 41.32 & 24.45 & 37.72 & 15.124 & 13.954 & 16.634 & 13.983 & 12.16 & 21.67 & 4.318 & 11118 \\ 3.5 & 3.504 & 52.15 & 39.85 & 24.12 & 35.64 & 15.674 & 13.92 & 17.447 & 13.937 & 12.17 & 21.01 & 4.695 & 11106 \\ 4.005 & 4.009 & 50.18 & 39.35 & 24.68 & 34.82 & 16.34 & 13.892 & 18.428 & 13.913 & 12.18 & 21.65 & 4.374 & 11102 \\ 4.496 & 4.508 & 48.52 & 38.81 & 24.98 & 34.05 & 17.092 & 13.867 & 19.526 & 13.888 & 12.24 & 21.81 & 4.327 & 11096 \\ 5.007 & 5.01 & 47.05 & 38.27 & 25.14 & 33.35 & 17.98 & 13.846 & 20.757 & 13.866 & 12.24 & 21.96 & 4.323 & 11090 \\ 5.512 & 5.519 & 45.8 & 37.77 & 25.24 & 32.73 & 18.965 & 13.832 & 22.151 & 13.859 & 12.28 & 22.03 & 4.309 & 11080 \\ 6.013 & 6.019 & 44.48 & 37.06 & 25.04 & 31.92 & 20.015 & 13.82 & 23.665 & 13.847 & 12.32 & 21.73 & 4.479 & 11074 \\ 6.51 & 6.504 & 43.7 & 36.77 & 25.18 & 31.59 & 21.134 & 13.817 & 25.256 & 13.85 & 12.43 & 21.88 & 4.5 & 11074 \\ 7.008 & 6.993 & 42.3 & 35.82 & 24.58 & 30.57 & 22.384 & 13.821 & 26.963 & 13.857 & 12.3 & 21.29 & 4.766 & 11065 \end{pmatrix}$$

$i2 := 1..9$

$$Mi22 := \begin{pmatrix} 3.016 & 3.017 & 21.46 & 20.76 & 20.48 & 20.76 & 15.414 & 14.258 & 16.91 & 14.239 & 20.24 & 20.44 & 4.507 & 0 \\ 3.498 & 3.504 & 17.45 & 16.42 & 15.72 & 16.35 & 15.978 & 14.23 & 17.692 & 14.186 & 14.86 & 15.51 & 4.471 & 0 \\ 3.994 & 3.997 & 15.8 & 14.98 & 14.68 & 15.07 & 16.661 & 14.206 & 18.676 & 14.154 & 14.16 & 14.57 & 4.494 & 0 \\ 4.509 & 4.501 & 15.15 & 14.35 & 14.1 & 14.46 & 17.483 & 14.186 & 19.799 & 14.121 & 13.55 & 13.98 & 4.463 & 0 \\ 5.012 & 4.999 & 14.48 & 13.7 & 13.48 & 13.83 & 18.399 & 14.172 & 21.048 & 14.099 & 12.92 & 13.34 & 4.487 & 0 \\ 5.507 & 5.502 & 14.12 & 13.36 & 13.19 & 13.51 & 19.391 & 14.161 & 22.448 & 14.084 & 12.64 & 13.05 & 4.488 & 0 \\ 6.004 & 6 & 14.03 & 13.29 & 13.14 & 13.45 & 20.444 & 14.143 & 23.954 & 14.066 & 12.58 & 13 & 4.493 & 0 \\ 6.507 & 6.505 & 14.1 & 13.36 & 13.2 & 13.5 & 21.603 & 14.138 & 25.628 & 14.064 & 12.58 & 13.04 & 4.485 & 0 \\ 6.993 & 6.997 & 14.11 & 13.38 & 13.2 & 13.51 & 22.844 & 14.146 & 27.393 & 14.083 & 12.51 & 13.02 & 4.488 & 0 \end{pmatrix}$$

$i3 := 1..9$

Now listing experimentally determined hose pressure drops. The values correspond to the closest nominal flow rates in the experimental heat exchanger data. First column is for raw hot side pressure drop and second column is for the raw cold side pressure drop

(1) is full
power
2 half power
3 isothermal

$$Mhosedrop := \begin{pmatrix} -0.318 & 0.363 \\ -0.212 & 0.47 \\ -0.101 & 0.618 \\ 0.029 & 0.755 \\ 0.225 & 0.895 \\ 0.39 & 1.052 \\ 0.553 & 1.207 \\ 0.746 & 1.391 \\ 0.948 & 1.584 \\ 1.17 & 1.787 \end{pmatrix} \qquad Mhosedrop2 := \begin{pmatrix} -0.318 & 0.363 \\ -0.212 & 0.47 \\ -0.101 & 0.618 \\ 0.029 & 0.755 \\ 0.225 & 0.895 \\ 0.39 & 1.052 \\ 0.553 & 1.207 \\ 0.746 & 1.391 \\ 0.948 & 1.584 \end{pmatrix}$$

half power and isothermal share same flow rates

Now creating additional matrixes to calculate perturbations in the data due to measurement
uncertainties

Uclflowmeter1 := 1.0034 Uhlflowmeter1 := 1.0052

Uclflowmeter2 := .9966 Uhlflowmeter2 := 0.9948

maximum heat transfer error matrices

$Mf2err_{i,1} := Mf22_{i,1} \cdot Uhlflowmeter2$ $Mf2err_{i,2} := Mf22_{i,2} \cdot Uclflowmeter1$

T1i value T1o value

$Mf2err_{i,3} := Mf22_{i,3} + -.16$ $Mf2err_{i,4} := Mf22_{i,4} + .16$

T2i value T2o value

$Mf2err_{i,5} := Mf22_{i,5} + -.16$ $Mf2err_{i,6} := Mf22_{i,6} + -.16$

Hot loop raw pressure drop

$Mf2err_{i,7} := Mf22_{i,7}$ $Mf2err_{i,8} := Mf22_{i,8}$

Cold loop raw pressure drop

$Mf2err_{i,9} := Mf22_{i,9}$ $Mf2err_{i,10} := Mf22_{i,10}$

$Mf2err_{i,11} := Mf22_{i,11}$ $Mf2err_{i,12} := Mf22_{i,12}$

$Mf2err_{i,13} := Mf22_{i,13}$ $Mf2err_{i,14} := Mf22_{i,14}$

half power error matrices

Now defining property values from matrixes

$Q1(Mf,i) := Mf_{i,1} \cdot gpm$ $Q2(Mf,i) := Mf_{i,2} \cdot gpm$ $Q3(Mf,i) := Mf_{i,13} \cdot gpm$

$T1i(Mf,i) := Mf_{i,3} \cdot °C - .73 °C$ $T2i(Mf,i) := Mf_{i,5} \cdot °C - .02 °C$

$T1o(Mf,i) := Mf_{i,4} \cdot °C - .21 °C$ $T2o(Mf,i) := Mf_{i,6} \cdot °C - .10 °C$

$$T3i(Mf,i) := Mf_{i,11}\,°C \qquad T3o(Mf,i) := Mf_{i,12}\,°C$$

$$tavg1(Mf,i) := \frac{\left(Mf_{i,3} - .73\right) + \left(Mf_{i,4} - .21\right)}{2} \qquad tavg2(Mf,i) := \frac{\left(Mf_{i,5} - .02\right) + \left(Mf_{i,6} - .1\right)}{2}$$

$$tavg3(Mf,i) := \frac{Mf_{i,9} + Mf_{i,10}}{2}$$

Now listing experimentally determined offsets for temperature difference and pressure

$$\Delta Photooffset := .54$$

$$\Delta Pcoldoffset := -.1$$

Considering the offset of ΔP

$$\Delta P1(Mf,i) := \left[\left(Mf_{i,7} - Mf_{i,8}\right) + \Delta Photooffset\right]\cdot psi$$

$$\Delta P2(Mf,i) := \left[\left(Mf_{i,9} - Mf_{i,10}\right) + \Delta Pcoldoffset\right]\cdot psi$$

Now calculating NTU relationships

$$C1(Mf,i) := \rho_1(tavg1(Mf,i))\cdot Q1(Mf,i)\cdot c_{p1}(tavg1(Mf,i))$$

$$C2(Mf,i) := \rho_2(tavg2(Mf,i))\cdot Q2(Mf,i)\cdot c_{p2}(tavg2(Mf,i))$$

$$Cmin(Mf,i) := \min(C1(Mf,i), C2(Mf,i)) \qquad Cmax(Mf,i) := \max(C1(Mf,i), C2(Mf,i))$$

$$Cr(Mf,i) := \frac{Cmin(Mf,i)}{Cmax(Mf,i)}$$

$$\varepsilon(Mf,i) := \frac{C1(Mf,i)\cdot(T1i(Mf,i) - T1o(Mf,i))}{Cmin(Mf,i)\cdot(T1i(Mf,i) - T2i(Mf,i) + 0)}$$

$$NTU(Mf,i) := \frac{1}{1 - Cr(Mf,i)}\cdot\ln\left(\frac{1 - \varepsilon(Mf,i)\cdot Cr(Mf,i)}{1 - \varepsilon(Mf,i)}\right)$$

$$U2(Mf,i) := \frac{NTU(Mf,i)\cdot Cmin(Mf,i)}{A_2}$$

$$h(Mf,i) := \frac{U2(Mf,i)\cdot\left(\frac{A_2}{A_1} + 1\right)}{1 - \frac{U2(Mf,i)\cdot\delta}{k_w}}$$

This section calculates values from the data, friction factor, reynolds, colburn, etc.

$$G1(Mf,i) := \frac{\rho_1(tavg1(Mf,i))\cdot Q1(Mf,i)}{A_{c1}} \qquad G2(Mf,i) := \frac{\rho_2(tavg2(Mf,i))\cdot Q2(Mf,i)}{A_{c2}}$$

$$Gp1(Mf,i) := \frac{4\cdot\rho_1(tavg1(Mf,i))\cdot Q1(Mf,i)}{\pi\cdot D_p^{\,2}} \qquad Gp2(Mf,i) := \frac{4\cdot\rho_2(tavg2(Mf,i))\cdot Q2(Mf,i)}{\pi\cdot D_p^{\,2}}$$

$$j1(Mf,i) := \frac{h(Mf,i)\cdot Pr_1(tavg1(Mf,i))^{\frac{2}{3}}}{G1(Mf,i)\cdot c_{p1}(tavg1(Mf,i))} \qquad j2(Mf,i) := \frac{h(Mf,i)\cdot Pr_2(tavg2(Mf,i))^{\frac{2}{3}}}{G2(Mf,i)\cdot c_{p2}(tavg2(Mf,i))}$$

The various friction factors calculated below represent different corrections applied. f1 is the basic form used to calculate the friction factor, while the hose designations have the experimental hose pressure drop subtracted from them. The h designation at the end is used to distinguish between the various runs with different numbers of flow rate sets.

$$f1(Mf,i) := \left[\Delta P1(Mf,i) - \frac{1.5\cdot(Gp1(Mf,i))^2}{2\cdot\rho_1(tavg1(Mf,i))}\right]\cdot\frac{D_h\cdot\rho_1(tavg1(Mf,i))}{2\cdot L_p\cdot G1(Mf,i)^2}$$

$$flwithhosef(Mf,i) := \left[\left[\Delta P1(Mf,i) - \left(Mhosedrop_{i,1} + \Delta Photooffset\right)\cdot psi\right] - \frac{1.5\cdot(Gp1(Mf,i))^2}{2\cdot\rho_1(tavg1(Mf,i))}\right]\cdot\frac{D_h\cdot\rho_1(tavg1(Mf,i))}{2\cdot L_p\cdot G1(Mf,i)^2}$$

$$f2(Mf,i) := \left[\Delta P2(Mf,1) - \frac{1.5\cdot(Gp2(Mf,i))^2}{2\cdot\rho_2(tavg2(Mf,i))}\right]\cdot\frac{D_h\cdot\rho_2(tavg2(Mf,i))}{2\cdot L_p\cdot G2(Mf,i)^2}$$

$$f2withhose(Mf,i) := \left[\left[\Delta P1(Mf,i) - \left(Mhosedrop_{i,2} + \Delta Pcoldoffset\right)\cdot psi\right] - \frac{1.5\cdot(Gp1(Mf,i))^2}{2\cdot\rho_1(tavg1(Mf,i))}\right]\cdot\frac{D_h\cdot\rho_1(tavg1(Mf,i))}{2\cdot L_p\cdot G1(Mf,i)^2}$$

$$flwithhoseh(Mf,i) := \left[\left[\Delta P1(Mf,i) - \left(Mhosedrop2_{i,1} + \Delta Photooffset\right)\cdot psi\right] - \frac{1.5\cdot(Gp1(Mf,i))^2}{2\cdot\rho_1(tavg1(Mf,i))}\right]\cdot\frac{D_h\cdot\rho_1(tavg1(Mf,i))}{2\cdot L_p\cdot G1(Mf,i)^2}$$

$$Re1(Mf,i) := \frac{G1(Mf,i)\cdot D_h}{\mu_1(tavg1(Mf,i))} \qquad Re2(Mf,i) := \frac{G2(Mf,i)\cdot D_h}{\mu_2(tavg2(Mf,i))}$$

$$Nu1(Mf,i) := \frac{h(Mf,i)\cdot L_p}{k_w}$$

Now calculating values from martin correlation

$$Nu_1(Q1) := \frac{h_1(Q1)\cdot L_p}{k_w}$$

$$Q_w := 1gpm, 1.02gpm .. 15gpm$$

Full power values

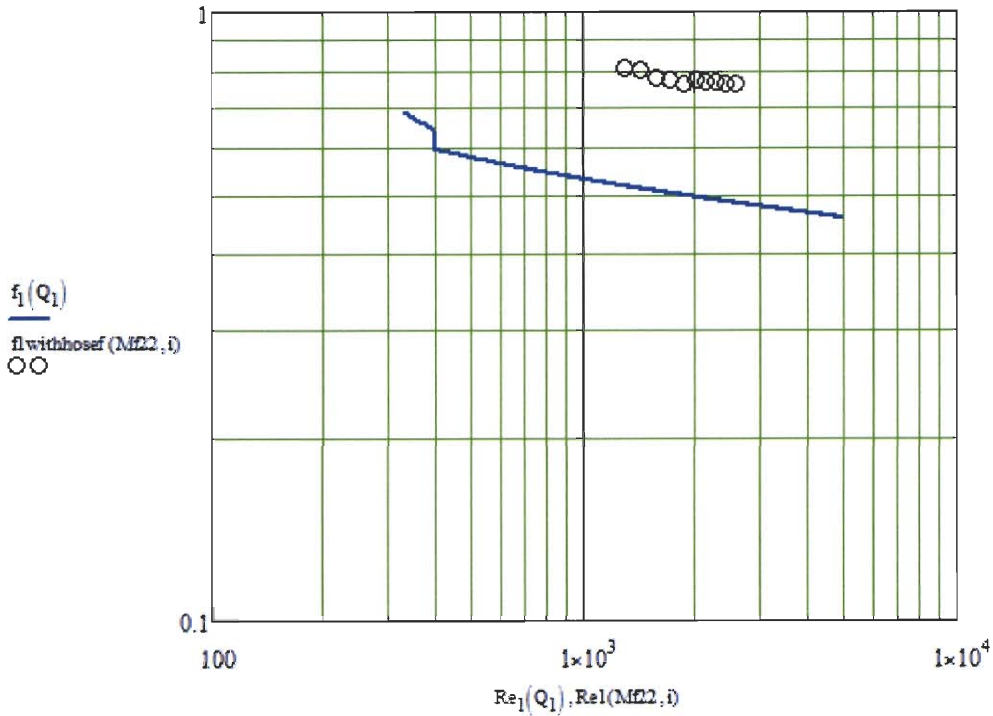


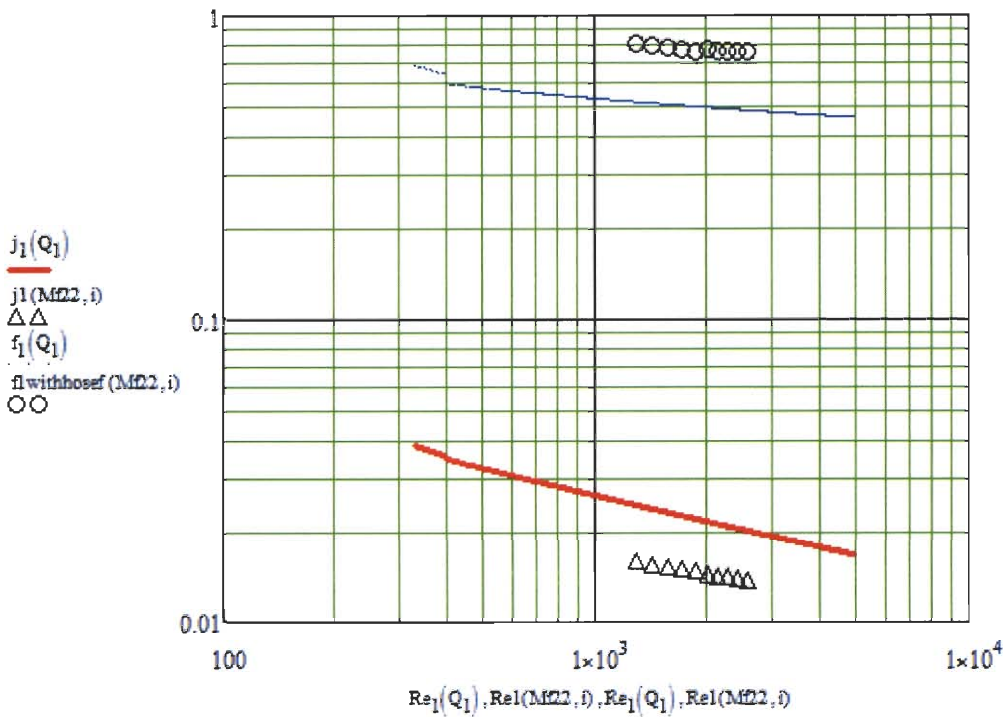

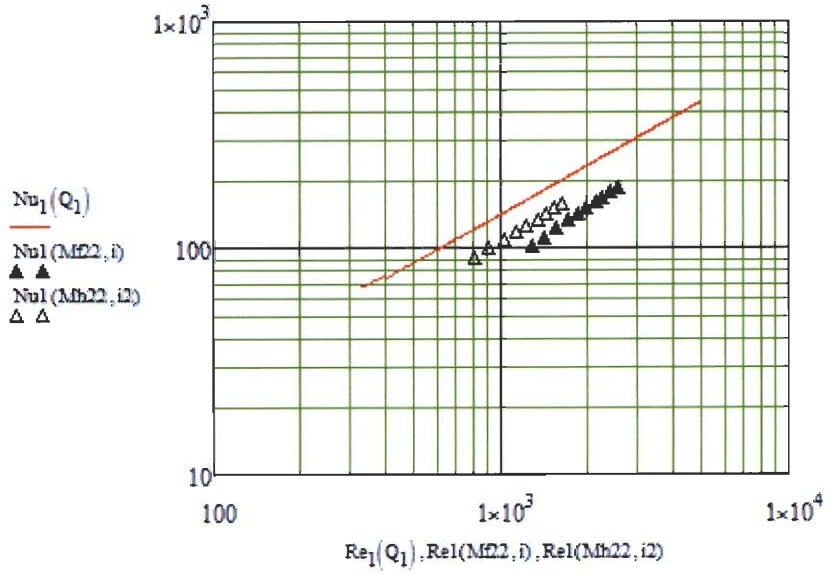


half power values

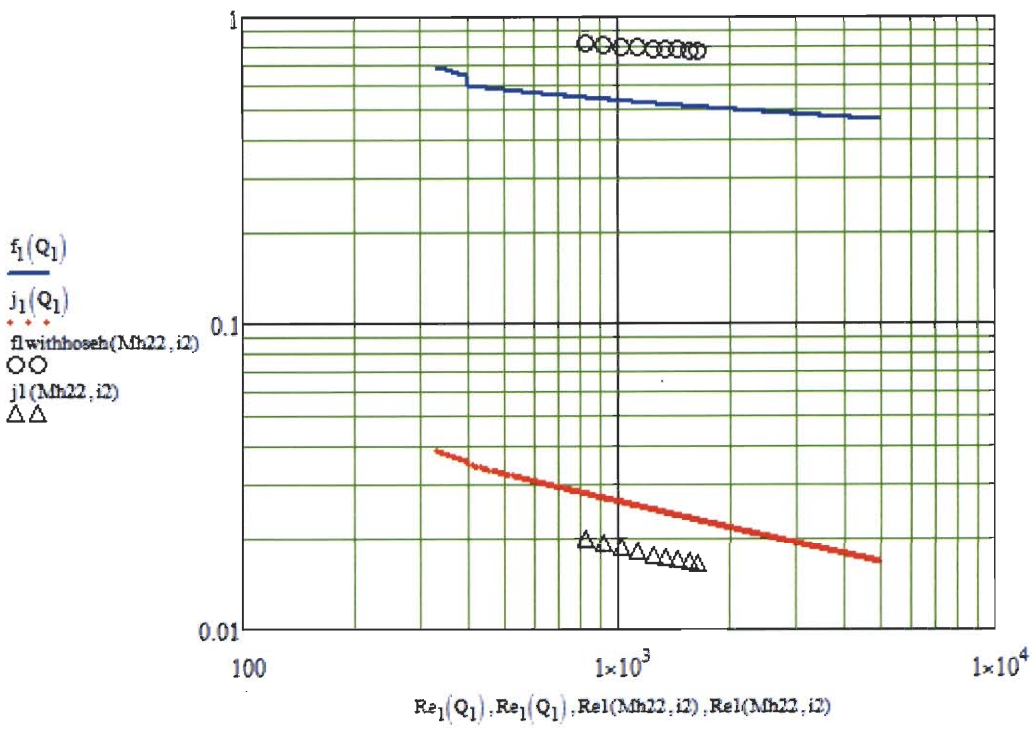

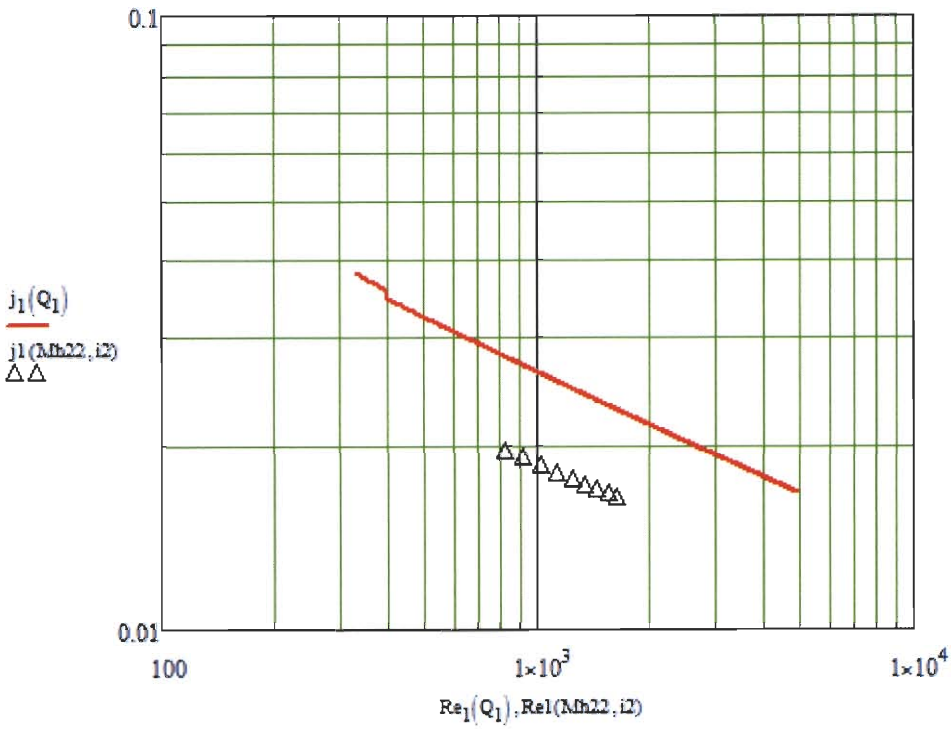


Isothermal pressure

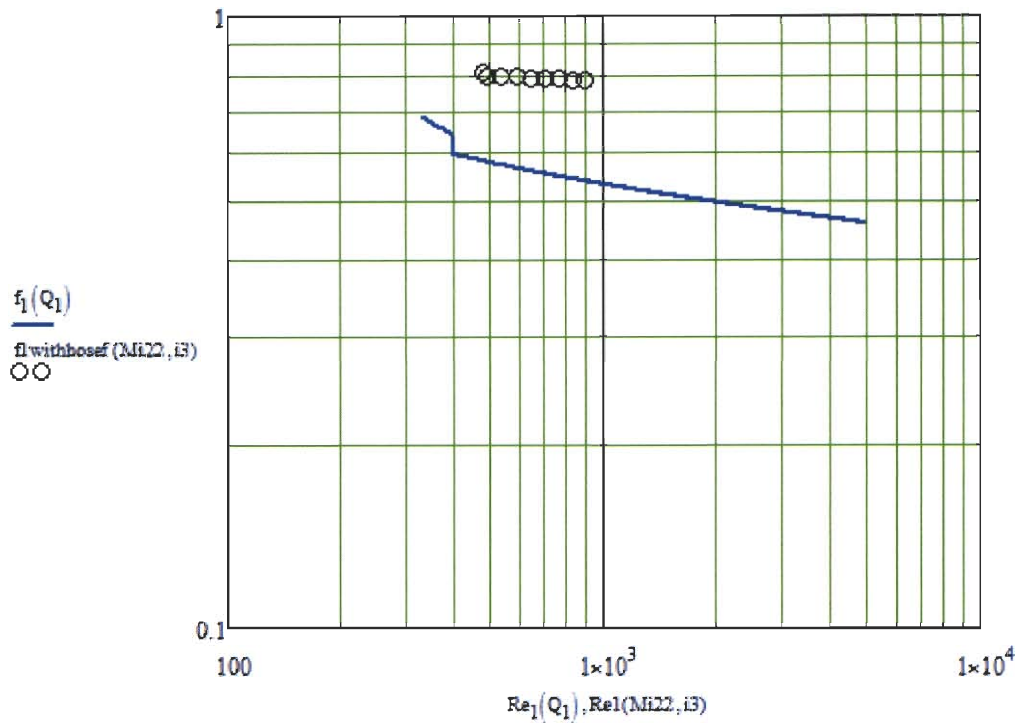

Now what follow is a calculation of the associated error for heat transfer, reynolds number, convection coefficient and friction factors

$$\Delta Tcityoffset := 0$$

$$\Delta T1(Mf, i) := T1i(Mf, i) - T1o(Mf, i)$$

$$\Delta T2(Mf, i) := T2o(Mf, i) - T2i(Mf, i)$$

$$\Delta T3(Mf, i) := T3o(Mf, i) - T3i(Mf, i)$$

$$mmdot1(Mf, i) := Q1(Mf, i) \cdot \rho_1(tavg1(Mf, i))$$

$$mmdot2(Mf, i) := Q2(Mf, i) \cdot \rho_2(tavg2(Mf, i))$$

$$mmdot3(Mf, i) := Q3(Mf, i) \cdot \rho_3(tavg3(Mf, i))$$

$$Qheat1(Mf, i) := mmdot1(Mf, i) \cdot c_{p1}(tavg1(Mf, i)) \cdot \Delta T1(Mf, i)$$

$$Qheat2(Mf, i) := mmdot2(Mf, i) \cdot c_{p2}(tavg2(Mf, i)) \cdot \Delta T2(Mf, i)$$

$$Qheat3(Mf, i) := mmdot3(Mf, i) \cdot c_{p3}(tavg3(Mf, i)) \cdot \Delta T3(Mf, i)$$

$$Qheatelectric(Mf, i) := Mf_{i, 14} \cdot W$$

$$Qhxmin(Mf, i) := \min(Qheat1(Mf, i), Qheat2(Mf, i))$$

$$Qhxmax(Mf, i) := \max(Qheat1(Mf, i), Qheat2(Mf, i))$$

$$Qhxavg(Mf, i) := \frac{Qheat1(Mf, 1) + Qheat2(Mf, i)}{2}$$

$$Qdiffhotvscold(Mf, i) := \frac{Qhxmax(Mf, i) - Qhxmin(Mf, i)}{Qhxmin(Mf, i)} \cdot 100$$

$$Qdiffhot(Mf, i) := \frac{Qheat1(Mf, i) - Qhxavg(Mf, i)}{Qhxavg(Mf, i)} \cdot 100$$

$$Qdiffcold(Mf, i) := \frac{Qheat2(Mf, i) - Qhxavg(Mf, i)}{Qhxavg(Mf, i)} \cdot 100$$

$$Qhxavgvselectric(Mf, i) := \frac{Qheatelectric(Mf, i) - Qhxavg(Mf, i)}{Qhxavg(Mf, i)} \cdot 100$$

$$Qhxavgvscity(Mf, i) := \frac{Qheat3(Mf, i) - Qhxavg(Mf, i)}{Qhxavg(Mf, i)} \cdot 100$$

Qdiffhotvscold represents comparison between the min and maximum experimental data. Qdiff hot and cold represent the heat transfer differences using the method used by muley and manglik 1999 asme paper.

Qdiffhot(Mf22, i) =

| |
|---|
| 1.0132 |
| 0.7778 |
| 1.3352 |
| 1.577 |
| 1.506 |
| 0.7629 |
| 1.0701 |
| 0.9713 |
| 0.9986 |
| 1.155 |

Qdiffhot(Mh22, i2) =

| |
|---|
| 1.3734 |
| 1.4828 |
| 1.3713 |
| 1.2279 |
| 1.1022 |
| 1.0158 |
| 1.2318 |
| 1.5327 |
| 1.456 |

Qdiffcold(Mf22, i) =

| |
|---|
| -1.0132 |
| -0.6811 |
| -0.0138 |
| 0.0402 |
| 0.2137 |
| 0.3477 |
| 0.5503 |
| 0.7025 |
| 0.7319 |
| 0.8408 |

Qdiffcold(Mh22, i2) =

| |
|---|
| -1.3734 |
| -0.8236 |
| -0.5171 |
| -0.2705 |
| -0.0147 |
| 0.191 |
| 0.24 |
| 0.5352 |
| 0.7404 |

Qhxavgvscity(Mf22, i) =

| |
|---|
| 2.5049 |
| 3.1214 |
| 2.8518 |
| 3.3536 |
| 3.024 |
| 3.2001 |
| 3.039 |
| 2.3682 |
| 2.9665 |
| 3.1252 |

Qhxavgvselectric(Mf22, i) =

| |
|---|
| 7.1054 |
| 6.7342 |
| 5.9698 |
| 5.9078 |
| 5.6672 |
| 5.4544 |
| 5.1221 |
| 4.9235 |
| 4.817 |
| 4.7068 |

Qdiffhotvscold(Mf22, i) =

| |
|---|
| 2.0471 |
| 1.4689 |
| 1.3492 |
| 1.5361 |
| 1.2895 |
| 0.4137 |
| 0.5169 |
| 0.267 |
| 0.2648 |
| 0.3116 |

Appendix B

MATHCAD for Fg3x8-14

GEA Fg3x8-14

**MathCAD format solution:**

## Test Heat Exchanger Fg3x8-14

Hot and cold water properties at Tf

$T_{hot\_water} := 50\,°C$ $T_{cold\_water} := 40\,°C$

Hot water (subscript 1) Cold water (subscript 2)

$\rho_1 := 985\frac{kg}{m^3}$ $\rho_2 := 994\frac{kg}{m^3}$

$c_{p1} := 4184\frac{J}{kg \cdot K}$ $c_{p2} := 4178\frac{J}{kg \cdot K}$

$k_1 := 0.639\frac{W}{m \cdot K}$ $k_2 := 0.628\frac{W}{m \cdot K}$

$\mu_1 := 471 \cdot 10^{-6}\frac{N \cdot s}{m^2}$ $\mu_2 := 654 \cdot 10^{-6}\frac{N \cdot s}{m^2}$

$Pr_1 := 3.02$ $Pr_2 := 4.34$

Thermal conductivity of the plate (Stainless Steel AISI 316)

$k_w := 13.4\frac{W}{m \cdot K}$

**Given information**

Volume flow rates for hot and cold water

$Q_1 := 10gpm$ $Q_2 := 10gpm$

Mass flow rates

$mdot_1(Q_1) := \rho_1 \cdot Q_1$ $mdot_1(Q_1) = 0.6214\frac{kg}{s}$

$mdot_2(Q_2) := \rho_2 \cdot Q_2$ $mdot_2(Q_2) = 0.6271\frac{kg}{s}$

**Geometric parameters:**

$N_p := 1$ Number of passes

$\beta := 60deg$ Corrugation inclination angle (chevron angle)

$N_t := 14$ Total number of plates

$D_p := \frac{3}{4}in$ Port diameter

$t_n := 0.087in$ spacing between plates

$\alpha := 40deg$ Corrugation Pitch angle

$\lambda := t_n \cdot \tan(\alpha)$ Corrugation Pitch (=wavelengtht) $\lambda = 0.073 \cdot in$

$\delta := 0.6mm$ Thickness of the plates

Use the dimensions of the test heat exchanger

$W_p := 3in$ $L_{p2p} := 7.2in$ $L_p := L_{p2p} - 1in$ $L_p = 6.2 \cdot in$

$H_p := t_n \cdot N_t$ $H_p = 1.218 \cdot in$

Number of wavelength per single plate

$$N_\lambda := \frac{W_p}{\lambda}$$

Number of channels for hot and cold fluid

$$N_{c1} := \frac{N_t}{2N_p} \qquad N_{c1} = 7$$

$$N_{c2} := \frac{N_t}{2N_p} - 1 \qquad N_{c2} = 6$$

Amplitude of corrugation and channel spacing

$$a := \frac{1}{2}\left(\frac{H_p}{N_t} - \delta\right) \qquad a = 0.0317 \cdot in \qquad 2 \cdot a = 0.0634 \cdot in \qquad 2 \cdot a - \delta = 0.087 \cdot in$$

Corrugation ratio γ

$\gamma := 4\cdot\frac{a}{\lambda}$ $\gamma = 1.7363$

Corrugated length

$$L_\lambda := \int_0^\lambda \sqrt{1 + \left(\frac{2\cdot\pi\cdot a}{\lambda}\right)^2 \cdot \cos\left(\frac{2\cdot\pi}{\lambda}\cdot x\right)^2}\, dx$$

Heat transfer area for hot fluid (fluid1)

$A_1 := 2\cdot L_\lambda \cdot N_\lambda \cdot L_p \cdot N_{c1}$ $A_1 = 0.3478\,m^2$

$A_2 := 2\cdot L_\lambda \cdot N_\lambda \cdot L_p \cdot N_{c2}$ $A_2 = 0.2982\,m^2$

Now setting the heat transfer area equal to the minimum area, which is A2

$A_{hx} := A_2$

Projected area for the plates

$A_{p1} := 2\cdot W_p \cdot L_p \cdot N_{c1}$ $A_{p2} := 2\cdot W_p \cdot L_p \cdot N_{c2}$

**Enlargement factor φ**

$\Phi := \frac{L_\lambda \cdot N_\lambda}{W_p}$ $\Phi = 2.0705$

Exact hydraulic diameter

$D_h := \frac{4\cdot a}{\Phi}$ $D_h = 1.555\,mm$

Surface area

$\beta_1 := \frac{A_1}{W_p \cdot 2\cdot a \cdot L_p \cdot N_{c1}}$ $\beta_1 = 2.2049 \times 10^3 \frac{1}{m}$

Minimum free-flow area

$A_{c1} := 2\cdot a \cdot W_p \cdot N_{c1}$ $A_{c1} = 1.3309\,in^2$

$A_{c2} := 2\cdot a \cdot W_p \cdot N_{c2}$ $A_{c2} = 1.1408\,in^2$

Mass velocity

$G_1(Q_1) := \frac{mdot_1(Q_1)}{A_{c1}}$ $v_1 := \frac{G_1(Q_1)}{\rho_1} = 0.7347\,\frac{m}{s}$

$Re_1(Q_1) := \frac{G_1(Q_1)\cdot D_h}{\mu_1}$ $Re_1(Q_1) = 2.3893 \times 10^3$

$$G_2(Q_2) := \frac{mdot_2(Q_2)}{A_{c2}} \qquad v_2 := \frac{G_2(Q_2)}{\rho_2} = 0.8572\frac{m}{s}$$

$$Re_2(Q_2) := \frac{G_2(Q_2)\cdot D_h}{\mu_2} \qquad Re_2(Q_2) = 2.0259 \times 10^3$$

**Friction factors**

Martin's correlation (1996) for the Darcy friction factor is modified by the Fanning friction factor.

Martin, H., 1996, A theoretical approach to predict the performance of chevron-type plate heat exchanger, Chem. Eng. Processing, Vol.35, pp. 301-310.

$$f_{o1}(Q_1) := \begin{cases} \left(1.56\cdot\ln(Re_1(Q_1)) - 3.0\right)^{-2} & \text{if } Re_1(Q_1) \geq 400 \\ \dfrac{16}{Re_1(Q_1)} & \text{otherwise} \end{cases}$$

$$f_{o2}(Q_2) := \begin{cases} \left(1.56\cdot\ln(Re_2(Q_2)) - 3.0\right)^{-2} & \text{if } Re_2(Q_2) \geq 400 \\ \dfrac{16}{Re_2(Q_2)} & \text{otherwise} \end{cases}$$

$$f_{m1}(Q_1) := \begin{cases} \dfrac{9.75}{Re_1(Q_1)^{0.289}} & \text{if } Re_1(Q_1) \geq 400 \\ \dfrac{149.25}{Re_1(Q_1)} + 0.9625 & \text{otherwise} \end{cases}$$

$$f_{m2}(Q_2) := \begin{cases} \dfrac{9.75}{Re_2(Q_2)^{0.289}} & \text{if } Re_2(Q_2) \geq 400 \\ \dfrac{149.25}{Re_2(Q_2)} + 0.9625 & \text{otherwise} \end{cases}$$

$$f_1(Q_1) := \left[\frac{\cos(\beta)}{\left(0.045\cdot\tan(\beta) + 0.09\cdot\sin(\beta) + \dfrac{f_{o1}(Q_1)}{\cos(\beta)}\right)^{0.5}} + \left(\frac{1 - \cos(\beta)}{\sqrt{3.8\cdot f_{m1}(Q_1)}}\right)\right]^{-2}$$

$$f_1(Q_1) = 0.4878$$

$$f_2(Q_2) := \left[ \frac{\cos(\beta)}{\left(0.045\cdot\tan(\beta) + 0.09\cdot\sin(\beta) + \frac{f_{o2}(Q_2)}{\cos(\beta)}\right)^{0.5}} + \left( \frac{1-\cos(\beta)}{\sqrt{3.8\cdot f_{m2}(Q_2)}} \right) \right]^{-2}$$

$$f_2(Q_2) = 0.4951$$

Heat transfer coefficients

$$h_1(Q_1) := \frac{k_1}{D_h}\cdot\left[0.205\cdot Pr_1^{\frac{1}{3}}\cdot 1^{\frac{1}{6}}\cdot\left(f_1(Q_1)\cdot Re_1(Q_1)^2\cdot\sin(2\cdot\beta)\right)^{0.374}\right]$$

$$h_1(Q_1) = 2.9684\times 10^4\cdot\frac{W}{m^2\cdot K}$$

$$h_2(Q_2) := \frac{k_2}{D_h}\cdot\left[0.205\cdot Pr_2^{\frac{1}{3}}\cdot 1^{\frac{1}{6}}\cdot\left(f_2(Q_2)\cdot Re_2(Q_2)^2\cdot\sin(2\cdot\beta)\right)^{0.374}\right]$$

$$h_2(Q_2) = 2.926\times 10^4\cdot\frac{W}{m^2\cdot K}$$

Overall heat teansfer coefficient

$$U_2(Q_1,Q_2) := \frac{1}{\frac{A_2}{h_1(Q_1)\cdot A_1} + \frac{\delta}{k_w} + \frac{1}{h_2(Q_2)}}$$

$$U_2(Q_1,Q_2) = 8.8778\times 10^3\cdot\frac{W}{m^2 K}$$

$$U_2(Q_1,Q_2)\cdot A_2 = 2.6469\times 10^3\cdot\frac{W}{K}$$

**Effectiveness-NTU Method**

$$C_1(Q_1) := mdot_1(Q_1)\cdot c_{p1} \qquad C_1(Q_1) = 2.6001\times 10^3\,\frac{m^2\cdot kg}{K\cdot s^3}$$

$$C_2(Q_2) := mdot_2(Q_2)\cdot c_{p2} \qquad C_2(Q_2) = 2.6201\times 10^3\,\frac{m^2\cdot kg}{K\cdot s^3}$$

$$C_{min}(Q_1, Q_2) := \min(C_1(Q_1), C_2(Q_2)) \qquad C_{min}(Q_1, Q_2) = 2.6001 \times 10^3 \frac{m^2 \cdot kg}{K \cdot s^3}$$

$$C_{max}(Q_1, Q_2) := \max(C_1(Q_1), C_2(Q_2)) \qquad C_{max}(Q_1, Q_2) = 2.6201 \times 10^3 \frac{m^2 \cdot kg}{K \cdot s^3}$$

$$C_r(Q_1, Q_2) := \frac{C_{min}(Q_1, Q_2)}{C_{max}(Q_1, Q_2)} \qquad C_r(Q_1, Q_2) = 0.9924$$

$$NTU(Q_1, Q_2) := \frac{U_2(Q_1, Q_2) \cdot A_2}{C_{min}(Q_1, Q_2)} \qquad NTU(Q_1, Q_2) = 1.018$$

Counterflow effectiveness

$$\varepsilon_{PHE}(Q_1, Q_2) := \frac{1 - \exp\left[-NTU(Q_1, Q_2) \cdot (1 - C_r(Q_1, Q_2))\right]}{1 - C_r(Q_1, Q_2) \cdot \exp\left[-NTU(Q_1, Q_2) \cdot (1 - C_r(Q_1, Q_2))\right]}$$

$$\varepsilon_{PHE}(Q_1, Q_2) = 0.5054$$

$Q_m := 1gpm, 2gpm .. 15gpm$

GBM 108

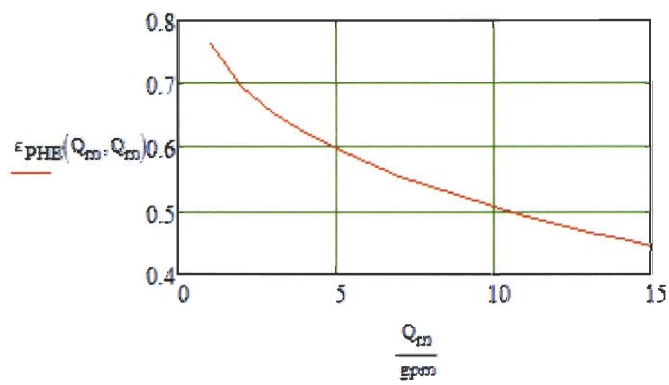


Heat transfer rate for the PHE

$$q(T_{1i}, T_{2i}, Q_1, Q_2) := \varepsilon_{PHE}(Q_1, Q_2) \cdot C_{min}(Q_1, Q_2) \cdot (T_{1i} - T_{2i})$$

Since $$\varepsilon_{PHE} = \frac{C_1 \cdot (T_{1i} - T_{1o})}{C_{min} \cdot (T_{1i} - T_{2i})} = \frac{C_2 \cdot (T_{2o} - T_{2i})}{C_{min} \cdot (T_{1i} - T_{2i})}$$

$$T_{1o}(T_{1i}, T_{2i}, Q_1, Q_2) := T_{1i} - \varepsilon_{PHE}(Q_1, Q_2) \cdot \frac{C_{min}(Q_1, Q_2)}{C_1(Q_1)} \cdot (T_{1i} - T_{2i})$$

$$T_{2o}(T_{1i}, T_{2i}, Q_1, Q_2) := T_{2i} - \varepsilon_{PHE}(Q_1, Q_2) \cdot \frac{C_{min}(Q_1, Q_2)}{C_2(Q_2)} \cdot (T_{1i} - T_{2i})$$

$$j_1(Q_1) := \frac{h_1(Q_1) \cdot Pr_1^{\frac{2}{3}}}{G_1(Q_1) \cdot c_{p1}}$$

$T_{1i} := 70\,°C$ $T_{2i} := 30\,°C$

$Q_m := 0.1gpm, 0.11gpm .. 12gpm$

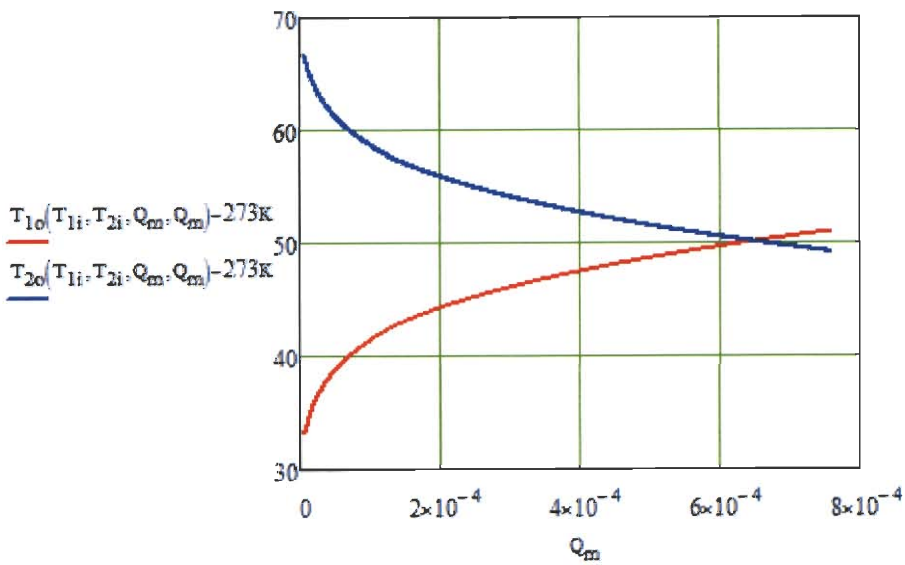


**Pressure Drop**

The frictional channel pressure drop

$$\Delta P_{fl}(Q_1) := \frac{2 \cdot f_1(Q_1) \cdot L_p}{D_h} \cdot \frac{G_1(Q_1)^2}{\rho_1} \cdot N_p \qquad \Delta P_{fl}(Q_1) = 7.6203 \cdot psi$$

$$\Delta P_{fl}(Q_2) := \frac{2 \cdot f_2(Q_2) \cdot L_p}{D_h} \cdot \frac{G_2(Q_2)^2}{\rho_2} \cdot N_p \qquad \Delta P_{fl}(Q_2) = 10.6228 \cdot psi$$

The connection and port pressure drop

$$G_{p1}(Q_1) := \frac{4 \cdot mdot_1(Q_1)}{\pi \cdot D_p^{\,2}} \qquad G_{p1}(Q_1) = 2.1803 \times 10^{3}\ \frac{kg}{m^2 \cdot s}$$

$$G_{p2}(Q_2) := \frac{4 \cdot mdot_2(Q_2)}{\pi \cdot D_p^{\,2}}$$

$$\Delta P_{p1}(Q_1) := 1.5 \cdot N_p \cdot \frac{G_{p1}(Q_1)^2}{2 \cdot \rho_1} \qquad \Delta P_{p1}(Q_1) = 0.525 \cdot psi$$

$$\Delta P_{p2}(Q_2) := 1.5 \cdot N_p \cdot \frac{G_{p2}(Q_2)^2}{2 \cdot \rho_2} \qquad \Delta P_{p2}(Q_2) = 0.5298 \cdot psi$$

$$\Delta P_1(Q_1) := \Delta P_{f1}(Q_1) + \Delta P_{p1}(Q_1) \qquad \Delta P_1(Q_1) = 8.1453 \cdot psi$$

$$\Delta P_2(Q_2) := \Delta P_{f2}(Q_2) + \Delta P_{p2}(Q_2) \qquad \Delta P_2(Q_2) = 11.1526 \cdot psi$$

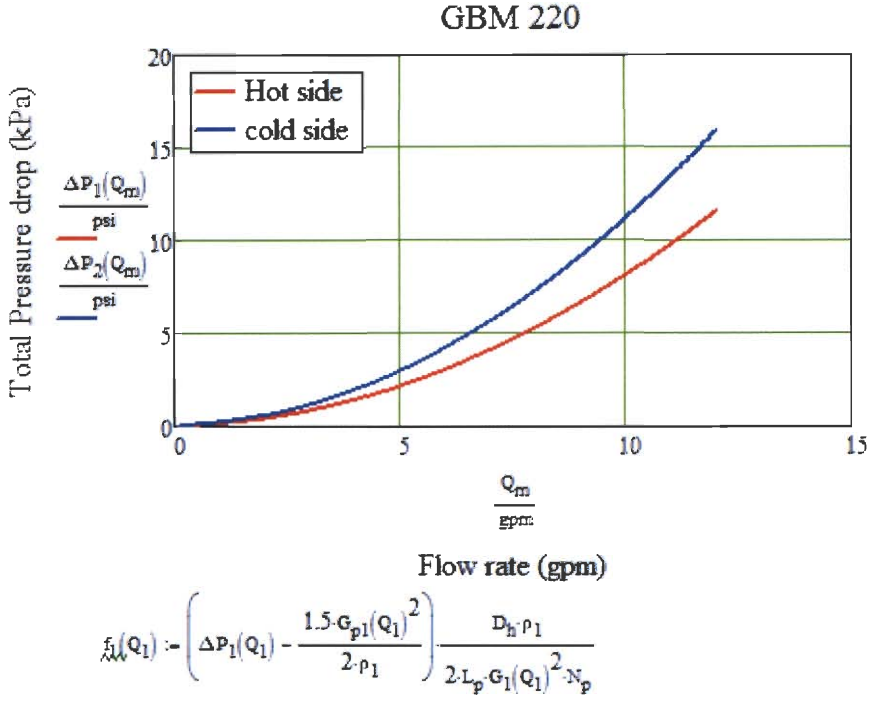


$$f_1(Q_1) := \left(\Delta P_1(Q_1) - \frac{1.5 \cdot G_{p1}(Q_1)^2}{2 \cdot \rho_1}\right) \cdot \frac{D_h \cdot \rho_1}{2 \cdot L_p \cdot G_1(Q_1)^2 \cdot N_p}$$

Experimental Data

ORIGIN := 1

$i := 1,2..10$

$M_{i,1} := i$

$$M_{i,2} := \frac{T_{1i} - 273K}{K}$$

$$M_{i,3} := \frac{T_{1o}(T_{1i}, T_{2i}, i\cdot gpm, i\cdot gpm) - 273.15K}{K}$$

$$M_{i,4} := \frac{T_{2i} - 273K}{K}$$

$$M_{i,5} := \frac{T_{2o}(T_{1i}, T_{2i}, i\cdot gpm, i\cdot gpm) - 273.15K}{K}$$

$$M_{i,6} := \frac{\Delta P_1(i\cdot gpm)}{psi} \qquad M_{i,7} := \frac{\Delta P_2(i\cdot gpm)}{psi}$$

Predictions

M =

| | 1 | 2 | 3 | 4 | 5 | 6 | 7 |
|---|---|---|---|---|---|---|---|
| 1 | 1 | 70.15 | 39.4647 | 30.15 | 60.3023 | 0.1271 | 0.1861 |
| 2 | 2 | 70.15 | 42.2945 | 30.15 | 57.4941 | 0.3827 | 0.5296 |
| 3 | 3 | 70.15 | 43.8669 | 30.15 | 55.9337 | 0.821 | 1.1316 |
| 4 | 4 | 70.15 | 45.1028 | 30.15 | 54.7072 | 1.416 | 1.9478 |
| 5 | 5 | 70.15 | 46.1367 | 30.15 | 53.6812 | 2.1648 | 2.9736 |
| 6 | 6 | 70.15 | 47.0321 | 30.15 | 52.7926 | 3.065 | 4.2059 |
| 7 | 7 | 70.15 | 47.8251 | 30.15 | 52.0057 | 4.1145 | 5.642 |
| 8 | 8 | 70.15 | 48.5383 | 30.15 | 51.2979 | 5.312 | 7.2797 |
| 9 | 9 | 70.15 | 49.1871 | 30.15 | 50.654 | 6.656 | 9.1171 |
| 10 | 10 | 70.15 | 49.7826 | 30.15 | 50.0631 | 8.1453 | 11.1526 |

Adding temperature dependent properties

Temperature dependent properties of water taken from table A.12 Thermal Design

temperature range of properties, in deg celsius

$$tx := \begin{pmatrix} 0 \\ 20 \\ 40 \\ 60 \\ 80 \\ 100 \end{pmatrix}$$

liquid density information, in kg/m3

$$dly := \begin{pmatrix} 1002 \\ 1000 \\ 994 \\ 985 \\ 974 \\ 960 \end{pmatrix}$$

$dly1 := dly$

$dls1 := lspline(tx, dly1)$

$\rho_1(t_{avg1}) := interp(dls1, tx, dly1, t_{avg1}) \cdot \frac{kg}{m^3}$

$dly2 := dly$

$dls2 := lspline(tx, dly2)$

$\rho_2(t_{avg2}) := interp(dls2, tx, dly2, t_{avg2}) \cdot \frac{kg}{m^3}$

$dly3 := dly$

$dls3 := lspline(tx, dly3)$

$\rho_3(t_{avg3}) := interp(dls3, tx, dly3, t_{avg3}) \cdot \frac{kg}{m^3}$

specific heat information, in J/(kg*K)

$$dcpy := \begin{pmatrix} 4217 \\ 4181 \\ 4178 \\ 4184 \\ 4196 \\ 4216 \end{pmatrix}$$

$dcp1 := dcpy$

$dcps1 := lspline(tx, dcp1)$

$c_{p1}(t_{avg1}) := interp(dcps1, tx, dcp1, t_{avg1}) \cdot \frac{J}{kg \cdot K}$

$dcp2 := dcpy$

$dcps2 := lspline(tx, dcp2)$

$c_{p2}(t_{avg2}) := interp(dcps2, tx, dcp2, t_{avg2}) \cdot \frac{J}{kg \cdot K}$

$dcp3 := dcpy$

$dcps3 := lspline(tx, dcp1)$

$c_{p3}(t_{avg3}) := interp(dcps3, tx, dcp3, t_{avg3}) \cdot \frac{J}{kg \cdot K}$

thermal conductivity information, in W/(m*K)

$$dky := \begin{pmatrix} .552 \\ .597 \\ .628 \\ .651 \\ .668 \\ .68 \end{pmatrix}$$

$dk1 := dky$

$dks1 := lspline(tx, dk1)$

$k_1(t_{avg1}) := interp(dks1, tx, dk1, t_{avg1}) \cdot \frac{W}{m \cdot K}$

$dk2 := dky$

$dks2 := lspline(tx, dk2)$

$k_2(t_{avg2}) := interp(dks2, tx, dk2, t_{avg2}) \frac{W}{m \cdot K}$

$dk3 := dky$

$dks3 := lspline(tx, dk3)$

$k_3(t_{avg3}) := interp(dks3, tx, dk3, t_{avg3}) \frac{W}{m \cdot K}$

absolute viscosity information, in N*s/m^2

$$dvsy := \begin{pmatrix} 1792 \\ 1006 \\ 654 \\ 471 \\ 355 \\ 288 \end{pmatrix}$$

$dv1 := dvsy$ $dv2 := dvsy$ $dv3 := dvsy$

$dvs1 := lspline(tx, dv1)$ $dvs2 := lspline(tx, dv2)$ $dvs3 := lspline(tx, dv3)$

$$\mu_1(t_{avg1}) := interp(dvs1, tx, dv1, t_{avg1}) \cdot 10^{-6} \cdot \frac{N \cdot s}{m^2}$$

$$\mu_2(t_{avg2}) := interp(dvs2, tx, dv2, t_{avg2}) \cdot 10^{-6} \cdot \frac{N \cdot s}{m^2}$$

$$\mu_3(t_{avg3}) := interp(dvs3, tx, dv3, t_{avg3}) \cdot 10^{-6} \cdot \frac{N \cdot s}{m^2}$$

Prantle number information

$$pry := \begin{pmatrix} 13.6 \\ 7.02 \\ 4.34 \\ 3.02 \\ 2.22 \\ 1.74 \end{pmatrix}$$

$pry1 := pry$ $pry2 := pry$ $pry3 := pry$

$prs1 := lspline(tx, pry1)$ $prs2 := lspline(tx, pry2)$ $prs3 := lspline(tx, pry3)$

$$Pr_1(t_{avg1}) := interp(prs1, tx, pry1, t_{avg1})$$

$$Pr_2(t_{avg2}) := interp(prs2, tx, pry2, t_{avg2})$$

$$Pr_3(t_{avg3}) := interp(prs3, tx, pry3, t_{avg3})$$

Experiments. For the model and data that follows, when regarding side A and side B of the heat exchangers, the hot side (A) will have a subscript 1, the cold side (B) will have a subscript 2

Description of matrix columns: 1) hot loop flow rate, 2) cold loop flow rate, 3) T1i, 4) T1o, 5) T2i, 6) T2o, 7) normalized hot loop inlet pressure, 8) normalized hot loop pressure outlet, 9) normalized cold loop inlet pressure, 10) normalized cold loop outlet pressure, 11) T3i, 12) T3o, 13) city water flow rate, 14) power applied to bulk heaters (accounts for voltage drop across shunts in power calc)

f represents full power, h represents half power, i represents isothermal

$$Mf22 := \begin{pmatrix} 3.01 & 3.003 & 95.97 & 64.26 & 42.59 & 73.12 & 24.092 & 23.676 & 19.073 & 17.877 & 12.35 & 33.83 & 4.302 & 25720 \\ 3.513 & 3.509 & 88.7 & 61.28 & 41.1 & 67.41 & 21.648 & 20.918 & 17.831 & 16.157 & 12.08 & 34.06 & 4.266 & 25697 \\ 4.011 & 4.02 & 84.19 & 59.85 & 40.86 & 64.17 & 20.468 & 19.38 & 17.553 & 15.406 & 11.96 & 34.05 & 4.263 & 25682 \\ 4.503 & 4.521 & 80.71 & 58.96 & 41.02 & 61.89 & 19.717 & 18.216 & 17.663 & 14.995 & 12.2 & 34.5 & 4.242 & 25688 \\ 4.997 & 4.992 & 77.5 & 57.87 & 40.78 & 59.7 & 19.16 & 17.157 & 17.777 & 14.527 & 11.97 & 34.4 & 4.23 & 25674 \\ 5.504 & 5.504 & 74.59 & 56.71 & 40.41 & 57.62 & 18.832 & 16.289 & 18.068 & 14.154 & 11.59 & 33.83 & 4.245 & 25669 \\ 6.014 & 6.027 & 73.07 & 56.7 & 41.23 & 56.91 & 18.997 & 15.878 & 18.782 & 14.132 & 12.98 & 34.58 & 4.377 & 25649 \\ 6.514 & 6.507 & 70.79 & 55.62 & 40.7 & 55.25 & 18.998 & 15.252 & 19.512 & 14.099 & 12.26 & 33.67 & 4.421 & 25645 \\ 7.001 & 7.014 & 69.11 & 54.94 & 40.55 & 54.1 & 19.657 & 15.249 & 20.319 & 14.069 & 12.24 & 34.01 & 4.383 & 25616 \\ 7.515 & 7.524 & 67.84 & 54.59 & 40.7 & 53.38 & 20.019 & 14.887 & 21.203 & 14.057 & 12.43 & 34.07 & 4.421 & 25613 \\ 8.007 & 8.067 & 66.21 & 53.75 & 40.35 & 52.17 & 20.438 & 14.536 & 22.237 & 14.04 & 12.34 & 33.87 & 4.442 & 25603 \\ 8.509 & 8.508 & 65.14 & 53.39 & 40.31 & 51.54 & 21.094 & 14.362 & 23.103 & 14.029 & 12.34 & 33.92 & 4.444 & 25606 \\ 9.009 & 9.035 & 63.85 & 52.72 & 40.04 & 50.64 & 21.715 & 14.099 & 24.205 & 14.021 & 12.25 & 33.64 & 4.492 & 25607 \\ 9.745 & 9.758 & 62.62 & 52.29 & 40.08 & 49.92 & 23.063 & 14.052 & 25.856 & 14.056 & 12.32 & 33.9 & 4.484 & 25594 \end{pmatrix}$$

$i := 1..14$

$$Mh22 := \begin{pmatrix} 3.011 & 3.001 & 59.88 & 41.95 & 28.48 & 45.56 & 14.726 & 14.246 & 15.518 & 14.193 & 12.59 & 25.08 & 4.247 & 14158 \\ 4 & 4.002 & 52.77 & 39.06 & 27.26 & 40.35 & 15.321 & 14.127 & 16.276 & 14.036 & 11.57 & 23.54 & 4.426 & 14155 \\ 4.498 & 4.5 & 50.91 & 38.66 & 27.62 & 39.25 & 15.729 & 14.102 & 16.816 & 14.02 & 12 & 23.8 & 4.492 & 14146 \\ 4.999 & 5.011 & 48.98 & 37.88 & 27.41 & 37.91 & 16.204 & 14.077 & 17.405 & 13.987 & 11.71 & 23.77 & 4.451 & 14131 \\ 5.527 & 5.531 & 47.81 & 37.71 & 27.82 & 37.32 & 16.742 & 14.065 & 18.089 & 13.974 & 12.14 & 24.06 & 4.478 & 14130 \\ 5.997 & 5.992 & 46.99 & 37.6 & 28.11 & 36.91 & 17.222 & 14.006 & 18.677 & 13.904 & 12.19 & 24.33 & 4.413 & 14120 \\ 6.505 & 6.504 & 46.23 & 37.52 & 28.44 & 36.57 & 17.845 & 13.99 & 19.451 & 13.889 & 12.56 & 24.63 & 4.441 & 14129 \\ 7.017 & 7.034 & 45.21 & 37.09 & 28.37 & 35.91 & 18.524 & 13.973 & 20.327 & 13.874 & 12.47 & 24.65 & 4.417 & 14124 \\ 7.503 & 7.5 & 44.31 & 36.68 & 28.24 & 35.33 & 19.227 & 13.961 & 21.139 & 13.862 & 12.29 & 24.47 & 4.414 & 14106 \\ 7.994 & 8.009 & 43.63 & 36.44 & 28.27 & 34.93 & 19.988 & 13.944 & 22.089 & 13.848 & 12.17 & 24.41 & 4.414 & 14091 \\ 8.528 & 8.525 & 43 & 36.19 & 28.28 & 34.56 & 20.824 & 13.936 & 23.122 & 13.843 & 12.29 & 24.43 & 4.478 & 14097 \\ 9.021 & 9.038 & 42.61 & 36.15 & 28.48 & 34.41 & 21.702 & 13.937 & 24.215 & 13.85 & 12.49 & 24.7 & 4.474 & 14091 \\ 9.782 & 9.741 & 42.08 & 36.08 & 28.7 & 34.22 & 23.141 & 13.965 & 25.825 & 13.899 & 12.65 & 24.87 & 4.456 & 14077 \end{pmatrix}$$

$i2 := 1..13$

$$Mi22 := \begin{pmatrix} 3.005 & 3.011 & 12.16 & 11.31 & 11.25 & 11.64 & 14.712 & 14.172 & 15.644 & 14.108 & 10.87 & 11.18 & 4.26 & 0 \\ 3.505 & 3.51 & 12.02 & 11.2 & 11.19 & 11.53 & 15.051 & 14.149 & 16.082 & 14.083 & 10.83 & 11.12 & 4.256 & 0 \\ 4.006 & 4.005 & 11.98 & 11.18 & 11.18 & 11.5 & 15.455 & 14.138 & 16.583 & 14.069 & 10.81 & 11.11 & 4.228 & 0 \\ 4.511 & 4.497 & 11.94 & 11.16 & 11.18 & 11.47 & 15.924 & 14.13 & 17.147 & 14.062 & 10.81 & 11.11 & 4.229 & 0 \\ 5.008 & 5.003 & 11.98 & 11.21 & 11.21 & 11.51 & 16.432 & 14.117 & 17.784 & 14.052 & 10.82 & 11.14 & 4.372 & 0 \\ 5.503 & 5.5 & 12 & 11.22 & 11.23 & 11.52 & 16.992 & 14.106 & 18.472 & 14.043 & 10.81 & 11.16 & 4.413 & 0 \\ 6.009 & 6.012 & 12.02 & 11.26 & 11.26 & 11.55 & 17.615 & 14.097 & 19.237 & 14.035 & 10.81 & 11.17 & 4.403 & 0 \\ 6.496 & 6.51 & 12.08 & 11.32 & 11.32 & 11.61 & 18.26 & 14.087 & 20.042 & 14.027 & 10.84 & 11.22 & 4.411 & 0 \\ 7.007 & 7.009 & 12.14 & 11.38 & 11.37 & 11.66 & 18.973 & 14.072 & 20.904 & 14.014 & 10.86 & 11.27 & 4.42 & 0 \\ 7.496 & 7.506 & 12.19 & 11.43 & 11.4 & 11.7 & 19.713 & 14.06 & 21.823 & 14 & 10.85 & 11.29 & 4.43 & 0 \\ 8.012 & 8.015 & 12.21 & 11.46 & 11.44 & 11.73 & 20.538 & 14.047 & 22.816 & 13.992 & 10.84 & 11.31 & 4.435 & 0 \\ 8.516 & 8.511 & 12.27 & 11.52 & 11.49 & 11.78 & 21.393 & 14.035 & 23.852 & 13.985 & 10.83 & 11.34 & 4.436 & 0 \\ 9.014 & 9.017 & 12.3 & 11.55 & 11.51 & 11.81 & 22.294 & 14.037 & 24.971 & 13.994 & 10.79 & 11.35 & 4.435 & 0 \\ 9.757 & 9.769 & 12.35 & 11.59 & 11.53 & 11.84 & 23.777 & 14.068 & 26.769 & 14.056 & 10.7 & 11.35 & 4.448 & 0 \end{pmatrix}$$

$i3 := 1..14$

Now listing experimentally determined hose pressure drops. The values correspond to the closest nominal flow rates in the experimental heat exchanger data. First column is for raw hot side pressure drop and second column is for the raw cold side pressure drop

(1) is full power
2 half power
3 isothermal

$$Mhosedrop := \begin{pmatrix} -0.318 & 0.363 \\ -0.212 & 0.47 \\ -0.101 & 0.618 \\ 0.029 & 0.755 \\ 0.225 & 0.895 \\ 0.39 & 1.052 \\ 0.553 & 1.207 \\ 0.746 & 1.391 \\ 0.948 & 1.584 \\ 1.17 & 1.787 \\ 1.385 & 2.001 \\ 1.634 & 2.234 \\ 1.891 & 2.49 \\ 2.302 & 2.888 \end{pmatrix}$$

$$Mhosedrop2 := \begin{pmatrix} -0.318 & 0.363 \\ -0.101 & 0.618 \\ 0.029 & 0.755 \\ 0.225 & 0.895 \\ 0.39 & 1.052 \\ 0.553 & 1.207 \\ 0.746 & 1.391 \\ 0.948 & 1.584 \\ 1.17 & 1.787 \\ 1.385 & 2.001 \\ 1.634 & 2.234 \\ 1.891 & 2.49 \\ 2.302 & 2.888 \end{pmatrix}$$

Now creating additional matrixes to calculate perturbations in the data due to measurement uncertainties

$Uclflowmeter1 := 1.0034$ $Uhlflowmeter1 := 1.0052$

$Uclflowmeter2 := .9966$ $Uhlflowmeter2 := 0.9948$

maximum heat transfer error matrices

$Mf2err_{i,1} := Mf22_{i,1} \cdot Uhlflowmeter1$ $Mf2err_{i,2} := Mf22_{i,2} \cdot Uclflowmeter2$

T1i value

$Mf2err_{i,3} := Mf22_{i,3} + .17$ $Mf2err_{i,4} := Mf22_{i,4} + 0$

T2i value

$Mf2err_{i,5} := Mf22_{i,5} + .17$ $Mf2err_{i,6} := Mf22_{i,6}$

Hot loop raw pressure drop

$Mf2err_{i,7} := Mf22_{i,7} \cdot 1.00285 + .049$ $Mf2err_{i,8} := Mf22_{i,8} \cdot .99715$

Cold loop raw pressure drop

$Mf2err_{i,9} := Mf22_{i,9}$ $Mf2err_{i,10} := Mf22_{i,10}$

$Mf2err_{i,11} := Mf22_{i,11}$ $Mf2err_{i,12} := Mf22_{i,12}$

$Mf2err_{i,13} := Mf22_{i,13}$ $Mf2err_{i,14} := Mf22_{i,14}$

half power error matrices

Now defining property values from matrixes

$$Q1(Mf,i) := Mf_{i,1}\cdot gpm \qquad Q2(Mf,i) := Mf_{i,2}\cdot gpm \qquad Q3(Mf,i) := Mf_{i,13}\cdot gpm$$

$$T1i(Mf,i) := Mf_{i,3}\,°C - .73\,°C \qquad T2i(Mf,i) := Mf_{i,5}\,°C - .02\,°C$$

$$T1o(Mf,i) := Mf_{i,4}\,°C - .21\,°C \qquad T2o(Mf,i) := Mf_{i,6}\,°C - .10\,°C$$

$$T3i(Mf,i) := Mf_{i,11}\,°C \qquad T3o(Mf,i) := Mf_{i,12}\,°C$$

$$tavg1(Mf,i) := \frac{\left(Mf_{i,3} - .73\right) + \left(Mf_{i,4} - .21\right)}{2} \qquad tavg2(Mf,i) := \frac{\left(Mf_{i,5} - .02\right) + \left(Mf_{i,6} - .1\right)}{2}$$

$$tavg3(Mf,i) := \frac{Mf_{i,9} + Mf_{i,10}}{2}$$

Now listing experimentally determined offsets for temperature difference and pressure

$$\Delta Photoffset := .54$$

$$\Delta Pcoldoffset := -.1$$

Considering the offset of
ΔP

$$\Delta P1(Mf,i) := \left(Mf_{i,7} + \Delta Photoffset\right)psi$$

$$\Delta P2(Mf,i) := \left(Mf_{i,8} + \Delta Pcoldoffset\right)psi$$

$$\Delta P1(Mf,i) := \left[\left(Mf_{i,7} - Mf_{i,8}\right) + \Delta Photoffset\right]\cdot psi$$

$$\Delta P2(Mf,i) := \left[\left(Mf_{i,9} - Mf_{i,10}\right) + \Delta Pcoldoffset\right]\cdot psi$$

Now calculating NTU relationships

$$C1(Mf,i) := \rho_1(tavg1(Mf,i)) \cdot Q1(Mf,i) \cdot c_{p1}(tavg1(Mf,i))$$

$$C2(Mf,i) := \rho_2(tavg2(Mf,i)) \cdot Q2(Mf,i) \cdot c_{p2}(tavg2(Mf,i))$$

$$Cmin(Mf,i) := \min(C1(Mf,i), C2(Mf,i)) \qquad Cmax(Mf,i) := \max(C1(Mf,i), C2(Mf,i))$$

$$Cr(Mf,i) := \frac{Cmin(Mf,i)}{Cmax(Mf,i)}$$

$$\varepsilon(Mf,i) := \frac{C1(Mf,i) \cdot (T1i(Mf,i) - T1o(Mf,i))}{Cmin(Mf,i) \cdot (T1i(Mf,i) - T2i(Mf,i) + 0)}$$

$$NTU(Mf,i) := \frac{1}{1 - Cr(Mf,i)} \cdot \ln\left(\frac{1 - \varepsilon(Mf,i) \cdot Cr(Mf,i)}{1 - \varepsilon(Mf,i)}\right)$$

$$U2(Mf,i) := \frac{NTU(Mf,i) \cdot Cmin(Mf,i)}{A_2}$$

$$h(Mf,i) := \frac{U2(Mf,i) \cdot \left(\frac{A_2}{A_1} + 1\right)}{1 - \frac{U2(Mf,i) \cdot \delta}{k_w}}$$

This section calculates values from the data, friction factor, reynolds, colburn, etc.

$$G1(Mf,i) := \frac{\rho_1(tavg1(Mf,i)) \cdot Q1(Mf,i)}{A_{c1}} \qquad G2(Mf,i) := \frac{\rho_2(tavg2(Mf,i)) \cdot Q2(Mf,i)}{A_{c2}}$$

$$Gp1(Mf,i) := \frac{4 \cdot \rho_1(tavg1(Mf,i)) \cdot Q1(Mf,i)}{\pi \cdot D_p^{\,2}} \qquad Gp2(Mf,i) := \frac{4 \cdot \rho_2(tavg2(Mf,i)) \cdot Q2(Mf,i)}{\pi \cdot D_p^{\,2}}$$

$$j1(Mf,i) := \frac{h(Mf,i) \cdot Pr_1(tavg1(Mf,i))^{\frac{2}{3}}}{G1(Mf,i) \cdot c_{p1}(tavg1(Mf,i))} \qquad j2(Mf,i) := \frac{h(Mf,i) \cdot Pr_2(tavg2(Mf,i))^{\frac{2}{3}}}{G2(Mf,i) \cdot c_{p2}(tavg2(Mf,i))}$$

$$f1(Mf,i) := \left[\Delta P1(Mf,i) - \frac{1.5\cdot(Gp1(Mf,i))^2}{2\cdot\rho_1(tavg1(Mf,i))}\right]\cdot\frac{D_h\cdot\rho_1(tavg1(Mf,i))}{2\cdot L_p\cdot G1(Mf,i)^2}$$

$$f1withhose(Mf,i) := \left[\left[\Delta P1(Mf,i) - \left(Mhosedrop_{i,1} + \Delta Photoffset\right)\cdot psi\right] - \frac{1.5\cdot(Gp1(Mf,i))^2}{2\cdot\rho_1(tavg1(Mf,i))}\right]\cdot\frac{D_h\cdot\rho_1(tavg1(Mf,i))}{2\cdot L_p\cdot G1(Mf,i)^2}$$

$$f2(Mf,i) := \left[\Delta P2(Mf,1) - \frac{1.5\cdot(Gp2(Mf,i))^2}{2\cdot\rho_2(tavg2(Mf,i))}\right]\cdot\frac{D_h\cdot\rho_2(tavg2(Mf,i))}{2\cdot L_p\cdot G2(Mf,i)^2}$$

$$f1withhoseh(Mf,i) := \left[\left[\Delta P1(Mf,i) - \left(Mhosedrop2_{i,1} + \Delta Photoffset\right)\cdot psi\right] - \frac{1.5\cdot(Gp1(Mf,i))^2}{2\cdot\rho_1(tavg1(Mf,i))}\right]\cdot\frac{D_h\cdot\rho_1(tavg1(Mf,i))}{2\cdot L_p\cdot G1(Mf,i)^2}$$

$$Re1(Mf,i) := \frac{G1(Mf,i)\cdot D_h}{\mu_1(tavg1(Mf,i))} \qquad Re2(Mf,i) := \frac{G2(Mf,i)\cdot D_h}{\mu_2(tavg2(Mf,i))}$$

$$Nu1(Mf,i) := \frac{h(Mf,i)\cdot L_p}{k_w}$$

Now calculating values from martin correlation

$$Nu_1(Q1) := \frac{h_1(Q1)\cdot L_p}{k_w}$$

$Q_{1i} := 1gpm, 1.02gpm .. 15gpm$

Full power values

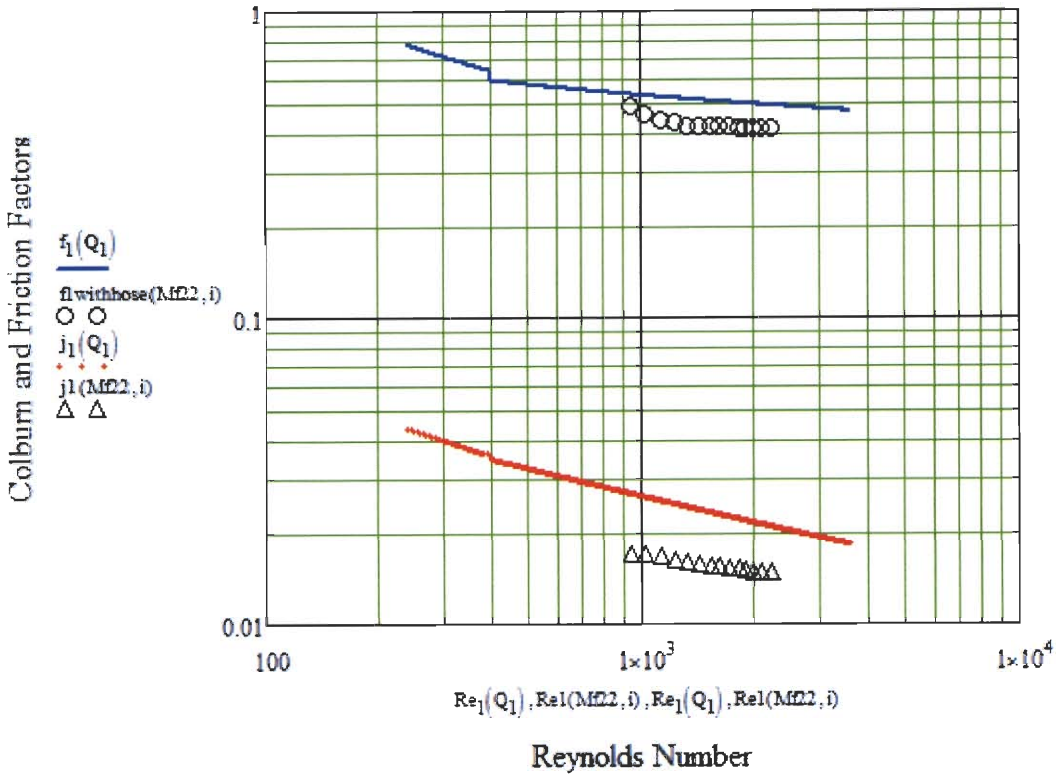


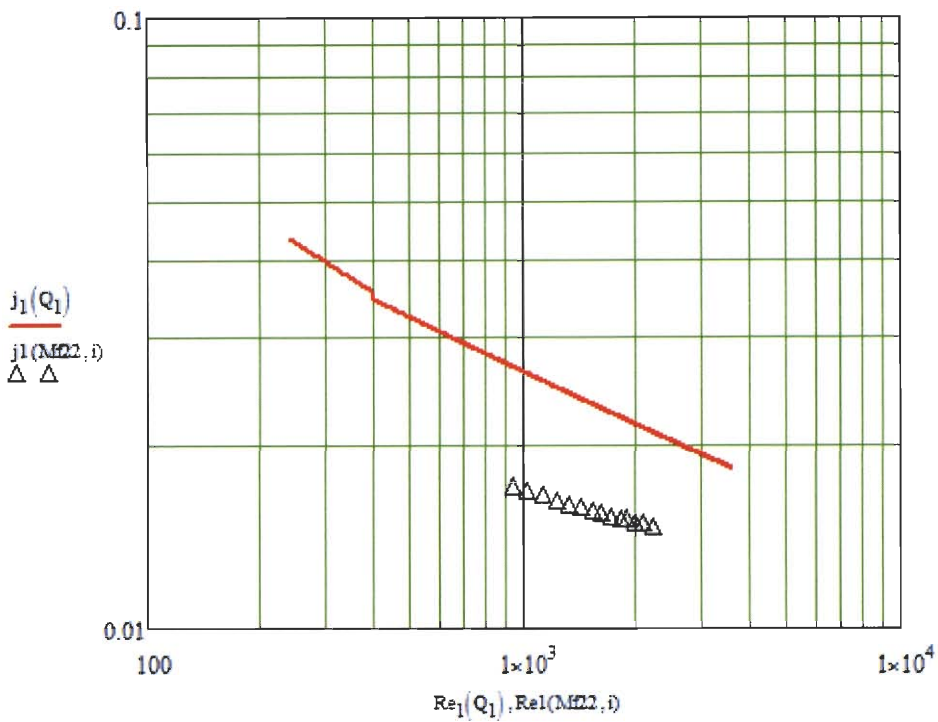

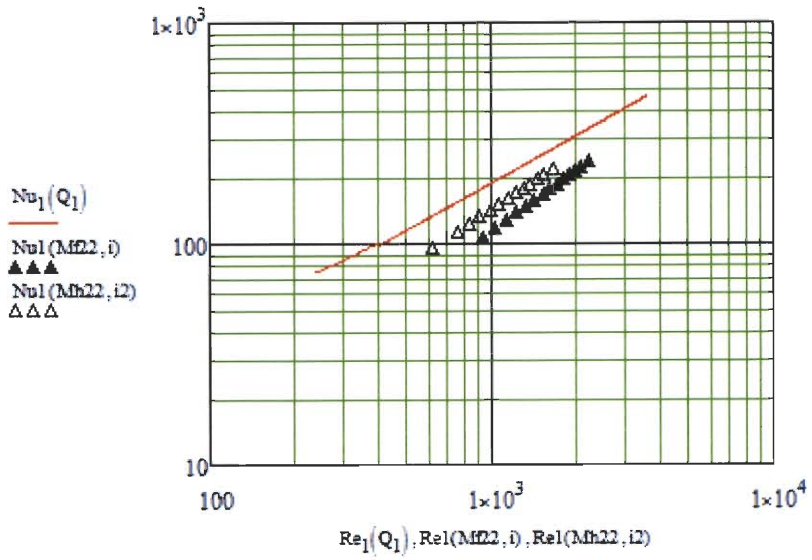


half power values

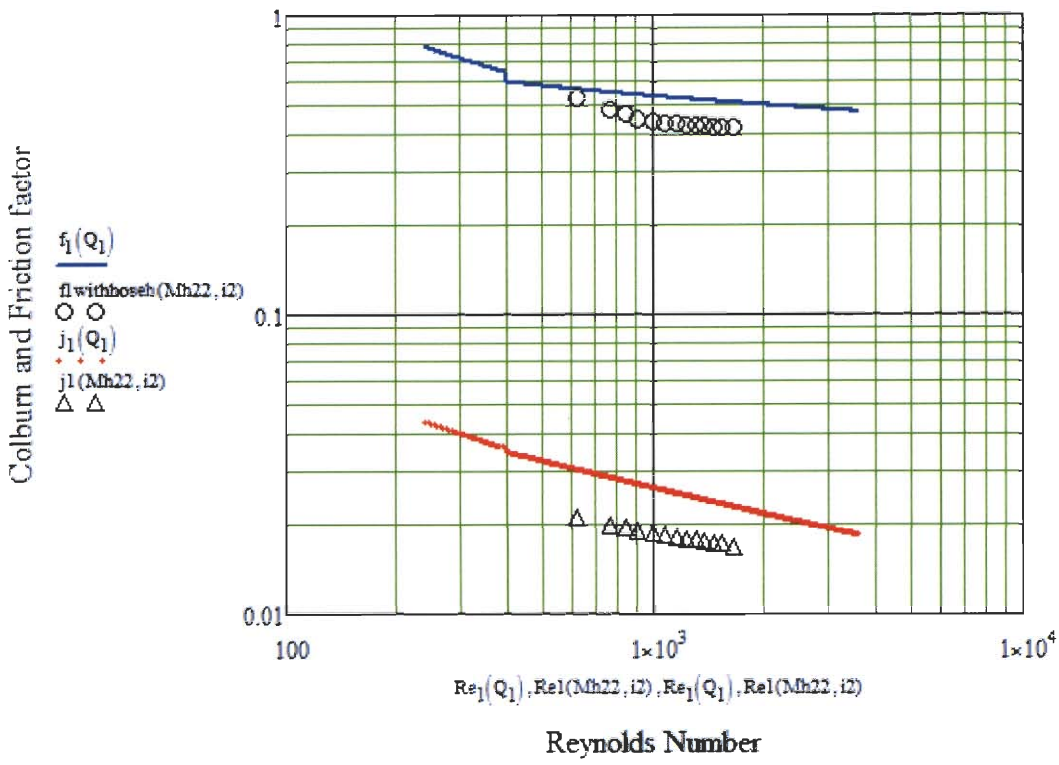

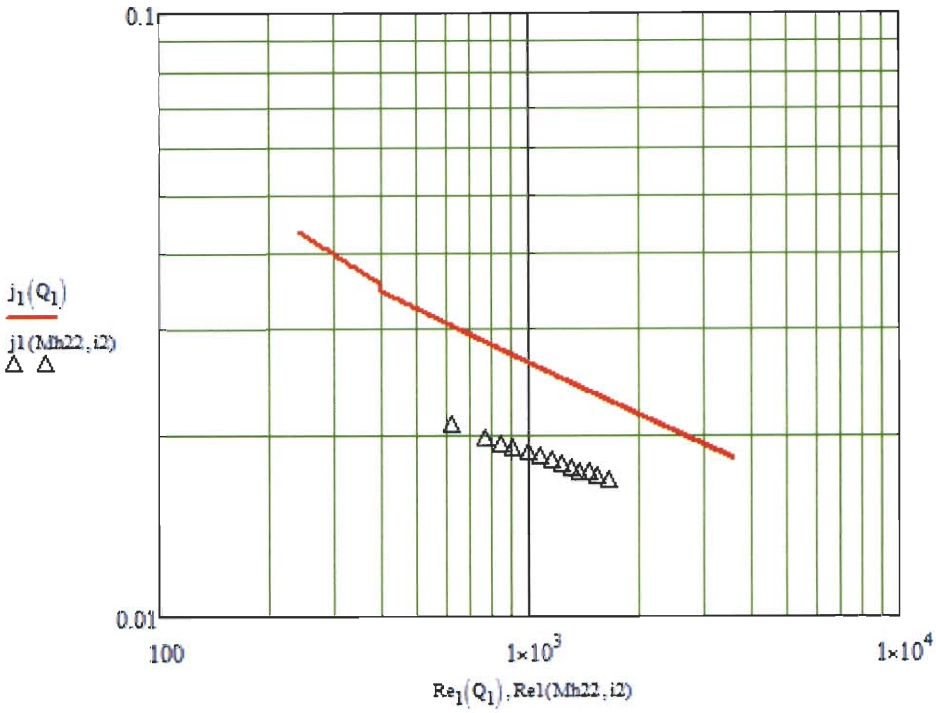


Isothermal pressure

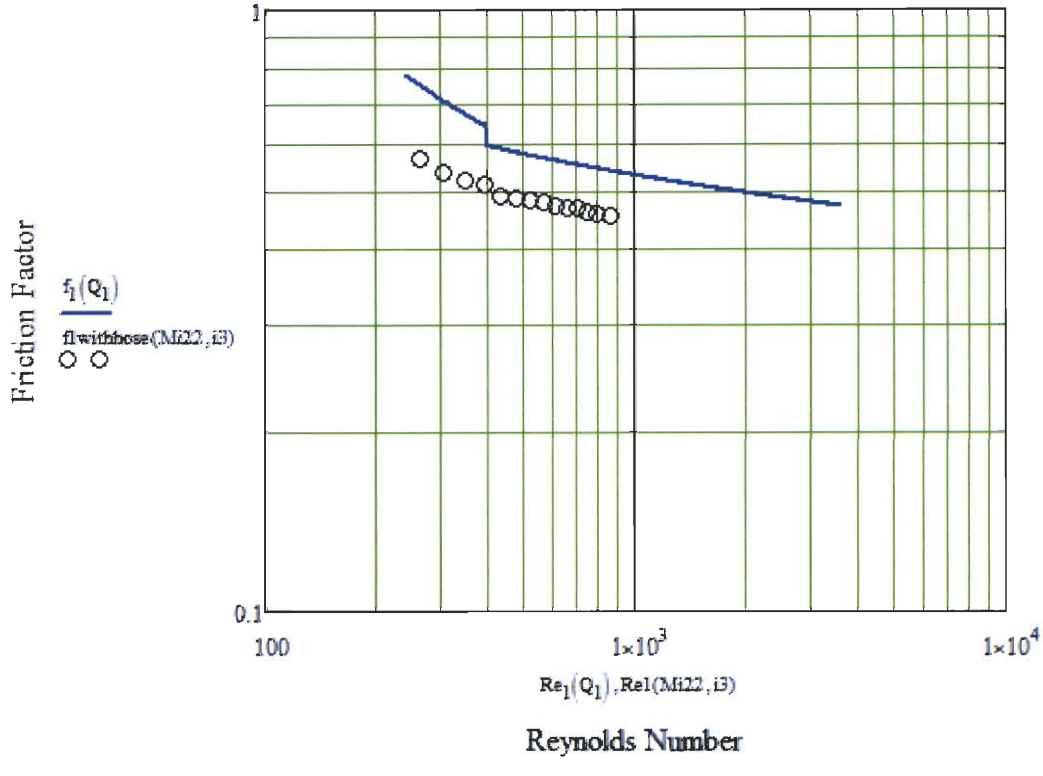

Now what follow is a calculation of the associated error for heat transfer, reynolds number, convection coefficient and friction factors

$$\Delta Tcityoffset := 0$$

$$\Delta T1(Mf, i) := T1i(Mf, i) - T1o(Mf, i)$$

$$\Delta T2(Mf, i) := T2o(Mf, i) - T2i(Mf, i)$$

$$\Delta T3(Mf, i) := T3o(Mf, i) - T3i(Mf, i)$$

$$mmdot1(Mf, i) := Q1(Mf, i) \cdot \rho_1(tavg1(Mf, i))$$

$$mmdot2(Mf, i) := Q2(Mf, i) \cdot \rho_2(tavg2(Mf, i))$$

$$mmdot3(Mf, i) := Q3(Mf, i) \cdot \rho_3(tavg3(Mf, i))$$

$$Qheat1(Mf, i) := mmdot1(Mf, i) \cdot c_{p1}(tavg1(Mf, i)) \cdot \Delta T1(Mf, i)$$

$$Qheat2(Mf, i) := mmdot2(Mf, i) \cdot c_{p2}(tavg2(Mf, i)) \cdot \Delta T2(Mf, i)$$

$$Qheat3(Mf, i) := mmdot3(Mf, i) \cdot c_{p3}(tavg3(Mf, i)) \cdot \Delta T3(Mf, i)$$

$$Qheatelectric(Mf, i) := Mf_{i, 14} \cdot W$$

$$Qhxmin(Mf, i) := \min(Qheat1(Mf, i), Qheat2(Mf, i))$$

$$Qhxmax(Mf, i) := \max(Qheat1(Mf, i), Qheat2(Mf, i))$$

$$Qhxavg(Mf, i) := \frac{Qheat1(Mf, 1) + Qheat2(Mf, i)}{2}$$

$$Qdiffhotvscold(Mf, i) := \frac{Qhxmax(Mf, i) - Qhxmin(Mf, i)}{Qhxmin(Mf, i)} \cdot 100$$

$$Qdiffhot(Mf, i) := \frac{Qheat1(Mf, i) - Qhxavg(Mf, i)}{Qhxavg(Mf, i)} \cdot 100$$

$$Qdiffcold(Mf, i) := \frac{Qheat2(Mf, i) - Qhxavg(Mf, i)}{Qhxavg(Mf, i)} \cdot 100$$

$$Qhxavgvselectric(Mf, i) := \frac{Qheatelectric(Mf, i) - Qhxavg(Mf, i)}{Qhxavg(Mf, i)} \cdot 100$$

$$Qhxavgvscity(Mf, i) := \frac{Qheat3(Mf, i) - Qhxavg(Mf, i)}{Qhxavg(Mf, i)} \cdot 100$$

Qdiffhotvscold represents comparison between the min and maximum experimental data. Qdiff hot and cold represent the heat transfer differences using the method used by muley and manglik 1999 asme paper. The tables below represent percentages.

Qdiffhot(Mf22, i) =

| |
|---|
| 0.8619 |
| 1.35 |
| 1.8209 |
| 1.6209 |
| 1.542 |
| 1.5349 |
| 1.468 |
| 1.5574 |
| 1.5602 |
| 1.5211 |
| 1.5426 |
| 1.4298 |
| 1.3907 |
| 1.3296 |

Qdiffhot(Mh22, i2) =

| |
|---|
| 1.1175 |
| 0.888 |
| 1.0152 |
| 1.0644 |
| 1.3094 |
| 1.6486 |
| 1.7168 |
| 1.7245 |
| 1.6754 |
| 1.5172 |
| 1.9889 |
| 1.8725 |
| 1.8066 |

Qdiffcold(Mf22, i) =

| |
|---|
| -0.8619 |
| -0.4624 |
| 0.297 |
| 0.6419 |
| 0.6964 |
| 0.8446 |
| 0.7042 |
| 0.797 |
| 0.9802 |
| 1.1566 |
| 1.1207 |
| 1.2101 |
| 1.3178 |
| 1.4238 |

Qdiffcold(Mh22, i2) =

| |
|---|
| -1.1175 |
| -0.0499 |
| -0.1316 |
| 0.1103 |
| $3.7771 \cdot 10^{-3}$ |
| 0.1467 |
| 0.2491 |
| 0.3658 |
| 0.4678 |
| 0.5887 |
| 0.739 |
| 0.755 |
| 0.8669 |

Qhxavgvscity(Mf22, i) =

| |
|---|
| 1.6139 |
| 2.77 |
| 2.4563 |
| 2.5721 |
| 2.8304 |
| 2.1702 |
| 2.4437 |
| 2.4506 |
| 3.0685 |
| 3.1364 |
| 3.1133 |
| 3.2861 |
| 3.3449 |
| 3.9278 |

Qhxavgvselectric(Mf22, i) =

| |
|---|
| 7.1496 |
| 6.6298 |
| 5.762 |
| 5.4208 |
| 5.3055 |
| 5.1279 |
| 5.1947 |
| 5.08 |
| 4.7674 |
| 4.5684 |
| 4.5656 |
| 4.4833 |
| 4.3735 |
| 4.2084 |

Qdiffhotvscold(Mf22, i) =

| |
|---|
| 1.7388 |
| 1.8208 |
| 1.5194 |
| 0.9727 |
| 0.8398 |
| 0.6846 |
| 0.7585 |
| 0.7544 |
| 0.5744 |
| 0.3603 |
| 0.4172 |
| 0.2171 |
| 0.072 |
| 0.0929 |

# Appendix C

## MATHCAD for GB220H-20

GEA GB220H-20

**MathCAD format solution:**

# Test Heat Exchanger GB220H-20

Hot and cold water properties at Tf

$T_{hot\_water} := 50\,°C$ $T_{cold\_water} := 40\,°C$

Hot water (subscript 1)

$\rho_1 := 985\frac{kg}{m^3}$

$c_{p1} := 4184\frac{J}{kg \cdot K}$

$k_1 := 0.639\frac{W}{m \cdot K}$

$\mu_1 := 471 \cdot 10^{-6}\frac{N \cdot s}{m^2}$

$Pr_1 := 3.02$

Cold water (subscript 2)

$\rho_2 := 994\frac{kg}{m^3}$

$c_{p2} := 4178\frac{J}{kg \cdot K}$

$k_2 := 0.628\frac{W}{m \cdot K}$

$\mu_2 := 654 \cdot 10^{-6}\frac{N \cdot s}{m^2}$

$Pr_2 := 4.34$

Thermal conductivity of the plate (Stainless Steel AISI 316)

$k_w := 13.4\frac{W}{m \cdot K}$

**Given information**

Volume flow rates for hot and cold water

$Q_1 := 10gpm$ $Q_2 := 10gpm$

Mass flow rates

$mdot_1(Q_1) := \rho_1 \cdot Q_1$ $mdot_1(Q_1) = 0.6214\frac{kg}{s}$

$mdot_2(Q_2) := \rho_2 \cdot Q_2$ $mdot_2(Q_2) = 0.6271\frac{kg}{s}$

**Geometric parameters:**

$N_p := 1$ Number of passes

$\beta := 60deg$ Corrugation inclination angle (chevron angle)

$N_t := 20$ Total number of plates

$D_p := \frac{3}{4}in$ Port diameter

$t_n := 0.087in$ spacing between plates

$\alpha := 40deg$ Corrugation Pitch angle

$\lambda := t_n \cdot \tan(\alpha)$ Corrugation Pitch (=wavelengtht) $\lambda = 0.073 \cdot in$

$\delta := 0.6mm$ Thickness of the plates

Use the dimensions of the test heat exchanger

$W_p := 3in$ $L_{p2p} := 11in$ $L_p := L_{p2p} - 1in$ $L_p = 10 \cdot in$

$H_p := t_n \cdot N_t$ $H_p = 1.74 \cdot in$

Number of wavelength per single plate

$$N_\lambda := \frac{W_p}{\lambda}$$

Number of channels for hot and cold fluid

$$N_{c1} := \frac{N_t}{2N_p} \qquad N_{c1} = 10$$

$$N_{c2} := \frac{N_t}{2N_p} - 1 \qquad N_{c2} = 9$$

Amplitude of corrugation and channel spacing

$$a := \frac{1}{2}\cdot\left(\frac{H_p}{N_t} - \delta\right) \qquad a = 0.0317 \cdot in \qquad 2 \cdot a = 0.0634 \cdot in \qquad 2 \cdot a + \delta = 0.087 \cdot in$$

Corrugation ratio $\gamma$

$\gamma := 4\frac{a}{\lambda}$ $\gamma = 1.7363$

Corrugated length

$$L_\lambda := \int_0^\lambda \sqrt{1 + \left(\frac{2\cdot\pi\cdot a}{\lambda}\right)^2 \cdot \cos\left(\frac{2\cdot\pi}{\lambda}\cdot x\right)^2}\, dx$$

Heat transfer area for hot fluid (fluid1)

$A_1 := 2\cdot L_\lambda \cdot N_\lambda \cdot L_p \cdot N_{t1}$ $A_1 = 0.8015\,m^2$

$A_2 := 2\cdot L_\lambda \cdot N_\lambda \cdot L_p \cdot N_{t2}$ $A_2 = 0.7213\,m^2$

Now setting the heat transfer area equal to the minimum area, which is A2

$A_1 := A_2$

Projected area for the plates

$A_{p1} := 2\cdot W_p \cdot L_p \cdot N_{t1}$ $A_{p2} := 2\cdot W_p \cdot L_p \cdot N_{t2}$

**Enlargement factor φ**

$\Phi := \frac{L_\lambda \cdot N_\lambda}{W_p}$ $\Phi = 2.0705$

Exact hydraulic diameter

$D_h := \frac{4\cdot a}{\Phi}$ $D_h = 1.555\,mm$

Minimum free-flow area

$A_{c1} := 2\cdot a\cdot W_p \cdot N_{c1}$ $A_{c1} = 1.9013\,in^2$

$A_{c2} := 2\cdot a\cdot W_p \cdot N_{c2}$ $A_{c2} = 1.7112\,in^2$

Surface area density

$\beta_1 := \frac{A_1}{W_p\cdot 2\cdot a\cdot L_p\cdot N_{t1}}$ $\beta_1 = 2.3151\times 10^3\,\frac{1}{m}$

Mass velocity

$G_1(Q_1) := \frac{mdot_1(Q_1)}{A_{c1}}$ $v_1 := \frac{G_1(Q_1)}{\rho_1} = 0.5143\,\frac{m}{s}$

$Re_1(Q_1) := \frac{G_1(Q_1)\cdot D_h}{\mu_1}$ $Re_1(Q_1) = 1.6725\times 10^3$

$$G_2(Q_2) := \frac{mdot_2(Q_2)}{A_{c2}} \qquad v_2 := \frac{G_2(Q_2)}{\rho_2} = 0.5715\frac{m}{s}$$

$$Re_2(Q_2) := \frac{G_2(Q_2)\cdot D_h}{\mu_2} \qquad Re_2(Q_2) = 1.3506 \times 10^3$$

**Friction factors**

Martin's correlation (1996) for the Darcy friction factor is modified by the Fanning friction factor.

Martin, H., 1996, A theoretical approach to predict the performance of chevron-type plate heat exchanger, Chem. Eng. Processing, Vol.35, pp. 301-310.

$$f_{o1}(Q_1) := \begin{cases} \left(1.56\cdot\ln\left(Re_1(Q_1)\right) - 3.0\right)^{-2} & \text{if } Re_1(Q_1) \geq 400 \\ \dfrac{16}{Re_1(Q_1)} & \text{otherwise} \end{cases}$$

$$f_{o2}(Q_2) := \begin{cases} \left(1.56\cdot\ln\left(Re_2(Q_2)\right) - 3.0\right)^{-2} & \text{if } Re_2(Q_2) \geq 400 \\ \dfrac{16}{Re_2(Q_2)} & \text{otherwise} \end{cases}$$

$$f_{m1}(Q_1) := \begin{cases} \dfrac{9.75}{Re_1(Q_1)^{0.289}} & \text{if } Re_1(Q_1) \geq 400 \\ \dfrac{149.25}{Re_1(Q_1)} + 0.9625 & \text{otherwise} \end{cases}$$

$$f_{m2}(Q_2) := \begin{cases} \dfrac{9.75}{Re_2(Q_2)^{0.289}} & \text{if } Re_2(Q_2) \geq 400 \\ \dfrac{149.25}{Re_2(Q_2)} + 0.9625 & \text{otherwise} \end{cases}$$

$$f_1(Q_1) := \left[\frac{\cos(\beta)}{\left(0.045\cdot\tan(\beta) + 0.09\cdot\sin(\beta) + \dfrac{f_{o1}(Q_1)}{\cos(\beta)}\right)^{0.5}} + \left(\frac{1-\cos(\beta)}{\sqrt{3.8\cdot f_{m1}(Q_1)}}\right)\right]^{-2}$$

$$f_1(Q_1) = 0.5039$$

$$f_2(Q_2) := \left[\frac{\cos(\beta)}{\left(0.045\cdot\tan(\beta) + 0.09\cdot\sin(\beta) + \frac{f_{o2}(Q_2)}{\cos(\beta)}\right)^{0.5}} + \left(\frac{1-\cos(\beta)}{\sqrt{3.8\cdot f_{m2}(Q_2)}}\right)\right]^{-2}$$

$$f_2(Q_2) = 0.5144$$

Heat transfer coefficients

$$h_1(Q_1) := \frac{k_1}{D_h}\cdot\left[0.205\cdot Pr_1^{\frac{1}{3}}\cdot 1^{\frac{1}{6}}\cdot\left(f_1(Q_1)\cdot Re_1(Q_1)^2\cdot\sin(2\cdot\beta)\right)^{0.374}\right]$$

$$h_1(Q_1) = 2.3011\times 10^4\,\frac{W}{m^2\cdot K}$$

$$h_2(Q_2) := \frac{k_2}{D_h}\cdot\left[0.205\cdot Pr_2^{\frac{1}{3}}\cdot 1^{\frac{1}{6}}\cdot\left(f_2(Q_2)\cdot Re_2(Q_2)^2\cdot\sin(2\cdot\beta)\right)^{0.374}\right]$$

$$h_2(Q_2) = 2.1917\times 10^4\,\frac{W}{m^2\cdot K}$$

Overall heat teansfer coefficient

$$U_2(Q_1,Q_2) := \frac{1}{\frac{A_2}{h_1(Q_1)\cdot A_1} + \frac{\delta}{k_w} + \frac{1}{h_2(Q_2)}}$$

$$U_2(Q_1,Q_2) = 7.4705\times 10^3\,\frac{W}{m^2 K}$$

$$U_2(Q_1,Q_2)\cdot A_2 = 5.3887\times 10^3\,\frac{W}{K}$$

**Effectiveness-NTU Method**

$C_1(Q_1) =$ ∎

$$C_1(Q_1) := mdot_1(Q_1)\cdot c_{p1}$$

$$C_2(Q_2) := mdot_2(Q_2)\cdot c_{p2}$$

$$C_2(Q_2) = 2.6201\times 10^3\,\frac{m^2\cdot kg}{K\cdot s^3}$$

$$C_{min}(Q_1, Q_2) := \min(C_1(Q_1), C_2(Q_2)) \qquad C_{min}(Q_1, Q_2) = 2.6001 \times 10^3 \frac{m^2 \cdot kg}{K \cdot s^3}$$

$$C_{max}(Q_1, Q_2) := \max(C_1(Q_1), C_2(Q_2)) \qquad C_{max}(Q_1, Q_2) = 2.6201 \times 10^3 \frac{m^2 \cdot kg}{K \cdot s^3}$$

$$C_r(Q_1, Q_2) := \frac{C_{min}(Q_1, Q_2)}{C_{max}(Q_1, Q_2)} \qquad C_r(Q_1, Q_2) = 0.9924$$

$$NTU(Q_1, Q_2) := \frac{U_2(Q_1, Q_2) \cdot A_2}{C_{min}(Q_1, Q_2)} \qquad NTU(Q_1, Q_2) = 2.0725$$

Counterflow effectiveness

$$\varepsilon_{PHE}(Q_1, Q_2) := \frac{1 - \exp\left[-NTU(Q_1, Q_2) \cdot (1 - C_r(Q_1, Q_2))\right]}{1 - C_r(Q_1, Q_2) \cdot \exp\left[-NTU(Q_1, Q_2) \cdot (1 - C_r(Q_1, Q_2))\right]}$$

$$\varepsilon_{PHE}(Q_1, Q_2) = 0.6763$$

$Q_m := 1gpm, 2gpm .. 15gpm$

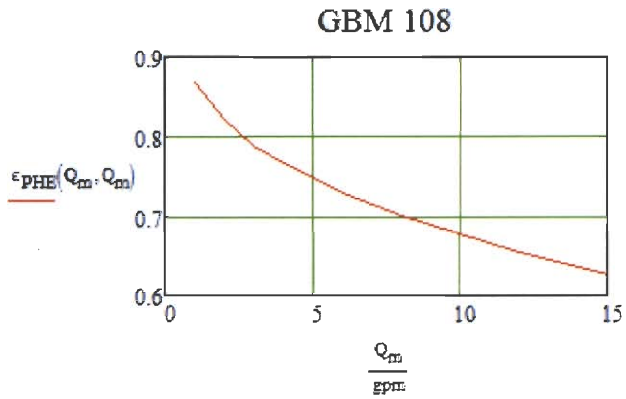


Heat transfer rate for the PHE

$$q(T_{1i}, T_{2i}, Q_1, Q_2) := \varepsilon_{PHE}(Q_1, Q_2) \cdot C_{min}(Q_1, Q_2) \cdot (T_{1i} - T_{2i})$$

Since $$\varepsilon_{PHE} = \frac{C_1 \cdot (T_{1i} - T_{1o})}{C_{min} \cdot (T_{1i} - T_{2i})} = \frac{C_2 \cdot (T_{2o} - T_{2i})}{C_{min} \cdot (T_{1i} - T_{2i})}$$

$$T_{1o}(T_{1i}, T_{2i}, Q_1, Q_2) := T_{1i} - \varepsilon_{PHE}(Q_1, Q_2) \cdot \frac{C_{min}(Q_1, Q_2)}{C_1(Q_1)} \cdot (T_{1i} - T_{2i})$$

$$T_{2o}(T_{1i}, T_{2i}, Q_1, Q_2) := T_{2i} + \varepsilon_{PHE}(Q_1, Q_2) \cdot \frac{C_{min}(Q_1, Q_2)}{C_2(Q_2)} \cdot (T_{1i} - T_{2i})$$

$$j_1(Q_1) := \frac{h_1(Q_1) \cdot Pr_1^{\frac{2}{3}}}{G_1(Q_1) \cdot c_{p1}}$$

$T_{1i} := 70\,°C$ $T_{2i} := 30\,°C$

$Q_m := 0.1gpm, 0.11gpm .. 12gpm$

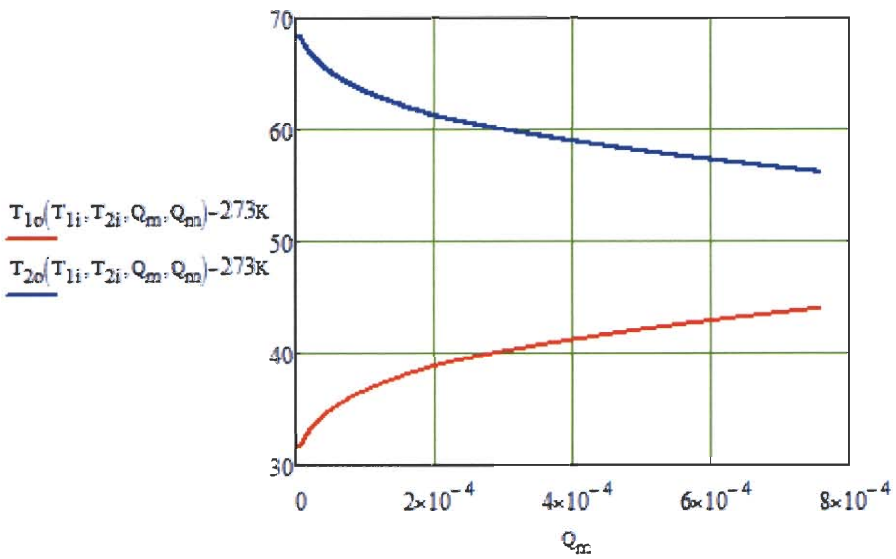


**Pressure Drop**

The frictional channel pressure drop

$$\Delta P_{f1}(Q_1) := \frac{2 \cdot f_1(Q_1) \cdot L_p}{D_h} \cdot \frac{G_1(Q_1)^2}{\rho_1} \cdot N_p \qquad \Delta P_{f1}(Q_1) = 6.2215 \cdot psi$$

$$\Delta P_{f2}(Q_2) := \frac{2 \cdot f_2(Q_2) \cdot L_p}{D_h} \cdot \frac{G_2(Q_2)^2}{\rho_2} \cdot N_p \qquad \Delta P_{f2}(Q_2) = 7.9119 \cdot psi$$

The connection and port pressure drop

$$G_{p1}(Q_1) := \frac{4 \cdot mdot_1(Q_1)}{\pi \cdot D_p^{\,2}} \qquad G_{p1}(Q_1) = 2.1803 \times 10^3 \ \frac{kg}{m^2 \cdot s}$$

$$G_{p2}(Q_2) := \frac{4 \cdot mdot_2(Q_2)}{\pi \cdot D_p^{\,2}}$$

$$\Delta P_{p1}(Q_1) := 1.5 \cdot N_p \cdot \frac{G_{p1}(Q_1)^2}{2 \cdot \rho_1} \qquad \Delta P_{p1}(Q_1) = 0.525 \cdot psi$$

$$\Delta P_{p2}(Q_2) := 1.5 \cdot N_p \cdot \frac{G_{p2}(Q_2)^2}{2 \cdot \rho_2} \qquad \Delta P_{p2}(Q_2) = 0.5298 \cdot psi$$

$$\Delta P_1(Q_1) := \Delta P_{f1}(Q_1) + \Delta P_{p1}(Q_1) \qquad \Delta P_1(Q_1) = 6.7464 \cdot psi$$

$$\Delta P_2(Q_2) := \Delta P_{f2}(Q_2) + \Delta P_{p2}(Q_2) \qquad \Delta P_2(Q_2) = 8.4417 \cdot psi$$

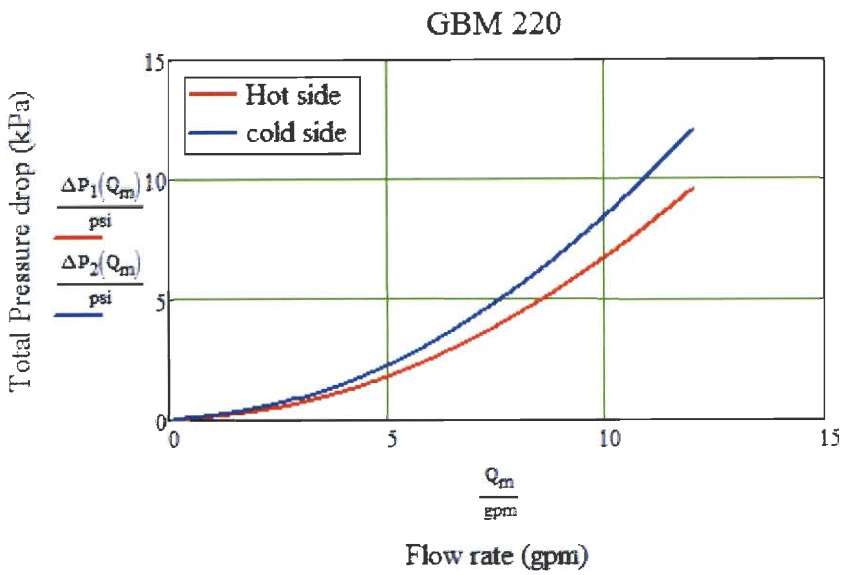


$$f_1(Q_1) := \left(\Delta P_1(Q_1) - \frac{1.5 \cdot G_{p1}(Q_1)^2}{2 \cdot \rho_1}\right) \cdot \frac{D_h \cdot \rho_1}{2 \cdot L_p \cdot G_1(Q_1)^2 \cdot N_p}$$

Experimental Data

ORIGIN := 1

$i := 1, 2 .. 10$

$M_{i,1} := i$

$$M_{i,2} := \frac{T_{1i} - 273K}{K}$$

$$M_{i,3} := \frac{T_{1o}(T_{1i}, T_{2i}, i \cdot gpm, i \cdot gpm) - 273.15K}{K}$$

$$M_{i,4} := \frac{T_{2i} - 273K}{K}$$

$$M_{i,5} := \frac{T_{2o}(T_{1i}, T_{2i}, i \cdot gpm, i \cdot gpm) - 273.15K}{K}$$

$$M_{i,6} := \frac{\Delta P_1(i \cdot gpm)}{psi} \qquad M_{i,7} := \frac{\Delta P_2(i \cdot gpm)}{psi}$$

Predictions

M =

| | 1 | 2 | 3 | 4 | 5 | 6 | 7 |
|---|---|---|---|---|---|---|---|
| 1 | 1 | 70.15 | 35.2955 | 30.15 | 64.4397 | 0.1201 | 0.1667 |
| 2 | 2 | 70.15 | 37.1478 | 30.15 | 62.6015 | 0.3566 | 0.4761 |
| 3 | 3 | 70.15 | 38.5009 | 30.15 | 61.2587 | 0.6863 | 0.8677 |
| 4 | 4 | 70.15 | 39.381 | 30.15 | 60.3854 | 1.18 | 1.4867 |
| 5 | 5 | 70.15 | 40.1342 | 30.15 | 59.6379 | 1.8003 | 2.2635 |
| 6 | 6 | 70.15 | 40.8009 | 30.15 | 58.9763 | 2.5454 | 3.1956 |
| 7 | 7 | 70.15 | 41.4038 | 30.15 | 58.378 | 3.4138 | 4.2809 |
| 8 | 8 | 70.15 | 41.957 | 30.15 | 57.829 | 4.4041 | 5.518 |
| 9 | 9 | 70.15 | 42.4699 | 30.15 | 57.32 | 5.5153 | 6.9053 |
| 10 | 10 | 70.15 | 42.9493 | 30.15 | 56.8443 | 6.7464 | 8.4417 |

Adding temperature dependent properties

Temperature dependent properties of water taken from table A.12 Thermal Design

temperature range of properties, in deg celsius

$$tx := \begin{pmatrix} 0 \\ 20 \\ 40 \\ 60 \\ 80 \\ 100 \end{pmatrix}$$

liquid density information, in kg/m3

$$dly := \begin{pmatrix} 1002 \\ 1000 \\ 994 \\ 985 \\ 974 \\ 960 \end{pmatrix}$$

$dly1 := dly$

$dls1 := lspline(tx, dly1)$

$\rho_1(t_{avg1}) := interp(dls1, tx, dly1, t_{avg1}) \cdot \frac{kg}{m^3}$

$dly2 := dly$

$dls2 := lspline(tx, dly2)$

$\rho_2(t_{avg2}) := interp(dls2, tx, dly2, t_{avg2}) \cdot \frac{kg}{m^3}$

$dly3 := dly$

$dls3 := lspline(tx, dly3)$

$\rho_3(t_{avg3}) := interp(dls3, tx, dly3, t_{avg3}) \cdot \frac{kg}{m^3}$

specific heat information, in J/(kg*K)

$$dcpy := \begin{pmatrix} 4217 \\ 4181 \\ 4178 \\ 4184 \\ 4196 \\ 4216 \end{pmatrix}$$

$dcp1 := dcpy$

$dcps1 := lspline(tx, dcp1)$

$c_{p1}(t_{avg1}) := interp(dcps1, tx, dcp1, t_{avg1}) \cdot \frac{J}{kg \cdot K}$

$dcp2 := dcpy$

$dcps2 := lspline(tx, dcp2)$

$c_{p2}(t_{avg2}) := interp(dcps2, tx, dcp2, t_{avg2}) \cdot \frac{J}{kg \cdot K}$

$dcp3 := dcpy$

$dcps3 := lspline(tx, dcp1)$

$c_{p3}(t_{avg3}) := interp(dcps3, tx, dcp3, t_{avg3}) \cdot \frac{J}{kg \cdot K}$

thermal conductivity information, in W/(m*K)

$$dky := \begin{pmatrix} .552 \\ .597 \\ .628 \\ .651 \\ .668 \\ .68 \end{pmatrix}$$

$dk1 := dky$

$dks1 := lspline(tx, dk1)$

$k_1(t_{avg1}) := interp(dks1, tx, dk1, t_{avg1}) \cdot \frac{W}{m \cdot K}$

$dk2 := dky$

$dks2 := lspline(tx, dk2)$

$k_2(t_{avg2}) := interp(dks2, tx, dk2, t_{avg2}) \frac{W}{m \cdot K}$

$dk3 := dky$

$dks3 := lspline(tx, dk3)$

$k_3(t_{avg3}) := interp(dks3, tx, dk3, t_{avg3}) \cdot \frac{W}{m \cdot K}$

absolute viscosity information, in N*s/m^2

$$dvsy := \begin{pmatrix} 1792 \\ 1006 \\ 654 \\ 471 \\ 355 \\ 288 \end{pmatrix}$$

$dv1 := dvsy$ $dv2 := dvsy$ $dv3 := dvsy$

$dvs1 := lspline(tx, dv1)$ $dvs2 := lspline(tx, dv2)$ $dvs3 := lspline(tx, dv3)$

$$\mu_1(t_{avg1}) := interp(dvs1, tx, dv1, t_{avg1}) \cdot 10^{-6} \cdot \frac{N \cdot s}{m^2}$$

$$\mu_2(t_{avg2}) := interp(dvs2, tx, dv2, t_{avg2}) \cdot 10^{-6} \cdot \frac{N \cdot s}{m^2}$$

$$\mu_3(t_{avg3}) := interp(dvs3, tx, dv3, t_{avg3}) \cdot 10^{-6} \cdot \frac{N \cdot s}{m^2}$$

Prantle number
information

$$pry := \begin{pmatrix} 13.6 \\ 7.02 \\ 4.34 \\ 3.02 \\ 2.22 \\ 1.74 \end{pmatrix}$$

$pry1 := pry$ $pry2 := pry$ $pry3 := pry$

$prs1 := lspline(tx, pry1)$ $prs2 := lspline(tx, pry2)$ $prs3 := lspline(tx, pry3)$

$$Pr_1(t_{avg1}) := interp(prs1, tx, pry1, t_{avg1})$$

$$Pr_2(t_{avg2}) := interp(prs2, tx, pry2, t_{avg2})$$

$$Pr_3(t_{avg3}) := interp(prs3, tx, pry3, t_{avg3})$$

Experiments. For the model and data that follows, when regarding side A and side B of the heat exchangers, the hot side (A) will have a subscript 1, the cold side (B) will have a subscript 2

Description of matrix columns: 1) hot loop flow rate, 2) cold loop flow rate, 3) T1i, 4) T1o, 5) T2i, 6) T2o, 7) normalized hot loop inlet pressure, 8) normalized hot loop pressure outlet, 9) normalized cold loop inlet pressure, 10) normalized cold loop outlet pressure, 11) T3i, 12) T3o, 13) city water flow rate, 14) power applied to bulk heaters (accounts for voltage drop across shunts in power calc)

f represents full power, h represents half power, i represents isothermal

$$Mf22 := \begin{pmatrix} 3.016 & 3.015 & 92.15 & 57.06 & 44.05 & 77.8 & 22.198 & 21.902 & 20.277 & 19.301 & 11.6 & 35.17 & 4.381 & 28283 \\ 3.511 & 3.506 & 85.06 & 54.6 & 42.5 & 71.67 & 20.249 & 19.699 & 18.996 & 17.696 & 11.68 & 34.84 & 4.45 & 28284 \\ 4.022 & 4.011 & 80.39 & 53.66 & 42.22 & 67.95 & 19.397 & 18.534 & 18.486 & 16.812 & 11.69 & 35.2 & 4.437 & 28278 \\ 4.504 & 4.536 & 76.39 & 52.44 & 41.73 & 64.56 & 18.633 & 17.414 & 18.198 & 16.089 & 11.41 & 34.66 & 4.49 & 28265 \\ 5.003 & 5.011 & 73.2 & 51.54 & 41.28 & 62.02 & 18.187 & 16.583 & 18.052 & 15.53 & 11.18 & 34.34 & 4.513 & 28261 \\ 5.497 & 5.507 & 70.69 & 50.99 & 41.11 & 60.11 & 18.195 & 16.143 & 17.828 & 14.861 & 11.26 & 34.44 & 4.529 & 28249 \\ 6.016 & 6.03 & 68.67 & 50.66 & 41.22 & 58.56 & 18.492 & 15.945 & 17.876 & 14.352 & 11.2 & 34.39 & 4.535 & 28229 \\ 7.021 & 7.019 & 65.48 & 49.97 & 41.19 & 56.14 & 19.143 & 15.535 & 18.721 & 14.064 & 11.22 & 34.43 & 4.536 & 28206 \\ 7.999 & 8.005 & 63.09 & 49.42 & 41.21 & 54.33 & 20.049 & 15.248 & 19.979 & 14.014 & 11.26 & 34.41 & 4.552 & 28189 \\ 8.999 & 9.018 & 61.56 & 49.35 & 41.63 & 53.3 & 21.225 & 15.041 & 21.45 & 13.986 & 11.16 & 35.08 & 4.382 & 28164 \\ 9.996 & 10.066 & 60.16 & 49.12 & 41.82 & 52.3 & 22.573 & 14.862 & 23.162 & 13.977 & 11.17 & 35.27 & 4.39 & 28132 \\ 11.005 & 11.016 & 58.97 & 48.9 & 41.9 & 51.51 & 24.182 & 14.74 & 24.883 & 14.022 & 11.2 & 35.4 & 4.377 & 28115 \end{pmatrix}$$

$i := 1..12$

$$Mh22 := \begin{pmatrix} 3.021 & 3.02 & 51.8 & 33.81 & 26.44 & 43.41 & 14.385 & 14.04 & 15.085 & 13.979 & 11.01 & 23.29 & 4.268 & 14216 \\ 3.516 & 3.523 & 50.87 & 34.91 & 27.94 & 43.03 & 16.726 & 16.149 & 15.591 & 14.229 & 11.91 & 24.7 & 4.218 & 14495 \\ 4.036 & 4.037 & 46.88 & 33.12 & 26.69 & 39.68 & 14.944 & 13.987 & 15.705 & 13.886 & 11.01 & 23.5 & 4.271 & 14208 \\ 4.508 & 4.511 & 46.83 & 34.19 & 28.01 & 39.94 & 17.032 & 15.764 & 16.286 & 14.164 & 11.89 & 24.41 & 4.375 & 14490 \\ 4.991 & 5.033 & 43.66 & 32.46 & 26.69 & 37.21 & 15.678 & 13.954 & 16.527 & 13.84 & 10.94 & 23.02 & 4.441 & 14199 \\ 5.498 & 5.528 & 44.2 & 33.77 & 28.18 & 37.98 & 17.686 & 15.524 & 17.202 & 14.118 & 11.98 & 24.5 & 4.373 & 14484 \\ 6 & 6.018 & 41.33 & 31.88 & 26.61 & 35.45 & 16.589 & 13.925 & 17.52 & 13.806 & 10.89 & 22.91 & 4.47 & 14187 \\ 6.996 & 7.038 & 39.65 & 31.48 & 26.62 & 34.22 & 17.672 & 13.897 & 18.71 & 13.777 & 10.89 & 22.92 & 4.478 & 14173 \\ 8.038 & 8.041 & 38.44 & 31.23 & 26.67 & 33.36 & 18.931 & 13.872 & 20.056 & 13.749 & 10.88 & 22.91 & 4.493 & 14157 \\ 9.012 & 9.027 & 37.42 & 30.93 & 26.63 & 32.61 & 20.287 & 13.851 & 21.537 & 13.73 & 10.86 & 22.91 & 4.512 & 14144 \\ 10.013 & 10.016 & 36.67 & 30.76 & 26.68 & 32.09 & 21.833 & 13.848 & 23.204 & 13.731 & 10.89 & 23 & 4.526 & 14128 \\ 11.016 & 11.019 & 36.04 & 30.61 & 26.72 & 31.65 & 23.621 & 13.895 & 25.065 & 13.811 & 10.88 & 23 & 4.533 & 14130 \end{pmatrix}$$

$i2 := 1..12$

$$Mi22 := \begin{pmatrix}
3.028 & 3.025 & 17.85 & 16.88 & 16.66 & 17.29 & 14.582 & 14.216 & 15.328 & 14.17 & 15.5 & 16.01 & 4.429 & 0 \\
3.488 & 3.497 & 13.51 & 12.57 & 12.53 & 13.05 & 14.623 & 14.039 & 15.44 & 14.022 & 11.88 & 12.38 & 4.28 & 0 \\
4.016 & 4.015 & 16.29 & 15.44 & 15.32 & 15.79 & 15.191 & 14.164 & 15.995 & 14.108 & 14.61 & 15.09 & 4.435 & 0 \\
4.522 & 4.518 & 13.05 & 12.27 & 12.33 & 12.67 & 15.386 & 14.02 & 16.261 & 13.988 & 11.87 & 12.24 & 4.269 & 0 \\
5.019 & 5.01 & 15.5 & 14.66 & 14.56 & 15.01 & 16.018 & 14.143 & 16.885 & 14.089 & 13.74 & 14.31 & 4.413 & 0 \\
5.506 & 5.516 & 13.08 & 12.32 & 12.38 & 12.7 & 16.325 & 14.011 & 17.242 & 13.961 & 11.9 & 12.29 & 4.266 & 0 \\
6.022 & 6.039 & 14.39 & 13.55 & 13.46 & 13.91 & 17.008 & 14.12 & 17.994 & 14.066 & 12.58 & 13.22 & 4.405 & 0 \\
7.021 & 7.017 & 14.23 & 13.53 & 13.55 & 13.83 & 18.144 & 14.099 & 19.216 & 14.048 & 13.05 & 13.42 & 4.44 & 0 \\
8.008 & 8.01 & 13.91 & 13.17 & 13.15 & 13.49 & 19.435 & 14.086 & 20.622 & 14.04 & 12.36 & 12.95 & 4.437 & 0 \\
9.004 & 9.017 & 13.61 & 12.89 & 12.9 & 13.21 & 20.893 & 14.071 & 22.215 & 14.031 & 12.17 & 12.73 & 4.416 & 0 \\
10.028 & 10.013 & 13.66 & 12.96 & 12.98 & 13.27 & 22.563 & 14.068 & 23.949 & 14.044 & 12.26 & 12.81 & 4.446 & 0 \\
11.007 & 11.029 & 13.84 & 13.14 & 13.15 & 13.43 & 24.389 & 14.123 & 25.934 & 14.15 & 12.34 & 12.96 & 4.457 & 0
\end{pmatrix}$$

$i3 := 1..12$

Now listing experimentally determined hose pressure drops. The values correspond to the closest nominal flow rates in the experimental heat exchanger data. First column is for raw hot side pressure drop and second column is for the raw cold side pressure drop

(1) is full power
2 half power
3 isothermal

$$Mhosedrop := \begin{pmatrix}
-0.318 & 0.363 \\
-0.212 & 0.47 \\
-0.101 & 0.618 \\
0.029 & 0.755 \\
0.225 & 0.895 \\
0.39 & 1.052 \\
0.553 & 1.207 \\
0.948 & 1.584 \\
1.385 & 2.001 \\
1.891 & 2.49 \\
2.433 & 3.023 \\
3.03 & 3.576
\end{pmatrix}$$

all three experimental runs share the same sets of flow rates

Now creating additional matrixes to calculate perturbations in the data due to measurement uncertainties

$Uclflowmeter1 := 1.0034$ $Uhlflowmeter1 := 1.0052$

$Uclflowmeter2 := .9966$ $Uhlflowmeter2 := 0.9948$

maximum heat transfer error matrices

$Mf2err_{i,1} := Mf22_{i,1} \cdot Uhlflowmeter1$ $Mf2err_{i,2} := Mf22_{i,2} \cdot Uclflowmeter1$

T1i value T1o value

$Mf2err_{i,3} := Mf22_{i,3} + .16$ $Mf2err_{i,4} := Mf22_{i,4} + -.16$

T2i value T2o value

$Mf2err_{i,5} := Mf22_{i,5} + -.16$ $Mf2err_{i,6} := Mf22_{i,6} + -.16$

Hot loop raw pressure drop

$Mf2err_{i,7} := Mf22_{i,7} \cdot 1.00285 + .049$ $Mf2err_{i,8} := Mf22_{i,8} \cdot .99715$

Cold loop raw pressure drop

$Mf2err_{i,9} := Mf22_{i,9}$ $Mf2err_{i,10} := Mf22_{i,10}$

$Mf2err_{i,11} := Mf22_{i,11}$ $Mf2err_{i,12} := Mf22_{i,12}$

$Mf2err_{i,13} := Mf22_{i,13}$ $Mf2err_{i,14} := Mf22_{i,14}$

half power error matrices

Now defining property values from matrixes

$$Q1(Mf,i) := Mf_{i,1}\cdot gpm \qquad Q2(Mf,i) := Mf_{i,2}\cdot gpm \qquad Q3(Mf,i) := Mf_{i,13}\cdot gpm$$

$$T1i(Mf,i) := Mf_{i,3}\,°C - .73\,°C \qquad T2i(Mf,i) := Mf_{i,5}\,°C - .02\,°C$$

$$T1o(Mf,i) := Mf_{i,4}\,°C - .21\,°C \qquad T2o(Mf,i) := Mf_{i,6}\,°C - .10\,°C$$

$$T3i(Mf,i) := Mf_{i,11}\,°C \qquad T3o(Mf,i) := Mf_{i,12}\,°C$$

$$tavg1(Mf,i) := \frac{\left(Mf_{i,3} - .73\right) + \left(Mf_{i,4} - .21\right)}{2} \qquad tavg2(Mf,i) := \frac{\left(Mf_{i,5} - .02\right) + \left(Mf_{i,6} - .1\right)}{2}$$

$$tavg3(Mf,i) := \frac{Mf_{i,9} + Mf_{i,10}}{2}$$

Now listing experimentally determined offsets for temperature difference and pressure

$$\Delta Photoffset := .54$$

$$\Delta Pcoldoffset := -.1$$

Considering the offset of
ΔP

$$\Delta P1(Mf,i) := \left[\left(Mf_{i,7} - Mf_{i,8}\right) + \Delta Photoffset\right]\cdot psi$$

$$\Delta P2(Mf,i) := \left[\left(Mf_{i,9} - Mf_{i,10}\right) + \Delta Pcoldoffset\right]\cdot psi$$

Now calculating NTU relationships

$$C1(Mf,i) := \rho_1(tavg1(Mf,i)) \cdot Q1(Mf,i) \cdot c_{p1}(tavg1(Mf,i))$$

$$C2(Mf,i) := \rho_2(tavg2(Mf,i)) \cdot Q2(Mf,i) \cdot c_{p2}(tavg2(Mf,i))$$

$$Cmin(Mf,i) := \min(C1(Mf,i), C2(Mf,i)) \qquad Cmax(Mf,i) := \max(C1(Mf,i), C2(Mf,i))$$

$$Cr(Mf,i) := \frac{Cmin(Mf,i)}{Cmax(Mf,i)}$$

$$\varepsilon(Mf,i) := \frac{C1(Mf,i) \cdot (T1i(Mf,i) - T1o(Mf,i))}{Cmin(Mf,i) \cdot (T1i(Mf,i) - T2i(Mf,i) + 0)}$$

$$NTU(Mf,i) := \frac{1}{1 - Cr(Mf,i)} \cdot \ln\left(\frac{1 - \varepsilon(Mf,i) \cdot Cr(Mf,i)}{1 - \varepsilon(Mf,i)}\right)$$

$$U2(Mf,i) := \frac{NTU(Mf,i) \cdot Cmin(Mf,i)}{A_2}$$

$$h(Mf,i) := \frac{U2(Mf,i) \cdot \left(\frac{A_2}{A_1} + 1\right)}{1 - \frac{U2(Mf,i) \cdot \delta}{k_w}}$$

This section calculates values from the data, friction factor, reynolds, colburn, etc.

$$G1(Mf,i) := \frac{\rho_1(tavg1(Mf,i)) \cdot Q1(Mf,i)}{A_{c1}} \qquad G2(Mf,i) := \frac{\rho_2(tavg2(Mf,i)) \cdot Q2(Mf,i)}{A_{c2}}$$

$$Gp1(Mf,i) := \frac{4 \cdot \rho_1(tavg1(Mf,i)) \cdot Q1(Mf,i)}{\pi \cdot D_p^{\,2}} \qquad Gp2(Mf,i) := \frac{4 \cdot \rho_2(tavg2(Mf,i)) \cdot Q2(Mf,i)}{\pi \cdot D_p^{\,2}}$$

$$j1(Mf,i) := \frac{h(Mf,i) \cdot Pr_1(tavg1(Mf,i))^{\frac{2}{3}}}{G1(Mf,i) \cdot c_{p1}(tavg1(Mf,i))} \qquad j2(Mf,i) := \frac{h(Mf,i) \cdot Pr_2(tavg2(Mf,i))^{\frac{2}{3}}}{G2(Mf,i) \cdot c_{p2}(tavg2(Mf,i))}$$

The various friction factors calculated below represent different corrections applied. f1 is the basic form used to calculate the friction factor, while the hose designations have the experimental hose pressure drop subtracted from them. The h designation at the end is used to distinguish between the various runs with different numbers of flow rate sets.

$$f1(Mf,i) := \left[\Delta P1(Mf,i) - \frac{1.5\cdot(Gp1(Mf,i))^2}{2\cdot\rho_1(tavg1(Mf,i))}\right]\cdot\frac{D_h\cdot\rho_1(tavg1(Mf,i))}{2\cdot L_p\cdot G1(Mf,i)^2}$$

$$f1withhosef(Mf,i) := \left[\left[\Delta P1(Mf,i) - \left(Mhosedrop_{i,1} + \Delta Photoffset\right)\cdot psi\right] - \frac{1.5\cdot(Gp1(Mf,i))^2}{2\cdot\rho_1(tavg1(Mf,i))}\right]\cdot\frac{D_h\cdot\rho_1(tavg1(Mf,i))}{2\cdot L_p\cdot G1(Mf,i)^2}$$

$$f2(Mf,i) := \left[\Delta P2(Mf,1) - \frac{1.5\cdot(Gp2(Mf,i))^2}{2\cdot\rho_2(tavg2(Mf,i))}\right]\cdot\frac{D_h\cdot\rho_2(tavg2(Mf,i))}{2\cdot L_p\cdot G2(Mf,i)^2}$$

$$f2withhose(Mf,i) := \left[\left[\Delta P1(Mf,i) - \left(Mhosedrop_{i,2} + \Delta Pcoldoffset\right)\cdot psi\right] - \frac{1.5\cdot(Gp1(Mf,i))^2}{2\cdot\rho_1(tavg1(Mf,i))}\right]\cdot\frac{D_h\cdot\rho_1(tavg1(Mf,i))}{2\cdot L_p\cdot G1(Mf,i)^2}$$

$$Re1(Mf,i) := \frac{G1(Mf,i)\cdot D_h}{\mu_1(tavg1(Mf,i))} \qquad Re2(Mf,i) := \frac{G2(Mf,i)\cdot D_h}{\mu_2(tavg2(Mf,i))}$$

$$Nu1(Mf,i) := \frac{h(Mf,i)\cdot L_p}{k_w}$$

Now calculating values from martin correlation

$$Nu_1(Q1) := \frac{h_1(Q1)\cdot L_p}{k_w}$$

$Q1_i := 1gpm, 1.02gpm .. 15gpm$

Full power values

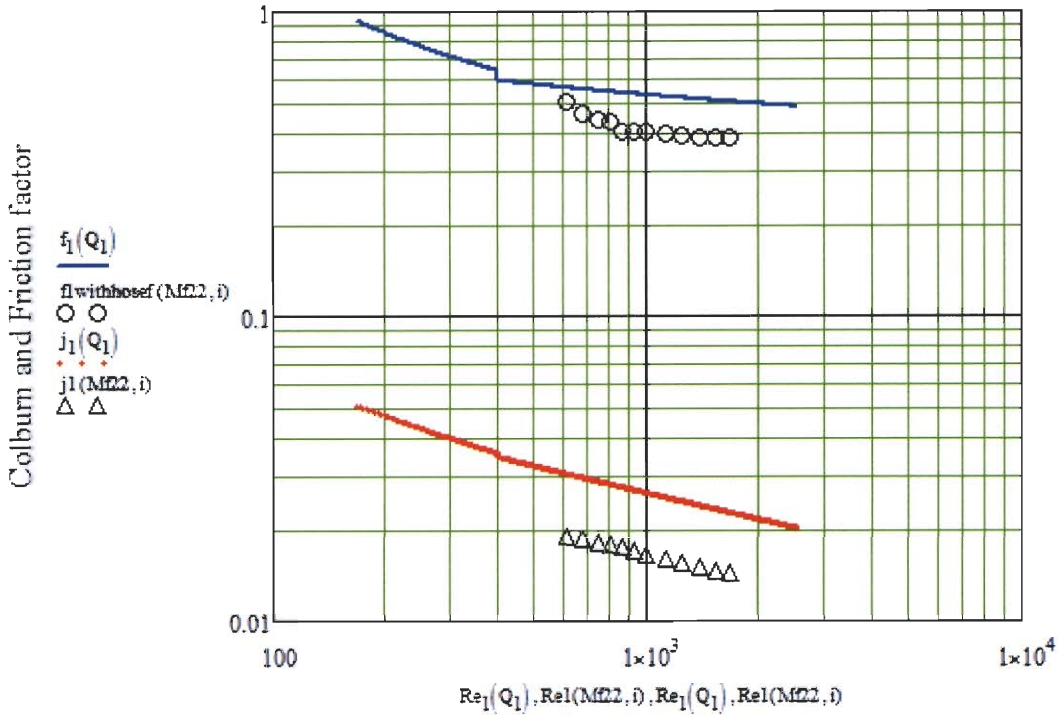


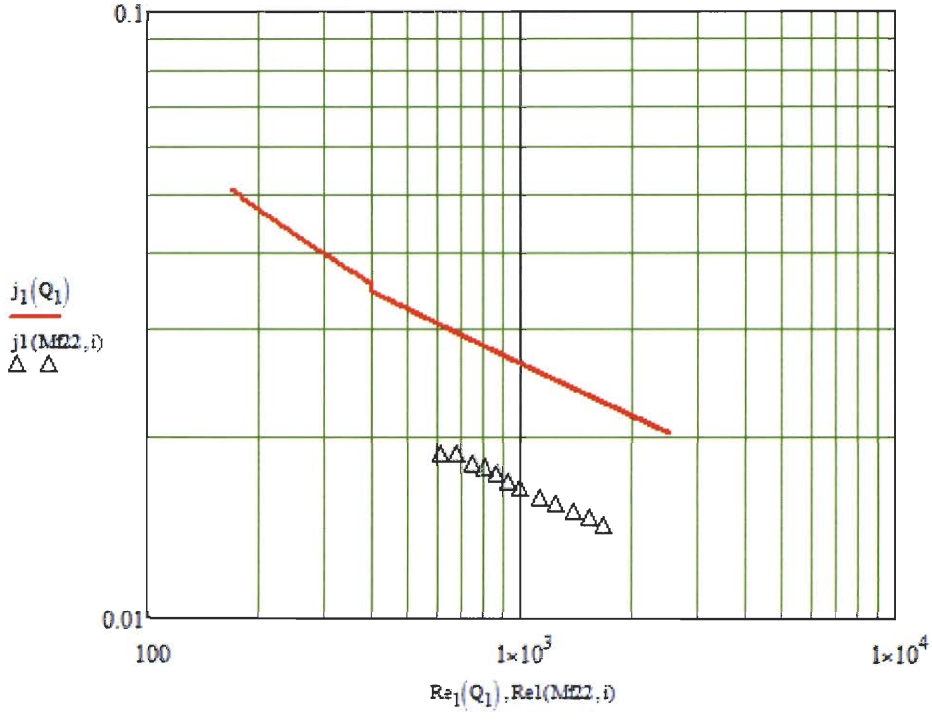

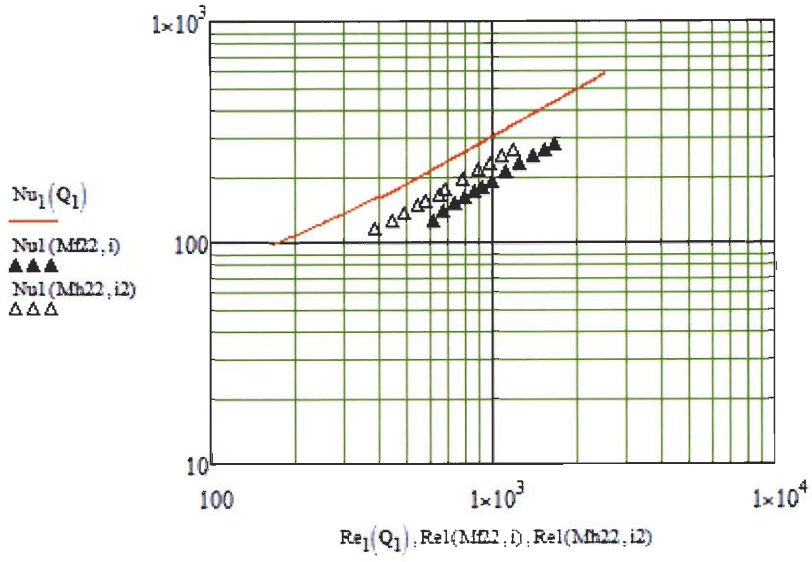


half power values

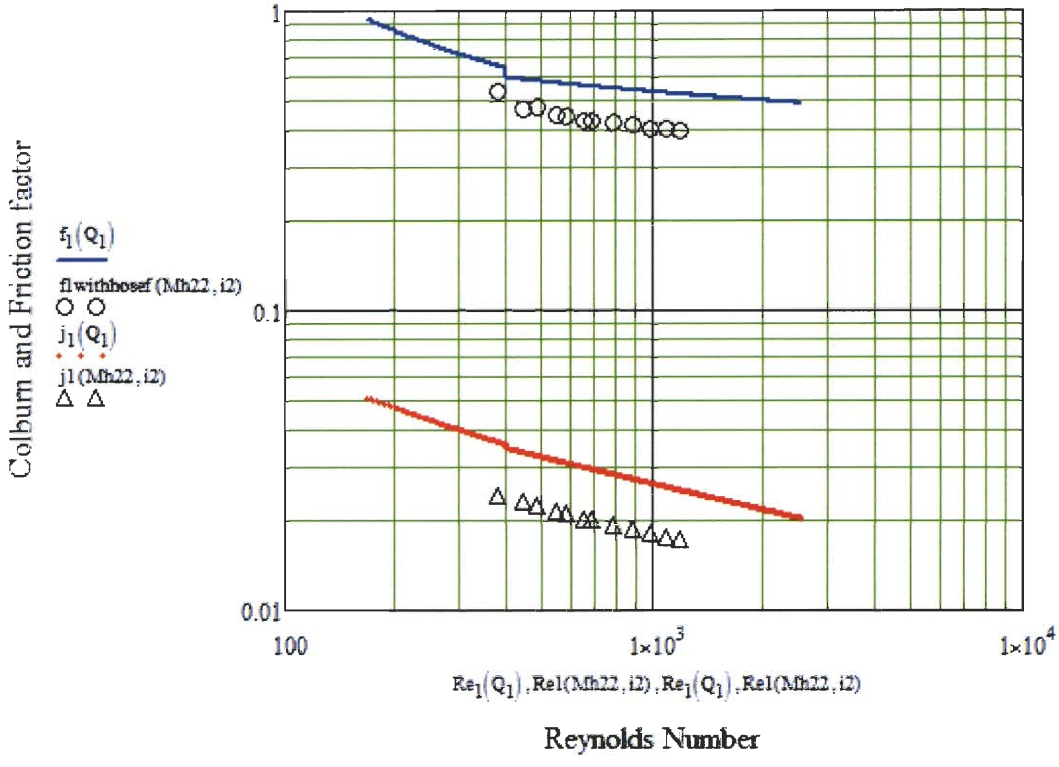

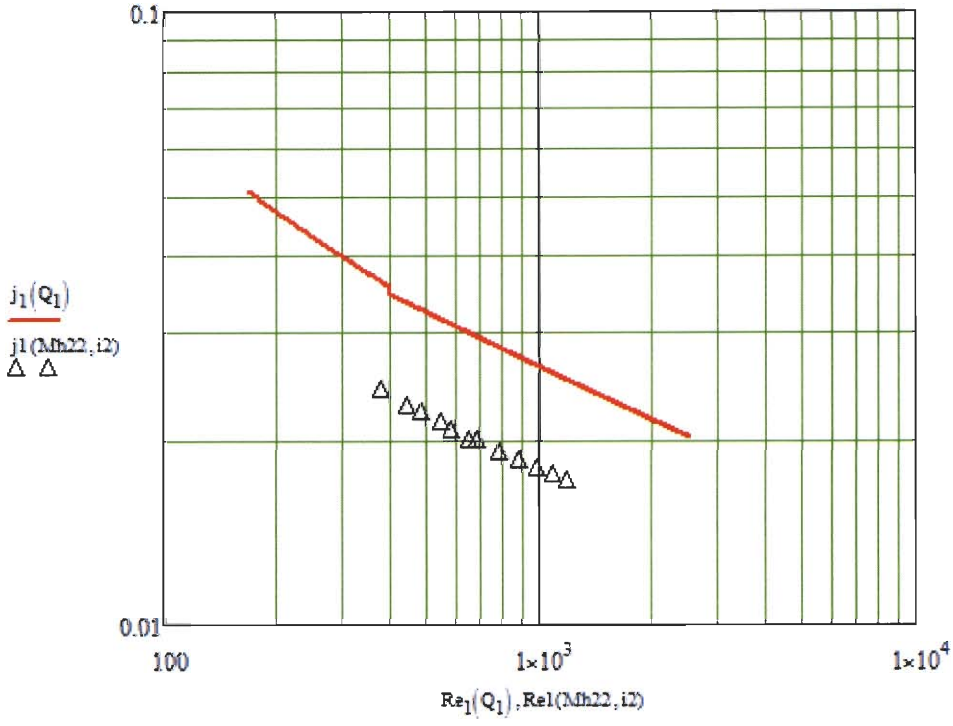


Isothermal pressure

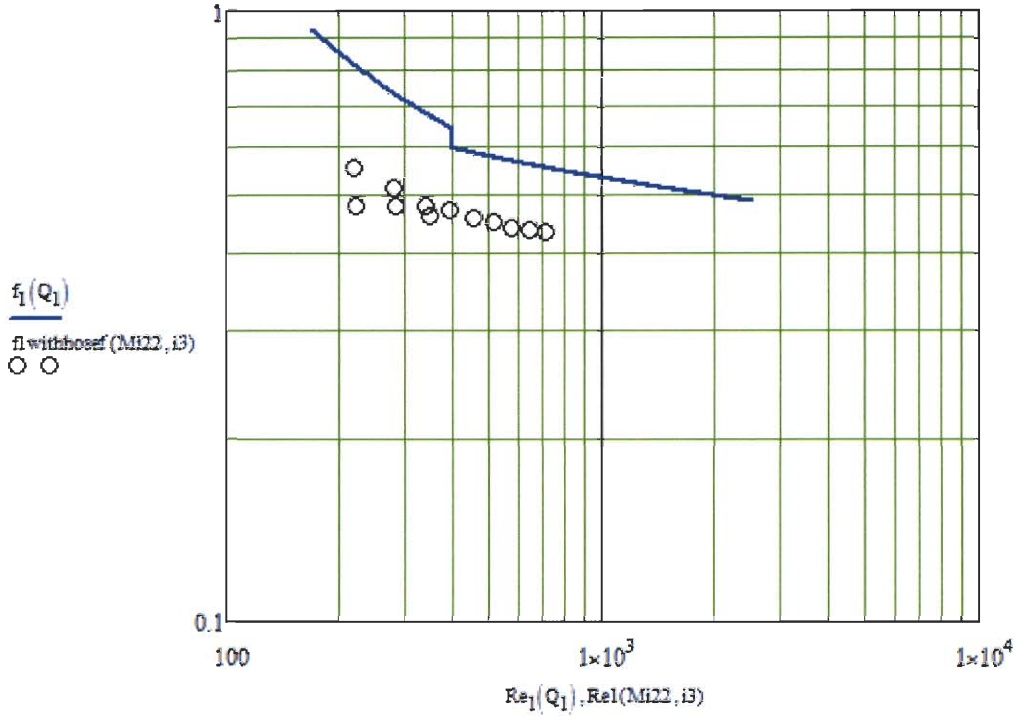

Now what follow is a calculation of the associated error for heat transfer, reynolds number, convection coefficient and friction factors

$$\Delta Tcityoffset := 0$$

$$\Delta T1(Mf, i) := T1i(Mf, i) - T1o(Mf, i)$$

$$\Delta T2(Mf, i) := T2o(Mf, i) - T2i(Mf, i)$$

$$\Delta T3(Mf, i) := T3o(Mf, i) - T3i(Mf, i)$$

$$mmdot1(Mf, i) := Q1(Mf, i) \cdot \rho_1(tavg1(Mf, i))$$

$$mmdot2(Mf, i) := Q2(Mf, i) \cdot \rho_2(tavg2(Mf, i))$$

$$mmdot3(Mf, i) := Q3(Mf, i) \cdot \rho_3(tavg3(Mf, i))$$

$$Qheat1(Mf, i) := mmdot1(Mf, i) \cdot c_{p1}(tavg1(Mf, i)) \cdot \Delta T1(Mf, i)$$

$$Qheat2(Mf, i) := mmdot2(Mf, i) \cdot c_{p2}(tavg2(Mf, i)) \cdot \Delta T2(Mf, i)$$

$$Qheat3(Mf, i) := mmdot3(Mf, i) \cdot c_{p3}(tavg3(Mf, i)) \cdot \Delta T3(Mf, i)$$

$$Qheatelectric(Mf, i) := Mf_{i,14} \cdot W$$

$$Qhxmin(Mf, i) := min(Qheat1(Mf, i), Qheat2(Mf, i))$$

$$Qhxmax(Mf, i) := max(Qheat1(Mf, i), Qheat2(Mf, i))$$

$$Qhxavg(Mf, i) := \frac{Qheat1(Mf, 1) + Qheat2(Mf, i)}{2}$$

$$Qdiffhotvscold(Mf, i) := \frac{Qhxmax(Mf, i) - Qhxmin(Mf, i)}{Qhxmin(Mf, i)} \cdot 100$$

$$Qdiffhot(Mf, i) := \frac{Qheat1(Mf, i) - Qhxavg(Mf, i)}{Qhxavg(Mf, i)} \cdot 100$$

$$Qdiffcold(Mf, i) := \frac{Qheat2(Mf, i) - Qhxavg(Mf, i)}{Qhxavg(Mf, i)} \cdot 100$$

$$Qhxavgvselectric(Mf, i) := \frac{Qheatelectric(Mf, i) - Qhxavg(Mf, i)}{Qhxavg(Mf, i)} \cdot 100$$

$$Qhxavgvscity(Mf, i) := \frac{Qheat3(Mf, i) - Qhxavg(Mf, i)}{Qhxavg(Mf, i)} \cdot 100$$

Qdiffhotvscold represents comparison between the min and maximum experimental data. Qdiff hot and cold represent the heat transfer differences using the method used by muley and manglik 1999 asme paper.

Qdiffhot(Mf22,i) =

| |
|---|
| 1.0628 |
| 1.7822 |
| 1.7046 |
| 1.7275 |
| 1.8436 |
| 1.2413 |
| 1.1269 |
| 1.0627 |
| 1.0436 |
| 1.0164 |
| 0.9214 |
| 0.7418 |

Qdiffhot(Mh22,i2) =

| |
|---|
| 1.5828 |
| 2.6414 |
| 1.833 |
| 2.8027 |
| 1.2119 |
| 2.2872 |
| 1.6009 |
| 1.3089 |
| 1.5908 |
| 1.5529 |
| 1.7603 |
| 1.938 |

Qdiffcold(Mf22,i) =

| |
|---|
| -1.0628 |
| -0.7518 |
| -0.2757 |
| -0.0855 |
| 0.1054 |
| 0.4461 |
| 0.4051 |
| 0.5702 |
| 0.5934 |
| 0.6631 |
| 0.7509 |
| 0.8988 |

Qdiffcold(Mh22,i2) =

| |
|---|
| -1.5828 |
| 0.2109 |
| -0.4798 |
| 0.7751 |
| -0.0528 |
| 1.0472 |
| 0.126 |
| 0.3325 |
| 0.5513 |
| 0.6593 |
| 0.7812 |
| 0.8376 |

Qhxavgvscity(Mf22,i) =

| |
|---|
| 2.1422 |
| 1.6964 |
| 2.4776 |
| 2.3841 |
| 2.3315 |
| 2.454 |
| 2.6876 |
| 2.6148 |
| 2.6574 |
| 2.0051 |
| 2.8299 |
| 2.7578 |

Qhxavgvselectric(Mf22,i) =

| |
|---|
| 6.0516 |
| 5.729 |
| 5.2071 |
| 4.9592 |
| 4.7442 |
| 4.3427 |
| 4.3117 |
| 4.054 |
| 3.967 |
| 3.802 |
| 3.5924 |
| 3.3755 |

Qdiffhotvscold(Mf22,i) =

| |
|---|
| 2.1483 |
| 2.5532 |
| 1.9858 |
| 1.8145 |
| 1.7363 |
| 0.7917 |
| 0.7189 |
| 0.4897 |
| 0.4475 |
| 0.351 |
| 0.1692 |
| 0.1559 |

# Appendix D

## MATHCAD for GB240H-20

GEA GB240H-20

**MathCAD format solution:**

# Test Heat Exchanger GB240H-20

Hot and cold water properties at Tf

$T_{hot\_water} := 50\,°C$ $T_{cold\_water} := 40\,°C$

Hot water (subscript 1) Cold water (subscript 2)

$\rho_1 := 985\,\frac{kg}{m^3}$ $\rho_2 := 994\,\frac{kg}{m^3}$

$c_{p1} := 4184\,\frac{J}{kg\cdot K}$ $c_{p2} := 4178\,\frac{J}{kg\cdot K}$

$k_1 := 0.639\,\frac{W}{m\cdot K}$ $k_2 := 0.628\,\frac{W}{m\cdot K}$

$\mu_1 := 471\cdot 10^{-6}\,\frac{N\cdot s}{m^2}$ $\mu_2 := 654\cdot 10^{-6}\,\frac{N\cdot s}{m^2}$

$Pr_1 := 3.02$ $Pr_2 := 4.34$

Thermal conductivity of the plate (Stainless Steel AISI 316)

$k_w := 13.4\,\frac{W}{m\cdot K}$

**Given information**

Volume flow rates for hot and cold water

$Q_1 := 10gpm$ $Q_2 := 10gpm$

Mass flow rates

$mdot_1(Q_1) := \rho_1\cdot Q_1$ $mdot_1(Q_1) = 0.6214\,\frac{kg}{s}$

$mdot_2(Q_2) := \rho_2\cdot Q_2$ $mdot_2(Q_2) = 0.6271\,\frac{kg}{s}$

**Geometric parameters:**

$N_p := 1$ Number of passes

$\beta := 60deg$ Corrugation inclination angle (chevron angle)

$N_t := 20$ Total number of plates

$D_p := 1in$ Port diameter

$t_n := 0.087in$ spacing between plates

$\alpha := 40deg$ Corrugation Pitch angle

$\lambda := t_n \cdot \tan(\alpha)$ Corrugation Pitch (=wavelengtht) $\lambda = 0.073 \cdot in$

$\delta := 0.6mm$ Thickness of the plates

Use the dimensions of the test heat exchanger

$W_p := 3in$ $L_{p2p} := 16.3in$ $L_p := L_{p2p} - 1.5in$ $L_p = 14.8 \cdot in$

$H_p := t_n \cdot N_t$ $H_p = 1.74 \cdot in$

Number of wavelength per single plate

$$N_\lambda := \frac{W_p}{\lambda}$$

Number of channels for hot and cold fluid

$$N_{c1} := \frac{N_t}{2N_p} \qquad N_{c1} = 10$$

$$N_{c2} := \frac{N_t}{2N_p} - 1 \qquad N_{c2} = 9$$

Amplitude of corrugation and channel spacing

$$a := \frac{1}{2} \cdot \left( \frac{H_p}{N_t} - \delta \right) \qquad a = 0.0317 \cdot in \qquad 2 \cdot a = 0.0634 \cdot in \qquad 2 \cdot a + \delta = 0.087 \cdot in$$

Corrugation ratio $\gamma$

$$\gamma := 4\cdot\frac{a}{\lambda} \qquad \gamma = 1.7363$$

Corrugated length

$$L_\lambda := \int_0^\lambda \sqrt{1 + \left(\frac{2\cdot\pi\cdot a}{\lambda}\right)^2 \cdot \cos\left(\frac{2\cdot\pi}{\lambda}\cdot x\right)^2}\, dx$$

Heat transfer area for hot fluid (fluid1)

$$A_1 := 2\cdot L_\lambda \cdot N_\lambda \cdot L_p \cdot N_{c1} \qquad A_1 = 1.1862\,m^2$$

$$A_2 := 2\cdot L_\lambda \cdot N_\lambda \cdot L_p \cdot N_{c2} \qquad A_2 = 1.0676\,m^2$$

Now setting the heat transfer area equal to the minimum area, which is A2

$$A_{1_{min}} := A_2$$

Projected area for the plates

$$A_{p1} := 2\cdot W_p \cdot L_p \cdot N_{c1} \qquad A_{p2} := 2\cdot W_p \cdot L_p \cdot N_{c2}$$

**Enlargement factor φ**

$$\Phi := \frac{L_\lambda \cdot N_\lambda}{W_p} \qquad \Phi = 2.0705$$

Exact hydraulic diameter

$$D_h := \frac{4\cdot a}{\Phi} \qquad D_h = 1.555\cdot mm$$

Minimum free-flow area

$$A_{c1} := 2\cdot a\cdot W_p \cdot N_{c1} \qquad A_{c1} = 1.9013\cdot in^2$$

$$A_{c2} := 2\cdot a\cdot W_p \cdot N_{c2} \qquad A_{c2} = 1.7112\cdot in^2$$

Mass velocity

$$G_1(Q_1) := \frac{mdot_1(Q_1)}{A_{c1}} \qquad v_1 := \frac{G_1(Q_1)}{\rho_1} = 0.5143\,\frac{m}{s}$$

$$Re_1(Q_1) := \frac{G_1(Q_1)\cdot D_h}{\mu_1} \qquad Re_1(Q_1) = 1.6725 \times 10^3$$

$$G_2(Q_2) := \frac{mdot_2(Q_2)}{A_{c2}} \qquad v_2 := \frac{G_2(Q_2)}{\rho_2} = 0.5715\,\frac{m}{s}$$

$$Re_2(Q_2) := \frac{G_2(Q_2)\cdot D_h}{\mu_2} \qquad Re_2(Q_2) = 1.3506 \times 10^3$$

**Friction factors**

Martin's correlation (1996) for the Darcy friction factor is modified by the Fanning friction factor.

Martin, H., 1996, A theoretical approach to predict the performance of chevron-type plate heat exchanger, Chem. Eng. Processing, Vol.35, pp. 301-310.

$$f_{o1}(Q_1) := \begin{cases} \left(1.56\cdot\ln(Re_1(Q_1)) - 3.0\right)^{-2} & \text{if } Re_1(Q_1) \geq 400 \\ \dfrac{16}{Re_1(Q_1)} & \text{otherwise} \end{cases}$$

$$f_{o2}(Q_2) := \begin{cases} \left(1.56\cdot\ln(Re_2(Q_2)) - 3.0\right)^{-2} & \text{if } Re_2(Q_2) \geq 400 \\ \dfrac{16}{Re_2(Q_2)} & \text{otherwise} \end{cases}$$

$$f_{m1}(Q_1) := \begin{cases} \dfrac{9.75}{Re_1(Q_1)^{0.289}} & \text{if } Re_1(Q_1) \geq 400 \\ \dfrac{149.25}{Re_1(Q_1)} + 0.9625 & \text{otherwise} \end{cases}$$

$$f_{m2}(Q_2) := \begin{cases} \dfrac{9.75}{Re_2(Q_2)^{0.289}} & \text{if } Re_2(Q_2) \geq 400 \\ \dfrac{149.25}{Re_2(Q_2)} + 0.9625 & \text{otherwise} \end{cases}$$

$$f_1(Q_1) := \left[\frac{\cos(\beta)}{\left(0.045\cdot\tan(\beta) + 0.09\cdot\sin(\beta) + \dfrac{f_{o1}(Q_1)}{\cos(\beta)}\right)^{0.5}} + \left(\frac{1-\cos(\beta)}{\sqrt{3.8\cdot f_{m1}(Q_1)}}\right)\right]^{-2}$$

$$f_1(Q_1) = 0.5039$$

$$f_2(Q_2) := \left[ \frac{\cos(\beta)}{\left( 0.045 \cdot \tan(\beta) + 0.09 \cdot \sin(\beta) + \frac{f_{o2}(Q_2)}{\cos(\beta)} \right)^{0.5}} + \left( \frac{1 - \cos(\beta)}{\sqrt{3.8 \cdot f_{m2}(Q_2)}} \right) \right]^{-2}$$

$$f_2(Q_2) = 0.5144$$

Heat transfer coefficients

$$h_1(Q_1) := \frac{k_1}{D_h} \cdot \left[ 0.205 \cdot Pr_1^{\frac{1}{3}} \cdot 1^{\frac{1}{6}} \cdot \left( f_1(Q_1) \cdot Re_1(Q_1)^2 \cdot \sin(2 \cdot \beta) \right)^{0.374} \right]$$

$$h_1(Q_1) = 2.3011 \times 10^4 \cdot \frac{W}{m^2 \cdot K}$$

$$h_2(Q_2) := \frac{k_2}{D_h} \cdot \left[ 0.205 \cdot Pr_2^{\frac{1}{3}} \cdot 1^{\frac{1}{6}} \cdot \left( f_2(Q_2) \cdot Re_2(Q_2)^2 \cdot \sin(2 \cdot \beta) \right)^{0.374} \right]$$

$$h_2(Q_2) = 2.1917 \times 10^4 \cdot \frac{W}{m^2 \cdot K}$$

Overall heat teansfer coefficient

$$U_2(Q_1, Q_2) := \frac{1}{\frac{A_2}{h_1(Q_1) \cdot A_1} + \frac{\delta}{k_w} + \frac{1}{h_2(Q_2)}}$$

$$U_2(Q_1, Q_2) = 7.4705 \times 10^3 \cdot \frac{W}{m^2 K}$$

$$U_2(Q_1, Q_2) \cdot A_2 = 7.9753 \times 10^3 \cdot \frac{W}{K}$$

**Effectiveness-NTU Method**

$$C_1(Q_1) := mdot_1(Q_1) \cdot c_{p1} \qquad C_1(Q_1) = 2.6001 \times 10^3 \frac{m^2 \cdot kg}{K \cdot s^3}$$

$$C_2(Q_2) := mdot_2(Q_2) \cdot c_{p2} \qquad C_2(Q_2) = 2.6201 \times 10^3 \frac{m^2 \cdot kg}{K \cdot s^3}$$

$$C_{min}(Q_1,Q_2) := \min(C_1(Q_1),C_2(Q_2)) \qquad C_{min}(Q_1,Q_2) = 2.6001 \times 10^3 \frac{m^2 \cdot kg}{K \cdot s^3}$$

$$C_{max}(Q_1,Q_2) := \max(C_1(Q_1),C_2(Q_2)) \qquad C_{max}(Q_1,Q_2) = 2.6201 \times 10^3 \frac{m^2 \cdot kg}{K \cdot s^3}$$

$$C_r(Q_1,Q_2) := \frac{C_{min}(Q_1,Q_2)}{C_{max}(Q_1,Q_2)} \qquad C_r(Q_1,Q_2) = 0.9924$$

$$NTU(Q_1,Q_2) := \frac{U_2(Q_1,Q_2)\cdot A_2}{C_{min}(Q_1,Q_2)} \qquad NTU(Q_1,Q_2) = 3.0673$$

Counterflow effectiveness

$$\varepsilon_{PHE}(Q_1,Q_2) := \frac{1-\exp\left[-NTU(Q_1,Q_2)\cdot(1-C_r(Q_1,Q_2))\right]}{1-C_r(Q_1,Q_2)\cdot\exp\left[-NTU(Q_1,Q_2)\cdot(1-C_r(Q_1,Q_2))\right]}$$

$$\varepsilon_{PHE}(Q_1,Q_2) = 0.7563$$

$Q_m := 1gpm, 2gpm .. 15gpm$

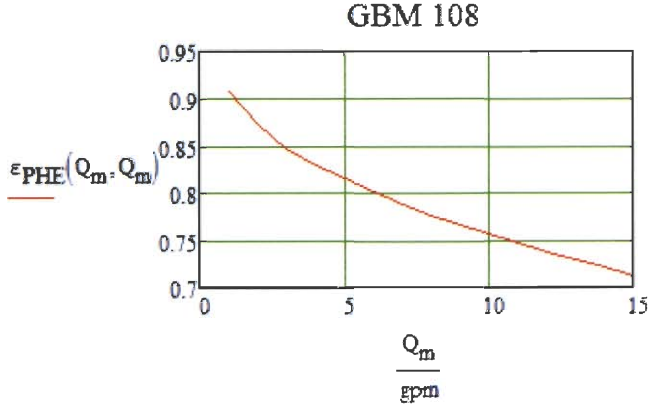


Heat transfer rate for the PHE

$$q(T_{1i},T_{2i},Q_1,Q_2) := \varepsilon_{PHE}(Q_1,Q_2)\cdot C_{min}(Q_1,Q_2)\cdot(T_{1i}-T_{2i})$$

Since $$\varepsilon_{PHE} = \frac{C_1\cdot(T_{1i}-T_{1o})}{C_{min}\cdot(T_{1i}-T_{2i})} = \frac{C_2\cdot(T_{2o}-T_{2i})}{C_{min}\cdot(T_{1i}-T_{2i})}$$

$$T_{1o}(T_{1i}, T_{2i}, Q_1, Q_2) := T_{1i} - \varepsilon_{PHE}(Q_1, Q_2) \cdot \frac{C_{min}(Q_1, Q_2)}{C_1(Q_1)} \cdot (T_{1i} - T_{2i})$$

$$T_{2o}(T_{1i}, T_{2i}, Q_1, Q_2) := T_{2i} + \varepsilon_{PHE}(Q_1, Q_2) \cdot \frac{C_{min}(Q_1, Q_2)}{C_2(Q_2)} \cdot (T_{1i} - T_{2i})$$

$$j_1(Q_1) := \frac{h_1(Q_1) \cdot Pr_1^{\frac{2}{3}}}{G_1(Q_1) \cdot c_{p1}}$$

$T_{1i} := 70\,°C$ $T_{2i} := 30\,°C$

$Q_m := 0.1gpm, 0.11gpm .. 12gpm$

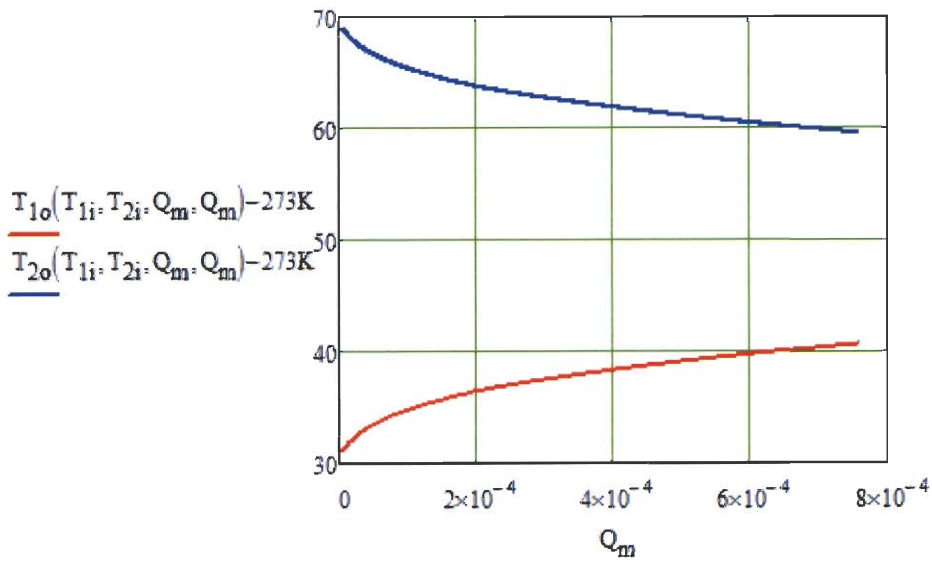


**Pressure Drop**

The frictional channel pressure drop

$$\Delta P_{f1}(Q_1) := \frac{2 \cdot f_1(Q_1) \cdot L_p}{D_h} \cdot \frac{G_1(Q_1)^2}{\rho_1} \cdot N_p \qquad \Delta P_{f1}(Q_1) = 9.2077 \cdot psi$$

$$\Delta P_{f2}(Q_2) := \frac{2 \cdot f_2(Q_2) \cdot L_p}{D_h} \cdot \frac{G_2(Q_2)^2}{\rho_2} \cdot N_p \qquad \Delta P_{f2}(Q_2) = 11.7096 \cdot psi$$

The connection and port pressure drop

$$G_{p1}(Q_1) := \frac{4 \cdot mdot_1(Q_1)}{\pi \cdot D_p^{\,2}} \qquad G_{p1}(Q_1) = 1.2264 \times 10^3 \ \frac{kg}{m^2 \cdot s}$$

$$G_{p2}(Q_2) := \frac{4 \cdot mdot_2(Q_2)}{\pi \cdot D_p^{\,2}}$$

$$\Delta P_{p1}(Q_1) := 1.5 \cdot N_p \cdot \frac{G_{p1}(Q_1)^2}{2 \cdot \rho_1} \qquad \Delta P_{p1}(Q_1) = 0.1661 \cdot psi$$

$$\Delta P_{p2}(Q_2) := 1.5 \cdot N_p \cdot \frac{G_{p2}(Q_2)^2}{2 \cdot \rho_2} \qquad \Delta P_{p2}(Q_2) = 0.1676 \cdot psi$$

$$\Delta P_1(Q_1) := \Delta P_{f1}(Q_1) + \Delta P_{p1}(Q_1) \qquad \Delta P_1(Q_1) = 9.3739 \cdot psi$$

$$\Delta P_2(Q_2) := \Delta P_{f2}(Q_2) + \Delta P_{p2}(Q_2) \qquad \Delta P_2(Q_2) = 11.8772 \cdot psi$$

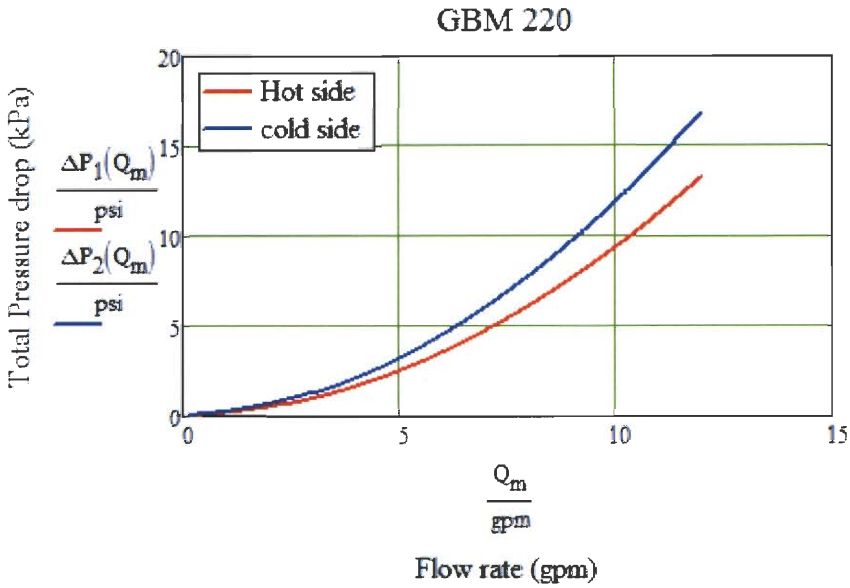


$$f_1(Q_1) := \left( \Delta P_1(Q_1) - \frac{1.5 \cdot G_{p1}(Q_1)^2}{2 \cdot \rho_1} \right) \cdot \frac{D_h \cdot \rho_1}{2 \cdot L_p \cdot G_1(Q_1)^2 \cdot N_p}$$

Experimental Data

ORIGIN := 1

$i := 1, 2 .. 10$

$M_{i,1} := i$

$$M_{i,2} := \frac{T_{1i} - 273K}{K}$$

$$M_{i,3} := \frac{T_{1o}(T_{1i}, T_{2i}, i \cdot gpm, i \cdot gpm) - 273.15K}{K}$$

$$M_{i,4} := \frac{T_{2i} - 273K}{K}$$

$$M_{i,5} := \frac{T_{2o}(T_{1i}, T_{2i}, i \cdot gpm, i \cdot gpm) - 273.15K}{K}$$

$$M_{i,6} := \frac{\Delta P_1(i \cdot gpm)}{psi} \qquad M_{i,7} := \frac{\Delta P_2(i \cdot gpm)}{psi}$$

Predictions

M =

| | 1 | 2 | 3 | 4 | 5 | 6 | 7 |
|---|---|---|---|---|---|---|---|
| 1 | 1 | 70.15 | 33.6986 | 30.15 | 66.0243 | 0.1716 | 0.2406 |
| 2 | 2 | 70.15 | 35.0896 | 30.15 | 64.644 | 0.5034 | 0.6799 |
| 3 | 3 | 70.15 | 36.134 | 30.15 | 63.6076 | 0.9608 | 1.2286 |
| 4 | 4 | 70.15 | 36.8266 | 30.15 | 62.9202 | 1.6486 | 2.1017 |
| 5 | 5 | 70.15 | 37.4279 | 30.15 | 62.3235 | 2.5117 | 3.1959 |
| 6 | 6 | 70.15 | 37.9669 | 30.15 | 61.7886 | 3.5473 | 4.5075 |
| 7 | 7 | 70.15 | 38.4598 | 30.15 | 61.2995 | 4.7531 | 6.0337 |
| 8 | 8 | 70.15 | 38.9167 | 30.15 | 60.8461 | 6.1271 | 7.772 |
| 9 | 9 | 70.15 | 39.3445 | 30.15 | 60.4216 | 7.6679 | 9.7205 |
| 10 | 10 | 70.15 | 39.7478 | 30.15 | 60.0213 | 9.3739 | 11.8772 |

Adding temperature dependent properties

Temperature dependent properties of water taken from table A.12 Thermal Design

temperature range of properties, in deg celsius

$$tx := \begin{pmatrix} 0 \\ 20 \\ 40 \\ 60 \\ 80 \\ 100 \end{pmatrix}$$

liquid density information, in kg/m3

$$dly := \begin{pmatrix} 1002 \\ 1000 \\ 994 \\ 985 \\ 974 \\ 960 \end{pmatrix}$$

$dly1 := dly$

$dls1 := lspline(tx, dly1)$

$\rho_1(t_{avg1}) := interp(dls1, tx, dly1, t_{avg1}) \cdot \frac{kg}{m^3}$

$dly2 := dly$

$dls2 := lspline(tx, dly2)$

$\rho_2(t_{avg2}) := interp(dls2, tx, dly2, t_{avg2}) \cdot \frac{kg}{m^3}$

$dly3 := dly$

$dls3 := lspline(tx, dly3)$

$\rho_3(t_{avg3}) := interp(dls3, tx, dly3, t_{avg3}) \cdot \frac{kg}{m^3}$

specific heat information, in J/(kg*K)

$$dcpy := \begin{pmatrix} 4217 \\ 4181 \\ 4178 \\ 4184 \\ 4196 \\ 4216 \end{pmatrix}$$

$dcp1 := dcpy$ $dcp2 := dcpy$

$dcps1 := lspline(tx, dcp1)$ $dcps2 := lspline(tx, dcp2)$

$$c_{p1}(t_{avg1}) := interp(dcps1, tx, dcp1, t_{avg1}) \cdot \frac{J}{kg \cdot K}$$

$$c_{p2}(t_{avg2}) := interp(dcps2, tx, dcp2, t_{avg2}) \cdot \frac{J}{kg \cdot K}$$

$dcp3 := dcpy$

$dcps3 := lspline(tx, dcp1)$

$$c_{p3}(t_{avg3}) := interp(dcps3, tx, dcp3, t_{avg3}) \cdot \frac{J}{kg \cdot K}$$

thermal conductivity information, in W/(m*K)

$$dky := \begin{pmatrix} .552 \\ .597 \\ .628 \\ .651 \\ .668 \\ .68 \end{pmatrix}$$

$dk1 := dky$ $dk2 := dky$

$dks1 := lspline(tx, dk1)$ $dks2 := lspline(tx, dk2)$

$$k_1(t_{avg1}) := interp(dks1, tx, dk1, t_{avg1}) \cdot \frac{W}{m \cdot K} \qquad k_2(t_{avg2}) := interp(dks2, tx, dk2, t_{avg2}) \frac{W}{m \cdot K}$$

$dk3 := dky$

$dks3 := lspline(tx, dk3)$

$$k_3(t_{avg3}) := interp(dks3, tx, dk3, t_{avg3}) \cdot \frac{W}{m \cdot K}$$

absolute viscosity information, in N*s/m^2

$$dvsy := \begin{pmatrix} 1792 \\ 1006 \\ 654 \\ 471 \\ 355 \\ 288 \end{pmatrix}$$

$dv1 := dvsy \qquad dv2 := dvsy \qquad dv3 := dvsy$

$dvs1 := lspline(tx, dv1) \qquad dvs2 := lspline(tx, dv2) \qquad dvs3 := lspline(tx, dv3)$

$$\mu_1(t_{avg1}) := interp(dvs1, tx, dv1, t_{avg1}) \cdot 10^{-6} \cdot \frac{N \cdot s}{m^2}$$

$$\mu_2(t_{avg2}) := interp(dvs2, tx, dv2, t_{avg2}) \cdot 10^{-6} \cdot \frac{N \cdot s}{m^2}$$

$$\mu_3(t_{avg3}) := interp(dvs3, tx, dv3, t_{avg3}) \cdot 10^{-6} \cdot \frac{N \cdot s}{m^2}$$

Prantle number
information

$$pry := \begin{pmatrix} 13.6 \\ 7.02 \\ 4.34 \\ 3.02 \\ 2.22 \\ 1.74 \end{pmatrix}$$

$pry1 := pry \qquad pry2 := pry \qquad pry3 := pry$

$prs1 := lspline(tx, pry1) \qquad prs2 := lspline(tx, pry2) \qquad prs3 := lspline(tx, pry3)$

$$Pr_1(t_{avg1}) := interp(prs1, tx, pry1, t_{avg1})$$

$$Pr_2(t_{avg2}) := interp(prs2, tx, pry2, t_{avg2})$$

$$Pr_3(t_{avg3}) := interp(prs3, tx, pry3, t_{avg3})$$

Experiments. For the model and data that follows, when regarding side A and side B of the heat exchangers, the hot side (A) will have a subscript 1, the cold side (B) will have a

Description of matrix columns: 1) hot loop flow rate, 2) cold loop flow rate, 3) T1i, 4) T1o, 5) T2i, 6) T2o, 7) normalized hot loop inlet pressure, 8) normalized hot loop pressure outlet, 9) normalized cold loop inlet pressure, 10) normalized cold loop outlet pressure, 11) T3i, 12) T3o, 13) city water flow rate, 14) power applied to bulk heaters (accounts for voltage drop across shunts in power calc)

f represents full power, h represents half power, i represents isothermal

$$Mf22 := \begin{pmatrix} 2.997 & 3.016 & 90.31 & 56.97 & 48.34 & 80.82 & 22.297 & 21.756 & 21.106 & 19.88 & 15.9 & 37.53 & 4.548 & 27089 \\ 3.514 & 3.515 & 84.65 & 55.64 & 47.7 & 75.71 & 20.42 & 19.541 & 19.648 & 17.985 & 15.94 & 38.51 & 4.363 & 27055 \\ 3.999 & 3.992 & 79.49 & 53.83 & 46.34 & 71.08 & 18.94 & 17.67 & 18.539 & 16.391 & 15.98 & 37.91 & 4.544 & 27044 \\ 4.517 & 4.515 & 75.71 & 52.93 & 45.88 & 67.8 & 18.365 & 16.616 & 18.176 & 15.471 & 15.88 & 37.74 & 4.571 & 27030 \\ 5.006 & 5.013 & 72.99 & 52.35 & 45.63 & 65.46 & 18.072 & 15.83 & 18.088 & 14.803 & 15.93 & 37.84 & 4.563 & 27029 \\ 5.511 & 5.523 & 71.84 & 53.08 & 46.69 & 64.7 & 18.212 & 15.411 & 18.304 & 14.378 & 16.06 & 38.83 & 4.357 & 27023 \\ 6.002 & 6.024 & 69.73 & 52.46 & 46.28 & 62.9 & 18.586 & 15.175 & 18.33 & 13.741 & 16.14 & 38.61 & 4.439 & 27008 \\ 6.523 & 6.516 & 67.47 & 51.51 & 45.54 & 60.92 & 18.851 & 14.767 & 19.027 & 13.702 & 15.67 & 37.91 & 4.21 & 27007 \\ 7.013 & 7.01 & 65.51 & 50.57 & 44.81 & 59.17 & 19.223 & 14.447 & 19.801 & 13.679 & 15.29 & 37.4 & 4.519 & 26996 \\ 7.509 & 7.523 & 65.68 & 51.72 & 46.16 & 59.54 & 20.013 & 14.502 & 20.658 & 13.687 & 15.26 & 39.02 & 4.18 & 26985 \\ 8.013 & 8.016 & 63.09 & 49.93 & 44.51 & 57.12 & 20.41 & 14.084 & 21.517 & 13.645 & 15.13 & 37.17 & 4.555 & 26974 \\ 8.519 & 8.513 & 63.72 & 51.34 & 46.09 & 57.95 & 21.379 & 14.198 & 22.474 & 13.661 & 15.3 & 39.16 & 4.194 & 26987 \\ 9.012 & 9.024 & 61.4 & 49.66 & 44.54 & 55.77 & 21.952 & 13.859 & 23.501 & 13.622 & 15.3 & 37.33 & 4.566 & 26964 \\ 9.522 & 9.524 & 62.15 & 51.02 & 46.04 & 56.69 & 22.966 & 13.912 & 24.571 & 13.649 & 15.36 & 39.2 & 4.217 & 26957 \\ 10.013 & 10.006 & 60.08 & 49.42 & 44.54 & 54.72 & 23.896 & 13.826 & 25.681 & 13.678 & 15.26 & 37.5 & 4.575 & 26975 \end{pmatrix}$$

$i := 1..15$

$$Mh22 := \begin{pmatrix} 3.018 & 3.011 & 51.97 & 34.43 & 29.55 & 46.16 & 14.452 & 13.872 & 15.04 & 13.657 & 14.4 & 25.93 & 4.4 & 13731 \\ 3.509 & 3.508 & 49.53 & 34.32 & 29.75 & 44.17 & 14.798 & 13.858 & 15.415 & 13.61 & 14.48 & 25.98 & 4.422 & 13728 \\ 4.017 & 4.01 & 47.28 & 33.91 & 29.62 & 42.31 & 15.224 & 13.845 & 15.889 & 13.588 & 14.37 & 25.64 & 4.527 & 13722 \\ 4.507 & 4.501 & 45.71 & 33.72 & 29.66 & 41.02 & 15.674 & 13.835 & 16.411 & 13.572 & 14.59 & 25.75 & 4.598 & 13721 \\ 4.999 & 5.009 & 44.78 & 33.93 & 30.11 & 40.29 & 16.192 & 13.835 & 17.035 & 13.567 & 14.74 & 26.54 & 4.339 & 13721 \\ 5.51 & 5.514 & 43.16 & 33.23 & 29.57 & 38.9 & 16.772 & 13.82 & 17.683 & 13.545 & 14.73 & 25.7 & 4.715 & 13717 \\ 6.009 & 6.005 & 42.99 & 33.86 & 30.36 & 38.92 & 17.377 & 13.81 & 18.368 & 13.533 & 14.85 & 26.62 & 4.374 & 13711 \\ 6.501 & 6.518 & 41.71 & 33.21 & 29.88 & 37.79 & 18.039 & 13.798 & 19.138 & 13.521 & 15.01 & 26.01 & 4.718 & 13702 \\ 7.001 & 7.015 & 41.64 & 33.74 & 30.52 & 37.87 & 18.751 & 13.79 & 19.939 & 13.516 & 15.06 & 26.96 & 4.348 & 13696 \\ 7.499 & 7.514 & 40.69 & 33.25 & 30.13 & 37.04 & 19.509 & 13.776 & 20.79 & 13.497 & 15.12 & 26.31 & 4.656 & 13693 \\ 8.007 & 8.006 & 40.8 & 33.81 & 30.78 & 37.26 & 20.335 & 13.772 & 21.695 & 13.501 & 15.18 & 27.2 & 4.31 & 13689 \\ 8.5 & 8.502 & 40.21 & 33.58 & 30.64 & 36.77 & 21.187 & 13.766 & 22.655 & 13.494 & 15.23 & 26.83 & 4.51 & 13681 \\ 9.004 & 9 & 39.91 & 33.62 & 30.75 & 36.56 & 22.11 & 13.76 & 23.685 & 13.494 & 15.26 & 26.96 & 4.477 & 13676 \\ 9.505 & 9.506 & 39.58 & 33.59 & 30.8 & 36.32 & 23.106 & 13.779 & 24.801 & 13.527 & 15.31 & 26.99 & 4.479 & 13668 \\ 10.006 & 10.012 & 39.45 & 33.73 & 31.02 & 36.26 & 24.181 & 13.82 & 25.982 & 13.596 & 15.28 & 27.39 & 4.358 & 13662 \end{pmatrix}$$

$i2 := 1..15$

$$Mi22 := \begin{pmatrix} 3.001 & 3.011 & 17.33 & 16.69 & 16.65 & 16.92 & 14.616 & 13.976 & 15.524 & 14.006 & 16.44 & 16.6 & 4.297 & 0 \\ 3.505 & 3.501 & 17.17 & 16.52 & 16.48 & 16.76 & 15.005 & 13.958 & 15.957 & 13.987 & 16.22 & 16.42 & 4.313 & 0 \\ 4.008 & 4.007 & 17.01 & 16.37 & 16.35 & 16.61 & 15.453 & 13.946 & 16.468 & 13.975 & 16.11 & 16.31 & 4.312 & 0 \\ 4.508 & 4.509 & 17.01 & 16.39 & 16.37 & 16.61 & 15.954 & 13.935 & 17.04 & 13.962 & 16.16 & 16.33 & 4.656 & 0 \\ 5.006 & 5.019 & 16.92 & 16.28 & 16.26 & 16.52 & 16.509 & 13.923 & 17.665 & 13.951 & 16.01 & 16.23 & 4.648 & 0 \\ 5.51 & 5.502 & 16.86 & 16.24 & 16.23 & 16.47 & 17.12 & 13.914 & 18.326 & 13.94 & 15.95 & 16.2 & 4.343 & 0 \\ 6.007 & 5.998 & 16.68 & 16.04 & 16.04 & 16.28 & 17.766 & 13.903 & 19.057 & 13.928 & 15.69 & 16 & 4.314 & 0 \\ 6.508 & 6.513 & 16.73 & 16.1 & 16.1 & 16.33 & 18.479 & 13.893 & 19.869 & 13.918 & 15.76 & 16.04 & 4.603 & 0 \\ 7.007 & 7.016 & 16.76 & 16.14 & 16.13 & 16.36 & 19.234 & 13.885 & 20.726 & 13.91 & 15.8 & 16.09 & 4.612 & 0 \\ 7.498 & 7.503 & 16.68 & 16.04 & 16.03 & 16.28 & 20.028 & 13.879 & 21.599 & 13.904 & 15.58 & 15.95 & 4.626 & 0 \\ 8.012 & 8.006 & 16.83 & 16.2 & 16.2 & 16.43 & 20.909 & 13.874 & 22.568 & 13.901 & 15.75 & 16.12 & 4.595 & 0 \\ 8.519 & 8.51 & 17.13 & 16.49 & 16.48 & 16.72 & 21.812 & 13.872 & 23.585 & 13.904 & 15.94 & 16.38 & 4.256 & 0 \\ 9.012 & 8.996 & 16.79 & 16.14 & 16.12 & 16.39 & 22.774 & 13.876 & 24.649 & 13.918 & 15.51 & 16.01 & 4.306 & 0 \\ 9.512 & 9.532 & 16.81 & 16.17 & 16.14 & 16.4 & 23.841 & 13.91 & 25.865 & 13.969 & 15.53 & 16.02 & 4.595 & 0 \\ 9.98 & 9.991 & 16.96 & 16.31 & 16.29 & 16.54 & 24.888 & 13.942 & 26.962 & 14.029 & 15.62 & 16.15 & 4.59 & 0 \end{pmatrix}$$

$i3 := 1..12$

Now listing experimentally determined hose pressure drops. The values correspond to the closest nominal flow rates in the experimental heat exchanger data. First column is for raw hot side pressure drop and second column is for the raw cold side pressure drop

(1) is full power
2 half power
3 isothermal

$$Mhosedrop := \begin{pmatrix} -0.318 & 0.363 \\ -0.212 & 0.47 \\ -0.101 & 0.618 \\ 0.029 & 0.755 \\ 0.225 & 0.895 \\ 0.39 & 1.052 \\ 0.553 & 1.207 \\ 0.746 & 1.391 \\ 0.948 & 1.584 \\ 1.17 & 1.787 \\ 1.385 & 2.001 \\ 1.634 & 2.234 \\ 1.891 & 2.49 \\ 2.162 & 2.768 \\ 2.433 & 3.023 \end{pmatrix}$$

all three experimental runs share the same sets of flow rates

Now creating additional matrixes to calculate perturbations in the data due to measurement uncertainties

Uclflowmeter1 := 1.0034 Uhlflowmeter1 := 1.0052

Uclflowmeter2 := .9966 Uhlflowmeter2 := 0.9948

maximum heat transfer error matrices

$Mf2err_{i,1} := Mf22_{i,1} \cdot Uhlflowmeter2$ $Mf2err_{i,2} := Mf22_{i,2} \cdot Uclflowmeter1$

T1i value T1o value

$Mf2err_{i,3} := Mf22_{i,3} + -.16$ $Mf2err_{i,4} := Mf22_{i,4} + .16$

T2i value T2o value

$Mf2err_{i,5} := Mf22_{i,5} + -.16$ $Mf2err_{i,6} := Mf22_{i,6} + -.16$

Hot loop raw pressure drop

$Mf2err_{i,7} := Mf22_{i,7} \cdot 1.00285 + .049$ $Mf2err_{i,8} := Mf22_{i,8} \cdot .99715$

Cold loop raw pressure drop

$Mf2err_{i,9} := Mf22_{i,9}$ $Mf2err_{i,10} := Mf22_{i,10}$

$Mf2err_{i,11} := Mf22_{i,11}$ $Mf2err_{i,12} := Mf22_{i,12}$

$Mf2err_{i,13} := Mf22_{i,13}$ $Mf2err_{i,14} := Mf22_{i,14}$

half power error matrices

Now defining property values from matrixes

$Q1(Mf,i) := Mf_{i,1} \cdot gpm$ $Q2(Mf,i) := Mf_{i,2} \cdot gpm$ $Q3(Mf,i) := Mf_{i,13} \cdot gpm$

$$T1i(Mf,i) := Mf_{i,3}\,°C - .73\,°C \qquad T2i(Mf,i) := Mf_{i,5}\,°C - .02\,°C$$

$$T1o(Mf,i) := Mf_{i,4}\,°C - .21\,°C \qquad T2o(Mf,i) := Mf_{i,6}\,°C - .10\,°C$$

$$T3i(Mf,i) := Mf_{i,11}\,°C \qquad T3o(Mf,i) := Mf_{i,12}\,°C$$

$$tavg1(Mf,i) := \frac{\left(Mf_{i,3} - .73\right) + \left(Mf_{i,4} - .21\right)}{2} \qquad tavg2(Mf,i) := \frac{\left(Mf_{i,5} - .02\right) + \left(Mf_{i,6} - .1\right)}{2}$$

$$tavg3(Mf,i) := \frac{Mf_{i,9} + Mf_{i,10}}{2}$$

Now listing experimentally determined offsets for temperature difference and pressure

$$\Delta Photoffset := .54$$

$$\Delta Pcoldoffset := -.1$$

Considering the offset of
ΔP

$$\Delta P1(Mf,i) := \left[\left(Mf_{i,7} - Mf_{i,8}\right) + \Delta Photoffset\right]\cdot psi$$

$$\Delta P2(Mf,i) := \left[\left(Mf_{i,9} - Mf_{i,10}\right) + \Delta Pcoldoffset\right]\cdot psi$$

Now calculating NTU relationships

$$C1(Mf,i) := \rho_1(tavg1(Mf,i)) \cdot Q1(Mf,i) \cdot c_{p1}(tavg1(Mf,i))$$

$$C2(Mf,i) := \rho_2(tavg2(Mf,i)) \cdot Q2(Mf,i) \cdot c_{p2}(tavg2(Mf,i))$$

$$Cmin(Mf,i) := \min(C1(Mf,i), C2(Mf,i)) \qquad Cmax(Mf,i) := \max(C1(Mf,i), C2(Mf,i))$$

$$Cr(Mf,i) := \frac{Cmin(Mf,i)}{Cmax(Mf,i)}$$

$$\varepsilon(Mf,i) := \frac{C1(Mf,i) \cdot (T1i(Mf,i) - T1o(Mf,i))}{Cmin(Mf,i) \cdot (T1i(Mf,i) - T2i(Mf,i) + 0)}$$

$$NTU(Mf,i) := \frac{1}{1 - Cr(Mf,i)} \cdot \ln\left(\frac{1 - \varepsilon(Mf,i) \cdot Cr(Mf,i)}{1 - \varepsilon(Mf,i)}\right)$$

$$U2(Mf,i) := \frac{NTU(Mf,i) \cdot Cmin(Mf,i)}{A_2}$$

$$h(Mf,i) := \frac{U2(Mf,i) \cdot \left(\frac{A_2}{A_1} + 1\right)}{1 - \frac{U2(Mf,i) \cdot \delta}{k_w}}$$

This section calculates values from the data, friction factor, reynolds, colburn, etc.

$$G1(Mf,i) := \frac{\rho_1(tavg1(Mf,i)) \cdot Q1(Mf,i)}{A_{c1}} \qquad G2(Mf,i) := \frac{\rho_2(tavg2(Mf,i)) \cdot Q2(Mf,i)}{A_{c2}}$$

$$Gp1(Mf,i) := \frac{4 \cdot \rho_1(tavg1(Mf,i)) \cdot Q1(Mf,i)}{\pi \cdot D_p^{\,2}} \qquad Gp2(Mf,i) := \frac{4 \cdot \rho_2(tavg2(Mf,i)) \cdot Q2(Mf,i)}{\pi \cdot D_p^{\,2}}$$

$$j1(Mf,i) := \frac{h(Mf,i) \cdot Pr_1(tavg1(Mf,i))^{\frac{2}{3}}}{G1(Mf,i) \cdot c_{p1}(tavg1(Mf,i))} \qquad j2(Mf,i) := \frac{h(Mf,i) \cdot Pr_2(tavg2(Mf,i))^{\frac{2}{3}}}{G2(Mf,i) \cdot c_{p2}(tavg2(Mf,i))}$$

The various friction factors calculated below represent different corrections applied. f1 is the basic form used to calculate the friction factor, while the hose designations have the experimental hose pressure drop subtracted from them. The h designation at the end is used to distinguish between the various runs with different numbers of flow rate sets.

$$f1(Mf,i) := \left[\Delta P1(Mf,i) - \frac{1.5\cdot(Gp1(Mf,i))^2}{2\cdot\rho_1(tavg1(Mf,i))}\right]\cdot\frac{D_h\cdot\rho_1(tavg1(Mf,i))}{2\cdot L_p\cdot G1(Mf,i)^2}$$

$$f1withhosef(Mf,i) := \left[\left[\Delta P1(Mf,i) - \left(Mhosedrop_{i,1} + \Delta Photoffset\right)\cdot psi\right] - \frac{1.5\cdot(Gp1(Mf,i))^2}{2\cdot\rho_1(tavg1(Mf,i))}\right]\cdot\frac{D_h\cdot\rho_1(tavg1(Mf,i))}{2\cdot L_p\cdot G1(Mf,i)^2}$$

$$f2(Mf,i) := \left[\Delta P2(Mf,1) - \frac{1.5\cdot(Gp2(Mf,i))^2}{2\cdot\rho_2(tavg2(Mf,i))}\right]\cdot\frac{D_h\cdot\rho_2(tavg2(Mf,i))}{2\cdot L_p\cdot G2(Mf,i)^2}$$

$$f2withhose(Mf,i) := \left[\left[\Delta P1(Mf,i) - \left(Mhosedrop_{i,2} + \Delta Pcoldoffset\right)\cdot psi\right] - \frac{1.5\cdot(Gp1(Mf,i))^2}{2\cdot\rho_1(tavg1(Mf,i))}\right]\cdot\frac{D_h\cdot\rho_1(tavg1(Mf,i))}{2\cdot L_p\cdot G1(Mf,i)^2}$$

$$Re1(Mf,i) := \frac{G1(Mf,i)\cdot D_h}{\mu_1(tavg1(Mf,i))} \qquad Re2(Mf,i) := \frac{G2(Mf,i)\cdot D_h}{\mu_2(tavg2(Mf,i))}$$

$$Nu1(Mf,i) := \frac{h(Mf,i)\cdot L_p}{k_w}$$

Now calculating values from martin correlation

$$Nu_1(Q1) := \frac{h_1(Q1)\cdot L_p}{k_w}$$

$$Q1_i := 1gpm, 1.02gpm .. 15gpm$$

Full power values

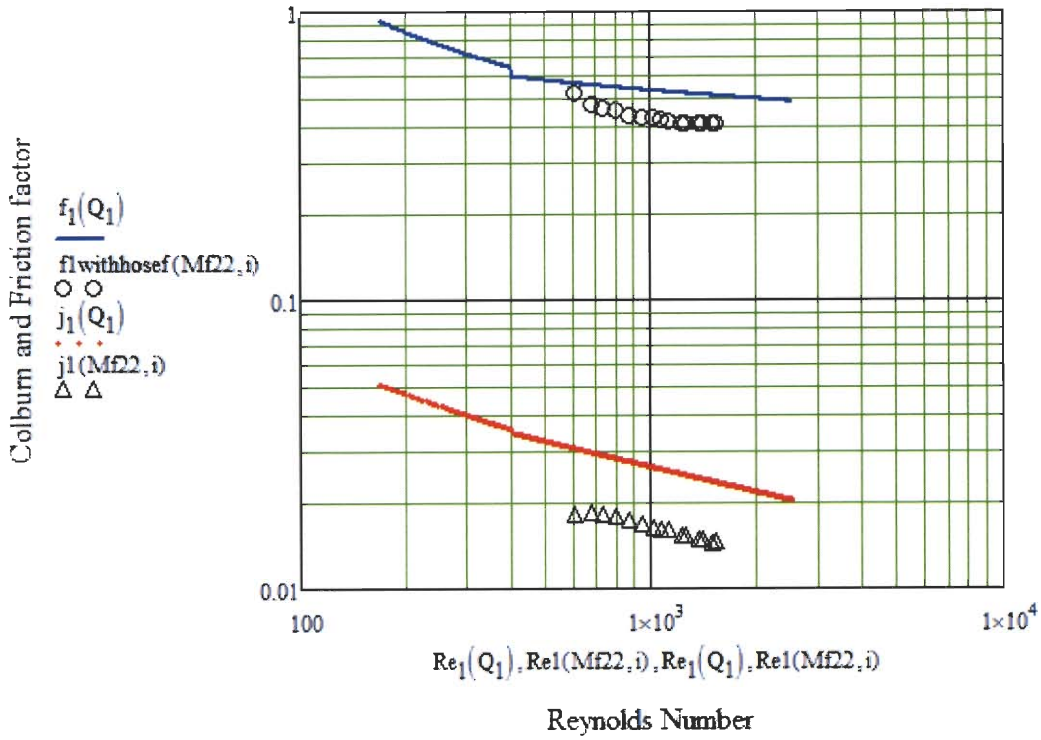


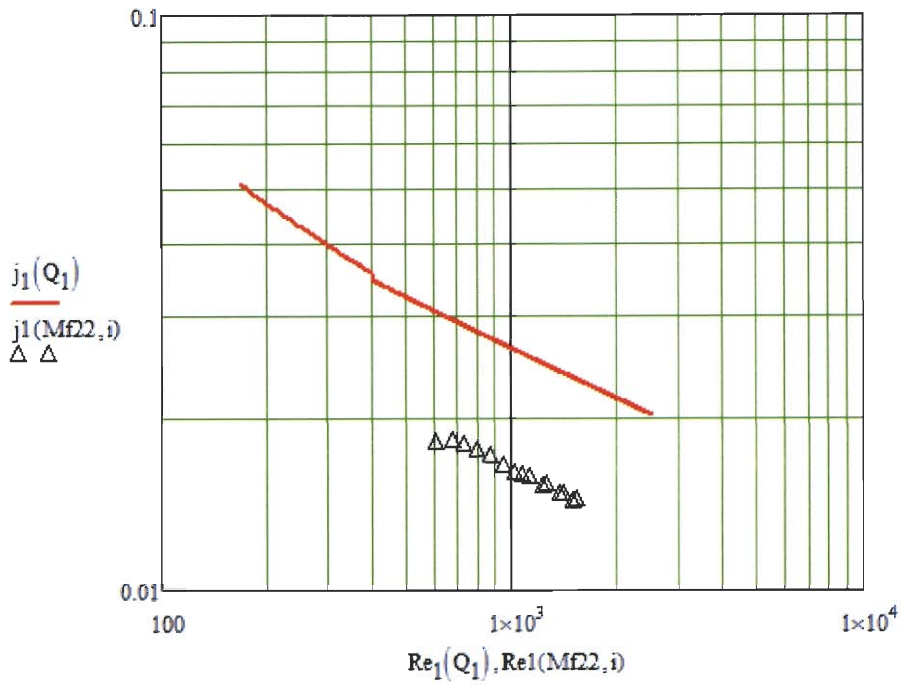

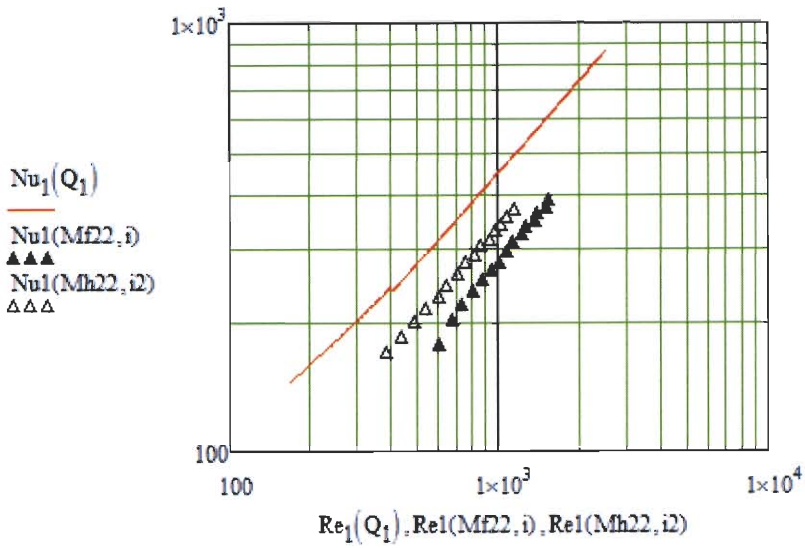


half power values

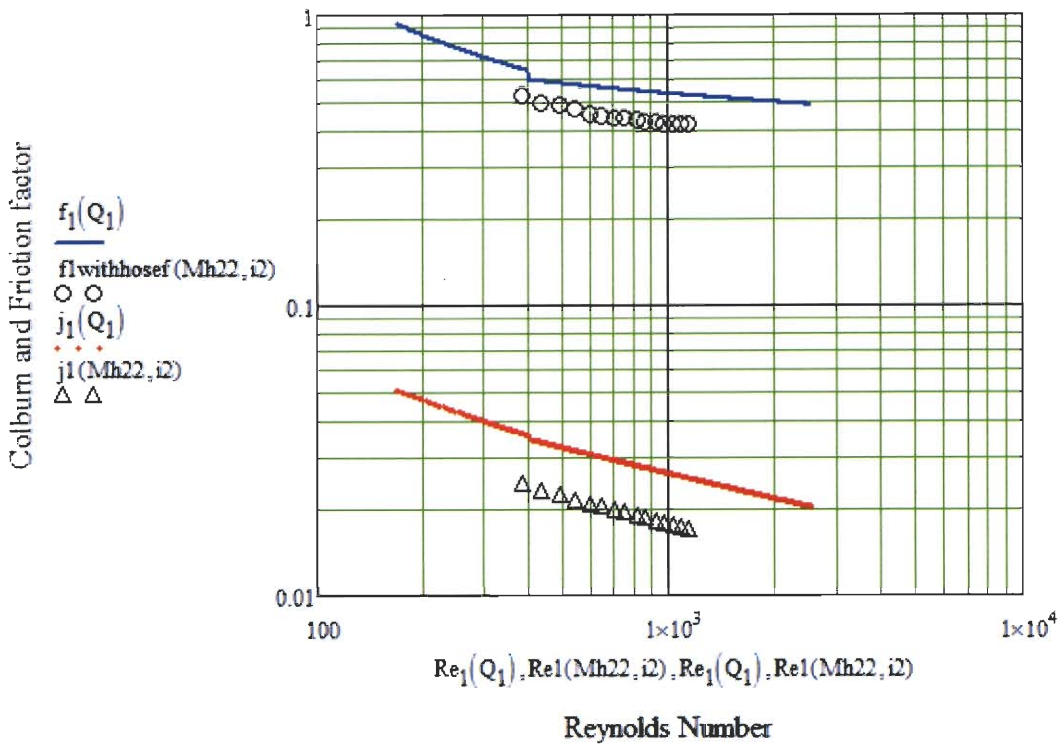

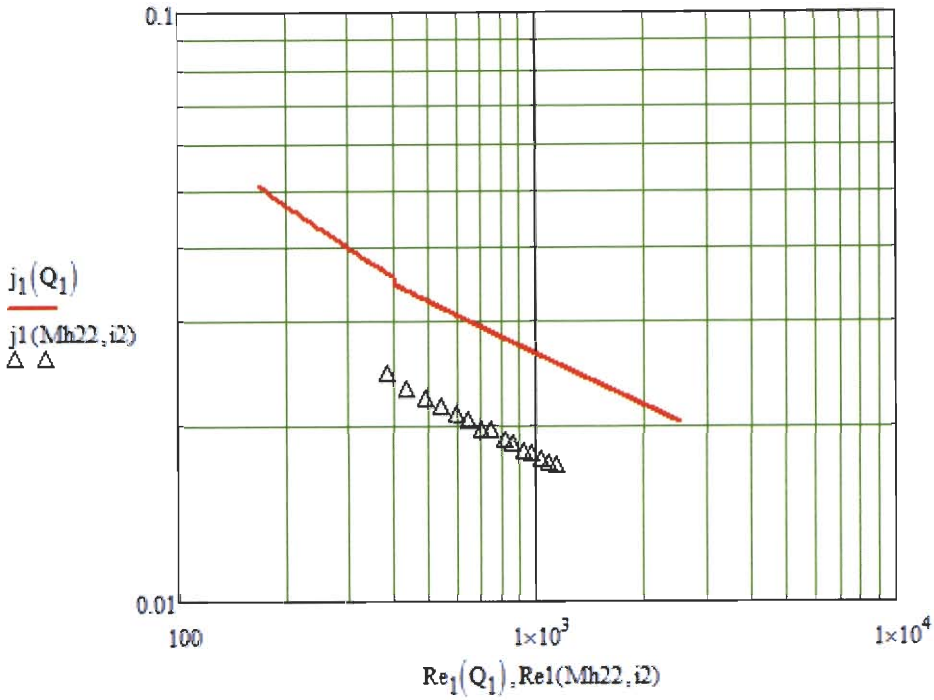


Isothermal pressure

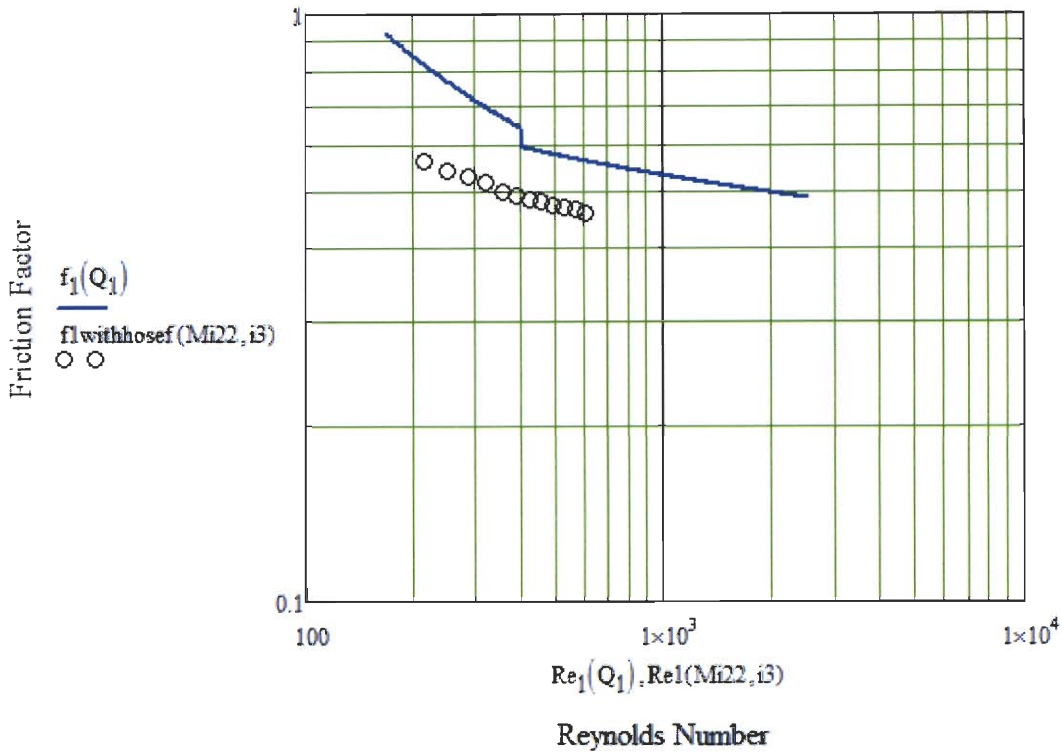

Now what follow is a calculation of the associated error for heat transfer, reynolds number, convection coefficient and friction factors

$$\Delta Tcityoffset := 0$$

$$\Delta T1(Mf,i) := T1i(Mf,i) - T1o(Mf,i)$$

$$\Delta T2(Mf,i) := T2o(Mf,i) - T2i(Mf,i)$$

$$\Delta T3(Mf,i) := T3o(Mf,i) - T3i(Mf,i)$$

$$mmdot1(Mf,i) := Q1(Mf,i)\cdot\rho_1(tavg1(Mf,i))$$

$$mmdot2(Mf,i) := Q2(Mf,i)\cdot\rho_2(tavg2(Mf,i))$$

$$mmdot3(Mf,i) := Q3(Mf,i)\cdot\rho_3(tavg3(Mf,i))$$

$$Qheat1(Mf,i) := mmdot1(Mf,i)\cdot c_{p1}(tavg1(Mf,i))\cdot\Delta T1(Mf,i)$$

$$Qheat2(Mf,i) := mmdot2(Mf,i)\cdot c_{p2}(tavg2(Mf,i))\cdot\Delta T2(Mf,i)$$

$$Qheat3(Mf,i) := mmdot3(Mf,i)\cdot c_{p3}(tavg3(Mf,i))\cdot\Delta T3(Mf,i)$$

$$Qheatelectric(Mf,i) := Mf_{i,14}\cdot W$$

$$Qhxmin(Mf,i) := min(Qheat1(Mf,i), Qheat2(Mf,i))$$

$$Qhxmax(Mf,i) := max(Qheat1(Mf,i), Qheat2(Mf,i))$$

$$Qhxavg(Mf,i) := \frac{Qheat1(Mf,1) + Qheat2(Mf,i)}{2}$$

$$Qdiffhotvscold(Mf,i) := \frac{Qhxmax(Mf,i) - Qhxmin(Mf,i)}{Qhxmin(Mf,i)}\cdot 100$$

$$Qdiffhot(Mf,i) := \frac{Qheat1(Mf,i) - Qhxavg(Mf,i)}{Qhxavg(Mf,i)}\cdot 100$$

$$Qdiffcold(Mf,i) := \frac{Qheat2(Mf,i) - Qhxavg(Mf,i)}{Qhxavg(Mf,i)}\cdot 100$$

$$Qhxavgvselectric(Mf,i) := \frac{Qheatelectric(Mf,i) - Qhxavg(Mf,i)}{Qhxavg(Mf,i)}\cdot 100$$

$$Qhxavgvscity(Mf,i) := \frac{Qheat3(Mf,i) - Qhxavg(Mf,i)}{Qhxavg(Mf,i)}\cdot 100$$

Qdiffhotvscold represents comparison between the min and maximum experimental data. Qdiff hot and cold represent the heat transfer differences using the method used by muley and manglik 1999 asme paper.

Qdiffhot(Mf22,i) =

| |
|---|
| 0.1497 |
| 1.7863 |
| 2.1581 |
| 2.1443 |
| 2.153 |
| 1.9512 |
| 1.6825 |
| 1.8746 |
| 2.1151 |
| 1.9211 |
| 2.1382 |
| 1.9507 |
| 1.9029 |
| 1.7709 |
| 2.1164 |

Qdiffhot(Mh22,i2) =

| |
|---|
| 1.4938 |
| 1.3477 |
| 1.2572 |
| 1.2237 |
| 1.3036 |
| 1.3258 |
| 1.1878 |
| 1.3684 |
| 0.9916 |
| 1.1281 |
| 1.0342 |
| 1.0992 |
| 1.007 |
| 0.9474 |
| 1.0738 |

Qdiffcold(Mf22,i) =

| |
|---|
| -0.1497 |
| 0.1411 |
| 0.3384 |
| 0.46 |
| 0.6882 |
| 0.6956 |
| 1.0246 |
| 1.0809 |
| 1.3097 |
| 1.2692 |
| 1.5012 |
| 1.3991 |
| 1.6022 |
| 1.6039 |
| 1.832 |

Qdiffcold(Mh22,i2) =

| |
|---|
| -1.4938 |
| -0.9472 |
| -0.6725 |
| -0.4603 |
| -0.6361 |
| -0.2141 |
| -0.3009 |
| -0.1771 |
| -0.2188 |
| 0.1049 |
| 0.018 |
| 0.2164 |
| 0.3462 |
| 0.4857 |
| 0.4354 |

Qhxavgvscity(Mf22,i) =

| |
|---|
| 2.1429 |
| 2.0224 |
| 3.1004 |
| 3.2866 |
| 3.1231 |
| 2.33 |
| 2.5563 |
| -3.7998 |
| 2.4017 |
| 1.8098 |
| 2.651 |
| 2.4038 |
| 2.7014 |
| 2.6181 |
| 3.5918 |

Qhxavgvselectric(Mf22,i) =

| |
|---|
| 6.6526 |
| 6.2094 |
| 5.9564 |
| 5.7723 |
| 5.526 |
| 5.4947 |
| 5.0868 |
| 5.0232 |
| 4.7375 |
| 4.7378 |
| 4.4491 |
| 4.6078 |
| 4.3033 |
| 4.2745 |
| 4.1022 |

Qdiffhotvscold(Mf22,i) =

| |
|---|
| 0.2999 |
| 1.6429 |
| 1.8135 |
| 1.6765 |
| 1.4548 |
| 1.2469 |
| 0.6512 |
| 0.7852 |
| 0.7949 |
| 0.6437 |
| 0.6276 |
| 0.544 |
| 0.2959 |
| 0.1644 |
| 0.2792 |

# Appendix E

## Averaged Experimental Results in Table Format

This appendix contains tables of the averaged experimental results of all measurements which were necessary to complete the intended study. The pressure drops are normalized with respect to the excitation voltage and have the appropriate hose pressure drops removed. The temperatures in the tables below have the offsets applied.

Data for Fp3x8-10

Maximum power

| HL flow (gpm) | HL flow (gpm) | T1i (C) | T1o (C) | T2i (C) | T2o (C) | DP hot (psi) | DP cold (psi) | T3i (C) | T3o (C) | City water flow (gpm) | electric power (W) |
|---|---|---|---|---|---|---|---|---|---|---|---|
| 3.015 | 3.015 | 93.59 | 66.48 | 36.98 | 63.22 | 1.439 | 2.219 | 12.91 | 30.82 | 4.526 | 22346 |
| 3.484 | 3.504 | 87.58 | 64.14 | 36.63 | 59.34 | 1.911 | 2.991 | 12.72 | 30.65 | 4.562 | 22342 |
| 3.994 | 4.002 | 83.11 | 62.44 | 36.45 | 56.59 | 2.453 | 3.789 | 12.7 | 30.7 | 4.562 | 22330 |
| 4.505 | 4.506 | 79.47 | 61.11 | 36.57 | 54.47 | 3.102 | 4.808 | 12.78 | 30.86 | 4.567 | 22329 |
| 4.993 | 4.995 | 76.71 | 60.14 | 36.79 | 52.99 | 3.757 | 5.889 | 12.56 | 31.29 | 4.403 | 22317 |
| 5.512 | 5.511 | 74.25 | 59.34 | 37.05 | 51.77 | 4.646 | 7.136 | 12.59 | 31.5 | 4.375 | 22302 |
| 6.004 | 6.01 | 72.26 | 58.51 | 37.1 | 50.65 | 5.469 | 8.448 | 12.56 | 31.58 | 4.352 | 22277 |
| 6.506 | 6.513 | 70.55 | 57.86 | 37.24 | 49.78 | 6.412 | 9.86 | 12.55 | 31.58 | 4.329 | 22269 |
| 6.992 | 6.996 | 69.14 | 57.33 | 37.4 | 49.08 | 7.386 | 11.327 | 12.58 | 31.83 | 4.307 | 22253 |
| 7.497 | 7.485 | 67.94 | 56.9 | 37.58 | 48.52 | 8.467 | 12.904 | 12.63 | 32 | 4.293 | 22254 |

Half power

| hl flow (gpm) | cl flow (gpm) | t1i (C) | t1o (C) | t2i (C) | t2o (C) | dp hot (psi) | dp cold (psi) | t3i (C) | t3o (C) | city flow (gpm) | electric power (W) |
|---|---|---|---|---|---|---|---|---|---|---|---|
| 3.008 | 3.007 | 54.74 | 41.11 | 24.43 | 37.62 | 1.488 | 2.288 | 12.16 | 21.67 | 4.318 | 11118 |
| 3.5 | 3.504 | 51.42 | 39.64 | 24.1 | 35.54 | 1.966 | 3.04 | 12.17 | 21.01 | 4.695 | 11106 |
| 4.005 | 4.009 | 49.45 | 39.14 | 24.66 | 34.72 | 2.549 | 3.897 | 12.18 | 21.65 | 4.374 | 11102 |
| 4.496 | 4.508 | 47.79 | 38.6 | 24.96 | 33.95 | 3.196 | 4.883 | 12.24 | 21.81 | 4.327 | 11096 |
| 5.007 | 5.01 | 46.32 | 38.06 | 25.12 | 33.25 | 3.909 | 5.996 | 12.24 | 21.96 | 4.323 | 11090 |
| 5.512 | 5.519 | 45.07 | 37.56 | 25.22 | 32.63 | 4.743 | 7.24 | 12.28 | 22.03 | 4.309 | 11080 |
| 6.013 | 6.019 | 43.75 | 36.85 | 25.02 | 31.82 | 5.642 | 8.611 | 12.32 | 21.73 | 4.479 | 11074 |

| | | | | | | | | | | | |
|---|---|---|---|---|---|---|---|---|---|---|---|
| 6.51 | 6.504 | 42.97 | 36.56 | 25.16 | 31.49 | 6.571 | 10.015 | 12.43 | 21.88 | 4.5 | 11074 |
| 7.008 | 6.993 | 41.57 | 35.61 | 24.56 | 30.47 | 7.615 | 11.522 | 12.3 | 21.29 | 4.766 | 11065 |

Isothermal data

| hl flow (gpm) | cl flow (gpm) | t1i (C) | t1o (C) | t2i (C) | t2o (C) | dp hot (psi) | dp cold (psi) | t3i (C) | t3o (C) | city flow (gpm) | electric power (W) |
|---|---|---|---|---|---|---|---|---|---|---|---|
| 3.016 | 3.017 | 20.73 | 20.55 | 20.46 | 20.66 | 1.474 | 2.308 | 20.24 | 20.44 | 4.507 | 0 |
| 3.498 | 3.504 | 16.72 | 16.21 | 15.7 | 16.25 | 1.96 | 3.036 | 14.86 | 15.51 | 4.471 | 0 |
| 3.994 | 3.997 | 15.07 | 14.77 | 14.66 | 14.97 | 2.556 | 3.904 | 14.16 | 14.57 | 4.494 | 0 |
| 4.509 | 4.501 | 14.42 | 14.14 | 14.08 | 14.36 | 3.268 | 4.923 | 13.55 | 13.98 | 4.463 | 0 |
| 5.012 | 4.999 | 13.75 | 13.49 | 13.46 | 13.73 | 4.002 | 6.054 | 12.92 | 13.34 | 4.487 | 0 |
| 5.507 | 5.502 | 13.39 | 13.15 | 13.17 | 13.41 | 4.84 | 7.312 | 12.64 | 13.05 | 4.488 | 0 |
| 6.004 | 6 | 13.3 | 13.08 | 13.12 | 13.35 | 5.748 | 8.681 | 12.58 | 13 | 4.493 | 0 |
| 6.507 | 6.505 | 13.37 | 13.15 | 13.18 | 13.4 | 6.719 | 10.173 | 12.58 | 13.04 | 4.485 | 0 |
| 6.993 | 6.997 | 13.38 | 13.17 | 13.18 | 13.41 | 7.75 | 11.726 | 12.51 | 13.02 | 4.488 | 0 |

Data for Fg3x8-14

Maximum power

| hl flow (gpm) | cl flow (gpm) | t1i (C) | t1o (C) | t2i (C) | t2o (C) | dp hot (psi) | dp cold (psi) | t3i (C) | t3o (C) | city flow (gpm) | electric power (W) |
|---|---|---|---|---|---|---|---|---|---|---|---|
| 3.01 | 3.003 | 95.24 | 64.05 | 42.57 | 73.02 | 0.734 | 0.833 | 12.35 | 33.83 | 4.302 | 25720 |
| 3.513 | 3.509 | 87.97 | 61.07 | 41.08 | 67.31 | 0.942 | 1.204 | 12.08 | 34.06 | 4.266 | 25697 |
| 4.011 | 4.02 | 83.46 | 59.64 | 40.84 | 64.07 | 1.189 | 1.529 | 11.96 | 34.05 | 4.263 | 25682 |
| 4.503 | 4.521 | 79.98 | 58.75 | 41 | 61.79 | 1.472 | 1.913 | 12.2 | 34.5 | 4.242 | 25688 |
| 4.997 | 4.992 | 76.77 | 57.66 | 40.76 | 59.6 | 1.778 | 2.355 | 11.97 | 34.4 | 4.23 | 25674 |
| 5.504 | 5.504 | 73.86 | 56.5 | 40.39 | 57.52 | 2.153 | 2.862 | 11.59 | 33.83 | 4.245 | 25669 |
| 6.014 | 6.027 | 72.34 | 56.49 | 41.21 | 56.81 | 2.566 | 3.443 | 12.98 | 34.58 | 4.377 | 25649 |
| 6.514 | 6.507 | 70.06 | 55.41 | 40.68 | 55.15 | 3 | 4.022 | 12.26 | 33.67 | 4.421 | 25645 |
| 7.001 | 7.014 | 68.38 | 54.73 | 40.53 | 54 | 3.46 | 4.666 | 12.24 | 34.01 | 4.383 | 25616 |
| 7.515 | 7.524 | 67.11 | 54.38 | 40.68 | 53.28 | 3.962 | 5.359 | 12.43 | 34.07 | 4.421 | 25613 |
| 8.007 | 8.067 | 65.48 | 53.54 | 40.33 | 52.07 | 4.517 | 6.196 | 12.34 | 33.87 | 4.442 | 25603 |
| 8.509 | 8.508 | 64.41 | 53.18 | 40.29 | 51.44 | 5.098 | 6.84 | 12.34 | 33.92 | 4.444 | 25606 |
| 9.009 | 9.035 | 63.12 | 52.51 | 40.02 | 50.54 | 5.725 | 7.694 | 12.25 | 33.64 | 4.492 | 25607 |
| 9.745 | 9.758 | 61.89 | 52.08 | 40.06 | 49.82 | 6.709 | 8.912 | 12.32 | 33.9 | 4.484 | 25594 |

Half power

| hl flow (gpm) | cl flow (gpm) | t1i (C) | t1o (C) | t2i (C) | t2o (C) | dp hot (psi) | dp cold (psi) | t3i (C) | t3o (C) | city flow (gpm) | electric power (W) |
|---|---|---|---|---|---|---|---|---|---|---|---|
| 3.011 | 3.001 | 59.15 | 41.74 | 28.46 | 45.46 | 0.798 | 0.962 | 12.59 | 25.08 | 4.247 | 14158 |
| 4 | 4.002 | 52.04 | 38.85 | 27.24 | 40.25 | 1.295 | 1.622 | 11.57 | 23.54 | 4.426 | 14155 |
| 4.498 | 4.5 | 50.18 | 38.45 | 27.6 | 39.15 | 1.598 | 2.041 | 12 | 23.8 | 4.492 | 14146 |
| 4.999 | 5.011 | 48.25 | 37.67 | 27.39 | 37.81 | 1.902 | 2.523 | 11.71 | 23.77 | 4.451 | 14131 |
| 5.527 | 5.531 | 47.08 | 37.5 | 27.8 | 37.22 | 2.287 | 3.063 | 12.14 | 24.06 | 4.478 | 14130 |
| 5.997 | 5.992 | 46.26 | 37.39 | 28.09 | 36.81 | 2.663 | 3.566 | 12.19 | 24.33 | 4.413 | 14120 |
| 6.505 | 6.504 | 45.5 | 37.31 | 28.42 | 36.47 | 3.109 | 4.171 | 12.56 | 24.63 | 4.441 | 14129 |
| 7.017 | 7.034 | 44.48 | 36.88 | 28.35 | 35.81 | 3.603 | 4.869 | 12.47 | 24.65 | 4.417 | 14124 |
| 7.503 | 7.5 | 43.58 | 36.47 | 28.22 | 35.23 | 4.096 | 5.49 | 12.29 | 24.47 | 4.414 | 14106 |
| 7.994 | 8.009 | 42.9 | 36.23 | 28.25 | 34.83 | 4.659 | 6.24 | 12.17 | 24.41 | 4.414 | 14091 |
| 8.528 | 8.525 | 42.27 | 35.98 | 28.26 | 34.46 | 5.254 | 7.045 | 12.29 | 24.43 | 4.478 | 14097 |
| 9.021 | 9.038 | 41.88 | 35.94 | 28.46 | 34.31 | 5.874 | 7.875 | 12.49 | 24.7 | 4.474 | 14091 |
| 9.782 | 9.741 | 41.35 | 35.87 | 28.68 | 34.12 | 6.874 | 9.038 | 12.65 | 24.87 | 4.456 | 14077 |

Isothermal data

| hl flow (gpm) | cl flow (gpm) | t1i (C) | t1o (C) | t2i (C) | t2o (C) | dp hot (psi) | dp cold (psi) | t3i (C) | t3o (C) | city flow (gpm) | electric power (W) |
|---|---|---|---|---|---|---|---|---|---|---|---|
| 3.005 | 3.011 | 11.43 | 11.1 | 11.23 | 11.54 | 0.858 | 1.173 | 10.87 | 11.18 | 4.26 | 0 |
| 3.505 | 3.51 | 11.29 | 10.99 | 11.17 | 11.43 | 1.114 | 1.529 | 10.83 | 11.12 | 4.256 | 0 |
| 4.006 | 4.005 | 11.25 | 10.97 | 11.16 | 11.4 | 1.418 | 1.896 | 10.81 | 11.11 | 4.228 | 0 |
| 4.511 | 4.497 | 11.21 | 10.95 | 11.16 | 11.37 | 1.765 | 2.33 | 10.81 | 11.11 | 4.229 | 0 |
| 5.008 | 5.003 | 11.25 | 11 | 11.19 | 11.41 | 2.09 | 2.837 | 10.82 | 11.14 | 4.372 | 0 |
| 5.503 | 5.5 | 11.27 | 11.01 | 11.21 | 11.42 | 2.496 | 3.377 | 10.81 | 11.16 | 4.413 | 0 |
| 6.009 | 6.012 | 11.29 | 11.05 | 11.24 | 11.45 | 2.965 | 3.995 | 10.81 | 11.17 | 4.403 | 0 |
| 6.496 | 6.51 | 11.35 | 11.11 | 11.3 | 11.51 | 3.427 | 4.624 | 10.84 | 11.22 | 4.411 | 0 |
| 7.007 | 7.009 | 11.41 | 11.17 | 11.35 | 11.56 | 3.953 | 5.306 | 10.86 | 11.27 | 4.42 | 0 |
| 7.496 | 7.506 | 11.46 | 11.22 | 11.38 | 11.6 | 4.483 | 6.036 | 10.85 | 11.29 | 4.43 | 0 |
| 8.012 | 8.015 | 11.48 | 11.25 | 11.42 | 11.63 | 5.106 | 6.823 | 10.84 | 11.31 | 4.435 | 0 |
| 8.516 | 8.511 | 11.54 | 11.31 | 11.47 | 11.68 | 5.724 | 7.633 | 10.83 | 11.34 | 4.436 | 0 |
| 9.014 | 9.017 | 11.57 | 11.34 | 11.49 | 11.71 | 6.366 | 8.487 | 10.79 | 11.35 | 4.435 | 0 |
| 9.757 | 9.769 | 11.62 | 11.38 | 11.51 | 11.74 | 7.407 | 9.825 | 10.7 | 11.35 | 4.448 | 0 |

Data for GB220H-20

Maximum power

| hl flow (gpm) | cl flow (gpm) | t1i (C) | t1o (C) | t2i (C) | t2o (C) | dp hot (psi) | dp cold (psi) | t3i (C) | t3o (C) | city flow (gpm) | electric power (W) |
|---|---|---|---|---|---|---|---|---|---|---|---|
| 3.016 | 3.015 | 91.42 | 56.85 | 44.03 | 77.7 | 0.614 | 0.613 | 11.6 | 35.17 | 4.381 | 28283 |
| 3.511 | 3.506 | 84.33 | 54.39 | 42.48 | 71.57 | 0.762 | 0.83 | 11.68 | 34.84 | 4.45 | 28284 |
| 4.022 | 4.011 | 79.66 | 53.45 | 42.2 | 67.85 | 0.964 | 1.056 | 11.69 | 35.2 | 4.437 | 28278 |
| 4.504 | 4.536 | 75.66 | 52.23 | 41.71 | 64.46 | 1.19 | 1.354 | 11.41 | 34.66 | 4.49 | 28265 |
| 5.003 | 5.011 | 72.47 | 51.33 | 41.26 | 61.92 | 1.379 | 1.627 | 11.18 | 34.34 | 4.513 | 28261 |
| 5.497 | 5.507 | 69.96 | 50.78 | 41.09 | 60.01 | 1.662 | 1.915 | 11.26 | 34.44 | 4.529 | 28249 |
| 6.016 | 6.03 | 67.94 | 50.45 | 41.2 | 58.46 | 1.994 | 2.317 | 11.2 | 34.39 | 4.535 | 28229 |
| 7.021 | 7.019 | 64.75 | 49.76 | 41.17 | 56.04 | 2.66 | 3.073 | 11.22 | 34.43 | 4.536 | 28206 |
| 7.999 | 8.005 | 62.36 | 49.21 | 41.19 | 54.23 | 3.416 | 3.964 | 11.26 | 34.41 | 4.552 | 28189 |
| 8.999 | 9.018 | 60.83 | 49.14 | 41.61 | 53.2 | 4.293 | 4.974 | 11.16 | 35.08 | 4.382 | 28164 |
| 9.996 | 10.066 | 59.43 | 48.91 | 41.8 | 52.2 | 5.278 | 6.162 | 11.17 | 35.27 | 4.39 | 28132 |
| 11.005 | 11.016 | 58.24 | 48.69 | 41.88 | 51.41 | 6.412 | 7.285 | 11.2 | 35.4 | 4.377 | 28115 |

Half power

| hl flow (gpm) | cl flow (gpm) | t1i (C) | t1o (C) | t2i (C) | t2o (C) | dp hot (psi) | dp cold (psi) | t3i (C) | t3o (C) | city flow (gpm) | electric power (W) |
|---|---|---|---|---|---|---|---|---|---|---|---|
| 3.021 | 3.02 | 51.07 | 33.6 | 26.42 | 43.31 | 0.663 | 0.743 | 11.01 | 23.29 | 4.268 | 14216 |
| 3.516 | 3.523 | 50.14 | 34.7 | 27.92 | 42.93 | 0.789 | 0.892 | 11.91 | 24.7 | 4.218 | 14495 |
| 4.036 | 4.037 | 46.15 | 32.91 | 26.67 | 39.58 | 1.058 | 1.201 | 11.01 | 23.5 | 4.271 | 14208 |
| 4.508 | 4.511 | 46.1 | 33.98 | 27.99 | 39.84 | 1.239 | 1.367 | 11.89 | 24.41 | 4.375 | 14490 |
| 4.991 | 5.033 | 42.93 | 32.25 | 26.67 | 37.11 | 1.499 | 1.792 | 10.94 | 23.02 | 4.441 | 14199 |
| 5.498 | 5.528 | 43.47 | 33.56 | 28.16 | 37.88 | 1.772 | 2.032 | 11.98 | 24.5 | 4.373 | 14484 |
| 6 | 6.018 | 40.6 | 31.67 | 26.59 | 35.35 | 2.111 | 2.507 | 10.89 | 22.91 | 4.47 | 14187 |
| 6.996 | 7.038 | 38.92 | 31.27 | 26.6 | 34.12 | 2.827 | 3.349 | 10.89 | 22.92 | 4.478 | 14173 |
| 8.038 | 8.041 | 37.71 | 31.02 | 26.65 | 33.26 | 3.674 | 4.306 | 10.88 | 22.91 | 4.493 | 14157 |
| 9.012 | 9.027 | 36.69 | 30.72 | 26.61 | 32.51 | 4.545 | 5.317 | 10.86 | 22.91 | 4.512 | 14144 |
| 10.013 | 10.016 | 35.94 | 30.55 | 26.66 | 31.99 | 5.552 | 6.45 | 10.89 | 23 | 4.526 | 14128 |
| 11.016 | 11.019 | 35.31 | 30.4 | 26.7 | 31.55 | 6.696 | 7.678 | 10.88 | 23 | 4.533 | 14130 |

Isothermal data

| hl flow (gpm) | cl flow (gpm) | t1i (C) | t1o (C) | t2i (C) | t2o (C) | dp hot (psi) | dp cold (psi) | t3i (C) | t3o (C) | city flow (gpm) | electric power (W) |
|---|---|---|---|---|---|---|---|---|---|---|---|
| 3.028 | 3.025 | 17.12 | 16.67 | 16.64 | 17.19 | 0.684 | 0.795 | 15.5 | 16.01 | 4.429 | 0 |
| 3.488 | 3.497 | 12.78 | 12.36 | 12.51 | 12.95 | 0.796 | 0.948 | 11.88 | 12.38 | 4.28 | 0 |
| 4.016 | 4.015 | 15.56 | 15.23 | 15.3 | 15.69 | 1.128 | 1.269 | 14.61 | 15.09 | 4.435 | 0 |
| 4.522 | 4.518 | 12.32 | 12.06 | 12.31 | 12.57 | 1.337 | 1.518 | 11.87 | 12.24 | 4.269 | 0 |
| 5.019 | 5.01 | 14.77 | 14.45 | 14.54 | 14.91 | 1.65 | 1.901 | 13.74 | 14.31 | 4.413 | 0 |
| 5.506 | 5.516 | 12.35 | 12.11 | 12.36 | 12.6 | 1.924 | 2.229 | 11.9 | 12.29 | 4.266 | 0 |
| 6.022 | 6.039 | 13.66 | 13.34 | 13.44 | 13.81 | 2.335 | 2.721 | 12.58 | 13.22 | 4.405 | 0 |
| 7.021 | 7.017 | 13.5 | 13.32 | 13.53 | 13.73 | 3.097 | 3.584 | 13.05 | 13.42 | 4.44 | 0 |
| 8.008 | 8.01 | 13.18 | 12.96 | 13.13 | 13.39 | 3.964 | 4.581 | 12.36 | 12.95 | 4.437 | 0 |
| 9.004 | 9.017 | 12.88 | 12.68 | 12.88 | 13.11 | 4.931 | 5.694 | 12.17 | 12.73 | 4.416 | 0 |
| 10.028 | 10.013 | 12.93 | 12.75 | 12.96 | 13.17 | 6.062 | 6.882 | 12.26 | 12.81 | 4.446 | 0 |
| 11.007 | 11.029 | 13.11 | 12.93 | 13.13 | 13.33 | 7.236 | 8.208 | 12.34 | 12.96 | 4.457 | 0 |

Data for GB240H-20
Maximum power

| hl flow (gpm) | cl flow (gpm) | t1i (C) | t1o (C) | t2i (C) | t2o (C) | dp hot (psi) | dp cold (psi) | t3i (C) | t3o (C) | city flow (gpm) | electric power (W) |
|---|---|---|---|---|---|---|---|---|---|---|---|
| 2.997 | 3.016 | 89.58 | 56.76 | 48.32 | 80.72 | 0.859 | 0.863 | 15.9 | 37.53 | 4.548 | 27089 |
| 3.514 | 3.515 | 83.92 | 55.43 | 47.68 | 75.61 | 1.091 | 1.193 | 15.94 | 38.51 | 4.363 | 27055 |
| 3.999 | 3.992 | 78.76 | 53.62 | 46.32 | 70.98 | 1.371 | 1.53 | 15.98 | 37.91 | 4.544 | 27044 |
| 4.517 | 4.515 | 74.98 | 52.72 | 45.86 | 67.7 | 1.72 | 1.95 | 15.88 | 37.74 | 4.571 | 27030 |
| 5.006 | 5.013 | 72.26 | 52.14 | 45.61 | 65.36 | 2.017 | 2.39 | 15.93 | 37.84 | 4.563 | 27029 |
| 5.511 | 5.523 | 71.11 | 52.87 | 46.67 | 64.6 | 2.411 | 2.874 | 16.06 | 38.83 | 4.357 | 27023 |
| 6.002 | 6.024 | 69 | 52.25 | 46.26 | 62.8 | 2.858 | 3.382 | 16.14 | 38.61 | 4.439 | 27008 |
| 6.523 | 6.516 | 66.74 | 51.3 | 45.52 | 60.82 | 3.338 | 3.934 | 15.67 | 37.91 | 4.21 | 27007 |
| 7.013 | 7.01 | 64.78 | 50.36 | 44.79 | 59.07 | 3.828 | 4.538 | 15.29 | 37.4 | 4.519 | 26996 |
| 7.509 | 7.523 | 64.95 | 51.51 | 46.14 | 59.44 | 4.341 | 5.184 | 15.26 | 39.02 | 4.18 | 26985 |
| 8.013 | 8.016 | 62.36 | 49.72 | 44.49 | 57.02 | 4.941 | 5.871 | 15.13 | 37.17 | 4.555 | 26974 |
| 8.519 | 8.513 | 62.99 | 51.13 | 46.07 | 57.85 | 5.547 | 6.579 | 15.3 | 39.16 | 4.194 | 26987 |
| 9.012 | 9.024 | 60.67 | 49.45 | 44.52 | 55.67 | 6.202 | 7.389 | 15.3 | 37.33 | 4.566 | 26964 |
| 9.522 | 9.524 | 61.42 | 50.81 | 46.02 | 56.59 | 6.892 | 8.154 | 15.36 | 39.2 | 4.217 | 26957 |
| 10.013 | 10.006 | 59.35 | 49.21 | 44.52 | 54.62 | 7.637 | 8.98 | 15.26 | 37.5 | 4.575 | 26975 |

Half power

| hl flow (gpm) | cl flow (gpm) | t1i (C) | t1o (C) | t2i (C) | t2o (C) | dp hot (psi) | dp cold (psi) | t3i (C) | t3o (C) | city flow (gpm) | electric power (W) |
|---|---|---|---|---|---|---|---|---|---|---|---|
| 3.018 | 3.011 | 51.24 | 34.22 | 29.53 | 46.06 | 0.898 | 1.02 | 14.4 | 25.93 | 4.4 | 13731 |
| 3.509 | 3.508 | 48.8 | 34.11 | 29.73 | 44.07 | 1.152 | 1.335 | 14.48 | 25.98 | 4.422 | 13728 |
| 4.017 | 4.01 | 46.55 | 33.7 | 29.6 | 42.21 | 1.48 | 1.683 | 14.37 | 25.64 | 4.527 | 13722 |
| 4.507 | 4.501 | 44.98 | 33.51 | 29.64 | 40.92 | 1.81 | 2.084 | 14.59 | 25.75 | 4.598 | 13721 |
| 4.999 | 5.009 | 44.05 | 33.72 | 30.09 | 40.19 | 2.132 | 2.573 | 14.74 | 26.54 | 4.339 | 13721 |
| 5.51 | 5.514 | 42.43 | 33.02 | 29.55 | 38.8 | 2.562 | 3.086 | 14.73 | 25.7 | 4.715 | 13717 |
| 6.009 | 6.005 | 42.26 | 33.65 | 30.34 | 38.82 | 3.014 | 3.628 | 14.85 | 26.62 | 4.374 | 13711 |
| 6.501 | 6.518 | 40.98 | 33 | 29.86 | 37.69 | 3.495 | 4.226 | 15.01 | 26.01 | 4.718 | 13702 |
| 7.001 | 7.015 | 40.91 | 33.53 | 30.5 | 37.77 | 4.013 | 4.839 | 15.06 | 26.96 | 4.348 | 13696 |
| 7.499 | 7.514 | 39.96 | 33.04 | 30.11 | 36.94 | 4.563 | 5.506 | 15.12 | 26.31 | 4.656 | 13693 |
| 8.007 | 8.006 | 40.07 | 33.6 | 30.76 | 37.16 | 5.178 | 6.193 | 15.18 | 27.2 | 4.31 | 13689 |
| 8.5 | 8.502 | 39.48 | 33.37 | 30.62 | 36.67 | 5.787 | 6.927 | 15.23 | 26.83 | 4.51 | 13681 |
| 9.004 | 9 | 39.18 | 33.41 | 30.73 | 36.46 | 6.459 | 7.701 | 15.26 | 26.96 | 4.477 | 13676 |
| 9.505 | 9.506 | 38.85 | 33.38 | 30.78 | 36.22 | 7.165 | 8.506 | 15.31 | 26.99 | 4.479 | 13668 |
| 10.006 | 10.012 | 38.72 | 33.52 | 31 | 36.16 | 7.928 | 9.363 | 15.28 | 27.39 | 4.358 | 13662 |

Isothermal data

| hl flow (gpm) | cl flow (gpm) | t1i (C) | t1o (C) | t2i (C) | t2o (C) | dp hot (psi) | dp cold (psi) | t3i (C) | t3o (C) | city flow (gpm) | electric power (W) |
|---|---|---|---|---|---|---|---|---|---|---|---|
| 3.001 | 3.011 | 16.6 | 16.48 | 16.63 | 16.82 | 0.958 | 1.155 | 16.44 | 16.6 | 4.297 | 0 |
| 3.505 | 3.501 | 16.44 | 16.31 | 16.46 | 16.66 | 1.259 | 1.5 | 16.22 | 16.42 | 4.313 | 0 |
| 4.008 | 4.007 | 16.28 | 16.16 | 16.33 | 16.51 | 1.608 | 1.875 | 16.11 | 16.31 | 4.312 | 0 |
| 4.508 | 4.509 | 16.28 | 16.18 | 16.35 | 16.51 | 1.99 | 2.323 | 16.16 | 16.33 | 4.656 | 0 |
| 5.006 | 5.019 | 16.19 | 16.07 | 16.24 | 16.42 | 2.361 | 2.819 | 16.01 | 16.23 | 4.648 | 0 |
| 5.51 | 5.502 | 16.13 | 16.03 | 16.21 | 16.37 | 2.816 | 3.334 | 15.95 | 16.2 | 4.343 | 0 |
| 6.007 | 5.998 | 15.95 | 15.83 | 16.02 | 16.18 | 3.31 | 3.922 | 15.69 | 16 | 4.314 | 0 |
| 6.508 | 6.513 | 16 | 15.89 | 16.08 | 16.23 | 3.84 | 4.56 | 15.76 | 16.04 | 4.603 | 0 |
| 7.007 | 7.016 | 16.03 | 15.93 | 16.11 | 16.26 | 4.401 | 5.232 | 15.8 | 16.09 | 4.612 | 0 |
| 7.498 | 7.503 | 15.95 | 15.83 | 16.01 | 16.18 | 4.979 | 5.908 | 15.58 | 15.95 | 4.626 | 0 |
| 8.012 | 8.006 | 16.1 | 15.99 | 16.18 | 16.33 | 5.65 | 6.666 | 15.75 | 16.12 | 4.595 | 0 |
| 8.519 | 8.51 | 16.4 | 16.28 | 16.46 | 16.62 | 6.306 | 7.447 | 15.94 | 16.38 | 4.256 | 0 |
| 9.012 | 8.996 | 16.06 | 15.93 | 16.1 | 16.29 | 7.007 | 8.241 | 15.51 | 16.01 | 4.306 | 0 |
| 9.512 | 9.532 | 16.08 | 15.96 | 16.12 | 16.3 | 7.769 | 9.128 | 15.53 | 16.02 | 4.595 | 0 |
| 9.98 | 9.991 | 16.23 | 16.1 | 16.27 | 16.44 | 8.513 | 9.91 | 15.62 | 16.15 | 4.59 | 0 |

# Appendix F

## Table of Experimental Hose Pressure Drops

These values are the averaged isothermal pressure drops for the hoses used to connect the heat exchangers in the test section. A 4 inch steel nipple was used in place of the heat exchanger, and the values below include the offsets listed in chapter 4.

Table F.1 Experimental hose pressure drop values

| Hot loop flow rate (gpm) | Hot loop hose pressure drop (psi) | Cold loop flow rate (gpm) | Cold loop hose pressure drop (psi) |
|---|---|---|---|
| 2.997 | 0.222 | 3.025 | 0.251 |
| 3.516 | 0.328 | 3.516 | 0.358 |
| 3.991 | 0.439 | 4.003 | 0.506 |
| 4.479 | 0.569 | 4.501 | 0.643 |
| 5.013 | 0.765 | 5.001 | 0.783 |
| 5.514 | 0.93 | 5.511 | 0.94 |
| 5.987 | 1.093 | 5.995 | 1.095 |
| 6.503 | 1.286 | 6.513 | 1.279 |
| 7.01 | 1.488 | 7.015 | 1.472 |
| 7.516 | 1.71 | 7.513 | 1.675 |
| 8.002 | 1.925 | 7.994 | 1.889 |
| 8.514 | 2.174 | 8.494 | 2.122 |
| 9.014 | 2.431 | 9.008 | 2.378 |
| 9.518 | 2.702 | 9.528 | 2.656 |
| 9.773 | 2.842 | 9.745 | 2.776 |

| | | | |
|---|---|---|---|
| 10.007 | 2.973 | 9.994 | 2.911 |

Table F.1 Continued

| Hot loop flow rate (gpm) | Hot loop hose pressure drop (psi) | Cold loop flow rate (gpm) | Cold loop hose pressure drop (psi) |
|---|---|---|---|
| 10.007 | 2.973 | 9.994 | 2.911 |
| 10.514 | 3.27 | 10.5 | 3.189 |
| 11.005 | 3.57 | 10.993 | 3.464 |
| 11.509 | 3.892 | 11.537 | 3.779 |
| 12.006 | 4.221 | 12.011 | 4.065 |
| 12.505 | 4.56 | 12.534 | 4.375 |

# Appendix G

## Power Measurement

This appendix discusses the equipment used to control and measure the power applied to the immersion heaters in the system. There are two immersion heaters in the hot loop, they were manufactured by Vulcan Electric and have the part number SF-1524B. They are flanged at one end, and are inserted into portions of the flow loop constructed by Andrew O'Neill. They are rated for 15kW each, giving a total heat generation capacity of 30kW. The maximum voltage they are rated for is 240V, and consist of a bundle of hairpin type heaters, with a stated heat flux density of 84W/in^2. They were connected to the EHMP 300-200 power supply through a set of high capacity voltage shunts placed in parallel on the return side of the current flow. This was a choice made from safety concerns, as was the decision to install fuses on the instrumentation wiring. The shunts were mounted on a board with rubber feet to ensure electrical isolation . This can be seen in Figure G.1.

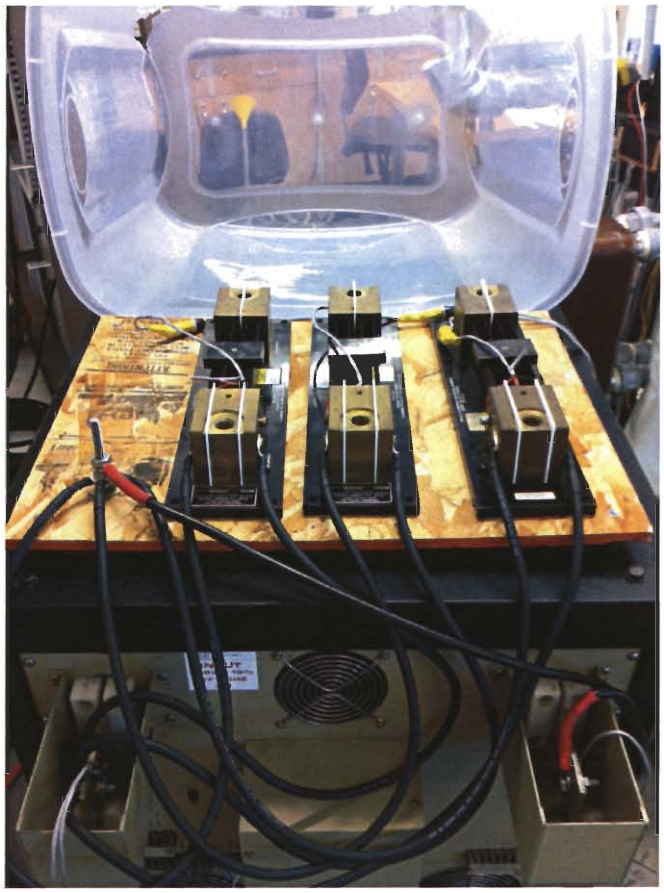

Figure G.1 Voltage shunts and rear of EHMP power supply

The voltage shunts were manufactured by Sensitive Instruments, and were modified from a previous experiment. They were calibrated after modification and had known resistances that can be seen in Table G.1, and each had a rated capacity of 50 A.

Table G.1 Shunt specifications

| | SH-5182 | SH-5186 | SH-5190 |
|---|---|---|---|
| Resistance (Ohms) | 0.007954 | 0.007954 | 0.007949 |
| Maximum variation of resistance (Ohms) | +-10E-6 | +-10E-6 | +-2*10E-6 |
| Uncertainty (%) | +-0.013 | +-0.013 | +-0.026 |

The voltage of the power supply was measure directly across the terminals with a SCXI-1122 module and appropriate mounting block. Voltage measurements of the shunts were taken with the SCXI-1102 module independently to verify that no stray currents would unknowingly surpass their rated capacities. The instrumentation and SCXI-1000 Chassis was mounted on a separate movable rack to again ensure that the user was isolated from any potential danger. The rack can be seen in Figure G.2. An earth safety ground was connected to module as was required by the operations manual.

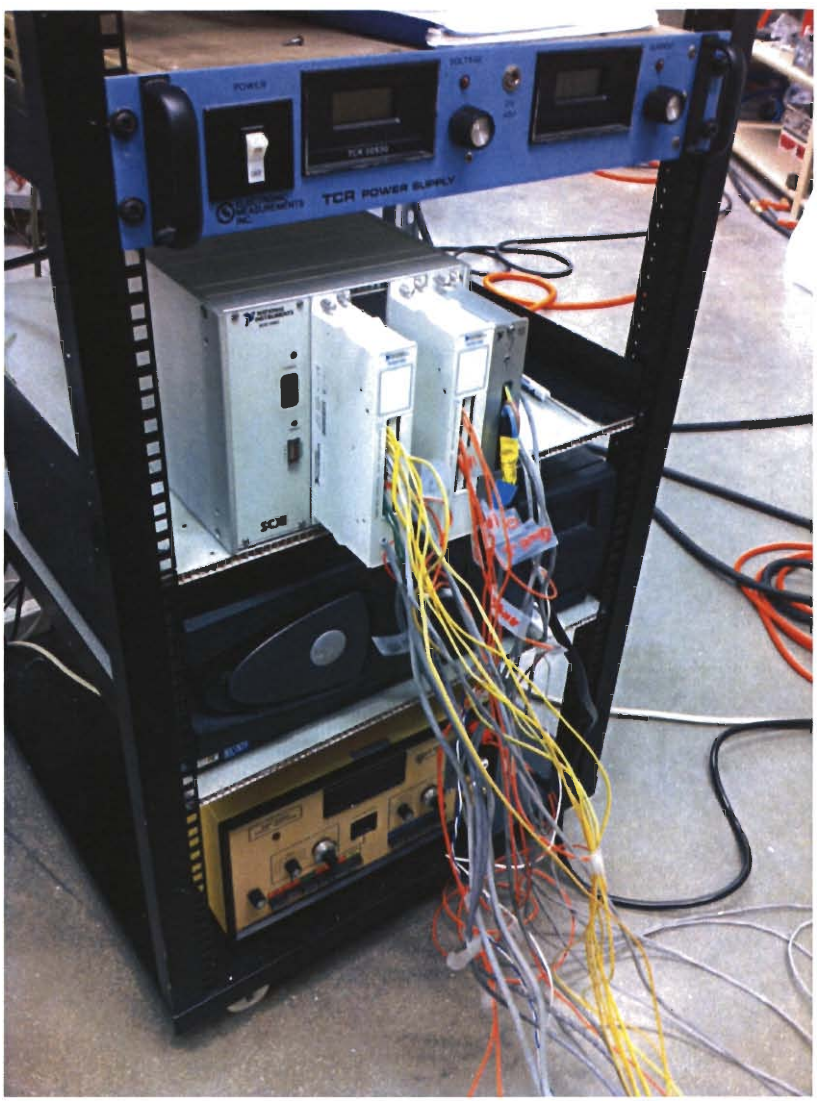


Figure G.2 Picture of data acquisition system

In order to measure such a high voltage, a gain of .01 was used, and was capable of reading the full power supply voltage at all operating conditions. At this gain, the module is capable of reading voltages in steps of 0.518V, and had a percent error of 0.22%. At the maximum level of heat generation, 30kW, the voltage output was 240V with a corresponding current of 125 DC Amps. The combined uncertainty of the shunts was 0.52%, coupled with an uncertainty of 0.05% for each shunt reading. Therefore, the total uncertainty of amperage was 0.67%. When the maximum uncertainties for voltage and amperage are applied for a full heat load to the immersion heaters, this resulted in an uncertainty of +-267W, which was in general agreement with the measured applied power.

# Appendix H

## Instrumentation and Experimental Equipment Information

This appendix contains the calibration reports of various instruments used in this experiment as well as specifications regarding various pieces of equipment installed in test stand.

Pressure Transducers

OMEGADYNE INC.

PRESSURE TRANSDUCER
FINAL CALIBRATION

0 - 100.00 PSIA
Excitation 10.000 Vdc

Job:
Model: PX32B1-100AV
Date: 12/23/2002
Calibrated: 0.00 - 100.00 PSIA

Serial: 130258
Tested By: RICK
Temperature Range: -40 to 135 F
Specfile: Px32..spf

| Pressure PSIA | Unit Data mVdc |
|---|---|
| 0.00 | 0.000 |
| 50.00 | 14.954 |
| 100.00 | 29.940 |
| 50.00 | 14.970 |
| 0.00 | 0.002 |

| | | |
|---|---|---|
| Balance | 0.120 | mVdc |
| Sensitivity | 29.940 | mVdc |
| In Resist | 350.30 | Ohms |
| Out Resist | 350.80 | Ohms |
| Shunt: | 25.776 | mVdc |

ELECTRICAL LEAKAGE: PASS
PRESSURE CONNECTION/FITTING: 1/8-27 NPT FEMALE
ELECTRICAL WIRING/CONNECTOR:

| | |
|---|---|
| Pin A | +INPUT |
| Pin B | +OUTPUT |
| Pin C | -OUTPUT |
| Pin D | -INPUT |
| Pins E&F | SHUNT |

This Calibration was performed using Instruments and Standards that are traceable to the United States National Institute of Standards Technology.

| S/N | Description | Range | Reference | Cal Cert |
|---|---|---|---|---|
| 1598/94-3 | 30/150 PSI DRUCK STD | 0 - 150 lbs | C-2502 | C-2502 |
| 3146A20557 | HP 34401A | Unit Under Test | C-2405 | C-2405 |

Q.A. Representative : Rick Swinker Date: 12-23-02

This transducer is tested to & meets published specifications. After final calibration our products are stored in a controlled stock room & considered in bonded storage. Depending on environment & severity of use factory calibration is recommended every one to three years after initial service installation date

Omegadyne, Inc., 149 Stelzer Court, Sunbury, OH 43074 (740) 965-9340
http://www.omegadyne.com email: info@omegadyne.com (800) USA-DYNE

Figure H.1 Cold loop test section outlet pressure transducer

OMEGADYNE INC.

PRESSURE TRANSDUCER
FINAL CALIBRATION

0 - 100.00 PSIA
Excitation 10.000 Vdc

Job:
Model: PX32B1-100AV
Date: 12/23/2002
Calibrated: 0.00 - 100.00 PSIA

Serial: 130259
Tested By: RICK
Temperature Range: -40 to 335 F
Specfile: Px32..spf

| Pressure PSIA | Unit Data mVdc |
|---|---|
| 0.00 | 0.000 |
| 50.00 | 15.011 |
| 100.00 | 29.905 |
| 50.00 | 15.036 |
| 0.00 | 0.011 |

| | | |
|---|---|---|
| Balance | 0.105 | mVdc |
| Sensitivity | 29.905 | mVdc |
| In Resist | 350.80 | Ohms |
| Out Resist | 350.80 | Ohms |
| Shunt: | 25.675 | mVdc |

ELECTRICAL LEAKAGE: PASS
PRESSURE CONNECTION/FITTING: 1/8-27 NPT FEMALE
ELECTRICAL WIRING/CONNECTOR:

| | |
|---|---|
| Pin A | +INPUT |
| Pin B | +OUTPUT |
| Pin C | -OUTPUT |
| Pin D | -INPUT |
| Pins E&F | SHUNT |

This Calibration was performed using Instruments and Standards that are traceable to the United States National Institute of Standards Technology.

| S/N | Description | Range | Reference | Cal Cert |
|---|---|---|---|---|
| 1598/94-3 | 30/150 PSI DRUCK STD | 0 - 150 lbs | C-2502 | C-2502 |
| 3146A20557 | HP 34401A | Unit Under Test | C-2405 | C-2405 |

Q.A. Representative : Rick Swisher Date: 12-23-02

This transducer is tested to & meets published specifications. After final calibration our products are stored in a controlled stock room & considered in bonded storage. Depending on environment & severity of use factory calibration is recommended every one to three years after initial service installation date

Omegadyne, Inc., 149 Stelzer Court, Sunbury, OH 43074 (740) 965-9340
http://www.omegadyne.com email: infc@omegadyne.com (800) USA-DYNE

Figure H.1 Hot loop test section outlet pressure transducer

OMEGADYNE INC.

PRESSURE TRANSDUCER
FINAL CALIBRATION

0 - 100.00 PSIA
Excitation 10.000 Vdc

Job:
Model: PX32B1-100AV
Date: 12/23/2002
Calibrated: 0.00 - 100.00 PSIA

Serial: 130260
Tested By: RICK
Temperature Range: -40 to 335 F
Specfile: Px32..spf

| Pressure PSIA | Unit Data mVdc |
|---|---|
| 0.00 | 0.000 |
| 50.00 | 14.999 |
| 100.00 | 30.012 |
| 50.00 | 15.015 |
| 0.00 | 0.014 |

| | | |
|---|---|---|
| Balance - | 0.065 | mVdc |
| Sensitivity | 30.012 | mVdc |
| In Resist | 350.10 | Ohms |
| Out Resist | 350.70 | Ohms |
| Shunt: | 25.521 | mVdc |

ELECTRICAL LEAKAGE: PASS
PRESSURE CONNECTION/FITTING: 1/8-27 NPT FEMALE
ELECTRICAL WIRING/CONNECTOR:

| | |
|---|---|
| Pin A | +INPUT |
| Pin B | +OUTPUT |
| Pin C | -OUTPUT |
| Pin D | -INPUT |
| Pins E&F | SHUNT |

This Calibration was performed using Instruments and Standards that are traceable to the United States National Institute of Standards Technology.

| S/N | Description | Range | Reference | Cal Cert |
|---|---|---|---|---|
| 1598/94-3 | 30/150 PSI DRUCK STD | 0 - 150 lbs | C-2502 | C-2502 |
| 3146A20557 | HP 34401A | Unit Under Test | C-2405 | C-2405 |

Q.A. Representative : Rick Swisher Date: 12-23-02

This transducer is tested to & meets published specifications. After final calibration our products are stored in a controlled stock room & considered in bonded storage. Depending on environment & severity of use factory calibration is recommended every one to three years after initial service installation date

Omegadyne, Inc., 149 Stelzer Court, Sunbury, OH 43074 (740) 965-9340
http://www.omegadyne.com email: info@omegadyne.com (800) USA-DYNE

Figure H.3 Hot loop inlet pressure transducer

O M E G A D Y N E  I N C.

PRESSURE TRANSDUCER
FINAL CALIBRATION

0.00 - 100.00 PSIA
Excitation 10.000 Vdc

Job: Serial: 257877
Model: PX32B1-100AV Tested By: CHRIS
Date: 9/2/2010 Temperature Range: -40 to 335 F
Calibrated: 0.00 - 100.00 PSIA Specfile: PX32

| Pressure PSIA | Unit Data mVdc |
|---|---|
| 0.00 | 0.045 |
| 50.00 | 14.998 |
| 100.00 | 30.028 |
| 50.00 | 15.010 |
| 0.00 | 0.051 |

| | | |
|---|---|---|
| Balance | 0.045 | mVdc |
| Sensitivity | 29.983 | mVdc |
| In Resist | 414.40 | Ohms |
| Out Resist | 350.50 | Ohms |
| 80% Shunt | 23.918 | mVdc |

ELECTRICAL LEAKAGE: PASS
PRESSURE CONNECTION/FITTING: 1/8-27 NPT FEMALE
ELECTRICAL WIRING/CONNECTOR: PIN A = +INPUT (EXC)
PIN B = +OUTPUT
PIN C = -OUTPUT
PIN D = -INPUT (EXC)
PINS E&F = SHUNT

This Calibration was performed using Instruments and Standards that are traceable to the United States National Institute of Standards Technology.

| S/N | Description | Range | Reference | Cal Cert |
|---|---|---|---|---|
| 1598 94-3 | AUTO Druck 30/150 ST | 0 - 150 PSIA | C-2502 | C-2502 |
| MY4100867 | AT34970A DMM | Unit Under Test | C-2473 | 908949730 |

Q.A. Representative : Chris Diaz Date: 9/2/2010
This transducer is tested to & meets published specifications. After final calibration our products are stored in a controlled stock room & considered in bonded storage. Depending on environment & severity of use factory calibration is recommended every one to three years after initial service installation date.

Omegadyne, Inc., 149 Stelzer Court, Sunbury, OH 43074 (740) 965-9340
http://www.omegadyne.com email: info@omegadyne.com (800) USA-DYNE

Figure H.4 Cold loop test section inlet pressure transducer

The calibration reports for the flow meters used in this study now follow.

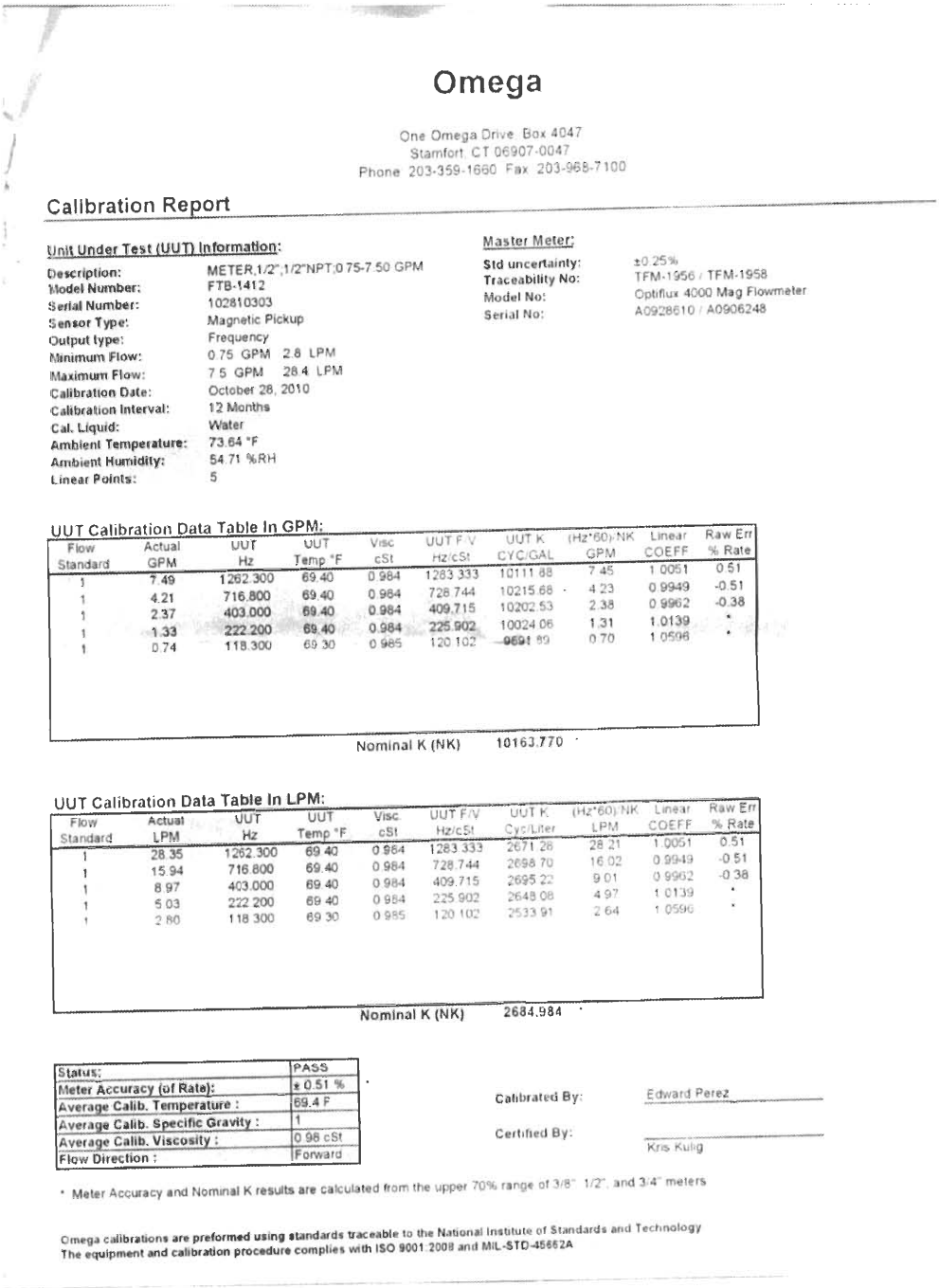

Omega

One Omega Drive, Box 4047
Stamford, CT 06907-0047
Phone: 203-359-1660 Fax: 203-968-7100

Calibration Report

Unit Under Test (UUT) Information:

| | |
|---|---|
| Description: | METER,1/2",1/2"NPT,0.75-7.50 GPM |
| Model Number: | FTB-1412 |
| Serial Number: | 102810303 |
| Sensor Type: | Magnetic Pickup |
| Output type: | Frequency |
| Minimum Flow: | 0.75 GPM 2.8 LPM |
| Maximum Flow: | 7.5 GPM 28.4 LPM |
| Calibration Date: | October 28, 2010 |
| Calibration Interval: | 12 Months |
| Cal. Liquid: | Water |
| Ambient Temperature: | 73.64 °F |
| Ambient Humidity: | 54.71 %RH |
| Linear Points: | 5 |

Master Meter:

| | |
|---|---|
| Std uncertainty: | ±0.25% |
| Traceability No: | TFM-1956 / TFM-1958 |
| Model No: | Optiflux 4000 Mag Flowmeter |
| Serial No: | A0928610 / A0906248 |

UUT Calibration Data Table In GPM:

| Flow Standard | Actual GPM | UUT Hz | UUT Temp °F | Visc cSt | UUT F/V Hz/cSt | UUT K CYC/GAL | (Hz*60)/NK GPM | Linear COEFF | Raw Err % Rate |
|---|---|---|---|---|---|---|---|---|---|
| 1 | 7.49 | 1262.300 | 69.40 | 0.984 | 1283.333 | 10111.88 | 7.45 | 1.0051 | 0.51 |
| 1 | 4.21 | 716.800 | 69.40 | 0.984 | 728.744 | 10215.68 | 4.23 | 0.9949 | -0.51 |
| 1 | 2.37 | 403.000 | 69.40 | 0.984 | 409.715 | 10202.53 | 2.38 | 0.9962 | -0.38 |
| 1 | 1.33 | 222.200 | 69.40 | 0.984 | 225.902 | 10024.06 | 1.31 | 1.0139 | * |
| 1 | 0.74 | 118.300 | 69.30 | 0.985 | 120.102 | 9691.89 | 0.70 | 1.0596 | * |

Nominal K (NK) 10163.770 *

UUT Calibration Data Table In LPM:

| Flow Standard | Actual LPM | UUT Hz | UUT Temp °F | Visc cSt | UUT F/V Hz/cSt | UUT K Cyc/Liter | (Hz*60)/NK LPM | Linear COEFF | Raw Err % Rate |
|---|---|---|---|---|---|---|---|---|---|
| 1 | 28.35 | 1262.300 | 69.40 | 0.984 | 1283.333 | 2671.26 | 28.21 | 1.0051 | 0.51 |
| 1 | 15.94 | 716.800 | 69.40 | 0.984 | 728.744 | 2698.70 | 16.02 | 0.9949 | -0.51 |
| 1 | 8.97 | 403.000 | 69.40 | 0.984 | 409.715 | 2695.22 | 9.01 | 0.9962 | -0.38 |
| 1 | 5.03 | 222.200 | 69.40 | 0.984 | 225.902 | 2648.06 | 4.97 | 1.0139 | * |
| 1 | 2.80 | 118.300 | 69.30 | 0.985 | 120.102 | 2533.91 | 2.64 | 1.0596 | * |

Nominal K (NK) 2684.984 *

| | |
|---|---|
| Status: | PASS |
| Meter Accuracy (of Rate): | ± 0.51 % |
| Average Calib. Temperature : | 69.4 F |
| Average Calib. Specific Gravity : | 1 |
| Average Calib. Viscosity : | 0.98 cSt |
| Flow Direction : | Forward |

Calibrated By: Edward Perez

Certified By: Kris Kulig

* Meter Accuracy and Nominal K results are calculated from the upper 70% range of 3/8", 1/2", and 3/4" meters

Omega calibrations are preformed using standards traceable to the National Institute of Standards and Technology
The equipment and calibration procedure complies with ISO 9001:2008 and MIL-STD-45662A

Figure H.5 Cooling loop flow meter

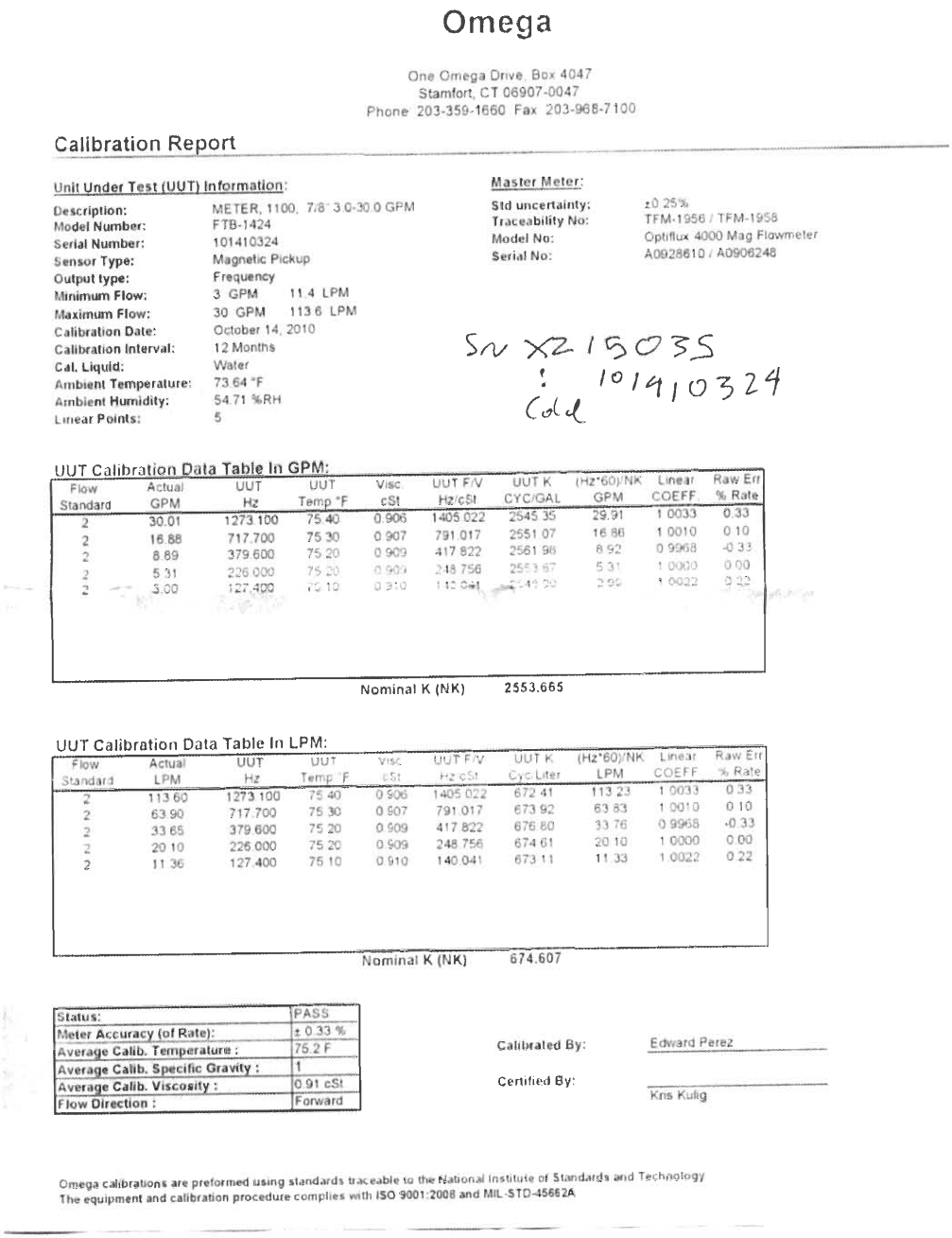

Omega

One Omega Drive, Box 4047
Stamford, CT 06907-0047
Phone: 203-359-1660 Fax: 203-968-7100

Calibration Report

Unit Under Test (UUT) Information:

| | |
|---|---|
| Description: | METER, 1100, 7/8" 3.0-30.0 GPM |
| Model Number: | FTB-1424 |
| Serial Number: | 101410324 |
| Sensor Type: | Magnetic Pickup |
| Output type: | Frequency |
| Minimum Flow: | 3 GPM 11.4 LPM |
| Maximum Flow: | 30 GPM 113.6 LPM |
| Calibration Date: | October 14, 2010 |
| Calibration Interval: | 12 Months |
| Cal. Liquid: | Water |
| Ambient Temperature: | 73.64 °F |
| Ambient Humidity: | 54.71 %RH |
| Linear Points: | 5 |

Master Meter:

| | |
|---|---|
| Std uncertainty: | ±0.25% |
| Traceability No: | TFM-1956 / TFM-1958 |
| Model No: | Optiflux 4000 Mag Flowmeter |
| Serial No: | A0928610 / A0906248 |

Sn XZ15035
: 101410324
Cold

UUT Calibration Data Table In GPM:

| Flow Standard | Actual GPM | UUT Hz | UUT Temp °F | Visc cSt | UUT F/V Hz/cSt | UUT K CYC/GAL | (Hz*60)/NK GPM | Linear COEFF | Raw Err % Rate |
|---|---|---|---|---|---|---|---|---|---|
| 2 | 30.01 | 1273.100 | 75.40 | 0.906 | 1405.022 | 2545.35 | 29.91 | 1.0033 | 0.33 |
| 2 | 16.88 | 717.700 | 75.30 | 0.907 | 791.017 | 2551.07 | 16.86 | 1.0010 | 0.10 |
| 2 | 8.89 | 379.600 | 75.20 | 0.909 | 417.822 | 2561.96 | 8.92 | 0.9968 | -0.33 |
| 2 | 5.31 | 226.000 | 75.20 | 0.909 | 248.756 | 2553.67 | 5.31 | 1.0000 | 0.00 |
| 2 | 3.00 | 127.400 | 75.10 | 0.910 | 140.041 | 2549.39 | 2.99 | 1.0022 | 0.22 |

Nominal K (NK) 2553.665

UUT Calibration Data Table In LPM:

| Flow Standard | Actual LPM | UUT Hz | UUT Temp °F | Visc cSt | UUT F/V Hz/cSt | UUT K Cyc/Liter | (Hz*60)/NK LPM | Linear COEFF | Raw Err % Rate |
|---|---|---|---|---|---|---|---|---|---|
| 2 | 113.60 | 1273.100 | 75.40 | 0.906 | 1405.022 | 672.41 | 113.23 | 1.0033 | 0.33 |
| 2 | 63.90 | 717.700 | 75.30 | 0.907 | 791.017 | 673.92 | 63.83 | 1.0010 | 0.10 |
| 2 | 33.65 | 379.600 | 75.20 | 0.909 | 417.822 | 676.60 | 33.76 | 0.9968 | -0.33 |
| 2 | 20.10 | 226.000 | 75.20 | 0.909 | 248.756 | 674.61 | 20.10 | 1.0000 | 0.00 |
| 2 | 11.36 | 127.400 | 75.10 | 0.910 | 140.041 | 673.11 | 11.33 | 1.0022 | 0.22 |

Nominal K (NK) 674.607

| | |
|---|---|
| Status: | PASS |
| Meter Accuracy (of Rate): | ± 0.33 % |
| Average Calib. Temperature : | 75.2 F |
| Average Calib. Specific Gravity : | 1 |
| Average Calib. Viscosity : | 0.91 cSt |
| Flow Direction : | Forward |

Calibrated By: Edward Perez

Certified By: Kris Kulig

Omega calibrations are preformed using standards traceable to the National Institute of Standards and Technology
The equipment and calibration procedure complies with ISO 9001:2008 and MIL-STD-45662A

Figure H.6 Cold loop flow meter calibration report

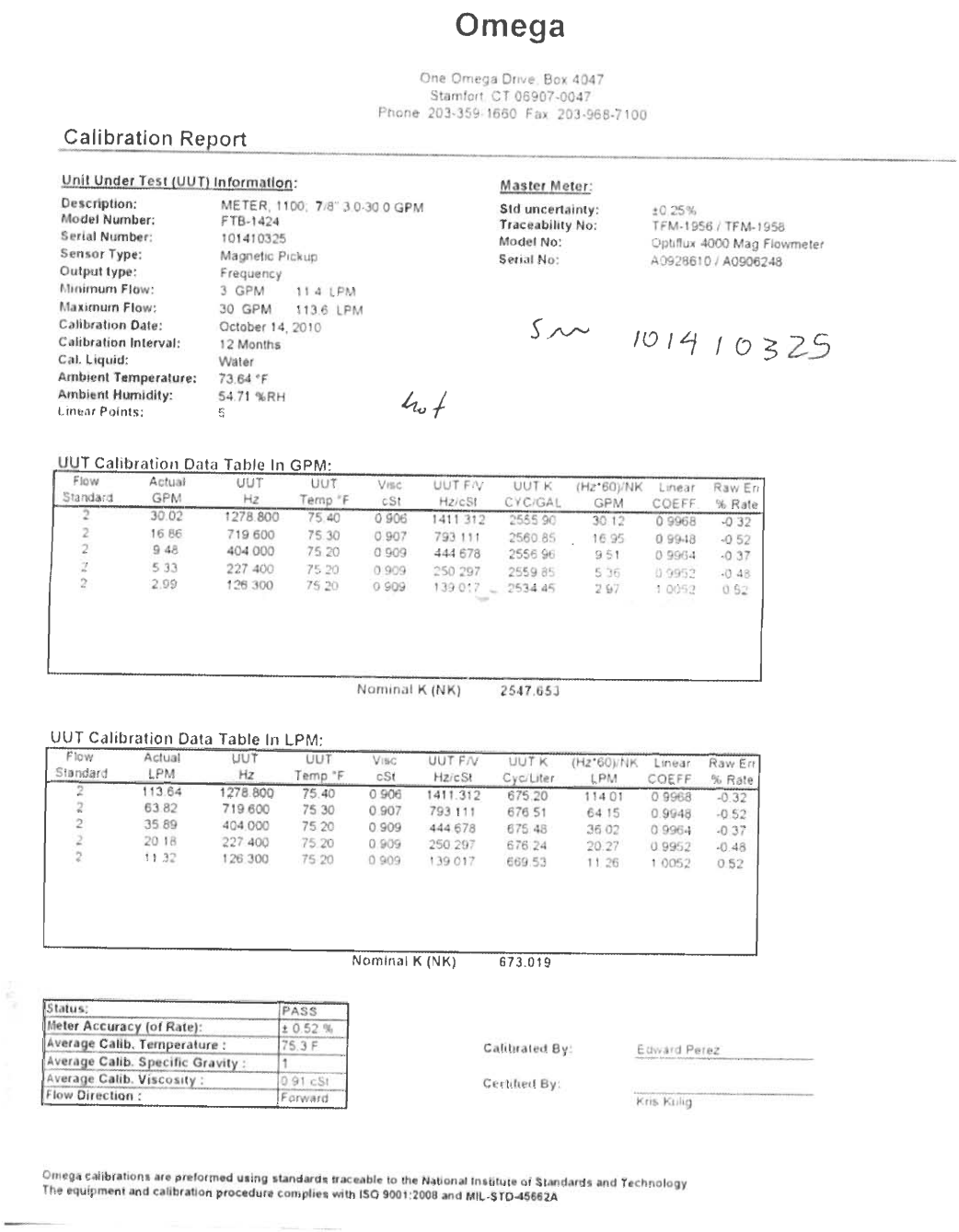

Omega

One Omega Drive, Box 4047
Stamford, CT 06907-0047
Phone: 203-359-1660 Fax: 203-968-7100

Calibration Report

**Unit Under Test (UUT) Information:**

| | |
|---|---|
| Description: | METER, 1100; 7/8" 3.0-30.0 GPM |
| Model Number: | FTB-1424 |
| Serial Number: | 101410325 |
| Sensor Type: | Magnetic Pickup |
| Output type: | Frequency |
| Minimum Flow: | 3 GPM 11.4 LPM |
| Maximum Flow: | 30 GPM 113.6 LPM |
| Calibration Date: | October 14, 2010 |
| Calibration Interval: | 12 Months |
| Cal. Liquid: | Water |
| Ambient Temperature: | 73.64 °F |
| Ambient Humidity: | 54.71 %RH |
| Linear Points: | 5 |

**Master Meter:**

| | |
|---|---|
| Std uncertainty: | ±0.25% |
| Traceability No: | TFM-1956 / TFM-1958 |
| Model No: | Optiflux 4000 Mag Flowmeter |
| Serial No: | A0928610 / A0906248 |

Sn 101410325

Hot

UUT Calibration Data Table In GPM:

| Flow Standard | Actual GPM | UUT Hz | UUT Temp °F | Visc cSt | UUT F/V Hz/cSt | UUT K CYC/GAL | (Hz*60)/NK GPM | Linear COEFF | Raw Er % Rate |
|---|---|---|---|---|---|---|---|---|---|
| 2 | 30.02 | 1278.800 | 75.40 | 0.906 | 1411.312 | 2555.90 | 30.12 | 0.9968 | -0.32 |
| 2 | 16.86 | 719.600 | 75.30 | 0.907 | 793.111 | 2560.85 | 16.95 | 0.9948 | -0.52 |
| 2 | 9.48 | 404.000 | 75.20 | 0.909 | 444.678 | 2556.96 | 9.51 | 0.9964 | -0.37 |
| 2 | 5.33 | 227.400 | 75.20 | 0.909 | 250.297 | 2559.85 | 5.36 | 0.9952 | -0.48 |
| 2 | 2.99 | 126.300 | 75.20 | 0.909 | 139.017 | 2534.45 | 2.97 | 1.0052 | 0.52 |

Nominal K (NK) 2547.653

UUT Calibration Data Table In LPM:

| Flow Standard | Actual LPM | UUT Hz | UUT Temp °F | Visc cSt | UUT F/V Hz/cSt | UUT K Cyc/Liter | (Hz*60)/NK LPM | Linear COEFF | Raw Er % Rate |
|---|---|---|---|---|---|---|---|---|---|
| 2 | 113.64 | 1278.800 | 75.40 | 0.906 | 1411.312 | 675.20 | 114.01 | 0.9968 | -0.32 |
| 2 | 63.82 | 719.600 | 75.30 | 0.907 | 793.111 | 676.51 | 64.15 | 0.9948 | -0.52 |
| 2 | 35.89 | 404.000 | 75.20 | 0.909 | 444.678 | 675.48 | 36.02 | 0.9964 | -0.37 |
| 2 | 20.18 | 227.400 | 75.20 | 0.909 | 250.297 | 676.24 | 20.27 | 0.9952 | -0.48 |
| 2 | 11.32 | 126.300 | 75.20 | 0.909 | 139.017 | 669.53 | 11.26 | 1.0052 | 0.52 |

Nominal K (NK) 673.019

| | |
|---|---|
| Status: | PASS |
| Meter Accuracy (of Rate): | ± 0.52 % |
| Average Calib. Temperature : | 75.3 F |
| Average Calib. Specific Gravity : | 1 |
| Average Calib. Viscosity : | 0.91 cSt |
| Flow Direction : | Forward |

Calibrated By: Edward Perez

Certified By: Kris Kulig

Omega calibrations are preformed using standards traceable to the National Institute of Standards and Technology
The equipment and calibration procedure complies with ISO 9001:2008 and MIL-STD-45662A

Figure H.7 Hot loop flow meter calibration report

System equipment

The figures that follow represent some of the performance characteristics of various critical components of the sytem.

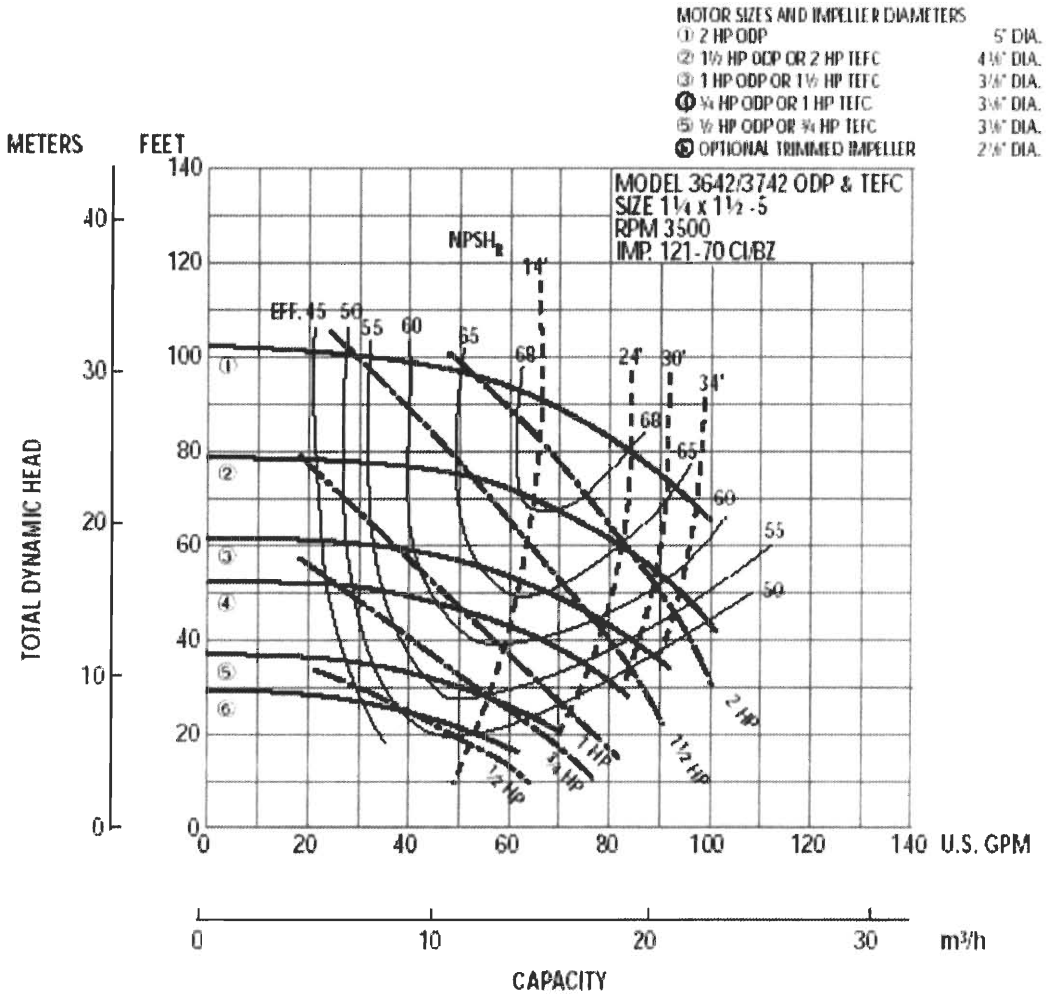


Figure H.8 Performance diagram of Goulds 3642 pump in hot loop

| | |
|---|---|
| Item | Centrifugal Pump Head |
| Type | Chemical Transfer, Straight |
| HP Required | 1/2 |
| RPM | 3450 |
| Inlet (In.) | 3/4 |
| Outlet (In.) | 3/4 |
| Use with Frame Number | 56J |
| Wetted Materials | Carbon, Ceramic, 304 SS, Viton |
| Impeller Material | 304 SS |
| Housing Material | 304 SS |
| Screw Material | 304 Stainless Steel |
| Seal Type | Mechanical |
| Seal Material | Carbon, Ceramic, Viton |
| Seal Application | Nonflammable Liquids Compatible with Pump Components |
| Max. Liquid Temp. (F) | 200 |
| GPM of Water @ 5 Ft. of Head | 38 |
| GPM of Water @ 10 Ft. of Head | 34.0 |
| GPM of Water @ 15 Ft. of Head | 32 |
| GPM of Water @ 20 Ft. of Head | 29 |
| GPM of Water @ 25 Ft. of Head | 26 |
| GPM of Water @ 30 Ft. of Head | 20 |
| GPM of Water @ 40 Ft. of Head | 5 |
| Max. Head (Ft.) | 50 |
| Max. GPM @ Head (Ft.) | 38 @ 5 |
| Best Efficiency GPM @ Head (Ft.) | 28 @ 22 |
| Min. GPM @ Head (Ft.) | 5 @ 40 |
| Best Efficiency Range GPM @ Head (Ft.) | 33 @ 12 to 24 @ 28 |
| Max. Specific Gravity | 1.0 |
| Max. Case Pressure (PSI) | 150 |
| Max. Fluid Viscosity | 31 SSU |
| Inlet Pressure (PSI) | 129 |
| Impeller Type | Closed |
| Duty | Continuous |
| Max. Dia. Solids (In.) | 1/8 |
| Port Rotation | 90¿ Increments |
| Drain Plug | No |
| Manufacturers Warranty Length | 1 Year |
| Application | Liquids Transfer, Circulation, Chemical Processing, Cooling, Pressure Boosting and Circulating |
| For Use With | Clear, Non-Abrasive, Non-Flammable Liquids Compatible with Pump Components |
| Height (In.) | 7-13/16 |
| Length (In.) | 3 |
| Width (In.) | 8-3/8 |
| Includes | Mounting Adapter, Hardware, Seal, O-ring |

H.9 Specifications for Dayton 4JMY2 pump head in cold loop

BALDOR • RELIANCE Product Information Packet: JM3107 - .5HP,3450RPM,3PH,60HZ,56J,3413M,OPEN,F1

| Part Detail | | | | | | | | | |
|---|---|---|---|---|---|---|---|---|---|
| Revision: | Q | Status: | PRD/A | Change #: | | | Proprietary: | No | |
| Type: | AC | Prod. Type: | 3413M | Elec. Spec: | 34WG2718 | | CD Diagram: | | |
| Enclosure: | OPEN | Mfg Plant: | | Mech. Spec: | 34F038 | | Layout: | | |
| Frame: | 56J | Mounting: | F1 | Poles: | 02 | | Created Date: | | |
| Base: | N | Rotation: | R | Insulation: | B | | Eff. Date: | 07-19-2006 | |
| Leads: | 9#18 | Literature: | | Elec. Diagram: | | | Replaced By: | | |
| Nameplate NP1256L | | | | | | | | | |
| CAT.NO. | JM3107 | | | | | | | | |
| SPEC. | 34F38-2718 | | | | | | | | |
| HP | .5 | | | | | | | | |
| VOLTS | 230/460 | | | | | | | | |
| AMP | 2.4/1.2 | | | | | | | | |
| RPM | 3450 | | | | | | | | |
| FRAME | 56J | | | HZ | | 60 | PH | 3 | |
| SER.F. | 1.60 | | | CODE | | N | DES | B | CLASS B |
| NEMA-NOM-EFF | 70 | | | PF | | 65 | | | |
| RATING | 40C AMB-CONT | | | | | | | | |
| CC | | | | USABLE AT 208V | | 3.1 | | | |
| DE | 6203 | | | ODE | | 6203 | | | |
| ENCL | OPEN | | | SN | | | | | |
| | SFA 2.8/1.4 | | | | | | | | |

Figure H.10 Baldor motor specifications

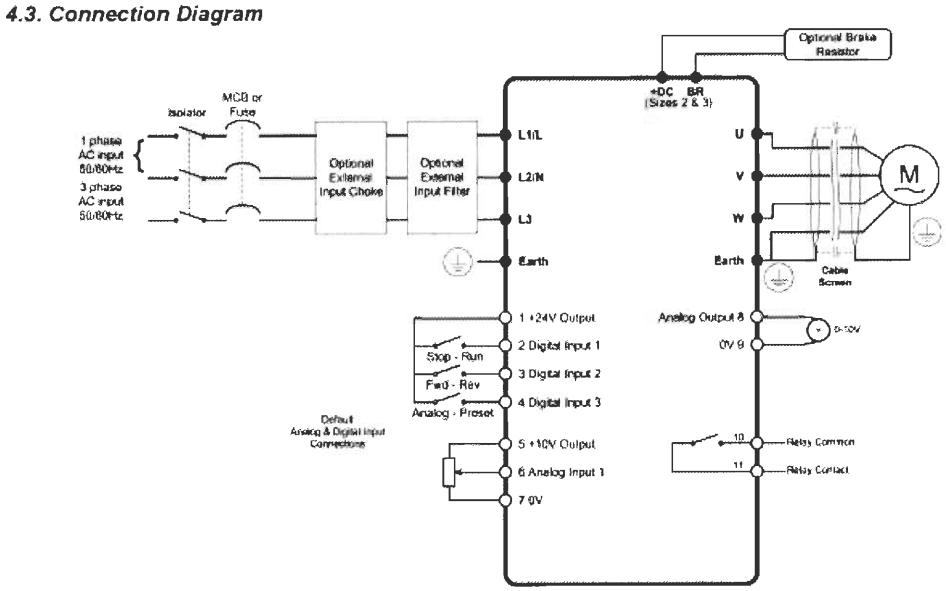


Figure H.10 Connection diagram for Invertek ODE-2-11005-1H012 drive

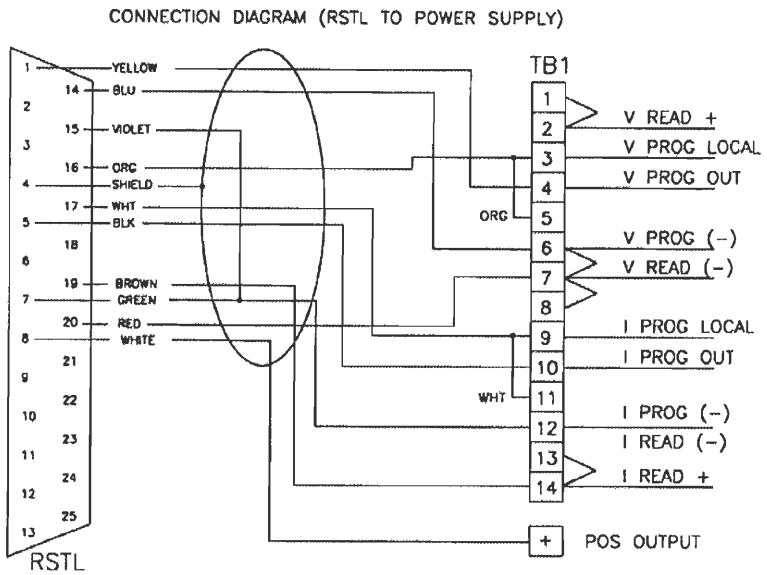


Figure 1 Connection Diagram (RSTL to Power Supply)

Figure H.11 Connection diagram for EMHP 300-200 60kW power supply

October 15, 2012
Copyright holder
Mechanical and Aeronautical Engineering
Western Michigan University
Parkview, Room G216
Kalamazoo, Michigan 4900-5343
Phone: (269) 276-3429

Dear Dr. Ho Sung Lee:
I would like to request your permission to include an excerpt of the following items in my thesis:

Lee, Ho Sung, "Thermal Design: heat sink, thermoelectric, compact heat exchanger, and solar cell," John Wiley & Sons Inc, Hoboken, New Jersey, 2010.

The figures 1.1, 2.1, and 2.2 will be helpful for the readers understanding of my analysis. The source will receive full credit in the manuscript.

For your convenience, I am including a space for your signature on the page to indicate your permission for my use of the above-mentioned. By signing below, you give ProQuest information and learning (former university Microfilms) the right to supply copies of this material on demand as part of Master Thesis. Please attach any other terms conditions for the purpose of the use of the item below. If you no longer hold the copyright to this work, please indicate to whom I should direct my request on the bottom of this page and return it to me.

Ho Sung Lee

10/15/2012
Date

Please return this letter in the self addressed, stamped envelope provided. Thank you for your time and attention to this matter.

Sincerely,
Andrew H. Pike